Integrating palaeontological and neontological perspectives to unravel the secrets of a third of vertebrate diversity



Daniel J. Delbarre

Worcester College

University of Oxford

A thesis submitted for the degree of

Doctor of Philosophy

Trinity 2017

Acknowledgements

First I wish to thank my supervisor, Matt Friedman, for everything he has done for me during my time at Oxford. Over the last four years, he has provided endless guidance, feedback, and support. Matt's knowledge of fish, fossils and evolutionary biology is vast, and as a supervisor, he seemed to be able to answer any question I asked, no matter how obscure. I could not have done this without you, thank you!

I also wish to thank Sam Giles, who became my second supervisor during my final year. Sam was a driving force in helping me to put my thesis together and making it through the latter stages of my DPhil. During the early stages of my time at Oxford, Sam was a great help in teaching me to segment in Mimics; some of the tricks she taught me saved me countless hours of frustration.

Early on in my DPhil I met Donald Davesne, who at the time, was also completing his PhD in fossil acanthomorph systematics. Despite the fact that these fossil fish had hardly been paid any attention for nearly 20 years, we both ended up working on them at the same time. I am grateful of the discussions we had over the course of my DPhil, particularly during the early days, when his insight into lampridomorph systematics was of considerable help.

I wish to thank the rest of the palaeobiology research group in Oxford (past and present). In particular, Roger Close, Mimi Beckett, John Clarke, Gemma Benevento, Andrzej Wolniewickz and César Espinoza Campuzano, who have provided much moral and academic support over the last four years.

I could not have completed my DPhil without the generous support of the curators and researchers who have let me study their collections. In particular, I must thank Zerina Johanson (NHMUK) who always went above and beyond to help, James Maclaine (NHMUK), Emma Bernard (NHMUK), Gäel Clément (MNHN) and Ursula Göhlich (NHMW).

I must indirectly thank the Leverhulme Trust for awarding Matt a grant, part of which he used to fund my DPhil. The Palaeontographical Society awarded me a small grant during my second year which enabled me to travel to museum collections and collect the data for the third chapter of my thesis.

The rest of the 2013 cohort of Earth Science DPhils also deserve my thanks. Although we did not see each other that much during the latter stages of our DPhils, we had many enjoyable meals and events earlier on. I also would like to thank everyone in office 40.17 for putting up with me and helping me to make it this far. Special thanks go to César for always lending an ear when I hit a roadblock in my work, and to Allison for our rowing gossip sessions that were an integral part of the day.

During my first year, the Worcester College MCR and everyone from Franks Building helped to make that year one of the most enjoyable periods of my life. I also thank my housemates, Dirk and Raj, for their company in our damp, beetle-infested house over the remainder of my time in Oxford.

Rowing for Worcester College Boat Club has been one of my most memorable experiences from my time at Oxford. I made many good friends and have lots of good memories from my time at the club - despite the lack of success on the water! I also thank the club for allowing me to learn to scull, which was the perfect way for me to unwind after a stressful day.

Of course, I must thank all of my family who have supported me over the last few years. Whether it was answering late night phone calls, sending me food, taking me to the Perch for lunch, or just listening to me ramble on about fish, I really appreciate your support.

Finally, I would like to thank Siân for her continued support and love. You are always there for me and I am not sure if I would have made it this far without you.

Abstract

There are over 18,500 living species of acanthomorph (spiny-rayed fishes), and they represent half of all living fish species and a third of extant vertebrates. They inhabit countless ecological niches, they are incredibly diverse, and they have developed a number of specialised morphological innovations. The earliest acanthomorphs are known from the Cenomanian, but they were neither diverse not abundant during the Cretaceous period. Following the end-Cretaceous extinction event, the acanthomorphs radiated, and by the Eocene they were anatomically modern. However, our understanding of the relationships between most fossil and living acanthomorphs, and the macroevolutionary processes behind their rise to dominance in the Recent, are poorly known. In this thesis, I aimed to develop our understanding of the evolution of the acanthomorphs by combining palaeontological and neontological data. I undertook three separate projects to accomplish this. First, I studied the anatomy two fossil representatives (†*Aipichthys pretiosus* and †'*Aipichthys*' *nuchalis*) of a primitive acanthomorph lineage, the lampridomorphs. I then placed these taxa in a phylogenetic analysis to reveal the pattern of character evolution leading to the crown-group. Second, I aimed to understand the morphological condition at the base of the acanthomorph tree by studying the relationships between two extinct groups (†Ctenothrissiformes and †Pattersonichthyiformes) that may have branched from the acanthomorph stem. Phylogenetic analyses utilising morphological and molecular data support a stem ctenosquamate placement for these taxa. Third, using a timescaled supertree, I studied the evolution of one of the major acanthomorph innovations, the protrusile upper jaw. The combination of palaeontological and neontological data provided deep insight into the evolution of the acanthomorphs, and allowed for the identification of patterns and processes that could not be identified from studying extant taxa in isolation.

Extended Abstract

The acanthomorphs (spiny-rayed fishes) are one of the largest groups of living vertebrates. Numbering over 18,500 species, the acanthomorphs represent half of all living fish species and a third of living vertebrates. They inhabit countless ecological niches, fulfil roles at a number of trophic levels, they are morphologically diverse, and they have developed a number of morphological innovations. Innovations include widespread traits such as jaw protrusion, pharyngognathy and defensive spines, as well as specialisations that are unique to subgroups of acanthomorphs (e.g. venom, limb-like appendages, cranial asymmetry and beaks). However, the acanthomorphs were not always as successful as they are in the Recent. The earliest known acanthomorph fossils are from the Late Cretaceous, where they were a relatively small part of the vertebrate assemblage. Only primitive, deeply-diverging lineages are known from the early Late Cretaceous. More advanced acanthomorphs are found in the fossil record during the late Late Cretaceous, but it is not until the Palaeogene when they start to flourish. By the Ypresian, a large number of extant lineages are represented by anatomically modern fossil taxa. Both the modern diversity of acanthomorphs and their rich fossil record have been of interest to scientists for over 150 years. However, our understanding of the relationships between most fossil and living acanthomorphs, and the macroevolutionary processes behind their Palaeogene radiation are poorly known. When combined, living and fossil data has the potential to provide insight into the origins of modern biodiversity and the evolution of life. In this thesis, I combine palaeontological and neontological data to understand the evolution of the acanthomorphs and their rise to dominance in Recent aquatic environments. I do this by using three case studies, with each one taking a separate approach and relying on different methodologies.

Some of the most primitive acanthomorph lineages have a rich fossil record spanning from the Late Cretaceous to the Recent. One of these lineages is the lampridomorphs, which are represented by oarfishes, opahs and their allies in modern oceans. In Chapter 2, I explored the anatomy and relationships of two primitive, Cenomanian lampridomorphs (†*Aipichthys pretiosus* and †'*Aipichthys*' *nuchalis*), with the aim of improving our understanding of early acanthomorph evolution.

Detailed anatomical descriptions of these two taxa are presented, followed by a phylogenetic analysis to understand how they are related to other lampridomorphs. I find that †*A. pretiosus* has a supraoccipital crest that is comprised of the supraoccipital, the frontal and the mesethmoid, and is distinct from all other species that were previously included within the genus, and branches much closer to the crown lampridomorphs. The fossil of †'*A.*' *nuchalis* was studied using a computed tomography (CT) scan, which revealed previously hidden anatomical features. As †*A. pretiosus* was the type species for †*Aipichthys*, †'*A.*' *nuchalis* and the three remaining species of this genus are referred to as †'*Aipichthys*'. I also find that †*Nardovelifer*, which was previously believed to be a crown lampridomorph (Veliferidae), is actually a stem lampridomorph as it lacks many veliferid and crown lampridomorph synapomorphies. Finally, †*Gigapteryx*, which was previously believed to be an acanthopterygian, is found to be one of the most deeply diverging lampridomorphs, united in a clade with †*Pycnosteroides*. These findings refine our understanding of the evolution of one of the most charismatic extant groups of acanthomorphs, and show how the unique lampridiform bodyplan may have evolved. Reconstructing relationships between extant and extinct taxa is the first step to building a tree of life. The phylogenetic analysis of the lampridomorphs in Chapter 2 provides new insights into the evolution of this group. Other primitive acanthomorph groups with poorly-known relationships between living and fossil members (e.g. Polymixiiformes and Beryciformes) would be ideal candidates for a similar approach as to the one taken here.

The origin of the acanthomorph clade was studied in Chapter 3. Two extinct groups of eurpyterygian fishes, the †ctenothrissiforms and †pattersonichthyiformes, have previously been attributed to branching close to, but outside of, the acanthomorph crown group. In this chapter, I aimed to study the anatomy and relationships of these extinct groups to understand the ancestral condition at the base of the acanthomorph tree. The anatomy of †*Aulolepis typus*, a †ctenothrissiform, was studied using a CT scan that revealed previously hidden features, such as the gill skeleton. †*Aulolepis*, another ctenothrissiform (†*Ctenothrissa*), and a †pattersonichthyiform (†*Pattersonichthys*) were then added to a novel morphological character matrix, which was analysed in isolation, and when combined with a molecular dataset, to understand how these taxa are related to the three extant eurypterygian lineages (Aulopiformes, Myctophiformes and Acanthomorpha). The datasets were analysed using parsimony and Bayesian methods, and Bayesian topological hypothesis tests. Collectively, the results of these analyses supported a stem ctenosquamate placement for the †ctenothrissiforms and †pattersonichthyiform

included in the analysis. However, two contrasting topologies were supported: one where all three taxa were arranged as a grade of stem ctenosquamates (hypothesis one) and the other where they were arranged as a monophyletic group (hypothesis two). Examination of the characters supporting the two topologies suggests that hypothesis one is more likely as it is supported by novel characters. In contrast, the second hypothesis appears to be supported by primitive characters that likely persisted up to the level of Eurypterygii. Understanding the primitive acanthomorph condition by studying taxa that branch outside the crown-group has the potential to provide great insight into the origins of the group. However, further study of other euteleostean groups is needed to ascertain the polarity of character evolution.

In Chapter 4, I studied the evolution of one of the major acanthomorph innovations: jaw protrusion. I built and timescaled a supertree containing 233 extant and 52 extinct fishes, of which all but 13 were acanthomorphs. I developed a novel metric, the jaw protrusion index (JPI), which was used to estimate the extent of protrusion in both living and fossil taxa. The evolution of jaw protrusion was mapped onto the phylogeny using ancestral character reconstruction, which allowed clade-specific patterns of protrusion to be visualised. Nearly all the non-acanthomorphs had limited protrusion, and only two primitive acanthomorph clades (Zeiogadiformes and Lampridomorpha) exhibited high levels of protrusion. The percomorphs displayed extensive heterogeneity in protrusile abilities, with some lineages adopting morphologies that were consistent with very low protrusion (e.g. Xiphidae), while others had extensive protrusion (e.g. Labridae). High protrusion was not necessarily clade-specific as origins of high protrusion were widespread across the phylogeny. The rate of evolution of the JPI was also studied using Bayesian evolutionary rates analyses. Well-supported increases in evolutionary rate were found in five areas of the tree: Zeiogadiformes, Lampridomorpha, Callionymidae + Dactylopteridae, a large unnamed percomorph clade (Clade A), and the branch leading to the slingjaw wrasse (*Epibulus insidiator*). When the evolutionary rates data was averaged across the tree through time, there was a sharp increase in median evolutionary rate around 88 Ma, after which it remained high. This suggests that the premaxillae of acanthomorphs were being modified during the Late Cretaceous and did not evolve in response to the end-Cretaceous extinction event. When fossil data was removed from the evolutionary rates analysis, the results were considerably different. The evolutionary rate was generally higher - especially at the base of the tree - and there were fewer well-supported shifts in evolutionary rate. Furthermore, when the evolutionary rates data was averaged across the tree, there was a near-constant trend, and there was no evidence for an increase in rate

during the Late Cretaceous. The discrepancy between the analyses where extinct taxa were included and excluded highlights the role that fossil data can have in the inference of macroevolutionary trends. In this instance, when fossil data is excluded it is not possible to detect the Late Cretaceous increase in evolutionary rate. The supertree approach taken in this Chapter has the potential to be applied to the study of other macroevolutionary traits in the acanthomorphs - and provide deep insight into their evolution.

In this thesis, the combination of palaeontological and neontological data has presented a powerful tool for delving into the evolutionary history of the acanthomorphs. If living and fossil taxa are treated are being part of the same system, and not as separate entities, then there is great potential to understand the evolution of modern diversity and the evolutionary processes that are responsible for it.

Contents

List of Figures **xv**

List of Tables **xvii**

Institutional Abbreviations **xix**

Anatomical Abbreviations **xxi**

Other Abbreviations **xxiii**

1 Introduction **1**

1.1 Interpreting and understanding evolution 1

1.1.1 Phylogenetic relationships 2

1.1.2 Macroevolutionary trends 6

1.2 Acanthomorpha and the "Second Age of Fishes" 7

1.2.1 Modern diversity and morphological innovation 7

1.2.2 The acanthomorph fossil record 12

1.2.3 Systematics and evolutionary history 16

1.3 Thesis aims and outline 20

2 Anatomy and relationships of †*Aipichthys pretiosus* and †'*Aipichthys*' *nuchalis* (Acanthomorpha: Lampridomorpha), with a review of Late Cretaceous relatives of oarfishes and their allies **23**

2.1 Introduction 24

2.2 Materials and methods 26

2.2.1 Computed tomography scanning 26

2.2.2 Phylogenetic analysis 26

2.2.3 Standard length estimation and body depth index 27

2.3 Systematic palaeontology 28

2.3.1 †*Aipichthys pretiosus* 28

2.3.2 †'*Aipichthys*' *nuchalis* 39

2.4 Phylogenetic relationships 50

2.4.1 Acanthomorpha 53
2.4.2 Clade A: Lampridomorpha 54
2.4.3 Clade α 55
2.4.4 Clade β 56
2.4.5 †'*Aipichthys*' + †*Freigichthys* 56
2.4.6 Clade C 57
2.4.7 Clade D 57
2.4.8 Clade γ 58
2.4.9 Clade δ and Lampridiformes 58
2.5 Discussion 60
2.5.1 The status of †*Paraipichthys* 60
2.5.2 †*Aipichthys* as a genus 61
2.5.3 †*Gigapteryx* as a lampridomorph 62
2.5.4 †*Nardovelifer* as a stem lampridiform 65
2.5.5 The palaeobiogeography and palaeoecology of Cretaceous lampridomorphs 66
2.5.6 Implications for lampridomorph evolution 68

3 Anatomy of †*Aulolepis typus*, and the phylogenetic position of †Ctenothrissiformes and †Pattersonichthyiformes 71
3.1 Introduction 71
3.2 Materials and methods 74
3.2.1 Computed tomography scanning 74
3.2.2 Phylogenetic analyses 77
3.2.3 Hypothesis testing 83
3.3 Systematic palaeontology 84
3.3.1 †*Aulolepis typus* 84
3.4 Phylogenetic analyses 94
3.4.1 Morphology only dataset 94
3.4.2 Combined dataset 98
3.5 Hypothesis tests 99
3.5.1 Morphology only dataset 100
3.5.2 Combined dataset 100
3.6 Discussion 102
3.6.1 Characters uniting Neoteleostei 102
3.6.2 †Ctenothrissiformes and †Pattersonichthyiformes as eurypterygians 104

3.6.3 †Ctenothrissiformes and †Pattersonichthyiformes as stem aulopiforms . . . 104
3.6.4 †Ctenothrissiformes and †Pattersonichthyiformes as stem ctenosquamates . . . 105
3.6.5 †Ctenothrissiformes + †Pattersonichthyiformes monophyly . 109
3.6.6 Refining the eurypterygian phylogeny . . . 110

4 A phylogenetic framework for investigating the evolution of jaw protrusion in acanthomorphs: fossil data exposes a Late Cretaceous shift in evolutionary rates 113
4.1 Introduction . . . 113
4.2 Materials and methods . . . 117
4.2.1 Jaw protrusion index . . . 117
4.2.2 Data collection . . . 122
4.2.3 Supertree construction . . . 123
4.2.4 Supertree dating . . . 123
4.2.5 Ancestral character reconstruction . . . 124
4.2.6 Evolutionary rates analyses . . . 125
4.2.7 Tempo of jaw protrusion evolution . . . 126
4.3 Results . . . 127
4.3.1 Jaw protrusion index . . . 127
4.3.2 Phylogenetic distribution of jaw protrusion . . . 127
4.3.3 Origins of significant jaw protrusion . . . 131
4.3.4 Evolutionary rates analyses . . . 132
4.3.5 Tempo of jaw protrusion evolution . . . 137
4.4 Discussion . . . 140
4.4.1 Jaw protrusion and morphology . . . 140
4.4.2 Jaw protrusion and macroevolution . . . 142
4.4.3 Inclusion of fossil data in macroevolution analyses . . . 146

5 Conclusion 149
5.1 The rise of the acanthomorphs: a few secrets revealed . . . 149
5.2 The evolution of primitive acanthomorph groups . . . 150
5.3 The origins of the acanthomorphs . . . 151
5.4 Acanthomorph macroevolution . . . 152
5.5 The importance of revisiting ‘old’ fossils . . . 153
5.6 Reconstructing relationships between living and fossil taxa . . . 155

5.7 Summary 156

References **157**

Appendices

A Scripts for phylogenetic analyses from Chapter 3 **181**
A.1 Parsimony analyses 181
A.2 Bayesian analyses 183
A.3 Hypothesis tests 184

B Supplementary tables for Chapter 4 **187**

C R scripts from Chapter 4 **195**
C.1 Supertree constraints and calibrations 195
C.2 Disparity between node estimates 198
C.3 `Evo.Rate.Time` 200

D The rise of jaw protrusion in spiny-rayed fishes closes the gap on elusive prey **205**

List of Figures

1.1 Acanthomorph diversity through geological time 13

2.1 †*Aipichthys pretiosus* NHMW 1857 XXXVIII 7: full specimen. . . . 29
2.2 †*Aipichthys pretiosus* NHMW 1857 XXXVIII 7: cranial and pectoral anatomy 31
2.3 †*Aipichthys pretiosus* NHMW 1857 XXXVIII 7: caudal anatomy . . 37
2.4 †'*Aipichthys*' *nuchalis* NHMUK PV OR 25770: full specimen 40
2.5 †'*Aipichthys*' *nuchalis* NHMUK PV OR 25770: full specimen (CT scan) 42
2.6 †'*Aipichthys*' *nuchalis* NHMUK PV OR 25770: cranial anatomy (CT scan) 44
2.7 †'*Aipichthys*' *nuchalis* NHMUK PV OR 25770: pelvic bones (CT scan) 50
2.8 Strict consensus tree of 29 parsimonious trees. 51
2.9 †*Paraipichthys lusitanicus* IST 561 and IST 560 61
2.10 †*Gigapteryx tethyestris* NHMUK P. 62521 63
2.11 †*Nardovelifer altipinnis* MSNV Na 519 64
2.12 Cretaceous lampridomorphs 67

3.1 †*Aulolepis typus* SMESC B. 9092: full specimen (CT scan) 86
3.2 †*Aulolepis typus* SMESC B. 9092: hyoid arch (CT scan) 88
3.3 †*Aulolepis typus* SMESC B. 9092: ventral branchial skeleton (CT scan) 89
3.4 †*Aulolepis typus* SMESC B. 9092: gill rakers (CT scan) 90
3.5 †*Aulolepis typus* SMESC B. 9092: dorsal branchial skeleton (CT scan) 91
3.6 †*Aulolepis typus* SMESC B. 9092: anterior vertebrae (CT scan) . . 92
3.7 †*Aulolepis typus* SMESC B. 9092: pelvic girdle (CT scan) 93
3.8 Strict consensus tree of four parsimonious trees (morphology only dataset) 95
3.9 Bayesian majority rule consensus tree (morphology only dataset) . . 96
3.10 Strict consensus tree of five parsimonious trees (combined dataset) . 97
3.11 Bayesian majority rule consensus tree (combined dataset) 99

3.12 Phylogenetic hypothesis tests (morphology only dataset) 101
3.13 Phylogenetic hypothesis tests (combined dataset) 103

4.1 Premaxilla measurements used to calculate the jaw protrusion index 117
4.2 The jaw protrusion index and premaxillary morphology 119
4.3 Correlation between the jaw protrusion index and data from Bellwood et al. (2015) 121
4.4 Histogram of the jaw protrusion indexes 128
4.5 The phylogenetic distribution of jaw protrusion 129
4.6 Regression of node ages and disparity between node estimates of the jaw protrusion index 131
4.7 Rate of evolution of the jaw protrusion index using the supertree containing living and fossil taxa 133
4.8 Rate of evolution of the jaw protrusion index using the supertree only containing living taxa 136
4.9 Relationship between the jaw protrusion index and age of the tips . 138

List of Tables

2.1 List of morphological characters: new characters (Lampridomorph analysis) . . . 27
2.2 Standard length and body depth of †'*Aipichthys*' and †*Freigichthys* 43
2.3 Character matrix (lampridomorph analysis) . . . 52

3.1 Sources of morphological data (†Ctenothrissiformes and †Pattersonichthyiformes analyses) . . . 75
3.2 List of morphological characters (†Ctenothrissiformes and †Pattersonichthyiformes analyses) . . . 78
3.3 GenBank accession numbers (†Ctenothrissiformes and †Pattersonichthyiformes analyses) . . . 81
3.4 Bayes factor interpretation . . . 83
3.5 Character matrix (†Ctenothrissiformes and †Pattersonichthyiformes analyses) . . . 94

4.1 Origins of high protrusion . . . 132
4.2 Posterior probabilities of shifts in evolutionary rate . . . 134

B.1 Taxa included in the jaw protrusion analyses . . . 188
B.2 Stratigraphic ages of extinct taxa . . . 192

Institutional Abbreviations

EY . . . . . The Hebrew University of Jerusalem, Jerusalem, Israel.

FSL . . . . . Faculté des Sciences de Lyon, Lyon, France.

IHNFG . . . . Instituto de Historia Natural y Ecología, Tuxtla Gutiérrez, Chiapas, Mexico.

IST . . . . . Instituto Superior Técnico, Lisbon, Portugal.

MNHN . . . . Muséum national d'Histoire naturelle, Paris, France.

MSNV . . . . Museo Civico di Storia Naturale di Verona, Verona, Italy.

NHMW . . . . Naturhistorisches Museum, Vienna, Austria

NHMUK . . . Natural History Museum, London, UK.

SMESC . . . . Sedgwick Museum of Earth Sciences, Cambridge, UK.

Anatomical Abbreviations

AfPt . . Anal-fin pterygiophore.

AfR . . . Anal-fin ray.

AfSp . . Anal-fin spine.

Ang . . . Anguloarticular.

Bas . . . Basisphenoid.

Bb . . . Basibranchial.

Bra . . . Branchial arch.

Brs . . . Branchiostegals.

Cb . . . Ceratobranchial.

Cer . . . Ceratohyal.

CerA . . Anterior ceratohyal.

CerP . . Posterior ceratohyal.

Cle . . . Cleithrum.

Cor . . . Coracoid.

Den . . . Dentary.

DfPt . . Dorsal-fin pterygiophore.

DfR . . . Dorsal-fin ray.

DfSp . . Dorsal-fin spine.

Eb . . . Epibranchial.

Ect . . . Ectopterygoid.

End . . . Endopterygoid.

Epi . . . Epiotic.

Epn . . . Epineural.

Epp . . . Epipleural.

Epu . . . Epural.

Fr . . . . Frontal.

Hb . . . Hypobranchial.

HHD . . Dorsal hypohyal.

HHV . . Ventral hypohyal.

Hmax . Hemaxanal complex.

Hs . . . . Haemal spine.

HsPu . . Haemal spine of preural centrum.

Hym . . Hyomandibula.

Hyp . . . Hypural.

Inf . . . Infraorbital.

Int . . . Interhyal.

Iop . . . Interopercle.

IW . . . Internal wings of pelvic bones.

Lac . . . Lacrimal.

LEth . . Lateral ethmoid.

Max . . Maxilla.

Mes . . . Mesethmoid.

Met . . . Metapterygoid.

MP . . . Median process of pelvic bones.

Nas . . . Nasal.

Nc . . . Neurocranium.

Ns . . . . Neural spine.

NsPu . . Neural spine of preural centrum.

Obs . . . Orbitosphenoid.

Op . . . Opercle.

Pal . . . Palatine.

Par . . . Parietal.

Pb . . . Pharyngobranchial.

PclD . . Dorsal postcleithrum.

PclV . . Ventral postcleithrum.

Pel . . . Pelvic bone.

PfR . . . Pectoral-fin ray.

PfRd . . Pectoral-fin radials.

Phy . . . Parhypural.

Pmx . . Premaxilla.

Pop . . . Preopercle.

PP . . . Posterior process of pelvic bones.

PRy . . Pelvic ray.

Psp . . . Parasphenoid.

PsUr . . Pseudourostylar complex.

Pt . . . . Posttemporal.

Pto . . . Pterotic.

Qu . . . Quadrate.

Ret . . . Retroarticular.

Sca . . . Scapula.

Scl . . . Supracleithrum.

Smx . . Supramaxilla.

Soc . . . Supraoccipital.

Sop . . . Subopercle.

Spn . . . Supraneural.

UP . . . Upper pharyngeal toothplate.

Uro . . . Uroneural.

V . . . . Vertebral centrum.

VRS . . Ventral ridge scale.

Numbers may follow some abbreviations when there is more than one structure (e.g. Hyp1 and Hyp2 to represent hypurals one and two respectively). Structures from the left and right sides are identified with (l) and (r), respectively.

Other Abbreviations

† . . . . . Used to identify extinct taxa (cf. Patterson and Rosen, 1977).

I believe that paleontologists and their fossil record do not have much of a reputation among ichthyologists who specialise on percomorphs.
Two reasons for this lack of regard are first, that paleontologists and their fossils have so far done virtually nothing to solve problems in percomorph phylogeny, and second, that the majority of fossil percomorphs seem to be too poorly preserved or too poorly described for it to be likely that they will ever contribute anything substantial to percomorph systematics.
But as a paleontologist, I could turn the charge around by asserting that ichthyologists working on percomorphs have done little to help paleontologists, and that this is the main reason why the percomorph fossil record seems unproductive and why many of the fossils are poorly described.

— C. Patterson (1993)

1 Introduction

Contents

1.1 Interpreting and understanding evolution 1
1.2 Acanthomorpha and the "Second Age of Fishes" . . . 7
1.3 Thesis aims and outline 20

1.1 Interpreting and understanding evolution

The Earth is home to numerous species of animals, plants, fungi, bacteria and other living organisms. It is estimated that there are between three and 100 million living species on Earth, although more conservative estimates predict five to ten million species (May, 2010; Mora et al., 2011). Of all the species that have lived since the planet's inception, 99.9% are extinct (Raup, 1991), which means that between five to ten billion species have existed on the planet over its history. As a consequence of this, Recent biodiversity presents only a snapshot into the evolutionary history of life. Although Recent biodiversity is highly diverse, there are some taxonomic groups, such as ginkgos (Plantae: Ginkgoospida), nautiluses (Animalia: Cephalopoda) and coelacanths (Animalia: Coelacanthi), which were once abundant, but are only represented by one or few species ('living fossils'), while other groups, like eurypterids (Animalia: †Merostomata), placoderms (Animalia:

†Placodermi) and pterosaurs (Animalia: †Pterosauromorpha), that are completely extinct and are not represented in modern biodiversity. One of the main goals of evolutionary biology specifically, and biology generally, is to reconstruct a 'tree of life' that shows how all organisms are related (Cracraft, 2002; Benton and Ayala, 2003; Cracraft and Donoghue, 2004; Pyron, 2011). By exclusively studying modern biodiversity, we would only be able to reconstruct a small portion of the tree of life, as many branches would be missing. The only way to fill in the gaps in the tree of life is to study the fossil record. The fossil record documents some of the earliest organisms to inhabit the planet over 3.8 Billion years ago (Dodd et al., 2017), major radiations of organisms (e.g. dinosaurs: Sereno, 1999; Fastovsky and Weishampel, 2016), and the origins of modern biodiversity. However, the fossil record can only tell us so much: soft tissues that degrade quickly are rarely preserved, we cannot directly observe how extinct organisms would have interacted and behaved, and the genetic basis for the morphology of extinct organisms is not retained in their fossils. Conversely, these are questions that can be answered for living species. Unique data can be collected from living and fossil species, that when combined can help to understand and interpret the evolution of life. In this section, I will summarise the ways in which palaeontological and neontological data can enable us to reconstruct evolutionary relationships and macroevolutionary patterns.

1.1.1 Phylogenetic relationships

If a group of organisms are viewed without a phylogenetic framework, or even a more primitive classification system, then they are simply an unordered assemblage that tells us little about the way in which they evolved. If we want to make sense of the bacteria, insects, fishes and mammals we see today, and their fossil ancestors, then these organisms must be placed in a system that allows us to understand how they are related to one another. Prior to the publication of *On The Origin of Species* (Darwin, 1859), organisms were classified without an evolutionary framework. Early philosophers like Aristotle started classifying organisms, but it was not until the work of Linnaeus (1735), the father of taxonomy, that a standardised

system was implemented. Following the acceptance of Darwin's evolutionary theory, most scientists tried to classify organisms in terms of ancestor-descendant relationships. But it was not until the 1960s – over 100 years after the publication of Darwin's work – that a more formal system was introduced. Hennig (1950) introduced the revolutionary concept of cladistics, where phylogenetic relationships are reconstructed based on shared characters, rather than ancestor-descendant relationships. Modern phylogenetic methods still rely on the principles set out by Hennig, but the availability of computational methods and the now commonplace use of molecular data, have revolutionised the art of reconstructing phylogenetic relationships. In this section, I briefly review the way in which phylogenetic relationships can be reconstructed, and the different types of data that can be used for phylogenetic inference and their applicability to extant and extinct taxa.

Phylogenetic relationships can be reconstructed using morphological and/or molecular data. Morphological data is collected from detailed anatomical study of the taxa of interest, of which, for phylogenetic purposes, observations are usually recorded in the form of characters with discrete states. Shared derived character states unite subsets of taxa in the taxon sample, which allows the relationships between them to be reconstructed. Morphological data is commonly analysed using parsimony, where the fewest character state changes, and consequently the shortest tree is preferred. However, model-based Bayesian methodologies are now also commonly used to analyse morphological data. When using molecular data, molecular sequences need to be carefully selected to ensure that they are phylogenetically informative: the rate of evolution has to be appropriate for the taxon sample. For example, an analysis containing species from the same genus would require different genes to an analysis containing completely different taxa (e.g. echinoderms and birds). Once molecular samples have been obtained, they need to be aligned to account for differences in sequence lengths because of insertions and deletions. Molecular data is analysed using model-based methods, such as Bayesian inference and maximum likelihood.

One of the major advantages of using morphological data for phylogenetic inference is that it can be collected from both living and fossil taxa. The impact of this is that all organisms, whether living or extinct, can be compared using the same metric, and the relationships between them can be deciphered. In most fossils, only the hard, mineralised structures are preserved, although in fossils from some Lagerstätten (e.g. the Jurassic Solnholfen Limestone) soft-tissue characters are preserved. Many fossils are incompletely preserved, disarticulated, or damaged during extraction and preparation. This can lead to many characters being coded as missing for fossil taxa, which reduces the power of phylogenetic methods to reconstruct relationships (Donoghue et al., 1989; Huelsenbeck, 1991; Smith, 1998; Anderson, 2001).

Even though it is not possible to extract molecular material from fossils, using a total-evidence approach, extinct taxa can be included in analyses in which molecular data is used. Datasets containing morphological and molecular data can be partitioned so that different evolutionary models can be applied to the different data types. Furthermore, the genes and codon positions of molecular data can be set as separate partitions as they may evolve at different rates. When using these methods the molecular data of fossil taxa is coded as 'missing', while the morphological data that is present in fossil taxa will still be used to place them among taxa for which genetic (and morphological) data has been obtained.

An additional approach, in which living and fossil taxa can be placed in the same phylogeny is through the construction of supertrees (Sanderson et al., 1998; Bininda-Emonds et al., 2002; Bininda-Emonds, 2004). A supertree is constructed from a set of independently-derived phylogenetic trees which are merged together. The set of trees can be stitched together informally, or formally, using a computational method (matrix representation with parsimony; Baum, 1992; Ragan, 1992; Bininda-Emonds and Sanderson, 2001). The input trees can contain different sets of taxa, which means that both molecular and morphological trees can be combined together. However, at least some of the taxa need to be found in multiple trees to ensure that they can be merged together; sometimes, a basic

phylogenetic tree that defines major taxonomic groups, is used as a source tree (e.g. Jetz et al., 2012; Clarke et al., 2016).

As well as being used to illustrate the relationships between a set of taxa, a phylogenetic tree can be also be used to display the temporal nature of evolution – the timing of diversification events. A phylogenetic tree can be timescaled using a variety of methods; selection depends on the source of the tree and the taxa included within it. With node-dating, the minimum and/or maximum ages of a sample of nodes in a phylogeny are calibrated using the stratigraphic ages of fossil taxa that can be assigned to each of the sampled nodes (Zuckerkandl and Pauling, 1962; Smith and Peterson, 2002; Near and Sanderson, 2004; Donoghue and Benton, 2007). The phylogenetic relationships need to be known *a priori*, so the dating analysis is usually undertaken after the phylogenetic tree has been constructed. Although fossil data is used for calibrating node-dating analyses, the phylogenetic trees are derived from molecular data, and consequently, they do not contain fossil taxa. Node-dating analyses use the node calibrations to calculate the rate of change in the molecular sequence data, and extrapolate this across the phylogeny. Tip-dating, or total evidence dating as it also known, uses the stratigraphic range of fossil taxa that are included in the phylogenetic analysis as calibrations to estimate the rate of evolution across the tree (Pyron, 2011; Ronquist et al., 2012; O'Reilly et al., 2015). As fossil and extant taxa are included in tip-dating analyses, both morphological and molecular data is included in datasets that are used for tip-dating purposes. Phylogenetic trees that are derived from morphological data and contain fossil taxa can be timescaled using methods where character data is not required and divergence times based on the age of fossil taxa (e.g. Ruta et al., 2006; Hedman, 2010; Lloyd et al., 2012; Bapst, 2013). Care is needed when selecting these methods as the results of some of these analyses can be unreliable (e.g. Bapst, 2014) and some methods can produce zero-length branches, which cannot be used with some downstream macroevolutionary analyses.

1.1.2 Macroevolutionary trends

As well as understanding the relationships between taxa, evolutionary biologists are also interested in understanding large-scale evolutionary patterns. By studying macroevolution, researchers can ask a variety of questions: why some lineages are extremely diverse while others are only represented by a few species, why some lineages go extinct yet others persist, how the evolution of traits and diversification patterns are linked, and the role that external factors, like changes in climate and the presence of other species, have on the evolution of a species or lineage.

The toolbox of an evolutionary biologist contains a variety of tools for studying macroevolutionary processes. Some of the most commonly used tools are phylogenetic comparative methods (PCMs), which usually require an underlying time-scaled phylogenetic tree; some PCMs can be used with a phylogeny that is not time-scaled (e.g. Friedman, 2009; Smith, 2012). Other macroevolutionary methods can be used without a phylogenetic framework; these include palaeobiological analyses where the taxa of interest are studied using time bins (e.g. Friedman, 2010). PCMs can be used to investigate trait evolution and diversification patterns. Trait evolution is studied using PCMs that reconstruct the evolution of a trait over a phylogeny and through evolutionary time. Traits can be discrete (e.g. presence of an anatomical structure) or continuous (e.g. body weight). In trait evolution analyses, both fossil and extant taxa can be included in the same dataset (Hunt and Slater, 2016). A common way of studying trait evolution is through the reconstruction of ancestral states, using the trait values of tips, and in some cases, calibrations from fossil data (Slater et al., 2012). Ancestral states are then estimated using a random walk model (e.g. Brownian motion, Ornstein-Uhlenbeck process) that estimates node values by interpolating between the values of the tips. Using random-walk processes, it is also possible to explore how the rate of evolution of a trait varies across a phylogeny (Collar et al., 2009; Eastman et al., 2011; Revell, 2012; Rabosky et al., 2014). Heterogeneity in evolutionary rate, which manifests itself as clade-specific rate shifts can be estimated using these models. It is also

possible to identify the direction and magnitude of rate shifts, allowing for in-depth study of traits across a phylogenetic tree.

Diversification patterns can be visualised as the accumulation or loss of lineages as a result of the net difference between origination and extinction rates. If rates of diversification are even across a phylogeny then the number of tips will be evenly distributed, but when clades contain varying numbers of tips then there may be heterogeneity in diversification rate (Cornwell and Nakagawa, 2017). Rates of speciation and extinction can both be estimated using PCMs. Many of these methods have been developed for use with molecular phylogenies. Including palaeontological data can be problematic, with discrepancies between estimates derived from palaeontological and neontological data – and difficulties integrating the two data types (Slater and Harmon, 2013; Hunt and Slater, 2016). However, recent methodological advances have shown some promise in allowing for the integration of extinct and extant taxa in diversification analyses (e.g. Pyron, 2011; Pyron and Burbrink, 2012; Ezard et al., 2013).

1.2 Acanthomorpha and the "Second Age of Fishes"

1.2.1 Modern diversity and morphological innovation

Despite the Cenozoic being traditionally known as the 'Age of Mammals', recent research has suggested that the "Second Age of Fishes" (Near et al., 2012) may be a more fitting name for this geological period (Friedman and Sallan, 2012; Near et al., 2012; Sibert and Norris, 2015). Following the end-Cretaceous extinction event, one lineage of actinopterygians, the acanthomorphs (Acanthomorpha) underwent a large radiation to become the dominant group of aquatic vertebrates. Numbering over 18,500 living species, the acanthomorphs represent a third of living vertebrate species (Stiassny et al., 2004), half of all living fish species, and there are over three times as many extant acanthomorph species as there are mammals. While the term 'acanthomorph' may not be as commonly known as 'mammal' or 'dinosaur', most people would undoubtedly recognise many of the hyper-diverse acanthomorphs.

Acanthomorphs have radiated to occupy countless ecological niches: from coral reefs to the deep abyss, freshwater caves to the open ocean. Although acanthomorphs inhabit both marine and freshwater environments, they are most diverse in marine habitats, especially coral reefs where approximately 25% of extant acanthomorph species are found (Price et al., 2014). Freshwater environments are dominated by another group of actinopterygians, the otophysans (Otophysi). However, acanthomorphs are still well-established in freshwater habitats, the most notable of which are the extremely diverse cichlids (Cichlidae) that inhabit the African Rift Valley Lakes. Moreover, acanthomorphs are ecologically important, fulfilling roles at a number of trophic levels. Many commercially important fish groups are acanthomorphs. These include gadiforms (cod, haddock and pollock), scombrids (tuna and mackerel) and pleuronectiforms (halibut, sole and plaice). Acanthomorphs exhibit incredible morphological diversity and they are characterised by a number of innovations that have enabled them to become one of the dominant groups of modern vertebrates. In the next few paragraphs, I briefly explore acanthomorph morphological diversity and discuss some of the key acanthomorph morphological innovations that have allowed them to dominate Recent aquatic environments.

1.2.1.1 General morphology

While most acanthomorphs are short and deep-bodied (Alexander, 1967a), their body shape can vary enormously. Some acanthomorphs are elongated and snake-like in appearance. This includes taxa like the flutemouths (Fistularidae) and the longest bony fish, the oarfish (*Regalecus glesne*), which can reach 11 m in length. At the other end of the scale, acanthomorphs like moonfish (Menidae), opah (Lampridae) and the ocean sunfish (*Mola mola*) are incredibly deeply bodied and short. The ocean sunfish also happens to be the largest bony fish, and can weigh up to 1000 kg. Other acanthomorphs have highly specialised morphologies, including extensive cranial asymmetry (Pleuronectiformes: flatfish), the ability to inflate like a balloon (Tetraodontidae: pufferfish), extreme sexual size dimorphism

(Lophiiformes: anglerfish) and a highly contorted appearance (e.g. *Hippocampus*: seahorses), to name a few examples.

1.2.1.2 Feeding

There are a number of adaptations that have enhanced the abilities of acanthomorphs to catch and process food. Acanthomorphs are one of five groups of actinopterygians that have evolved the ability to use jaw protrusion to feed (Westneat, 2004; Wainwright et al., 2015). Upper jaw protrusion, where a modified premaxilla is protruded anteriorly, has been described as a major vertebrate innovation (Schaeffer and Rosen, 1961; Gosline, 1980; Holzman et al., 2008; Bellwood et al., 2015; Wainwright and Longo, 2017) and could have been, at least partly, responsible for the success of the acanthomorphs (Schaeffer and Rosen, 1961; Bellwood et al., 2015). When an acanthomorph protrudes its jaw, not only is its jaw brought closer to its prey, but the rapid protrusion of the jaw also creates a pressure differential, which enables the fish to feed using suction feeding (Alexander, 1967b; Motta, 1984). Not all acanthomorphs use suction feeding, but protrusion is widespread across Acanthomorpha. Those acanthomorphs that do use upper jaw protrusion utilise it to different extents, with some taxa possessing highly modified premaxillae that are extremely protrusile: the slingjaw wrasse (*Epibulus insidiator*), for example, can protrude its premaxillae 65% of the length of its head (Westneat and Wainwright, 1989).

Another key acanthomorph feeding innovation is the evolution of pharyngognathy. Many actinopterygian lineages possess a second set of jaws, known as the pharyngeal jaws, which consist of posterior elements of the gill skeleton (Wainwright, 2005). Pharyngognathy, a condition that has evolved at least six times in the acanthomorphs (Wainwright et al., 2012), is where the ancestral pharyngeal jaw mechanism has been modified in such a way that it is more robust and able to process much tougher prey (Wainwright et al., 2012; Wainwright and Longo, 2017). Pharyngognathy enables acanthomorphs with this derived condition to eat a wider range of prey by allowing for the consumption and processing of hard shelly prey,

such as molluscs and crustaceans (Wainwright, 1988; Hulsey, 2006). Furthermore, the evolution of pharyngognathy may have allowed for the primary and pharyngeal jaws to evolve independently (Liem, 1973; Hulsey et al., 2006).

Jaw protrusion and pharyngognathy may be two of the most well-known acanthomorph feeding innovations, but there are numerous other ways in which acanthomorphs are adapted to feed. Some acanthomorph lineages do not rely on protrusion and have modified their primary jaws to fulfil other functions. Two of the most notable are swords and beaks. Some acanthomorphs have modified their jaw bones to form a sword-like weapon. In swordfish (Xiphiidae) and marlins (Istiophoridae), their elongated premaxillae are used for swiping and striking prey (Domenici et al., 2014; Habegger et al., 2015). Beaks have evolved independently in two lineages of acanthomorphs: parrotfish (Scaridae) and pufferfish (Tetraodontiformes). Their beaks, which are modified premaxillae and dentition, are used for consuming different diets: one scrapes algae from coral (parrotfish) while the other eats hard, shelly prey (pufferfish). Like the parrotfish and pufferfish, many acanthomorphs have modified dentition to allow them to catch and process food. Some taxa have completely lost their dentition, while others have developed long fangs (e.g. Anoplogastridae: fangtooths) or even teeth that superficially resemble mammalian dentition (e.g. the sheepshead, *Archosargus probatocephalus*).

Modifications to the jaws are not the only way in which acanthomorphs are adapted to feed. Some have feeding adaptations that allow them to consume large volumes of food. The black swallower fish (*Chiasmodon niger*) has an expandable stomach that allows it to consume large prey, typically other fish, whole. Other acanthomorphs have adaptations that can draw prey towards them. A notable example are females of deep-sea anglerfish (Lophiidae), which have a modified dorsal fin ray that acts as lure to attract prey.

1.2.1.3 Locomotion

Most acanthomorphs move in a way that is typical for teleosts. Propulsion is generated from undulations of the dorsal and caudal fins, and oscillation of the

pectoral fins, while paired appendages control depth and braking (Alexander, 1967a; Webb, 1984; Lauder and Drucker, 2004). Many acanthomorphs, particularly those that inhabit reef environments, are short and deeply-bodied, and highly manoeuvrable (Alexander, 1967a). Predatory acanthomorphs equipped with sword-like bills (Xiphiidae and Istiophoridae) are capable of swimming at high speeds ($\geq$ 100 km/h; Videler, 1993), although they more commonly swim at much slower speeds (Block et al., 1992). Other acanthomorphs (e.g. Scombridae: tunas) are powerful swimmers that are adapted to migrating large distances (Videler, 1993).

Despite acanthomorphs being fish, not all of their locomotory adaptations enhance their swimming abilities. Two groups of acanthomorphs, frogfish (Antenariidae) and mudskippers (Gobiidae), have modified paired appendages that resemble limbs. Frogfish can use their 'limbs' to slowly traverse the substrate (Pietsch and Grobecker, 1987), while mudskippers are amphibious and can use their 'limbs' to skip across terrestrial environments (Harris, 1960). Like the mudskipper, flying fish (Exocoetidae) are also adapted to moving while out of the water. They can use their large wing-like pectoral fins to glide up to 10 m above the surface of the water for distances reaching 400 m (Davenport, 1994).

1.2.1.4 Defence

The name acanthomorph, meaning spiny-form, is derived from one of their characteristic features, defensive fin spines (Johnson and Patterson, 1993; Patterson, 1993; Wainwright and Longo, 2017), which are used for deterring predators (Hoogland et al., 1956). The presence of fin spines in the dorsal and anal fins is an acanthomorph synapomorphy, although spines can also be found in the pelvic and pectoral fins. Fin spines are widespread in the acanthomorphs, although some groups, including primitive lineages such as Gadiformes and Lampridiformes, do not possess spines. Some acanthomorphs have additional armour to provide further protection against predation. For example, fishes of the family Triglidae have bony plates on their skulls, and sometimes their bodies too. Mechanical defence mechanisms are not the only way in which acanthomorphs can defend themselves. Flying fish (discussed

above) are able to evade predators by gliding above the surface of the water. Many acanthomorphs are able to use poison and venom to defend themselves. There are at least 11 independent origins of venom in the acanthomorphs (Smith and Wheeler, 2006), and the world's most venomous and poisonous fishes, the reef stonefish (*Synanceia verrucosa*) and pufferfish (*Takifugu*) respectively, are acanthomorphs.

1.2.2 The acanthomorph fossil record

The evolutionary history of the acanthomorphs is well documented by a rich fossil record (Fig. 1.1). The earliest known acanthomorph fossils are from the early Late Cretaceous (Cenomanian: 100.5 – 93.9 Ma), up until the Recent. Collectively, these deposits unveil the form of primitive acanthomorphs and their role in Mesozoic aquatic environments, record changes in acanthomorph diversity and abundance through time, and enable us to understand the origins of modern biodiversity. In this section, I will explore how the evolution of the acanthomorphs is documented in the fossil record. To do this, I concentrate on the period of time when the acanthomorphs underwent most of their evolution: the Cenomanian up until the Ypresian. By the Ypresian most modern lineages are represented in the fossil record (Greenwood et al., 1966; Patterson, 1993; Maisey, 1996), and beyond this period further acanthomorph evolution was "mere tinkering" (Patterson, 1993: p. 53).

Recent molecular estimates of the origin of crown group Acanthomorpha range between 162.5 – 127.0 Ma (Betancur-R et al., 2013; Near et al., 2013; Chen et al., 2014), which leaves a gap of at least 26.5 Ma between these estimates and the earliest known acanthomorph fossils. However, in the earliest deposits in which acanthomorphs are found, they are a relatively small part of the vertebrate assemblage (Patterson, 1993). The discord between molecular estimates for the origin of Acanthomorpha and the fossil record may be because early acanthomorphs were rare (Friedman, 2010). Therefore, the probability of finding fossils of the earliest acanthomorphs is low, and there may be a lag between the molecular estimates for the origin of the clade and the appearance of acanthomorphs in the fossil record.

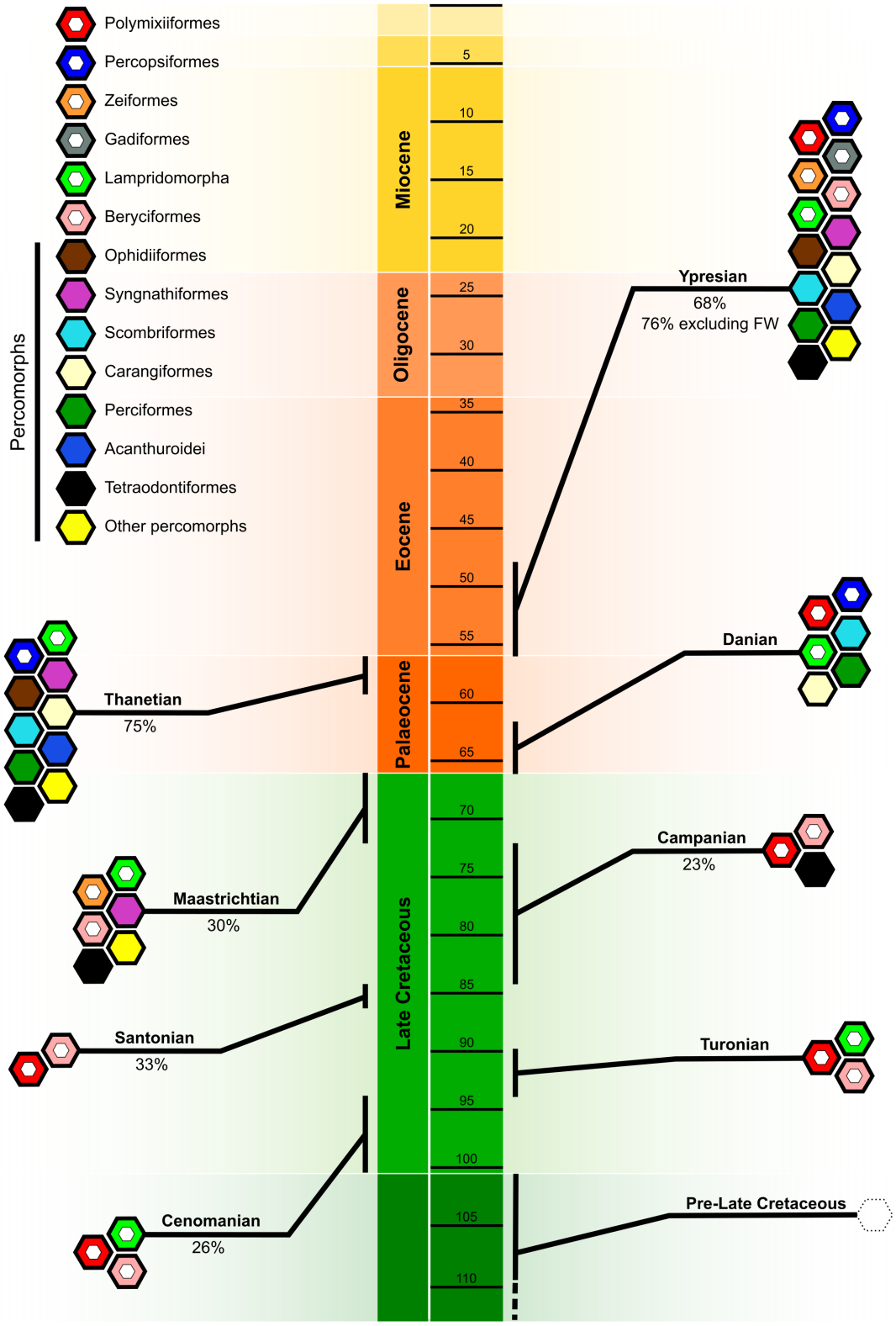

Figure 1.1: Acanthomorph diversity through geological time. Lineages of acanthomorphs that are found in geological periods from the early Late Cretaceous until the Ypresian. Hexagons show the lineages that are known from each period. Percentages under period names refer to the proportion of teleost genera that are acanthomorphs. The percentage data was obtained from Patterson (1993). FW = freshwater.

In Late Cretaceous deposits, acanthomorphs were a relatively small part of the vertebrate assemblage: up to 33% of all teleost genera were acanthomorphs (Patterson, 1993). Of all known acanthomorph fossils from the start of the Cenomanian (100.5 Ma) up until the end of the Campanian (72.1 Ma), the vast majority are primitive, deeply diverging (i.e. non-percomorph) taxa (Fig. 1.1). These are almost exclusively polymixiforms (e.g. †*Berycopsis*, †*Homonotichtys*), lampridomorphs (e.g. †'*Aipichthys*', †*Zoqueichthys*) and beryciforms (e.g. †*Hoplopteryx*, †*Plesioberyx*). There are possibly stem group tetraodontiforms, a derived percomorph lineage, present as far back as the Cenomanian (†*Plectocretacius*, †*Protriacanthus*). However, the attribution of these fossils remains controversial (see Arcila et al., 2015), with some doubting the tetraodontiform affinity of these taxa (e.g. Dornburg et al., 2014). While most Late Cretaceous acanthomorphs can be attributed to extant lineages, there are some that appear to represent extinct groups, such as the †sphenocephaliforms, †*Sphenocephalus* (Campanian) and †*Xenyllion* (Cenomanian). In Maastrichtian deposits, taxa from a greater number of extant clades are known – including a number of percomorph lineages. This includes zeiforms (e.g. †*Cretzeus*), lampridomorphs (e.g. †*Nardovelifer*), beryciforms (e.g. †*Lissoberyx nardoensis*), batrachoidiforms (e.g. †*Bacchiaichthys*), sygnathoids (e.g. †*Gasterorhamphosus zuppichinii*) and tetraodontiforms (e.g. †*Cretatriacanthus*). Of the six Late Cretaceous stages, acanthomorphs are known from more deposits in the Cenomanian than any of the other stages. These Cenomanian deposits include the English Chalk, United Kingdom, which yields exceptionally well-preserved, three-dimensional skulls (Woodward, 1902; Patterson, 1964), the Lebanese deposits of Hakel, Hadjoula and Namoura (Woodward, 1942; Gaudant, 1978c; Gayet, 1980a), of which the fossils of Hakel have been known since the time of the crusades, as well as Djebel Tselfat in Morocco, the Judean Hills in Palestine, and Komen in Slovenia. Other notable Late Cretaceous deposits include Sahel Alma in Lebanon (Santonian), Westphalia in Germany (Campanian), and Nardo in Italy (Maastrichtian).

Acanthomorphs are poorly represented in the first Palaeogene stage, the Danian (66.0 – 61.6 Ma), because of a lack of deposits representing environments

that would have been inhabited by acanthomorphs (Patterson, 1993). However, a small number of acanthomorph groups are represented (Fig. 1.1): polymixiiforms (†*Berycopsis lindstromi*), percopsiforms (e.g. †*McConichthys*), lampridomorphs (e.g. †*Bathysoma*), scombriforms (e.g. †*Landanichthys*), carangiforms (e.g. †*Prolates herbeti*) and perciforms (e.g. †*Proserranus lundensis*). Danian acanthomorphs are known from deposits in France (Mont Aimé), Sweden (Saltholm) and the United States of America (Tullock formation). In the more recent Thanetian (59.2 – 56.0 Ma) deposits, there are fossils representing a large number of acanthomorph lineages, with 75% of all known teleost genera from this period being acanthomorphs (Patterson, 1993). Furthermore, the majority of acanthomorphs are from percomorph lineages. Lineages not represented prior to the Thanetian include ophidiiforms (e.g. †*Eolamprogrammus*), acanthuroids (e.g. †*Avitoluvarus*), and ephippids (e.g. †*Exellia proxima*). Notable Thanetian acanthomorph deposits include the Stolleklint Clay of Denmark and the Danata formation of Turkmenistan.

The Ypresian (56.0 – 47.8 Ma), the first stage of the Eocene, is represented by a number of deposits containing acanthomorphs. Most notably, the numerous, exquisitely preserved acanthomorphs from the Monte Bolca locality of Italy (Blot, 1969) make it one of the most important acanthomorph deposits; at least 190 species and 78 acanthomorph families are known from here (Bannikov, 2014b; Fig. 1.1). Two other important Ypresian acanthomorph deposits are the Mo Clay of Denmark (Bonde, 1987), which overlies the Paleocene Stolleklint, and the London Clay (United Kingdom), which is known for preserving three-dimensional skulls (Casier, 1966). Due to the sheer number of known acanthomorphs from this period, it would be impractical, and beyond the scope of this work, to discuss them all here. However, Bannikov (2014b) presents a good overview of the taxonomic diversity found during this period.

1.2.3 Systematics and evolutionary history

1.2.3.1 Classification and relationships

One of the earliest classifications of fish is that of the palaeontologist Agassiz (1844), who classified fish into four 'orders' based on scale morphology. Agassiz's classification was shortly superseded by that of Müller (1846), who introduced taxonomic groups, such as Teleostei and Holostei, which are still in use today. However, although all of the acanthomorphs were placed in Teleostei, they were split across five teleost orders: Acanthopteri, Anacanthini, Pharyngognathi, Plectognathi and Lophobranchii. Following the publication of *On the Origin of Species* (Darwin, 1859), attempts were made to explore the links between taxonomic groups, including teleost fish (e.g. Haeckel, 1866; Gill, 1872; Haeckel, 1889, 1895; Boulenger, 1904). Early to mid 20th Century work on teleost classification (e.g. Berg, 1940; Bertin and Arambourg, 1958) led to further refinements, although the classification systems in use during this time were essentially modified 19th Century systems (Greenwood et al., 1966; Patterson and Rosen, 1977).

The acanthomorphs were first united as a monophyletic group in the seminal paper of Rosen (1973) discussing the interrelationships of higher euteleostean fishes. Furthermore, Rosen presented hypotheses for how two other euteleostean groups are related to the acanthomorphs, with the lanternfishes (Myctophiformes) as the sister group to Acanthomorpha, collectively known as Ctenosquamata, and the lizardfishes (Aulopiformes) as sister group to Ctenosquamata, collectively known as Eurypterygii. Rosen's Acanthomorpha is highly supported by a number of studies. This includes morphological (Lauder and Liem, 1983; Stiassny, 1986; Johnson, 1992; Stiassny and Moore, 1992; Johnson and Patterson, 1993; Grande et al., 2013), molecular (Chen et al., 2003; Dettai and Lecointre, 2005; Broughton, 2010; Near et al., 2012; Betancur-R et al., 2013; Grande et al., 2013; Near et al., 2013; Chen et al., 2014), and combined morphology and molecular analyses (Davis, 2010; Davesne et al., 2016). However, while Acanthomorpha is almost unanimously supported, some analyses do not recover Eurypterygii and/or Ctenosquamata (e.g. Broughton, 2010; Chen et al., 2014).

While Acanthomorpha as a clade is widely supported by a number of studies, internal acanthomorph relationships are much less well-defined. Prior to the establishment of Acanthomorpha, Greenwood et al. (1966) split acanthomorphs into three groups: Paracanthopterygii, Acanthopterygii and Atherinomorpha. Rosen (1973) retained these groups, placing the paracanthopterygians as the most deeply diverging acanthomorphs, with the atherinomorphs and a new clade, Percomorpha, united as acanthopterygians. There have been numerous attempts to understand the relationships among paracanthopterygians specifically (Rosen and Patterson, 1969; Grande et al., 2013; Davesne et al., 2016) as well as various large-scale attempts looking at acanthomorph or teleost relationships generally. However, there is still little consensus on which lineages should be placed within Paracanthopterygii, the relationships between those lineages, and whether the paracanthopteyrgians are even a monophyletic group (see Grande et al., 2013 for a brief review). Furthermore, the placement of another clade of primitive acanthomorphs, Lampridiformes, is also not secure, with some analyses placing the lampridiforms as the most deeply diverging acanthomorph clade (Johnson and Patterson, 1993; Broughton, 2010; Davesne et al., 2016), as sister group to the paracanthopterygians (Betancur-R et al., 2013) and as sister group to the acanthopterygians (Near et al., 2012; Grande et al., 2013; Near et al., 2013).

The vast majority of acanthomorphs are acanthopterygians – less than 4% of acanthomorphs branch from outside Acanthopterygii (Near et al., 2013). Excluding the beryciforms, all other acanthopterygians are percomorphs. The original Percomorpha of Rosen (1973) included the percomorphs of modern usage alongside Beryciformes, Lampridiformes and Zeiformes – all three lineages were subsequently removed, while the atherinomorphs were added to Percomorpha (Johnson and Patterson, 1993). The sheer number of percomorphs – 17,500 extant species split into approximately 250 families – has made the "percomorph problem" (Johnson and Patterson, 1993: p. 555), reconstructing percomorph interrelationships, difficult to resolve. While synapomorphies are known for most percomorph lineages (e.g. Wiley and Johnson, 2010), broad relationships across Percomorpha are poorly

defined by morphological characters; there are no large-scale morphological analyses of percomorphs. Despite the apparent lack of progress in resolving percomorph relationships using morphology, there has been substantial progress using molecular methods. The results of recent large-scale, molecular analyses are broadly congruent across Percomorpha, and Acanthomorpha, as a whole. All four of the recent large-scale molecular analyses including acanthomorphs (Near et al., 2012; Betancur-R et al., 2013; Near et al., 2013; Chen et al., 2014) recover Beryciformes as sister group to Percomorpha, Ophidiiformes and Batrachoidiformes as the most primitive percomorph lineages, and a monophyletic Tetraodontiformes + Lophiiformes + Caproidae, to name a few, of many examples.

1.2.3.2 Placement of fossil taxa

In early classifications (i.e. pre-1900), the inclusion of fossil taxa was not consistent between researchers. The early classification system of Agassiz (1844) was derived from his observations of the fossil record, although many subsequent efforts (e.g. Müller, 1846; Cope, 1871; Gill, 1872) were derived primarily from studying extant taxa. During the early 1900s, Woodward (1901) finished publishing his four-part *Catalogue of Fossil Fishes*, which was hugely influential and led to the inclusion of fossil taxa in all major attempts to classify teleosts over the next five decades (Patterson, 1977). However, the focus on fossil taxa may have actually hindered progress due to the lack of an understanding of the relationships between extant lineages; Patterson (1977: p. 362) eloquently summarises the situation: "the fossil record is dumb until it is interpreted by concepts derived from living organisms". The onset of cladistics (Hennig, 1950; Hennig, 1965) allowed researchers to place fossil taxa amongst extinct taxa based on the characters they share, rather than having to assign ancestor-descendant relationships between them. Furthermore, phylogenetic frameworks allowed for the placement of fossils among living taxa. In this section, I will explore the various attempts at placing acanthomorph fossils in phylogenetic analyses.

Our knowledge of the relationships between fossil taxa from primitive (i.e. non-percomorph) acanthomorph lineages is extremely variable. Some lineages have received little, or no, attention, while others have been extensively studied. Here I will briefly discuss the placement of fossils from all major non-percomorph clades. The relationships between fossil and living beardfishes (Polymixiformes) are completely unknown; a relatively recent acanthomorph macroevolutionary analysis (Friedman, 2009) placed the polymixiforms in a polytomy. The phylogenetic position of fossil percopsiforms (trout perches and their allies) was considered by Rosen and Patterson (1969) and formally studied by Murray and Wilson (1999). The fossil gadiforms have received some attention (e.g. Fedotov and Bannikov, 1989; Endo, 2002), although they have never been formally placed in a phylogeny. Fossil zeiforms are one of the most-studied acanthomorph groups. They have been included in three phylogenetic analyses: Tyler and Santini (2005), Santini et al. (2006), and more recently, Davesne et al. (2017). The relationships between lampridiforms, which are now regarded as part of a larger assemblage, Lampridomorpha, have been widely studied. Deeply diverging fossil lampridomorphs – formerly known as aipichthyoids – have received much of this attention (Otero and Gayet, 1995, 1996; Otero, 1997; Alvarado-Ortega and Than-Marchese, 2012; Davesne et al., 2014; Murray and Wilson, 2014). Fossil beryciforms (squirrelfish) have been included in a number of phylogenetic analyses (Stewart, 1984; Moore, 1993; Otero et al., 1995). However, many beryciform fossil taxa, particularly holocentroids, can only be placed in polytomies as the relationships between them and living taxa are poorly known.

The majority of extinct percomorphs have been placed at the family level, as is customary when describing fossil taxa, but relatively few have been included in a phylogenetic analysis. As a consequence, we know approximately where most fossil percomorphs would be placed on a phylogeny, but we do not know their exact position. Fossil representatives from some lineages have received considerable attention from researchers. Fossil tetraodontiforms have been included in a number of analyses (Tyler and Sorbini, 1996; Santini and Tyler, 2003, 2004; Tyler and Santini, 2005; Arcila et al., 2015; Close et al., 2016), although, as mentioned

earlier in this chapter, there is still some controversy over the affinities of some fossil taxa that have been attributed to Tetraodontiformes. The relationships of fossil tetraodontiforms are perhaps the most well-studied of all fossil percomorphs. Some other percomorph lineages may not have received as much attention as the tetraodontiforms, but have been included one or a small number of analyses; this includes fossil representatives of Sygnathoidei (Orr, 1995), Scombroidei (Monsch, 2000; Fierstine and Monsch, 2002), Pleuronectiformes (Friedman, 2008), Xiphiodei (Fierstine et al., 2008), Acanthuroidei (Bannikov and Tyler, 1995) and Lophiiformes (Carnevale and Pietsch, 2010, 2012). However, if you consider the large number of percomorph fossils from sites like Bolca (see above; Bannikov, 2014b), then to date, only a small percentage of those taxa have been included in a phylogenetic analysis.

The evolution of the acanthomorphs can be understood not just by understanding the phylogenetic position of fossil acanthomorphs, but also the position of fossil taxa that branch outside of Acanthomorpha. In particular, those that branch from the stem of Acanthomorpha and other major extant groups (Aulopiformes, Ctenosquqmata, Myctophiformes) have the potential to provide a deep insight into the evolution of the acanthomorphs. †Ctenothrissiformes has been regarded as sister group to the acanthomorphs (Rosen, 1973), although other researchers support a myctophiform placement (Greenwood et al., 1966; Goody, 1969), while Zehren (1979) did not find enough support to place †Ctenothrissiformes, Myctophiformes or another fossil group, †Pattersonichthyiformes, as sister group to the acanthomorphs. Other fossil taxa with uncertain eurypterygian placements include †*Nematonotus* and †*Sardinoides*.

1.3 Thesis aims and outline

So far in this chapter, I have briefly discussed the ways in which we can understand evolution, and the applicability of palaeontological and neontological data. I then introduced the acanthomorphs, a major radiation of fishes that dominate Recent aquatic environments, and discussed the innovations behind their success, their fossil record, and our current understanding of acanthomorph interrelationships.

Molecular phylogenetics have helped to resolve and refine our understanding of the links between extant acanthomorph lineages. However, our understanding of how fossil taxa are related to living acanthomorphs is still severely limited, with relatively few phylogenetic hypotheses describing these relationships. In this thesis, by combining palaeontological and neontological data, and using a variety of phylogenetic and macroevolutionary methods, I aim to develop our understanding of the evolutionary history of the acanthomorphs. My research is split into three separate projects, which explore the relationships of primitive acanthomorphs, the origins of the acanthomorph and eurypterygian fishes, and the evolution of one of the major acanthomorph innovations, the protrusile upper jaw. In each project, I take a different approach and use different methods to illustrate the ways in which our understanding of acanthomorph evolution can be enriched by studying living and fossil taxa in tandem. The next three chapters will be devoted to the three projects, before I bring my findings together in a final concluding chapter. Below, I present a brief summary of the three project-based chapters.

Chapter 2: anatomy and relationships of Cretaceous lampridomorphs

In this chapter, I aim to improve our understanding of the relationships of a primitive, extant acanthomorph clade, the lampridomorphs. Detailed anatomical descriptions of two Cretaceous lampridomorphs (†*Aipichthys pretiosus* and †'*Aipichthys*' *nuchalis*) are presented. I then include these taxa in a morphological phylogenetic analysis containing 10 extant and 17 extinct taxa.

Chapter 3: relationships of †Ctenothrissiformes and †Pattersonichthyiformes

Here, I aim to understand the origins of acanthomorph diversity by studying two extinct groups that have been attributed to diverging from the acanthomorph stem: †Ctenothrissiformes and †Pattersonichthyiformes. I begin by describing the internal anatomy of the †ctenothrissiform †*Aulolepis typus*. I then place

†*Aulolepis*, †*Ctenothrissa* (†Ctenothrissiformes) and †*Pattersonichthys* (†Pattersonichthyiformes) amongst extant eurypterygian lineages in a phylogenetic analysis, using morphological and molecular data.

Chapter 4: evolution of jaw protrusion

In this project, I aim to investigate the evolution of a major feeding innovation, jaw protrusion, and understand the role that palaeontological and neontological data has in reconstructing macroevolutionary patterns. First, I build and timescale an informal supertree containing 233 extant and 52 extinct fishes. Then, using a novel metric, I evaluate the extent of protrusion in each taxon and map this data onto the supertree. Finally, I undertake two evolutionary rates analyses, one including and one excluding fossil data to understand how rates of evolutionary change vary across the phylogeny, and evaluate the role that fossil data plays in reconstructing these patterns.

2

Anatomy and relationships of †*Aipichthys pretiosus* and †'*Aipichthys*' *nuchalis* (Acanthomorpha: Lampridomorpha), with a review of Late Cretaceous relatives of oarfishes and their allies

Contents

2.1 Introduction 24
2.2 Materials and methods 26
2.3 Systematic palaeontology 28
2.4 Phylogenetic relationships 50
2.5 Discussion 60

This chapter has been published in the *Journal of Systematic Palaeontology* as a co-authored article with Donald Davesne and Matt Friedman (Delbarre et al., 2016), except for the final section (2.5.6), which is new. The majority of the work in this chapter is my own. I described both of the fossil taxa, built and rendered the computed tomography scan of †'*Aipichthys*' *nuchalis*, produced 11 of the 12 figures, added the additional taxa and characters to the morphological matrix (this was based on the existing character matrix of Davesne et al., 2014), interpreted

the results of the phylogenetic analysis (e.g clade synapomorphies and character optimisations) and wrote the manuscript. Donald Davesne suggested improvements to the phylogenetic analysis, ran the analysis and produced the corresponding figure. Matt Friedman conceived the initial idea for this chapter.

2.1 Introduction

†*Aipichthys* is one of the oldest-known members of Acanthomorpha (spiny-rayed fishes), a group that comprises one third of modern vertebrate species (Stiassny et al., 2004). †*Aipichthys* contains five Cenomanian species: the type species †*Aipichthys pretiosus* Steindachner, 1860, plus †*Aipichthys minor* (Pictet, 1850), †*Aipichthys velifer* Woodward 1901, †*Aipichthys nuchalis* (Dixon, 1850) and †*Aipichthys oblongus* Gayet, 1980a. Most species of †*Aipichthys* derive from the Lebanese Lagerstätten of Hakel and Hadjoula, and it is these examples that provide the most detailed picture of anatomy in the genus (e.g. Gayet, 1980a; Otero and Gayet, 1996). †*Aipichthys pretiosus* and †*A. nuchalis* are not known from Lebanese deposits, and are only found in Cenomanian deposits from Komen, Slovenia and the English Chalk of the United Kingdom, respectively.

The affinities of †*Aipichthys* to both fossil and extant acanthomorphs has undergone substantial revision since the genus was established. Early interpretations placed †*Aipichthys* in the percomorph families Ephippidae (spadefishes; Dixon, 1850), Carangidae (jacks; Woodward, 1887; Gregory, 1933) and Scorpidae (Kyphosidae of modern usage) (sea chubs; Boulenger, 1904). By contrast, more recent interpretations view †*Aipichthys* and remaining †'Aipichthyidae' (†*Paraipichthys lusitanicus* Gaudant, 1978a, and †*Freigichthys elleipsis* Otero, 1997) as related to deeply diverging branches of Acanthomorpha: Beryciformes (Regan, 1911a), Paracanthopterygii (Gayet, 1980a) and Lampridiformes (Patterson, 1964, 1968; Rosen and Patterson, 1969; Oelschläger, 1983; Patterson, 1993). The first phylogenetic analyses to include †'Aipichthyidae' united them with another fossil family, †'Aipichthyoididae', to form the superfamily †'Aipichthyoidea' (Otero and Gayet, 1995, 1996). This in turn was placed as the sister group of Euacanthomorpha, a result echoed by a further analysis

using the same dataset (Alvarado-Ortega and Than-Marchese, 2012). None of these studies included Lampridiformes (oarfish and allies), a major early-diverging lineage of acanthomorphs (Johnson and Patterson, 1993; Olney et al., 1993). Davesne et al. (2014) recently re-evaluated the affinities of †'aipichthyoids' using a wider sample of living lineages, and found that they represent a grade of stem lampridiforms.

Species of †*Aipichthys* are known in varying detail. †*A. velifer*, †*A. minor* and, to a lesser degree, †*A. oblongus*, have been well described (e.g. Patterson, 1964; Gayet, 1980a) and are represented in all phylogenetic analyses incorporating †'aipichthyoids'. However the two remaining species of †*Aipichthys*, †*A. pretiosus* and †*A. nuchalis*, have not been included in any of these studies. The principal goals of this paper are to review the anatomy of these species from Slovenia and England, and to determine their phylogenetic placement relative to other species of †*Aipichthys* and among †'aipichthyoids' more generally. Restudy of each of these poorly known examples of †*Aipichthys* has potential to provide additional insights. First, †*A. pretiosus* is the type species of †*Aipichthys*, and thus is important for assessing the attribution of other species to the genus. Second, †*A. nuchalis* is one of the few non-Tethyan †'aipichthyoids' known, and the only example preserved in three dimensions rather than as a compression fossil.

As a consequence of the meagre anatomical details available in published accounts (Woodward, 1887; Gorjanovic-Kramberger, 1895), †*A. pretiosus* and †*A. nuchalis* have been excluded from previous phylogenetic analyses. Consequently, their affinity to other nominal species of †*Aipichthys* is assumed but has not been formally tested. Based on our re-examination of †*A. pretiosus* (using conventional methods) and †*A. nuchalis* (using high-resolution micro computed tomography [µCT] scanning), we provide new descriptions of these enigmatic species, and investigate their relationships to one another, to other nominal species of †*Aipichthys*, and among Lampridomorpha (*sensu* Davesne et al., 2014) more generally.

2.2 Materials and methods

2.2.1 Computed tomography scanning

†*Aipichthys nuchalis* was scanned at the Natural History Museum, London, United Kingdom using a Metris X-Tek HMX ST 225 CT scanner. The CT scan was segmented using the commercial biomedical software Mimics (Materialise, 2015; version 15.01). Local thresholds of grey values were used to create masks that differentiate between the fossil and the surrounding matrix. Individual masks were then combined to produce a model of the whole specimen. For a more in-depth explanation of processing CT scans of fossil material, see Abel et al. (2012). Blender (Blender Foundation, 2013; version 2.69) was used to light the models and produce renderings for the figures.

2.2.2 Phylogenetic analysis

We analysed the phylogenetic placements of †*Aipichthys pretiosus* and †*A. nuchalis* by including these species in the character-by-taxon matrix of Davesne et al. (2014), which itself is largely based on matrices presented earlier by Otero and Gayet (1995, 1996) and Alvarado-Ortega and Than-Marchese (2012). We also included seven new characters (Table 2.1) and two other taxa: the earliest putative crown lampridiform †*Nardovelifer altipinnis* Sorbini and Sorbini, 1999, from the Late Cretaceous (Campanian–Maastrichtian) of Italy and †*Gigapteryx tethyestris* Forey et al., 2003, an *incertae sedis* acanthopterygian. Contrary to Davesne et al. (2014), we did not include †*Paraipichthys lusitanicus* in the analysis because of the dubious status of the paratype specimen (see Discussion). Character states were coded using Nexus Data Editor (Page, 2001; version 0.5) and then analysed using PAUP* (Swofford, 2003; version 4.0b10). The branch-and-bound algorithm was used to search for the most parsimonious trees, from which a strict consensus tree was derived. PAUP* was subsequently used to calculate the consistency index, homoplasy index, retention index and the rescaled consistency index. A bootstrap analysis was subsequently run with PAUP* with a heuristic search option and 1000 replicates to calculate

Table 2.1: New characters included in the lampridomorph phylogenetic analysis. Characters are in addition to those of Davesne et al. (2014)

Character number	Character	References
68	Dentition on oral surface of the premaxilla: **(0)** present; **(1)**, absent	Sorbini and Sorbini, 1999
69	Articular process of the premaxilla: **(0)**, absent; **(1)**, present	Rosen and Patterson, 1969; Stiassny, 1986
70	Dentition on the oral surface of the dentary: **(0)**, present; **(1)**, absent	Sorbini and Sorbini, 1999
71	Dentition on the endopterygoid: **(0)**, present; **(1)**, absent	Sorbini and Sorbini, 1999
72	Suborbital shelf: **(0)**, absent; **(1)**, present	Smith and Bailey, 1962; Rosen, 1973; Otero, 1997
73	Middle regions of three most anterior haemal spines closely attached: **(0)**, absent; **(1)**, present	Sorbini and Sorbini, 1999
74	Ventral ridge scales: **(0)**, absent; **(1)**, present	Patterson, 1964; Otero and Gayet, 1996

support values for each node. The Bremer indexes were estimated automatically using a PAUP* script generated by TreeRot (Sorenson, 1999; version 2).

2.2.3 Standard length estimation and body depth index

The type and only specimen of †*A. nuchalis* is incomplete posteriorly. We therefore derived an estimated standard length using the following procedure: We measured †*A. nuchalis* as well as †*Aipichthys minor* and †*Aipichthys velifer* from the most anterior point to the posterior end of the 11th caudal vertebrae (the most posterior part of †*A. nuchalis*) (measurement A). The standard length (measurement B) of †*A. minor* and †*A. velifer* was also recorded. For †*A. minor* and †*A. velifer*, measurement B was then divided by measurement A to produce a ratio. This was repeated on a number of specimens of †*A. minor* and †*A. velifer*. The smallest and largest ratios were then multiplied with measurement A of †*A. nuchalis* to give an estimated size range. †*A. minor* and †*A. velifer* were used in this calculation as they represent taxa with different numbers of vertebrae, and are both known from a number of specimens. †*Aipichthys oblongus* and †*Freigichthys* were not used as †*A. oblongus* is only known from one disarticulated specimen, and †*Freigichthys* is only known from one articulated specimen.

The body depth index was calculated by dividing the height of the hemax-anal complex by measurement A.

2.3 Systematic palaeontology

Infraclass **Teleostei** Müller, 1846

Subcohort **Neoteleostei** Nelson, 1969

Infracohort **Eurypterygii** Rosen, 1973

Section **Ctenosquamata** Rosen, 1973

Subsection **Acanthomorpha** Rosen, 1973

Superorder **Lampridomorpha** *sensu* Davesne et al., 2014

2.3.1 †*Aipichthys pretiosus*

Genus †***Aipichthys*** Steindachner, 1860

†***Aipichthys pretiosus*** Steindachner, 1860

(Figs. 2.1, 2.2, 2.3)

1860 †*Aipichtys pretiosus* Steindachner: 763, pl. 1, fig. 1.

1882 †*Aipichthys pretiosus* Steindachner; Bassani: 262.

1895 †*Aipichthys pretiosus* Steindachner; Gorjanovic-Kramberger: 46, pl. 2, fig. 3.

1901 †*Aipichthys pretiosus* Steindachner; Woodward: 427.

1946 †*Aipichthys pretiosus* Steindachner; d'Erasmo: 113, fig. 30.

1964 †*Aipichthys pretiosus* Steindachner; Patterson: 393.

Diagnosis. Lampridomorph similar only to †*Aspesaipichthys* Taverne, 2004 and †*Aipichthyoides* Gayet, 1980b with supraoccipital, frontal and mesethmoid contributing to a long sagittal crest. The anterior edge of the crest is not thickened, and unlike the condition seen in †'*Aipichthys*', †*Freigichthys* and †*Gigapteryx*. Differs from all Cretaceous lampridomorphs, except some specimens of †*Errachidia pentaspinosa* Murray and Wilson, 2014, in possessing 12 abdominal and 14 caudal vertebrae. The first three haemal spines are closely associated with each other. This condition is not seen in other Cretaceous lampridomorphs. Similar to †'Aipichthyoididae' and

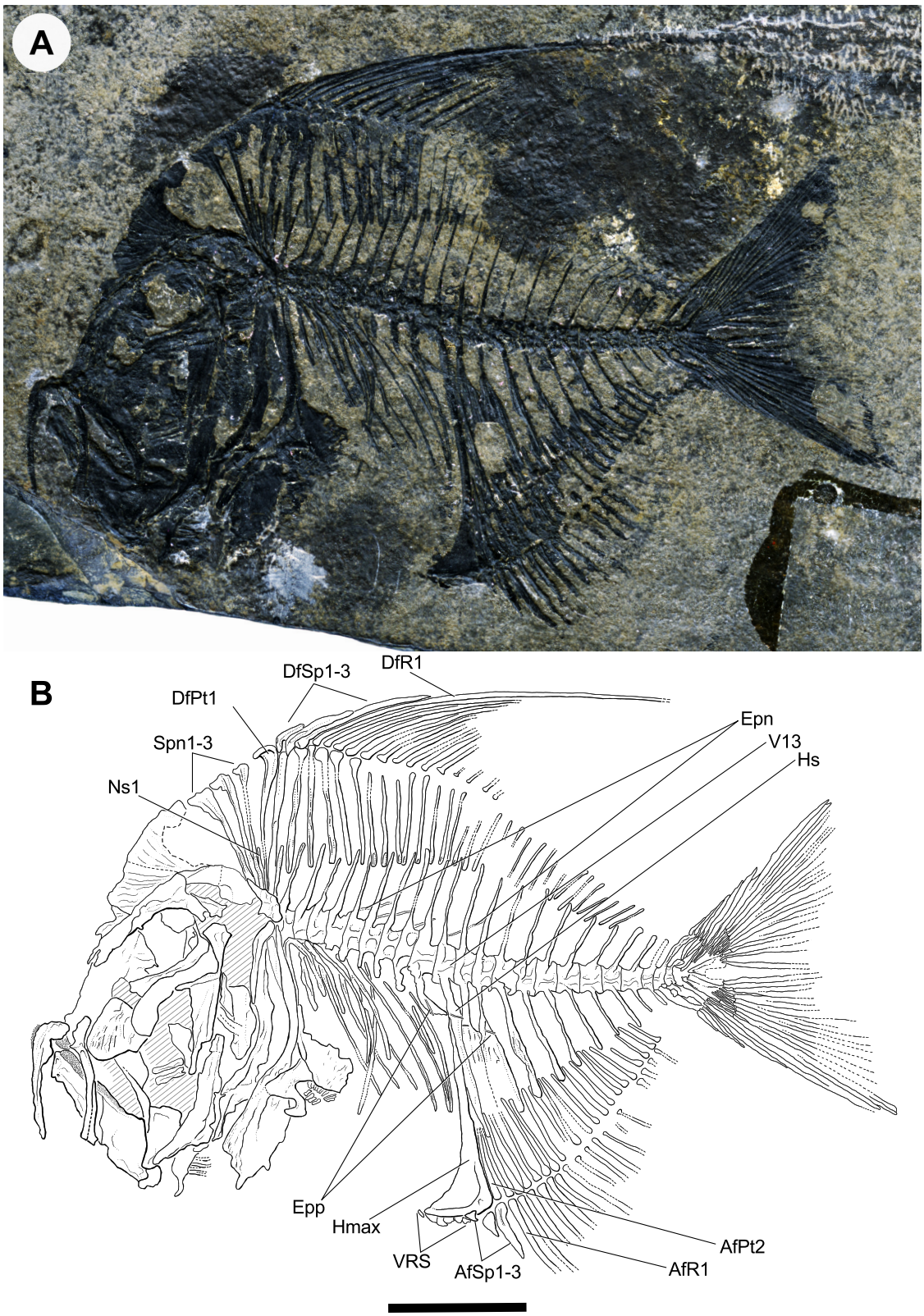

Figure 2.1: †*Aipichthys pretiosus*, holotype NHMW 1857 XXXVIII 7. **A,** specimen photograph (photograph by M. Friedman). **B,** interpretative drawing. Light grey diagonal hatching in B indicates damaged areas that could not be interpreted. Scale bar represents 10 mm.

Lampridiformes in having the lower hypurals fused together. Retains six hypurals, unlike †*Aspesaipichthys* and †*Aipichthyoides* where there has been a reduction to five.

Material. Holotype NHMW 1857. XXXVIII. 7., an articulated specimen preserved in left-lateral view. One other specimen from an unrecorded locality in Lesina has been reported (Gorjanovic-Kramberger, 1892, 1895). The location of this fossil has not been mentioned since 1895, and its present whereabouts are unknown.

Occurrence. Volčji Grad, Komen, Slovenia. Komen Limestone (Steindachner, 1860; Bassani, 1882; Cavin et al., 2000). This horizon is dated to the Cenomanian based on the presence of the mollusc †*Chondrodonta* spp. and the foraminiferan †*Broeckina* (*Pastrikella*) *balcanica* (Cavin et al., 2000).

Notes. The status of †*A. pretiosus* as the type species for †*Aipichthys* is unambiguous as Steindachner (1860) was the first to use the generic name †*Aipichthys* when he described †*A. pretiosus*. Although †'*Aipichthys*' *minor* and †'*Aipichthys*' *nuchalis* were described before †*A. pretiosus* by Pictet (1850) and Dixon (1850) respectively, they were only assigned to †*Aipichthys* by Woodward (1901). When first described by Steindachner (1860) the genus was originally named †*Aipichtys*, although the alternative spelling, †*Aipichthys*, has since been used almost exclusively (e.g. Bassani, 1882; Gorjanovic-Kramberger, 1895; Woodward, 1901, 1902; Patterson, 1964). †*Aipichthys* has become the recognized spelling though prevailing usage, although some of the older literature uses the original spelling (e.g. Steindachner, 1860; Hay, 1903).

2.3.1.1 Description

Measurements and meristics. Standard length of 47 mm and 60 mm total length. There are 26 vertebrae present: 12 abdominal and 14 caudal. Fin formulae are as follows: dorsal, III + 22?; anal, III + 17?; caudal, 6+I+9/8+I+5; pectoral, 12–14?; pelvic, ? The predorsal formula is: 0+0+0/x+x/.

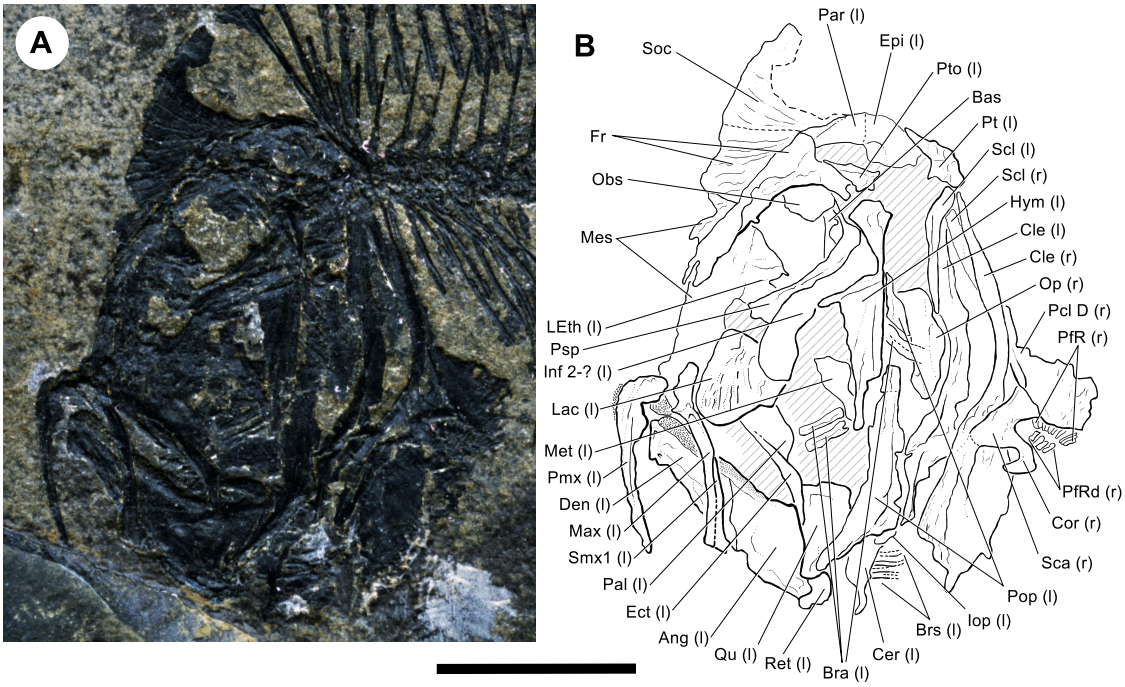

Figure 2.2: †*Aipichthys pretiosus*, holotype NHMW 1857 XXXVIII 7. **A,** specimen photograph (photograph by M. Friedman). **B,** interpretative drawing. Light grey diagonal hatching in B indicates damaged areas that could not be interpreted. Scale bar represents 10 mm.

Skull. The head is approximately two and a half times tall as it is long, although the neurocranium is of equal height and length (Figs. 2.1, 2.2). The substantial sagittal crest is nearly as large as the remainder of the skull. Although the skull is articulated, poor surface detail of component ossifications make detailed interpretation difficult. Bones that can be identified include: frontal, supraoccipital, parietal, epiotic, pterotic, orbitosphenoid, basisphenoid, parasphenoid, mesethmoid and lateral ethmoid.

The frontal forms the roof of the skull and defines the dorsal margin of the orbit. No canals or pores are apparent, but this likely reflects poor preservation. The conspicuous sagittal crest of the skull is composed of three bones: supraoccipital, frontal and mesethmoid. A number of ridges ornament the crest, and are aligned perpendicular to its anterodorsal border. The posterior part of the crest is composed of the supraoccipital, which makes the largest contribution of the three constituent bones. The supraoccipital projects posterodorsally to the level of the first supraneural. The posterior region of the supraoccipital is

incomplete, and it is unclear whether its hind margin would have been convex or concave. Anteriorly, the supraoccipital contacts the smaller frontal, which forms the middle part of the crest. The frontal in turn joins the mesethmoid, the most anterior and smallest part of the crest.

Both the parietal and epiotic are poorly preserved. No surface features can be discerned on the unremarkable parietal. The posterior margin, where the parietal meets the epiotic, cannot be detected. The epiotic bears a groove marking the point of articulation with the dorsal arm of the posttemporal.

The dorsal surface of the pterotic bears a large open groove for the frontal branch of the sensory canal. There is a lateral opening for the preopercular branch, although it is unclear whether this would have taken the form of a pore or open indentation (*sensu* Otero and Gayet, 1996: pp. 320–321, fig. 6) in life due to poor preservation.

The orbitosphenoid lies in the posterodorsal corner of the orbit. The basisphenoid forms an elongated strut between the posterior margin of the orbit and the parasphenoid. The anterior surface of the bone is straight, but its posterior margin is concave. The parasphenoid is elongated with a gentle ventral curve. The anterior apex of the parasphenoid is obscured by the overlying lacrimal and mesethmoid. The ascending process of the parasphenoid forms the posterior margin of the orbit.

As well as forming part of the sagittal crest, the mesethmoid forms the most anterior part of the skull, inserting medially below the frontals. It is unclear where this ventral component of the mesethmoid ends and the more posteriorly positioned lateral ethmoid starts. The posterior border of the lateral ethmoid is easily discerned, although the most ventral part appears to be missing as it does not overlie the parasphenoid or articulate with the lacrimal.

Jaws. Preserved elements of the upper jaw include the left premaxilla, maxilla and one supramaxilla (Figs. 2.1, 2.2). These bones have been rotated anteroventrally, and are not in a natural position relative to the rest of the skull. The premaxilla has

an elongated alveolar process, similar in length to the maxilla, and has small teeth along its oral margin. The ascending and articular processes are distinct. The dorsal extent of these processes is not preserved. The full length of the maxilla is preserved dorsal to the premaxilla. It has a process at its anterior end for articulation with the premaxilla. The supramaxilla is approximately half the length of the maxilla. It is not clear whether a second smaller supramaxilla may have also been present.

The lower jaw is complete and remains in life position (Figs. 2.1, 2.2). The posterior border of the dentary is 'V'-shaped, where it articulates with the anguloarticular. The small retroarticular is positioned to the posterior end of the anguloarticular. The dorsal margin of the dentary is thickened and bears a band of teeth along its oral margin. Three pores are visible near the ventral margin of the dentary, and mark the position of the sensory canal. There is a modest coronoid process.

Infraorbital series. The lacrimal is the only ossification of the infraorbital series that can be clearly discerned (Figs. 2.1, 2.2). Only the anterior and ventral margins of the lacrimal are intact, but it appears that the complete bone would have been ovoid with a long vertical axis. It is not possible to determine whether there would have been a dorsal process. The lateral surface of the lacrimal is ornamented with at least six thick, parallel ridges that correspond with branches of the underlying sensory canals. The remaining infraorbitals can only be detected as a length of bone, with divisions between individual ossifications unclear.

Suspensorium. Preserved elements of the suspensorium include the hyomandibula, metapterygoid, quadrate, ectopterygoid and palatine (Figs. 2.1, 2.2). No symplectic or endopterygoid are visible. The body of the hyomandibula is narrow, and bears a single articular facet at its dorsal terminus. The hyomandibula bears a large anterior process, which, although not complete, projects to approximately mid-orbit. No posterior process can be seen. The poorly preserved metapterygoid lies anterior to the ventral shaft of the hyomandibula. The quadrate is a large triangular bone, widest dorsally and tapering into an articular condyle ventrally.

The ectopterygoid is positioned to the anterior margin of the quadrate and the ventral margin of the palatine. The posterior part of the palatine is expanded dorsally into a semi-circular plate. The anterior end of the palatine is obscured by the overlying lacrimal.

Opercular series. The preoperculum, operculum and a small part of the interoperculum are preserved (Figs. 2.1, 2.2). The preoperculum is more complete ventrally, with much of its dorsal limb missing. The preoperculum is elongated along the dorsal-ventral axis, curving anteriorly at the ventral terminus. No pores are visible, but there is a well-developed groove for the sensory canal. The operculum appears to be from the right side and is presented in medial view. This bone is generally smooth, although there is a low, vertical ridge.

Ventral hyoid arch and gill skeleton. There are four, or possibly five, branchiostegals preserved in articulation with what is most likely the anterior ceratohyal (Figs. 2.1, 2.2). The anterior ceratohyal is only well preserved along its ventral margin. Thus it is not possible to comment on whether any foramen or groove is present. The branchiostegals are gently curved and appear relatively short. However, it seems likely that they are incompletely preserved distally.

The branchial arches can be seen in two places: anteroventral to the metapterygoid and hyomandibula, and where part of the dorsal limb of the preoperculum is missing (Figs. 2.1, 2.2). However, no significant features are apparent in these fragmentary remains.

Axial skeleton. The vertebral column is complete and consists of 12 abdominal and 14 caudal centra (Figs. 2.1, 2.3). Neural spines, haemal spines and ribs are well preserved, and some epineurals and epipleurals can also be distinguished. The first three abdominal centra are obscured by overlying material, but can be identified based on their corresponding neural spines. Each centrum is deeper than long.

Each centrum bears a neural arch with an elongated neural spine. The most anterior spines are quite short, but become successively longer in the middle of

the column, with the neural spine of the last abdominal centrum being the longest. Transverse processes can be seen on the last six abdominal vertebrae. They are successively longer and thicker posteriorly. Haemal arches of the caudal vertebrate bear elongated spines. The first three haemal spines are long, broad and closely associated with each other. The more posterior haemal spines are much narrower and become successively shorter posteriorly. All neural and haemal spines appear to be fused to the their respective centra except for the haemal spines of the second and third preural centra. These two haemal spines also support some of the procurrent rays of the ventral caudal fin skeleton. Further detail concerning the most posterior vertebrae is given in the section on the caudal fin skeleton below.

Ribs are present on the transverse processes of the abdominal vertebrae. The ribs are long and gently curved, and each rib bears a groove along its length. Some epineurals and epipleurals are present, although they are poorly preserved and incomplete. Epineurals from the right side can be seen on some of the more posterior abdominal vertebrae (vertebrae 8–11), and also the first caudal vertebra, although there may have been more in life. The epineurals originate on the neural arches of corresponding vertebrae. They all appear to originate from a similar level, although this cannot be clearly seen, as they are not from the exposed side of the specimen. The epipleurals appear to originate on the haemal arches of the first three caudal vertebrae and the transverse processes of the last abdominal vertebra. There are three supraneurals arranged in the following predorsal formula: 0+0+0/x+x/. The third supraneural is incomplete, with only the dorsal and ventral parts remaining. All three are of a similar length, and each is expanded distally to form an enlarged head.

Median fins. The dorsal, anal and caudal fins are preserved in articulation (Figs. 2.1, 2.3). The dorsal fin is supported by 32 pterygiophores. The first pterygiophore is distinct from the others with its sickle-shaped head. The first and second pterygiophores insert in the space between the first and second neural spines. Subsequent pterygiophores insert individually (3–7, 12), in pairs (8–11, 13–24, 31–32)

and in triplets (25–30) between neural spines. Pterygiophores decrease progressively in size toward the posterior of the series. There are three fin spines in the dorsal fin; they articulate with the first three pterygiophores. The length of successive fin spines increases, with each spine being approximately twice the length of that preceding it. There are 22 rays visible posterior to the spines. However, quality of preservation deteriorates posteriorly, and the absence of rays from posterior radials is almost certainly an artefact. The first ray is extremely long, but the subsequent rays are substantially shorter. The first ray is segmented, but this cannot be seen on any of the other rays. Most of the rays are incomplete distally; after the tenth ray, they can only be identified by the most proximal sections. No branching can be seen on the rays. The spines and rays are articulated in a 1:1 ratio with the pterygiophores. It appears that the number of pterygiophores present represents the true number, so there would have likely been 29 rays in life.

The anal fin comprises 22 pterygiophores, three spines, but only 17 rays are preserved. Some of the rays in the middle and posterior of the fin are not preserved. The first pterygiophore ('hemaxanal complex') is the largest and most robust of the series, and has an anteriorly pointing, sickle-shaped hook at its ventral end. The other pterygiophores are substantially shorter and narrower. They are all of a similar height, although there is a slight decrease toward the end of the series. The first anal-fin spine is very small, with the second spine 2.5 times the size of the first, and the third spine twice the size of the second. The first, second and possibly third spines articulate with the first pterygiophore. As with the dorsal fin, the preservation quality of the rays deteriorates posteriorly. The first and second rays are successively longer than the third spine. Distal parts of the rays are missing starting with the third ray, so it is not possible to comment on the full extent of their length. The rays appear to be in a 1:1 ratio with the pterygiophores. It seems likely that there would have been approximately 20 rays in life.

The caudal fin contains 11 procurrent (six dorsal, five ventral) and 19 principal rays (10 dorsal, nine ventral), with a formula of 6+I+9/8+I+5. The shorter outermost procurrent rays and some of the principal rays where the dorsal

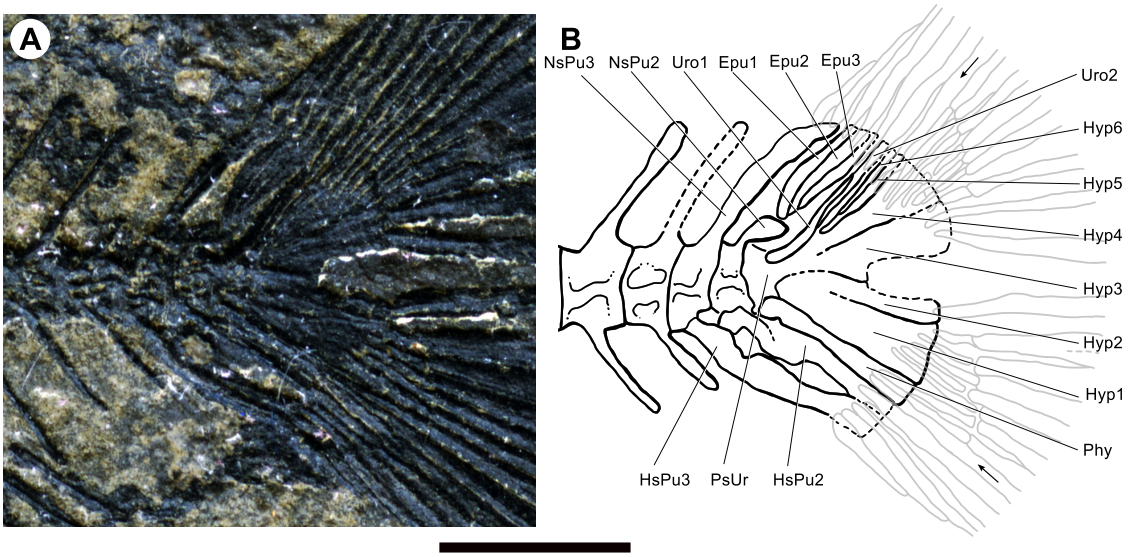

Figure 2.3: †*Aipichthys pretiosus*, holotype NHMW 1857 XXXVIII 7. **A,** specimen photograph (photograph by M. Friedman). **B,** interpretative drawing. In B, fin rays are shown in light grey. Arrows indicate the first principal ray in the upper and lower parts of the fin. Scale bar represents 5 mm.

and ventral lobes meet do not bifurcate. The first and last principal rays do not bifurcate. Two of the principal rays in the dorsal lobe bifurcate twice. All other rays bifurcate once. All rays except the most anterior procurrent rays show some degree of segmentation. With the exception of the first and the last, all principal rays are segmented once proximally. This segmentation is more conspicuous than anywhere else in the caudal fin, and similar to the condition seen in other lampridomorphs (e.g. †*Zoqueichthys*; Alvarado-Ortega and Than-Marchese, 2012: fig. 6). Some of the principal rays are also segmented distally. No rays appear to be segmented along their length. There is considerable overlap of the rays with the hypurals of the caudal skeleton.

The caudal fin skeleton includes the second and third preural centra, the pseudourostylar complex, three epurals, two uroneurals, six hypurals and one parhypural. The neural and haemal spine of the third preural vertebra are both elongated. The neural spine articulates with the first two procurrent rays of the dorsal lobe. The haemal spine articulates with the first three procurrent rays of the ventral lobe. The haemal spine of the second preural vertebra articulates with the procurrent rays, but its small, leaf-shaped neural spine articulates with

the first epural. The epurals are bound closely together. The first is the longest, with the other two successively shorter. Details of the pseudourostylar complex (the first preural plus first ural vertebra) are difficult to discern. It is unclear whether a second ural vertebra was present. The first uroneural is associated with the dorsal part of the pseudourostylar complex. This is in articulation with the second uroneural, which articulates with the last of the dorsal procurrent rays. Ventrally, the pseudourostylar complex articulates with the parhypural. The parhypural articulates with the first two principal rays of the ventral lobe. It is closely associated with the first hypural, but is not fused to it. A large part of hypural three and some of hypural two are missing. Hypural one is large and plate-like, articulating with the majority of the principal rays of the ventral lobe. Hypural two is much smaller, and articulates with a single ray. Only the proximal parts of the first and second hypurals are fused to one another. It is unclear whether they were also fused to the pseudourostylar complex. Fusion between other hypurals is not apparent, although it is hard to distinguish the borders of the distal parts of the third and fourth hypurals. The third hypural is a large plate-like bone, and may have been larger than the first hypural if complete. The fourth hypural is also plate-like, although smaller than the previous. Hypurals five and six are substantially smaller and shorter than any of the others.

Paired fins and girdles. The preserved components of the pectoral girdle are incomplete and represent bones from both the right and left sides of the specimen (Figs. 2.1, 2.2). No supratemporal can be seen. The body of the posttemporal is circular with a dorsal arm overlying the epiotic and a small remnant of the ventral arm.

Both the left and right supracleithra and cleithra are preserved. Each supracleithrum is tall and smooth with a large dorsoventral groove on its external surface. Of the two cleithra, the right one is the most complete. They are tall bones, and preserved dorsally only as thickened ridges representing the anterior

margins of the bones. Ventrally, there is a large plate-like posterior process. All parts of the cleithra appear unornamented.

The medial surface of the scapula, coracoid and postcleithrum of the right side is visible. Little of the scapula is visible, and the connection between it and the coracoid is hard to discern. The ventral part of the coracoid is broken, but the dorsal part is complete and appears to articulate with part of the cleithrum under the plate-like expansion. Part of the dorsal postcleithrum is preserved. The anterior margin is intact and bears a thickened ridge. The posterior margin of the dorsal postcleithrum is broken and incomplete. No part of the ventral postcleithrum can be seen. The pectoral girdle articulates with four distinct pectoral radials collectively bearing 12–14 pectoral rays. Only the proximal ends of the rays are visible as dorsal postcleithrum obscures distal parts of the fin.

The pelvic girdle is not preserved.

Squamation. There appear to be a few ventral ridge scales preserved along the lower margin of the hemaxanal complex (Fig. 2.1). The form of the scales is not clearly visible.

2.3.2 †'*Aipichthys*' *nuchalis*

Genus †'***Aipichthys***' Steindachner, 1860

†'***Aipichthys***' **nuchalis** (Dixon, 1850)

(Figs. 2.4, 2.5, 2.6, 2.7)

1850 †*Microdon nuchalis* Dixon: 369, pl. 32, fig. 7.

1887 †*Platax* (?) *nuchalis* (Dixon); Woodward: 342.

1901 †*Aipichthys nuchalis* (Dixon); Woodward: 429.

1902 †*Aipichthys nuchalis* (Dixon); Woodward: 4.

1964 †*Aipichthys nuchalis* (Dixon); Patterson: 303.

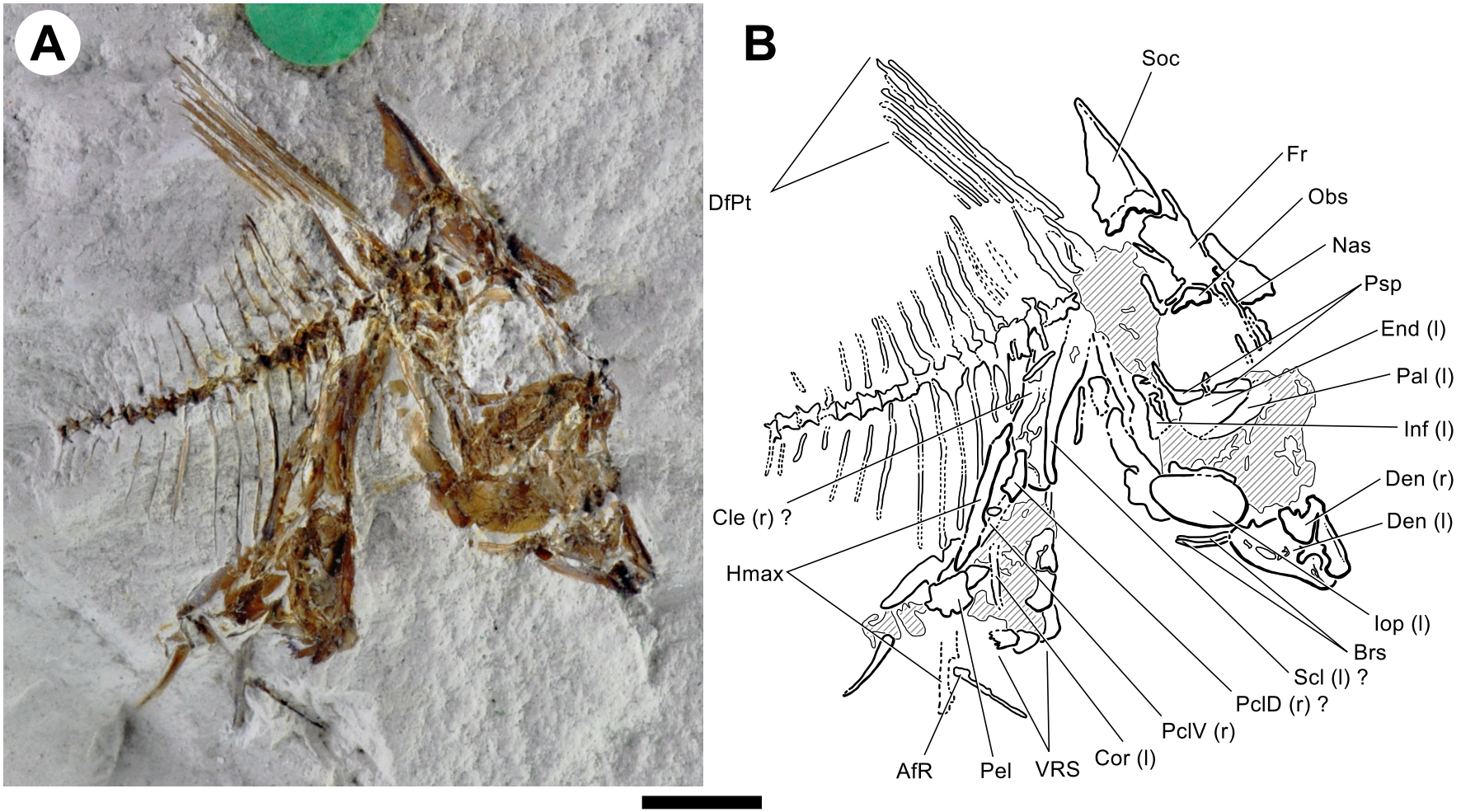

Figure 2.4: †'*Aipichthys*' *nuchalis*, holotype NHMUK PV OR 25770. **A,** specimen photograph (photograph by M. Friedman). **B,** interpretative drawing. Light grey shading in B indicates damaged areas that could not be interpreted. Scale bar represents 5 mm.

Diagnosis. Lampridomorpha with only the supraoccipital contributing to the sagittal crest; unlike †'Aipichthyoididae', †*Nardovelifer* and Lampridiformes where the frontal also contributes to the structure. The crest has a thickened anterior margin and a concave posterior margin. This condition is the same as is found in †*Freigichthys*, †*Gigapteryx* and other species of †'*Aipichthys*'. Has 11 abdominal vertebrae like †'*A.*' *velifer*, †'*A.*' *minor* and †*Freigichthys*. Body of greater depth than is known for †*Freigichthys* or any other species of †'*Aipichthys*' (Table 2.2).

Material. The Holotype and only known specimen. NHMUK PV OR 25770, an incomplete and partially articulated skeleton.

Occurrence. Upper Cenomanian English Chalk. According to Dixon (1850), the holotype was found in a chalk pit near Washington, Sussex, United Kingdom. It was likely from either the Zig Zag Chalk Formation of the Grey Chalk Subgroup or the Holywell Nodular Chalk Formation of the White Chalk Subgroup (Hopson, 2005). Woodward (1902: p. 5) states the specimen is probably from the 'zone of [†]*Holaster subglobosus*', although the exact horizon was not recorded when the specimen was collected. The zone of †*Holaster subglobosus* does not fully correspond with modern zones, and is represented by the lower part of the †*Neocardioceras judii* and the upper part of the †*Acanthoceras rhotomangense* zones (Caldwell and Cooper, 1999). The range of these zones is 93.49–94.86Ma (Hardenbol et al., 1998).

2.3.2.1 Description

The exposed right side of the specimen (Fig. 2.4) consists of broken sections through bones, and shows poor detail, leaving many of the anatomical features hard to discern. The following description is primarily based on features from the unprepared left side as observed in CT models (Fig. 2.5) unless otherwise specified.

Measurements and meristics. The specimen is incomplete posteriorly and measures 22 mm from the anterior edge of the frontal to the last preserved caudal vertebra. It likely would have been between 23–25 mm standard length in life based

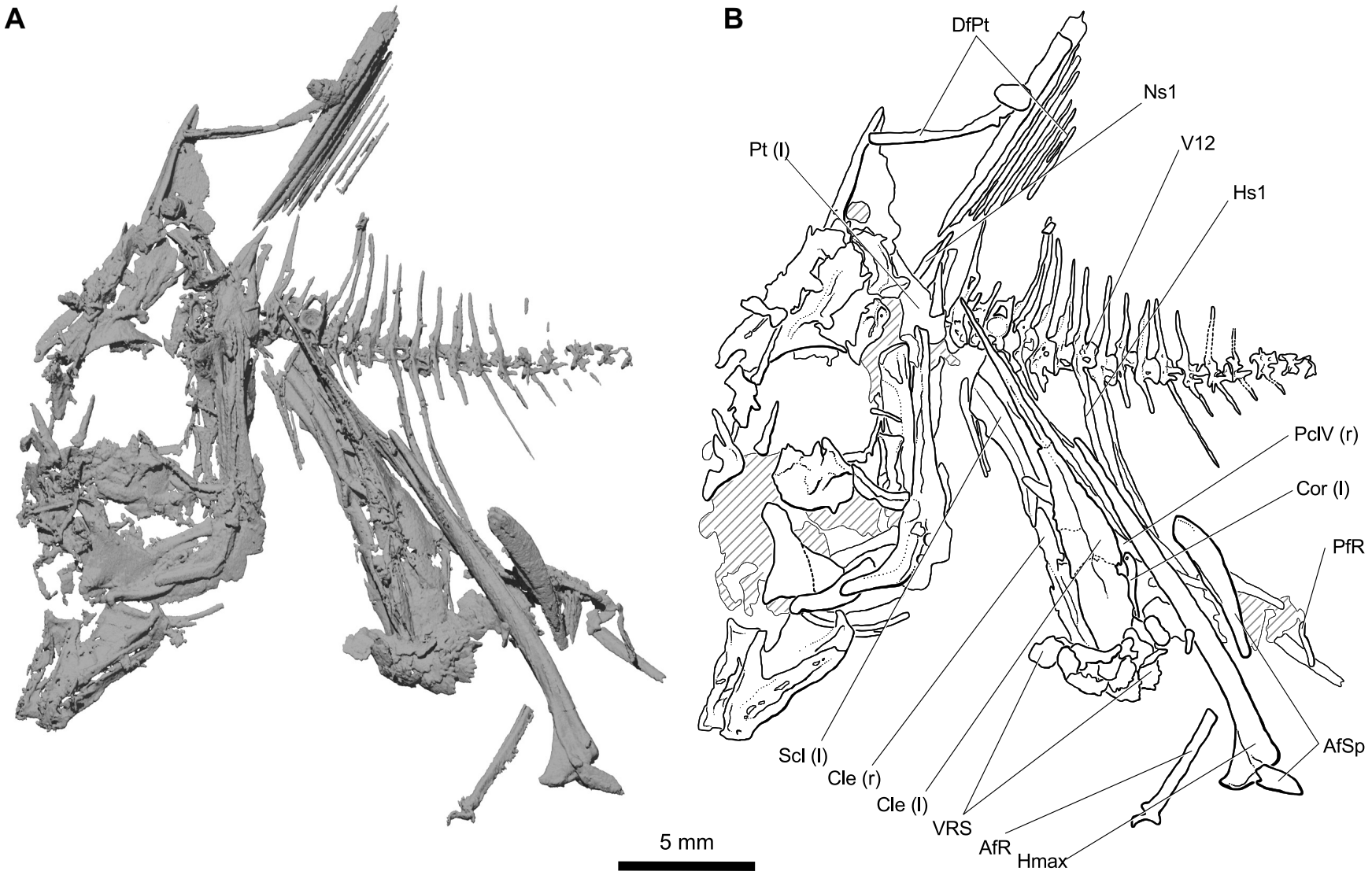

Figure 2.5: †'*Aipichthys*' *nuchalis*, holotype NHMUK PV OR 25770. **A,** computed tomography scan in left lateral view (virtual reconstruction by D. J. Delbarre). **B,** interpretative drawing. Light grey shading in B indicates damaged areas that could not be interpreted. Scale bar represents 5 mm.

on an extrapolation of measurements of †'*A.*' *minor* and †'*A.*' *velifer* (Table 2.2). There are 11 abdominal vertebrae and 11 preserved caudal vertebrae; additional caudal vertebrae would have been present in life as there is no trace of the caudal skeleton. The median fins are represented by a small number of elements: 10 pterygiophores from the dorsal fin, plus two fin spines and a pterygiophore from the anal fin. Much of the pectoral girdle is preserved, although only two fin rays are preserved. The two pelvic bones are present, but poorly preserved.

Table 2.2: Standard length and body depth of †'*Aipichthys*' and †*Freigichthys*. Measurements are indicated by [1] when they are estimated using the procedure described in the method section and [2] when based on estimates from the literature. Averages are given with the standard deviation (S.D.).

Species	Standard length		Body depth index	
	Range of standard length [number of specimens measured]	Average ± S.D.	Range of body depth [number of specimens measured]	Average ± S.D.
†'*Aipichthys*' *nuchalis*	23 – 25 mm[1] [1]	–	0.63 [1]	–
†'*Aipichthys*' *minor*	22.9 – 48.5 mm [13]	35.8 ± 6.1	0.36 – 0.46 [6]	0.42 ± 0.04
†'*Aipichthys*' *velifer*	25.7 – 63.2 mm [8]	40.8 ± 14.5	0.33 – 0.45 [6]	0.38 ± 0.04
†'*Aipichthys*' *oblongus*	70 mm[2] [1]	–	–	–
†*Freigichthys*	55.5 mm [1]	–	0.33 [1]	–

Skull. The skull (Figs. 2.4, 2.5, 2.6) is incomplete and some regions, especially the posterior section, appear to be compressed. Identifiable bones include the frontal, supraoccipital, parietal, pterotic, orbitosphenoid, parasphenoid, nasal and lateral ethmoid.

The frontal occupies much of the anterodorsal region of the skull, forming the anterior roof of the skull and framing the dorsal margin of the orbit. The frontal is fractured in a number of places, and the posterior section of the frontal is severely crushed. The dorsolateral margin of the orbit forms a lateral supraorbital shelf, which has a fully ossified sensory canal. Otherwise, the dorsal surface of the bone is smooth, and does not contribute to the sagittal crest of the skull. Instead, this conspicuous feature is formed exclusively by the supraoccipital. This bone forms a tall crest with a slight concave curve to the posterodorsal margin. The surface of the crest is smooth and flat with the exception of a thickened ridge along its anterior margin.

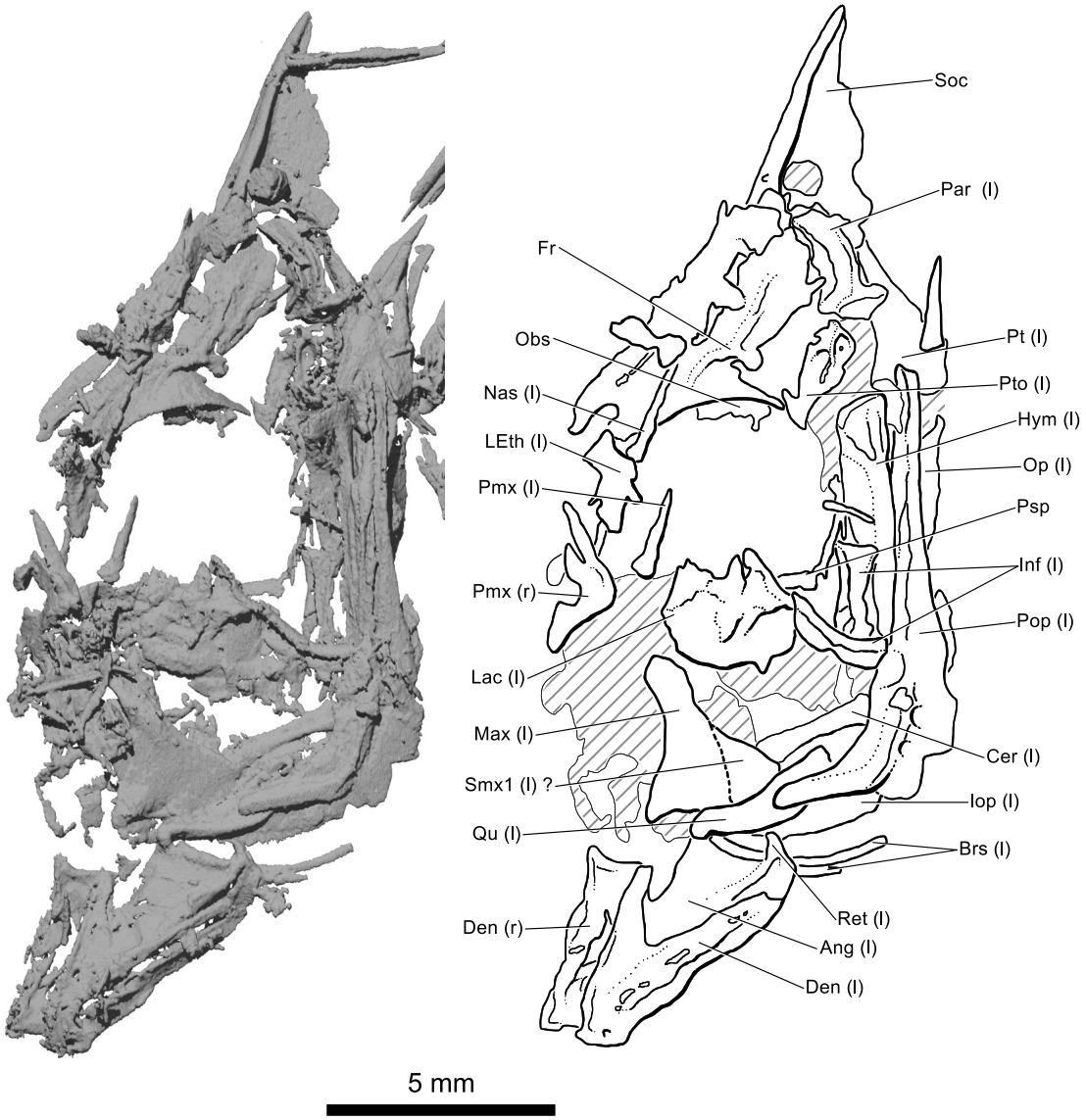

Figure 2.6: Cranial anatomy of †'*Aipichthys*' *nuchalis*, holotype NHMUK PV OR 25770. **A,** computed tomography scan in left lateral view (virtual reconstruction by D. J. Delbarre). **B,** interpretative drawing. Light grey shading in B indicates damaged areas that could not be interpreted. Scale bar represents 5 mm.

The parietal is incompletely preserved. A ledge-like facet at the anterior end of the bone appears to mark the articulation with the supratemporal. This facet originates at the top of what remains of the anterior end of the parietal, extends in a posteroventral direction before turning roughly 80 degrees and continuing anteriorly before terminating.

The incomplete pterotic preserves a surprising amount of anatomical detail. It bears an ovoid process on its ventral face, which has been interpreted as an

attachment point for branchial elevators in other †'aipichthyoids' (Otero and Gayet, 1996: pp. 320-321). A gutter for a sensory line extends along the length of the dorsal surface of the bone, and exits the lateral surface of the bone. It is not clear whether this exit assumes the form of an open groove or a dorsally enclosed foramen.

The poorly preserved orbitosphenoid partially separates the orbits. The parasphenoid is a long, straight bone, with a fracture in the orbital region dividing the bone in two. The posterior end of the parasphenoid is poorly preserved, and shows some traces of the ascending process. No part of the parasphenoid is preserved posterior to the orbit. Anterior to the fracture, the parasphenoid is only visible on the right side of the fossil, although it is crushed against the lacrimal so little detail can be discerned. Overlying fragments of bone completely obscure the anterior end of the parasphenoid.

The long, thin nasal has been displaced and extends anteroventrally from the surface of the supraorbital shelf of the frontal and terminates adjacent to the premaxilla. The lateral ethmoid has been displaced to overlie the nasal. It is incompletely preserved and presumably would have been larger in life.

Jaws. The premaxilla, maxilla and possibly a supramaxilla of the upper jaw are preserved (Figs. 2.4, 2.5, 2.6). Both premaxillae are displaced from life position. The more complete right premaxilla is found on the left side of the specimen in external view, while the ascending process of the left premaxilla – the only remaining preserved component of the bone – is on the right side of the specimen. The premaxilla has a tall, slender ascending processes and a distinct, shorter articular process, and is approximately half the height of the ascending process. The length of the alveolar process is nearly equal to the height of the ascending process, although the alveolar process is incomplete posteriorly so it presumably would have been longer in life. Small teeth are visible along the oral margin of the bone. The maxilla consists of a plate-like posterior half that assumes a semi-circular shape. The bone narrows considerably near its anterior end, which is produced as an arm-like extension. The anterior end of the maxilla is obscured

by unidentifiable fragments of bone. The maxilla is oriented at a steep angle, suggesting an upturned orientation of the mouth. It is possible that there is a supramaxilla on the dorsal surface of the maxilla. There is no clear margin to distinguish between the two, but if there were just one bone, the maxilla would be much deeper than in other species of †'*Aipichthys*'.

Both sets of the lower jaws are present, although the left mandible is more complete (Figs. 2.4, 2.5, 2.6). Both jaws have rotated posteroventrally relative to life position. The jaws are triangular in shape. The dentary bears small teeth along its dorsal margin. Posteriorly, the dentary is 'V'-shaped where it articulates with the anguloarticular. The coronoid process projects from the posterodorsal apex of the jaw, and is composed of the upper limb of the dentary and the anguloarticular. There is a facet on the posteroventral corner of the anguloarticular where the lower jaw articulates with the quadrate. No retroarticular can be seen. A series of elongated pores for the mandibular sensory canal extend along the dentary above its ventral margin. The preservation of these structures becomes less clear posteriorly, so an exact count of pores is not possible. However, at least two pores were present.

Infraorbital series. The infraorbital series is represented by the lacrimal and presumably the second and third infraorbitals, which together define the ventral margin of the orbit (Figs. 2.4, 2.5, 2.6). The lacrimal is large and ovoid. The margin of the lacrimal is hard to detect as it has been compressed onto underlying structures, but its lateral surface does not appear to have been smooth. There is a well-developed process on the dorsolateral surface of the lacrimal. The process has a number of projections radiating distally along the surface of the lacrimal, with an ascending process protruding over the dorsal margin of the bone. These radial projections would have presumably housed the underlying sensory canal. The second and third infraorbitals are narrow bones, with a groove for the sensory line on the external surface. They lie in sequence posterior to the lacrimal, with the second infraorbital being slightly larger than the third.

Suspensorium. The only bones of the suspensorium that are preserved well enough to merit description are the hyomandibula, quadrate, endopterygoid and palatine (Figs. 2.4, 2.5, 2.6). The splint-like hyomandibula extends ventrally from its articulation with the skull. It bears a large dorsal articular facet and carries a lateral ridge that extends most of the length of the bone. A plate-like process extends from the anterior margin of the hyomandibula, but appears to be incomplete. The quadrate is shaped like an elongated triangle. The quadrate narrows towards the anteroventral apex, where it bears a well-developed articular condyle. The endopterygoid and palatine can only be seen in medial view on the exposed side, as both the lacrimal and the parasphenoid obscure them from view on the other side. The endopterygoid appears to take the form of an oval, elongated along the anterior–posterior axis. The palatine is medial to the endopterygoid. Both the anterior and posterior ends of the palatine are not preserved. Both bones bear small teeth.

Opercular series. The opercular series is preserved only on the left side, where it consists of the opercle, preopercle and interopercle (Figs. 2.4, 2.5, 2.6). The opercle is incomplete, with large areas of the posterior and dorsal margins missing, and the remaining dorsal half of the bone crushed against the medial face of the preopercle. The bone is flat with a generally smooth surface. The preopercle has a long thin dorsal arm and a short anteroventral arm forming a boomerang shape, with a slightly obtuse angle of 110 degrees between the two arms. The ventral portion of the preopercle is well preserved, but the preservational quality deteriorates dorsally, where little detail can be discerned. The underlying sensory canal is accommodated by a flange along most of the length of the lateral surface. However, two pores can be seen where the dorsal and anteroventral arms meet. The interopercle is positioned ventral to the preopercle. This bone is incomplete and poorly preserved along the exposed ventral margin. The interopercle is flat with a fairly smooth surface.

Ventral hyoid arch and gill skeleton. Two branchiostegals and the anterior ceratohyal are preserved, although these are partially concealed by overlying bones (Figs. 2.4, 2.5, 2.6). The two branchiostegals are positioned along the ventral surface of the lower jaw. They are thin and curved. The posterior branchiostegal is longer than the other, although the anterior one appears to be broken. The anterior ends of the branchiostegals are obscured from view by the lower jaw. Both ends of the anterior ceratohyal are obscured, but it is clearly a long bone. A groove for the hyoid artery extends along the length of the bone. No 'beryciform' foramen can be seen.

Axial skeleton. The vertebral column is incomplete with much of the caudal section missing (Figs. 2.4, 2.5). Altogether there are 22 centra present, 11 abdominal and 11 caudal. The first three abdominal centra are obscured from view on the left side and undetectable from the right side, but can be identified based on their well-developed neural spines. Preservation of the vertebral column deteriorates posteriorly, with the most posterior vertebrae very incomplete. The anterior and posterior ends of the individual centra are circular in section with deeply concave articular surfaces as seen on centrum seven, which has rotated to clearly show the articular facet. Fine bony laminae occupy the lateral surfaces of the centra and separate them into upper and lower cavities.

Many of the neural spines are broken and incomplete, but spines become increasingly longer until the seventh vertebra. Posterior to this point, neural spines become successively shorter. Haemal arches are present on the first nine caudal centra, but complete spines are only preserved on the first two caudal centra. The spines project posteroventrally from the centra.

Broken fragments of pleural ribs are associated with some of the centra.

No intermuscular bones are visible, but this might reflect resolution limits of the scan.

No supraneurals are preserved.

Median fins. The fins are incompletely preserved, and many components that are present are displaced (Figs. 2.4, 2.5). Ten long pterygiophores are all that remains of the dorsal-fin skeleton. It is not clear where the first radial would have inserted. An anal-fin ray is preserved, although distally it is incomplete. There is a large, thick hemaxanal complex with an anteriorly facing sickle-like hook at its ventral apex. Two anal-fin spines are preserved. The first of these spines is one of the smaller anterior spines, which is found in articulation with the hemaxanal complex. The second spine is much larger than the first, and it has a sulcus running along the posterior margin.

Paired fins and girdles. The posttemporal is preserved only on the left hand side of the specimen, whereas the other preserved elements of the pectoral girdle are represented by right and left bones that have been shifted posteriorly and rotated to the left (Figs. 2.4, 2.5).

The posttemporal overlies the skull dorsal to the hyomandibula and the preopercle. The main body of the posttemporal is circular and smooth, and bears a long anterodorsal process that would have articulated with the epiotic.

Only the left supracleithrum is preserved. It assumes the shape of an elongated oval, with a thick ridge extending along the anterior margin of the lateral surface. Cleithra from both sides of the specimen are preserved, although both are incomplete. The cleithrum is dorsoventrally elongated and terminates dorsally with a narrow apex. Ventral ridge scales obscure the ventral tips of both cleithra. The lateral surface of the cleithrum has a raised ridge along the anterior margin. A robust rod-like ventral postcleithrum is preserved on the prepared side. A dorsal postcleithrum also appears to be preserved on this side.

Only the left coracoid can be clearly identified, where it is associated with the posterior margin of the left cleithrum. It is incompletely preserved, with only the posterior section present. The coracoid is an elongated bone with a raised posterior margin. Dorsally, the coracoid curves anteriorly, to form a large fenestra.

Two poorly preserved fin rays represent the only remains of the pectoral fin.

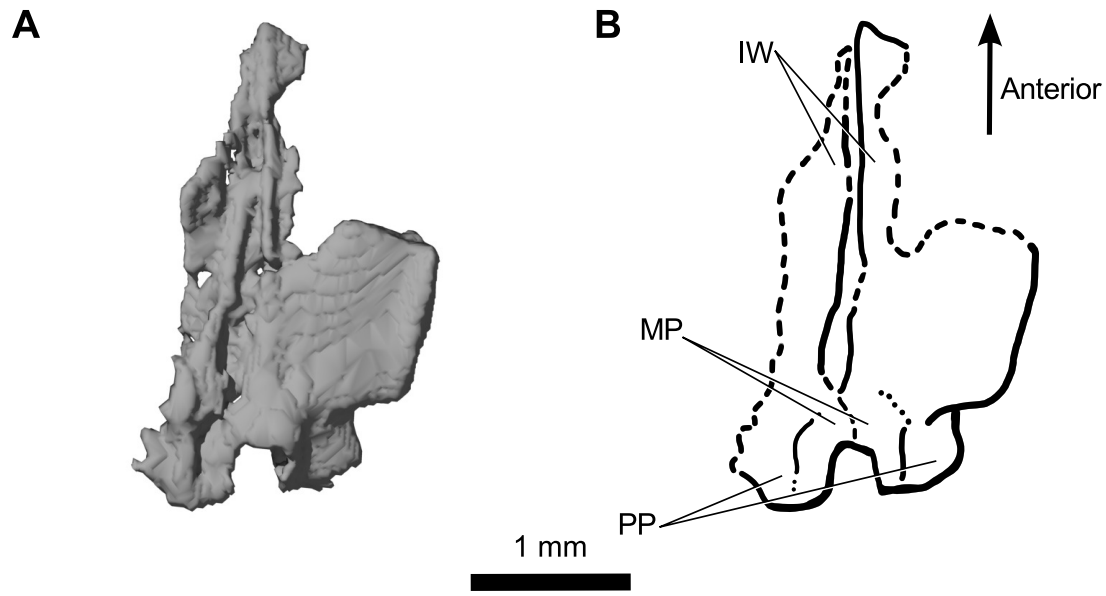

Figure 2.7: Pelvic bones of †'*Aipichthys*' *nuchalis*, holotype NHMUK PV OR 25770. **A,** computed tomography scan in ventral view (virtual reconstruction by D. J. Delbarre). B, interpretative drawing. Scale bar represents 1 mm.

On the exposed side of the specimen, the two pelvic bones appear to be joined by the medial processes (Figs. 2.4, 2.7). One half of the pelvis is highly incomplete, with only remnants visible, but most of the posterior section of the other half is present. The pelvic bones are triangular, and taper toward a point anteriorly. Posteriorly, each bone has a short posterior process medial to an articular facet for the pelvic-fin rays. The two pelvis bones diverge anterior to the medial process.

Squamation. There are a small number of thickened ventral ridge scales preserved below the pectoral girdle (Figs. 2.4, 2.5). Most of the scales have been crushed, but the scales are clearly ctenoid *sensu lato*, having a toothed posterior edge. No other scales are preserved in this specimen.

2.4 Phylogenetic relationships

We used the matrix presented by Davesne et al. (2014) as the basis of our analysis, and included seven new characters (Table 2.1) and four new species. We were able to code the states of 45 characters for †*Aipichthys pretiosus*, 28 characters

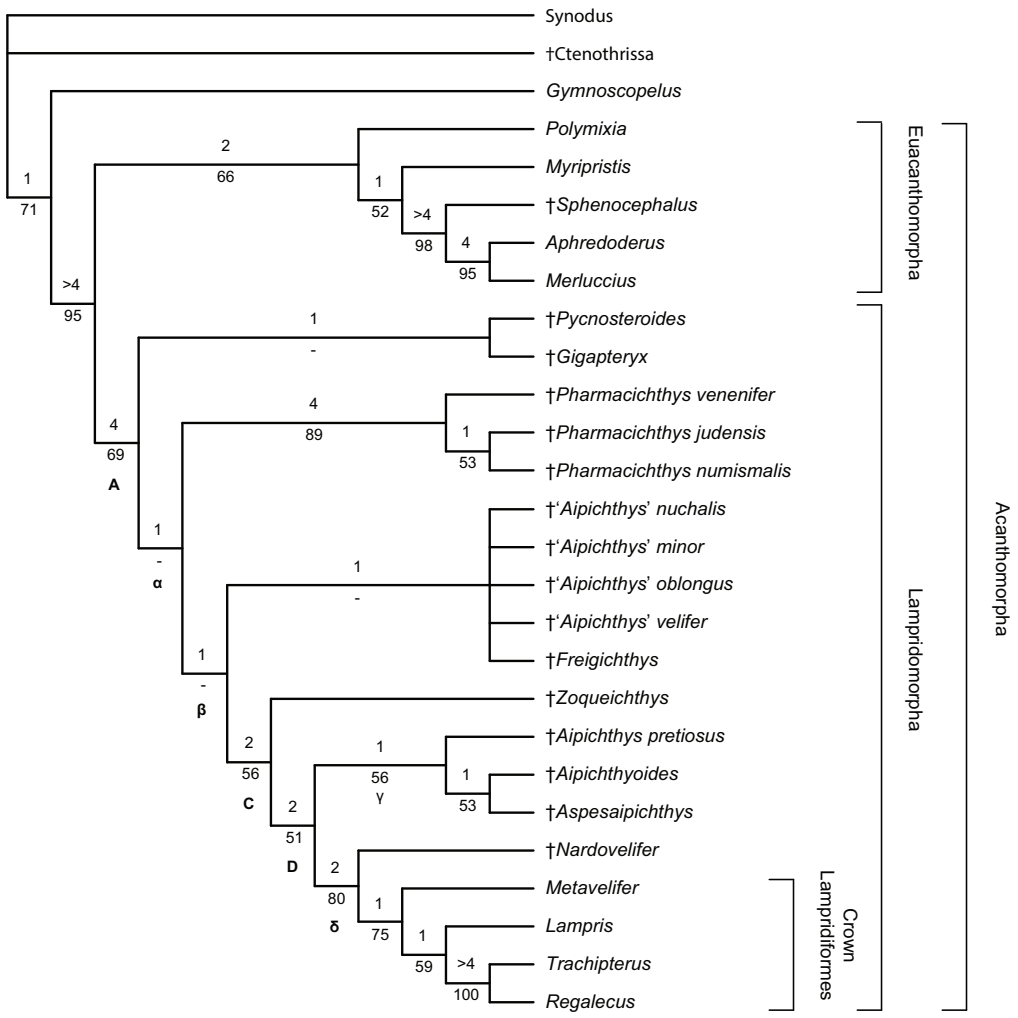

Figure 2.8: Strict consensus tree of 29 parsimonious trees. Tree length = 183, consistency index = 0.45, homoplasy index = 0.55, retention index = 0.70, rescaled consistency index = 0.31. Bremer indexes are above the branches, bootstrap indexes are below. Letters below branches are clade names. Clades with Greek letters as names are new. All other clades are from Davesne et al. (2014).

for †'*Aipichthys*' *nuchalis*, 60 characters for †*Gigapteryx* and 54 characters for †*Nardovelifer* (Table 2.3). The branch and bound analysis retained 29 trees, from which a strict consensus tree was produced (Fig. 2.8; tree length = 183 steps, consistency index = 0.45, homoplasy index = 0.55, retention index = 0.70, rescaled consistency index = 0.31).

The topology we recovered here is considerably different to that of Davesne et al. (2014). Instead of the lampridomorphs being split into two clades (Clades B and C *sensu* Davesne et al., 2014), they are united into one large clade. The internal

Table 2.3: Character matrix used in the phylogenetic analysis. The matrix is that of Davesne et al. (2014) with seven new characters, four new taxa, †*Paraipichthys* removed and revised coding for †*Aspesaipichthys* and †*Pycnosteroides*.

Taxa	Characters														
	1–5	6–10	11–15	16–20	21–25	26–30	31–35	36–40	41–45	46–50	51–55	56–60	61–65	66–70	71–74
Synodus	00000	00000	00000	0----	-0000	01000	00000	00000	00000	00000	00000	?0000	00000	00010	1000
Gymnoscopelus	00200	00001	00000	0----	-0000	11000	10100	00000	00000	00010	00000	00100	00000	00000	0100
†*Ctenothrissa*	00000	00000	00000	00000	0?001	00000	0000?	?0000	00000	00000	00000	00000	?01??	00010	0100
†*Pharmacichthys venenifer*	00001	01000	000??	10010	01??1	101?0	00101	00111	01100	11010	00000	01100	001??	200?0	1?00
†*Pharmacichthys numismalis*	000?1	01000	00000	10010	01??1	1???0	00101	00112	01100	11010	00000	01100	001??	20010	0000
†*Pharmacichthys judensis*	00001	01??0	000??	10010	01??1	1???0	00?01	00112	01?00	11010	00000	?1100	0?1??	2001?	??00
†*Aipichthyoides*	?00?0	11100	00011	11101	01??1	111?0	0010?	00011	01100	11001	10011	11100	001??	10000	?101
†'*Aipichthys*' *velifer*	00100	01100	00111	10010	11??1	11100	00100	00011	01100	11000	00000	11100	001??	20000	0001
†'*Aipichthys*' *oblongus*	0???0	01?00	00110	10010	1???1	1???0	00100	00011	01100	11000	00000	111?0	001??	?0???	0?0?
†'*Aipichthys*' *minor*	00100	01100	00110	10010	11??1	111?0	00100	00011	01100	11000	00000	11100	001??	20000	0001
†*Freigichthys*	00?00	01100	?0111	10010	11??1	1???0	00100	00011	01100	11000	??0?0	111?0	00110	100??	?1??
†*Aspesaipichthys*	00???	?????	?????	?????	????1	01??0	000??	??011	01?00	1?000	11011	1110?	?????	?????	0?0?
†*Zoqueichthys*	000?0	011?0	000??	11001	01??1	1?1?0	00100	00011	01100	11000	00000	11100	00110	00000	0001
†*Pycnosteroides*	?0000	011?0	00010	10010	?1??1	10100	00101	00102	01000	11100	00000	11110	001??	21000	0?00
Polymixia	10000	00000	00011	10000	01100	10200	00101	00000	01000	11100	00000	11010	00001	100?0	0100
Sphenocephalus	20100	001?1	10011	10010	01??1	00201	1011?	??200	01000	11101	00000	11011	00001	1?000	0000
Aphredoderus	00200	01111	10011	10010	01100	01201	10111	11200	01000	11101	01110	11011	10001	10000	0000
Merluccius	20200	01111	10011	10000	01111	01201	11111	113-0	00000	00111	11110	11011	10000	10000	1000
Myripristis	10000	00000	00011	10000	01100	00101	10101	01100	01000	11000	10000	11001	00110	11000	1100
Metavelifer	01210	11000	010??	11001	01001	10210	00100	11212	01100	11000	01110	11100	10110	00111	1010
Lampris	01210	11000	010??	11001	01011	01210	0110-	11212	00100	00001	11110	11100	11110	00111	?000
Trachipterus	01210	110?0	010??	0----	-1001	01210	0211-	113-2	10111	--101	11010	11010	11110	20010	1000
Regalecus	01210	110?0	010??	0----	-1001	01210	0211-	113-2	10111	-----	1---0	11010	11110	20◇1◇	1000
†'*Aipichthys*' *nuchalis*	?????	??100	???1?	10010	1???1	11??0	???0?	?????	????0	11???	?????	????0	???10	??000	0001
†*Aipichthys pretiosus*	0????	????0	00?1?	111?1	0???1	1???0	?0100	00011	011?0	11000	00?1?	11100	?0???	??000	??11
†*Nardovelifer altipinnis*	112?0	11??0	0????	1?011	0????	112?0	?010?	??112	01100	11000	01010	1110?	011??	10010	0000
†*Gigapteryx tethyestris*	?00?0	01101	000??	10010	11??1	1???0	00101	00001	01?00	110?0	00000	11100	0?1??	21000	0000

◇ Multiple states present (0 and 1)

branching structure of the Lampridomorpha highlights how character evolution may have occurred along the backbone of this clade. However, as with the topology of Davesne et al. (2014), many of these clades are weakly supported by Bootstrap and Bremer indexes (Fig. 2.8). Our analysis shows that †*A. pretiosus*, the type species for †*Aipichthys*, is not closely related to other species attributed to the genus, and in fact has greater affinity to the †'Aipichthyoididae'. The inclusion of †*A. pretiosus* and †*Nardovelifer* helps to resolve the polytomy between †*Aipichthyoides*, †*Aspesaipichthys* and crown Lampridiformes. Whilst †'*Aipichthys*' *velifer* and †*Freigichthys* were resolved as sister taxa in the original analysis, they are placed in a polytomy with †'*A.*' *nuchalis*, †'*Aipichthys*' *minor* and †'*Aipichthys*' *oblongus* in this analysis. We also find that †*Gigapteryx* and †*Pycnosteroides* are united as sister taxa, and collectively they are the most deeply branching lampridomorphs.

Below is a breakdown of the major clades – and the synapomorphies that define them – that were recovered in our phylogenetic analysis. When discussing synapomorphies presented by Davesne et al. (2014) we do not discuss them in detail (e.g. character state reversals within a clade) unless they are new characters, or when changes we have made to the character matrix have resulted in different character optimizations. The clade names used below correspond with the names from Figure 2.8.

2.4.1 Acanthomorpha

We found nine characters that are synapomorphies of Acanthomorpha. These include all eight synapomorphies proposed by Davesne et al. (2014): the frontal branch of the sensory canal opening in a groove (character 14: $0 \rightarrow 1$), a developed sagittal crest (character 16: $0 \rightarrow 1$), the dorsal limb of the posttemporal is firmly bound to the epiotic (character 22: $0 \rightarrow 1$), dorsal-fin spines (character 42: $0 \rightarrow 1$), presence of a hemaxanal complex (character 46: $0 \rightarrow 1$), anal-fin spines (character 47: $0 \rightarrow 1$), urodermals absent (character 56: $0 \rightarrow 1$) and dermal caudal scutes absent (character 57: $0 \rightarrow 1$). The anterior epineurals originating on the centra or transverse processes (character 35: $0 \rightarrow 1$) was considered a synapomorphy of Euacanthomorpha by

Davesne et al. (2014), which had convergently evolved in †*Pycnosteroides* Woodward, 1942 + †*Pharmacichthys* Woodward, 1942. Changes in the topology of our tree suggest this character is diagnostic for Acanthomorpha and was reversed in Clade β.

We found strong support for the placement of our four additional taxa within Acanthomorpha. We found eight synapomorphies in †*Gigapteryx* (characters 16: 1, 22: 1, 35: 1, 42:1, 46: 1, 47: 1, 56: 1, 57: 1), four in †'*A.*' *nuchalis* (characters 14: 1, 16: 1, 46: 1, 47: 1), seven in †*A. pretiosus* (characters 14: 1, 16: 1, 42: 1, 46: 1, 47: 1, 56: 1, 57: 1) and six in †*Nardovelifer* (characters 16: 1, 42: 1, 46: 1, 47: 1, 56: 1, 57: 1). The character states of the other acanthomorph synapomorphies could not be determined, except one character in †*A. pretiosus* (character 35: 0), which is optimized as a reversal in Clade β.

2.4.2 Clade A: Lampridomorpha

Davesne et al. (2014) proposed nine synapomorphies for Lampridomorpha. We recovered four of these characters as unambiguous synapomorphies for lampridomorphs: absence of the antorbital (character 7: $0 \rightarrow 1$), a single articular head of the hyomandibula (character 25: $0 \rightarrow 1$), first dorsal pterygiophore inserts anterior to the second neural spine (character 40: $0 \rightarrow 1$) and contact between the coracoid and the pelvic girdle (character 63: $0 \rightarrow 1$). Two of the lampridomorph synapomorphies of Davesne et al. (2014) were not unambiguously supported as lampridomorph synapomorphies. Firstly, an ascending process of the lacrimal (character 8: $0 \rightarrow 1$) is not present in †*Pharmacichthys* but found in all of the other deeply branching lampridomorph lineages. This character can be optimized as either a lampridomorph synapomorphy with a reversal in †*Pharmacichthys*, or as convergently evolved in †*Pycnosteroides* + †*Gigapteryx* and Clade β. Secondly, hypurostegy of the caudal-fin rays (character 58: $0 \rightarrow 1$) is present in Myctophiformes and most lampridomorphs but absent in Euacanthomorpha, so it could be optimized as a reversal in Euacanthomorpha or homoplastic in myctophiforms and lampridomorphs. With the changes to the topology of the tree, we found that two of the lampridomorph synapomorphies (characters 39: $0 \rightarrow 1$, 43: $0 \rightarrow 1$) proposed by Davesne et al.

(2014) are synapomorphic of Clade α. A medial join between the internal wings of the pelvic bones (character 64: $0 \rightarrow 1$) was also considered to be a synapomorphy of lampridomorphs by Davesne et al. (2014). However, the states of this character could not be determined in †*Pharmacichthys*, †*Pycnosteroides* and †*Gigapteryx*, so it is unclear whether the character is diagnostic of Lampridomorpha or one of the constituent clades instead. We also recovered three additional characters as synapomorphies for lampridomorphs. These included a concave posterior edge of the sagittal crest (character 19: $0 \rightarrow 1$), seven pelvic fin rays (character 66: $0 \rightarrow 2$) and loss of the suborbital shelf (character 72: $1 \rightarrow 0$). For two of these characters, the states change higher up in the tree. Character 19 reverses back to the ancestral state ($1 \rightarrow 0$), whilst character 66 is homoplastic in †*Freigichthys* ($2 \rightarrow 1$) and Clade C, where the optimization is ambiguous ($2 \rightarrow 0$ or $2 \rightarrow 1$).

All seven of the unambiguous synapomorphies are present in †*Gigapteryx*. Three and two respectively are present in †'*A.*' *nuchalis* (characters 19: 1, 25: 1, 72: 0) and †*A. pretiosus* (characters 25: 1, 40: 1). States for the other synapomorphies in these two taxa could not be determined. †*Nardovelifer* has four synapomorphies (characters 7: 1, 19: 1, 63: 1, 72: 0), although the state for character 19 is homoplastic, as †*Nardovelifer* is placed within Clade C where there is a reversal to the ancestral condition. Two of the character states found in †*Nardovelifer* (characters 40: 2, 66: 1) differ from those diagnostic of lampridomorphs, as †*Nardovelifer* is placed high in the tree where different character states are found. The state of character 25 could not be determined in †*Nardovelifer*.

2.4.3 Clade α

Clade α is a new unnamed clade recovered from our analysis and includes all lampridomorphs except †*Pycnosteroides* + †*Gigapteryx*. This clade is supported by two synapomorphies that were previously considered to be synapomophies of lampridomorphs by Davesne et al. (2014). The two characters are: all supraneurals anterior to the first neural spine (character 39: $0 \rightarrow 1$) and an elongated and unbranched first soft ray of the dorsal fin (character 43: $0 \rightarrow 1$).

†*Gigapteryx* does not have one of the synapomorphies of Clade α (character 39: 0), whilst the state could not be determined for the other character. The placement of †*A. pretiosus* and †*Nardovelifer* within Clade α was well supported, as the two synapomorphies were present in both taxa. The states of the two synapomorphies could not be determined in †'*A.*' *nuchalis*.

2.4.4 Clade β

The new unnamed clade, Clade β, contains all lampridomorphs except †*Pycnosteroides* + †*Gigapteryx* and †*Pharmacichthys*. We identified three synapomorphies that unite the included taxa: absence of a 'beryciform' foramen (character 27: 0 $\rightarrow$ 1), the anterior epineurals originating on the neural arches or spines (character 35: 1 $\rightarrow$ 0) and ventral ridge scales present (character 74: 0 $\rightarrow$ 1). Ventral ridge scales are lost higher up the tree in Clade δ.

Two synapomorphies are present in both †'*A.*' *nuchalis* (characters 27: 1, 74: 1) and †*A. pretiosus* (characters 35: 0, 74: 1), whilst the other character state could not be determined. †*Nardovelifer* only has one synapomorphy present (characters 27: 1), as one of the other characters was missing; absence of the final character was optimized as a reversal for Clade δ, which †*Nardovelifer* is part of.

2.4.5 †'*Aipichthys*' + †*Freigichthys*

Within Clade β, the deepest branch is a polytomy containing all four species of †'*Aipichthys*' + †*Freigichthys*. The genera †'*Aipichthys*' and †*Freigichthys* are defined by three synapomorphies: reduction to one supramaxilla (character 3: 0 $\rightarrow$ 1), presence of an interfrontal flat (character 13: 0 $\rightarrow$ 1) and a thickened anterior edge of the sagittal crest (character 21: 0 $\rightarrow$ 1). †'*A.*' *nuchalis* has a thickened anterior edge of the sagittal crest, but the states of the other two characters could not be determined. In this analysis, †'*Aipichthys*' and †*Freigichthys* are placed in a polytomy. In the original analysis of Davesne et al. (2014) some of the relationships were defined by a homoplastic character: the preopercular sensory canal in the pterotic opening laterally through an indentation in †'*A.*' *velifer* and †*Freigichthys* (character 15: 1),

but opening through a pore in †'*A.*' *oblongus* and †'*A.*' *minor* (character 15: 0). As this character state could not be determined in †'*A.*' *nuchalis*, the relationships between these taxa are not resolved further in this phylogenetic analysis.

2.4.6 Clade C

In our analysis we recovered Clade C of Davesne et al. (2014). This clade is supported by three synapomorphies: two previously described by Davesne et al. (2014) and one additional character. The three characters are: the frontal forms part of the sagittal crest (character 17: 0 → 1), the crest has a convex posterior border (character 19: 1 → 0) and the crest is long, extending from the nasal to the occiput (character 20: 0 → 1). Davesne et al. (2014) found that Character 19 was a synapomorphy of their Clade B. Clade B was not recovered in our analysis.

Both †*A. pretiosus* and †*Nardovelifer* have a long sagittal crest (character 20: 1). The frontal forms part of the crest of †*A. pretiosus* (character 17: 1). The crest of †*Nardovelifer* is broken in a number of places, so it is unclear whether the frontal forms part of this structure. The sagittal crest of †*Nardovelifer* has a convex posterior border (character 19: 1), and this appears to be homoplastic. The posterior border of the crest is missing in †*A. pretiosus*.

2.4.7 Clade D

Clade D contains all the taxa of Clade C except †*Zoqueichthys* Alvarado-Ortega and Than-Marchese, 2012. In the original analysis of Davesne et al. (2014) †*Aipichthyoides*, †*Aspesaipichthys* and crown Lampridiformes are placed in a polytomy, but with the additional taxa and characters here, the relationships are resolved. Davesne et al. (2014) recovered three characters that support Clade D. We found that two of these characters supported Clade D in our analysis: the mesethmoid located medially or posteriorly to the lateral ethmoids (character 6: 0 → 1) and fusion of the lower hypurals (character 54: 0 → 1). The first character state could not be determined in †*A. pretiosus*, but is present in †*Nardovelifer*. The lower hypurals are not completely fused in †*A. pretiosus*, but are fused proximally and free

distally, in the manner Otero and Gayet (1996) described for the †'Aipichthyoididae' (e.g. Davesne et al., 2014: fig. 3b). In †*Nardovelifer* the lower hypurals are fused in the middle region, but not proximally or distally. In our analysis we did not find support for the third synapomorphy of Davesne et al. (2014) – having five or fewer hypurals (character 51: 0 → 1). Both †*A. pretiosus* and †*Nardovelifer* have six hypurals, not five. Within Clade D, it now seems likely that six hypurals is the ancestral state, as †*A. pretiosus*, †*Nardovelifer*, *Metavelifer* and *Velifer* also show the general condition of six hypurals (Oelschläger, 1983). It appears that both †*Aipichthyoides* + †*Aspesaipichthys* and *Lampris* + *Trachipterus* + *Regalecus* convergently lost the sixth hypural. Thus possessing five or fewer hypurals should no longer be considered a synapomorphy of Clade D.

2.4.8 Clade γ

Clade γ is another new unnamed clade, uniting †*A. pretiosus* and †*Aipichthyoides* + †*Aspesaipichthys*. This clade has one synapomorphy: the mesethmoid forming part of the sagittal crest (character 18: 0 → 1), which is present in †*A. pretiosus* and †*Aipichthyoides*, although this character is unknown in †*Aspesaipichthys*. The fusion of the lower hypurals to the pseudourostylar centrum (character 55: 0 → 1) is a possible character shared by these three taxa. In both †*Aipichthyoides* and †*Aspesaipichthys*, the lower hypurals are fused to the pseudourostylar centrum, but this state cannot be determined in †*A. pretiosus*, so it could be an exclusive synapomorphy of †*Aipichthyoides* + †*Aspesaipichthys*, or unite all three taxa. There is only one synapomorphy that unites †*Aipichthyoides* and †*Aspesaipichthys*, but excludes †*A. pretiosus*: the presence of five or fewer hypurals (character 51: 0 → 1).

2.4.9 Clade δ and Lampridiformes

Davesne et al. (2014) recovered 14 synapomorphies for Lampridiformes. We found that some of these characters are synapomorphies of another clade, Clade δ, where †*Nardovelifer* is the sister taxon to crown Lampridiformes. There are seven synapomorphies for Clade δ. These are: the ascending process of the premaxilla

is longer than the alveolar process (character 2: 0 → 1), supramaxillae are absent (character 3: 0 → 2), there are seven or fewer branchiostegals (character 28: 1 → 2), the first dorsal pterygiophore is anterior of the first neural spine (character 40: 1 → 2), the upper hypurals are fused together (character 52: 0 → 1), absence of an articular process on the premaxilla (character 69: 1 → 0) and loss of the ventral ridge scales (character 74: 1 → 0). †*Nardovelifer* has all of these synapomorphies. Five of these characters (characters 2, 3, 28, 40, 52) were previously recognized as synapomorphies of Lampridiformes by Davesne et al. (2014), while the two other characters (characters 69, 74) are new additions to the matrix. †*Nardovelifer* is also united with *Lampris*, *Regalecus* and *Trachipterus* by a reduction to three pectoral fin radials (character 62: 0 → 1). However, *Velifer* has four radials, so the reduction to three radials could either be a synapomorphy with a reversal in veliferids, or it may have evolved independently in †*Nardovelifer* and crown Lampridiformes excluding veliferids. A reduction from three to two supraneurals (character 38: 0 → 1) could also be diagnostic of Clade δ. Three supraneurals is the primitive condition for acanthomorphs, but crown Lampridiformes have two or fewer supraneurals. All the crown lampridiforms in our analysis have one or fewer supraneurals, but some veliferids have two supraneurals.

The crown lampridiforms are united by five characters. Two of these were considered synapomorphic by Davesne et al. (2014): the upper hypurals are fused to the second ural centrum (character 53: 0 → 1) and the dorsal and ventral postcleithra are fused together (character 61: 0 → 1). The final three characters are new additions: dentition is absent on the premaxilla (character 68: 0 → 1), dentary (character 70: 0 → 1) and endopterygoid (character 71: 0 → 1). Two of these characters are not optimized as unambiguous synapomorphies: the absence of dentition on both the lower and upper jaws. Dentition is only present on the jaws in some of the elongated lampridiforms, which are typically recovered as a monophyletic group (Wiley et al., 1998; Grande et al., 2013). Therefore, the absence of dentition on the lower and upper jaws are either synapomorphies of Lampridiformes with the states reversed in the elongated forms, or jaw dentition

was lost separately in veliferids and lamprids. †*Nardovelifer* has none of these lampridiform synapomorphies.

Four of the 14 Lampridiformes synapomorphies presented by Davesne et al. (2014) are either synapomorphies of Clade δ or the Lampridiformes. These characters are unknown in †*Nardovelifer* so it is not possible to say which of the two clades they are diagnostic of. The four characters are: absence of an ascending process of the lacrimal (character 8: $1 \rightarrow 0$), presence of a frontal vault or cradle (character 12: $0 \rightarrow 1$), no epineurals on the caudal vertebrae (character 36: $0 \rightarrow 1$) and no epipleurals (character 37: $0 \rightarrow 1$).

2.5 Discussion

2.5.1 The status of †*Paraipichthys*

†*Paraipichthys lusitanicus*, the only species of the genus, from Cenomanian deposits in Portugal was described and assigned to the †'Aipichthyidae' by Gaudant (1978a). In the phylogenetic hypotheses of Otero and Gayet (1995, 1996), Otero (1997) and Alvarado-Ortega and Than-Marchese (2012) †*Paraipichthys* was recovered as the sister group to †'*Aipichthys*, while Davesne et al. (2014) found †*Paraipichthys* to be a more deeply diverging lampridomorph.

†*Paraipichthys* is only known from two specimens: the holotype (IST 561; Fig. 2.9A) and the paratype (IST 560; Fig. 2.9B). The holotype shows only the anterior part of the skeleton (cranium, opercles, pectoral and pelvic fins, anterior portions of the anal fin and vertebral column), however it is poorly preserved and only a few useful characters can be observed. By contrast, the paratype is a well-preserved caudal fin with several posterior vertebrae and part of a dorsal fin. The majority of the characters in previous phylogenetic analyses were coded from the paratype. However, there is no overlap between these two specimens; they are oriented differently and the paratype appears to be from a considerably larger animal than the holotype. Further to this, both the holotype and the paratype appear to be preserved in different sediments, and are possibly from different horizons. Therefore we recommend that the paratype should be referred to as cf. †*Paraipichthys*,

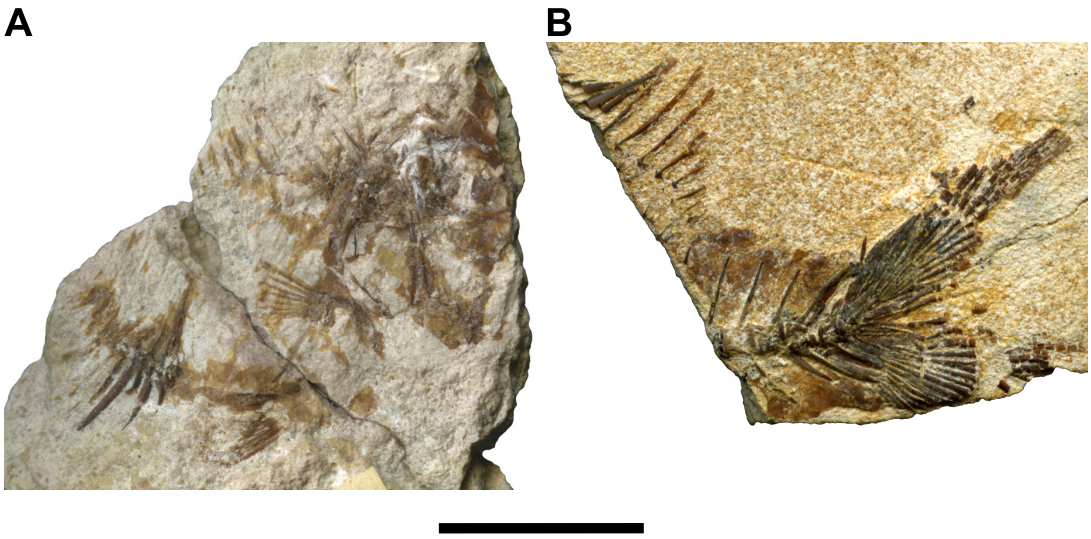

Figure 2.9: A, †*Paraipichthys lusitanicus*, IST 561 (holotype). **B,** cf. †*Paraipichthys lusitanicus*, IST 560 (paratype of †*P. lusitanicus*). Photographs by D. Davesne. Scale bar represents 10 mm.

until new specimens can show overlap between the anterior and caudal regions of †*Paraipichthys*, and confirm whether the holotype and paratype represent the same genus and species. The few characters that could be coded from the holotype led us to remove †*Paraipichthys* from our analysis. If individually the holotype and paratype are consistent with a placement inside Lampridomorpha, their position relative to other lampridomorphs cannot then be determined with any confidence.

2.5.2 †*Aipichthys* as a genus

Our analysis shows that †*Aipichthys pretiosus* is distinct from all other species that have been subsequently assigned to the genus †*Aipichthys*, and thus we now recommend those taxa (formerly known as †*Aipichthys velifer*, †*Aipichthys minor*, †*Aipichthys oblongus* and †*Aipichthys nuchalis*) should temporarily be referred to as †'*Aipichthys*' rather than †*Aipichthys*, which we reserve for †*A. pretiosus*. Under Article 60 of the International Code of Zoological Nomenclature (International Commission on Zoological Nomenclature, 2000), the junior homonym (i.e. †'*Aipichthys*') should be replaced by an established synonymous name or if one is not available then a new substitute name should be used. Both synonymous names for †*Aipichthys* are preoccupied: *Microdon* Dixon, 1850 is preoccupied by an

extant dipteran insect (family Syrphidae) and *Platax* Pictet, 1850 is preoccupied by an unrelated extant acanthomorph (family Ephippidae). This and previous analyses (e.g. Alvarado-Ortega and Than-Marchese, 2012; Davesne et al., 2014) show strong morphological similarity between †'*Aipichthys*' and †*Freigichthys*; it could be proposed that the concept of †*Freigichthys* could be expanded to accommodate species of †'*Aipichthys*'.

In †*Freigichthys* and †'*A.*' *velifer* the preopercular branch of the pterotic opens through an indentation, but it opens through a pore in the rest of †'*Aipichthys*'. This character has resolved some of the relationships amongst these taxa in previous studies (Alvarado-Ortega and Than-Marchese, 2012; Davesne et al., 2014), but all species of †'*Aipichthys*' and †*Freigichthys* are placed in a polytomy here. Despite close morphological similarity between these two genera, †*Freigichthys* possesses a number of characters that distinguish it from †'*Aipichthys*'. These include: presence of seven rather than six pelvic fin rays, presence of a suborbital shelf that also includes the lacrimal, pterygiophores with smooth median laminae and spines with longitudinal ridges (Otero, 1997). Overall, despite the close morphological similarity between †'*Aipichthys*' and †*Freigichthys* these taxa seem too dissimilar to incorporate into the same genus. Therefore we recommend the usage of †'*Aipichthys*' for †'*A.*' *velifer*, †'*A.*' *minor*, †'*A.*' *oblongus* and †'*A.*' *nuchalis* until the relationships between these taxa and †*Freigichthys* can be refined.

2.5.3 †*Gigapteryx* as a lampridomorph

†*Gigapteryx tethyestris* is the only species of the genus, and it is only known from one specimen (Fig. 2.10). However, in Forey et al. (2003) the figures are labelled as †*Gigapteryx tethyensis*, and in the abstract as well as on the holotype specimen itself, it has been named †*Gigapteryx lebanonensis*. Both of these species names appear to be erroneous. There are no other records of a †*G. tethyensis* and Forey et al. (2003) mention that †*G. tethyestris* is the only species of the genus. They also explain the origin of the name †*G. tethyestris* in text. In their paper, Forey et al. (2003) also describe another new genus and species: †*Paracentrus lebanonensis*. Presumably the



Figure 2.10: Specimen photograph of †*Gigapteryx tethyestris*, holotype NHMUK P. 62521 (photograph by D. J. Delbarre). Scale bar represents 10 mm.

authors have accidentally referred to †*Gigapteryx* using this species name, as they consistently refer to †*P. lebanonensis* in the text and only refer to †*G. lebanonensis* in the abstract. To summarize, †*G. tethyestris* is the only known species of †*Gigapteryx*, and both of the alternative names mentioned above should be disregarded.

When they originally described †*Gigapteryx*, Forey et al. (2003) placed it as Acanthopterygii *incertae sedis*. They identified one euacanthomorph synapomorphy from Johnson and Patterson (1993) in †*Gigapteryx*: the anterior epineural originating on the centrum, rather than the neural arch. However, they could not find any other euacanthomorph synapomorphies. They also identify two characters that suggest an affinity with acanthopterygians: presence of pelvic fin spines and a reduced number of pelvic fin radials. However, the authors did not consider whether †*Gigapteryx* was related to any of the taxa that we now refer to as lampridomorphs.

In our analysis, we find that †*Gigapteryx* is the sister taxon to †*Pycnosteroides*, and together they are sister taxa to all other lampridomorphs (Clade α). We



Figure 2.11: Specimen photograph of †*Nardovelifer altipinnis*, holotype MSNV Na 519 (photographs by M. Friedman). This specimen is split into a number of pieces. Individual photographs of these pieces were digitally re-aligned to produce this figure. Scale bar represents 50 mm.

found all nine of our lampridomorph synapomorphies in †*Gigapteryx*, and this clade was relatively well supported by Bootstrap and Bremer support indexes (Fig. 2.8). Furthermore, we believe that the characters identified by Forey et al. (2003) do not sufficiently justify an affinity to Euacanthomorpha or Acanthopterygii. The anterior epineurals originating on the centrum appears to be a synapomorphy of acanthomorphs, rather than a synapomorphy of Euacanthomorpha as suggested by Johnson and Patterson (1993). The anterior epineurals originate on the centrum in †*Pycnosteroides*, †*Gigapteryx* and †*Pharmacichthys* – the most deeply branching lampridomorphs. In Clade β, which excludes these three genera, there appears to be a character reversal where the anterior epineurals originate on the neural arches or spines. The presence of pelvic fin spines appears to be homoplastic for †*Pycnosteroides* + †*Gigapteryx* and acanthopterygians. However, some molecular phylogenies show Lampridiformes to be the sister group to the Euacanthopterygii

(e.g. Near et al., 2013). If this is the case, the presence of pelvic spines could be a synapomorphy of Lampridomorpha + Euacanthopterygii, and subsequently lost in Clade α. Finally, we have not been able to find a description of the pelvic radials in any of the fossil lampridomorphs used in our analysis. In extant lampridiforms, at least some of the pelvic radials are typically cartilaginous (Olney et al., 1993). Therefore, we do not believe this character can be used to place fossil taxa relative to living groups, as it is impossible to say whether the number of radials preserved is the true number.

In light of the new evidence we have presented here, we recommend that †*Gigapteryx* should no longer be classified as Acanthopterygii *incertae sedis*. Instead, †*Gigapteryx* should be considered to be part of the Lampridomorpha.

2.5.4 †*Nardovelifer* as a stem lampridiform

†*Nardovelifer* (Fig. 2.11) is generally regarded as a member of the extant lampridiform radiation and placed within Veliferidae, despite showing a number of characters not present in other veliferids or indeed other lampridiforms (Sorbini and Sorbini, 1999). As well as the characters identified by Sorbini and Sorbini (1999: dentition on the jaws and endopterygoid) we identified a number of primitive acanthomorph characters that exclude †*Nardovelifer* from veliferids specifically and crown lampridiforms generally. †*Nardovelifer* also retains the primitive condition of upper hypurals autogenous to the ural centra and postcleithra formed from two separate bones. On this basis of this evidence, we conclude that †*Nardovelifer* falls outside the lampridiform crown. In doing so, it helps to fill the structural gap between crown lampridiforms and the more distantly related †'aipichthyoids'. Our reinterpretation of †*Nardovelifer* also revises the minimum age for the divergence between Veliferidae and other extant lampridiforms to the early Palaeogene, rather than the late Late Cretaceous as presented in Davesne et al. (2014: fig. 7).

2.5.5 The palaeobiogeography and palaeoecology of Cretaceous lampridomorphs

Lampridomorphs outside of Clade C are exclusively found in Cenomanian deposits. The deposits in Lebanon (Hakel, Hadjoula and Namoura) yield the most taxa from this clade, including †*Pycnosteroides levispinosus* (Hay, 1903) (Fig. 2.12A), †*Gigapteryx* (Fig. 2.10), †*Pharmacichthys numismalis* Gayet, 1980a (Fig. 2.12B), †*Pharmacichthys venenifer* Woodward, 1942 (Fig. 2.12C), †'*A.*' *minor* (Fig. 2.12D), †'*A.*' *velifer* (Fig. 2.12E), †'*A.*' *oblongus* and †*Freigichthys* (Fig. 2.12F). †*Pharmacichthys judensis* Gayet, 1980b, and †'*A.*' *nuchalis* (Figs. 2.4, 2.5, 2.6, 2.7) derive from separate deposits in Palestine and England respectively. With the exception of the English Chalk, all of these deposits were of similar palaeolatitude. Within Clade C, some of the most deeply diverging branches represent Cenomanian taxa: †*Zoqueichthys* (Fig. 2.12G) from Mexico, †*A. pretiosus* (Figs. 2.1, 2.2, 2.3) from Slovenia and †*Aipichthyoides* (Fig. 2.12H) from Palestine, but no examples from Lebanon. †*Aspesaipichthys* (Fig. 2.12I) is found in Campanian–Maastrichtian deposits from Nardò Italy, along with †*Nardovelifer altipinnis* (Fig. 2.11). Two *incertae sedis* lampridomorphs, †*Errachidia pentaspinosa* and †*Homalopagus multispinosus* Murray and Wilson, 2014, are also known from Cenomanian–Turonian deposits in Morocco. No crown lampridiforms are known from the Cretaceous. The relative abundance of lampridomorphs from Lebanese sites might either indicate genuinely high diversity in these settings or reflect more exhaustive sampling. There appear to be collecting or preservation biases against small fishes in deposits like the English Chalk Group. It is possible that the rarity of lampridomorphs from these sediments represents taphonomic – rather than biological – signal.

With the exception of †*Nardovelifer*, lampridomorphs from the Cretaceous are morphologically very similar (e.g. Fig. 2.12): small (< 100 mm standard length), deep-bodied, with long, tall dorsal and anal fins, and have a moderately protusible premaxilla. †*Nardovelifer* is morphologically distinct (Fig. 2.11) and bears the greatest resemblance to the extant lampridiforms, especially the anatomically generalized veliferids. It is nearly an order of magnitude larger than other Cretaceous

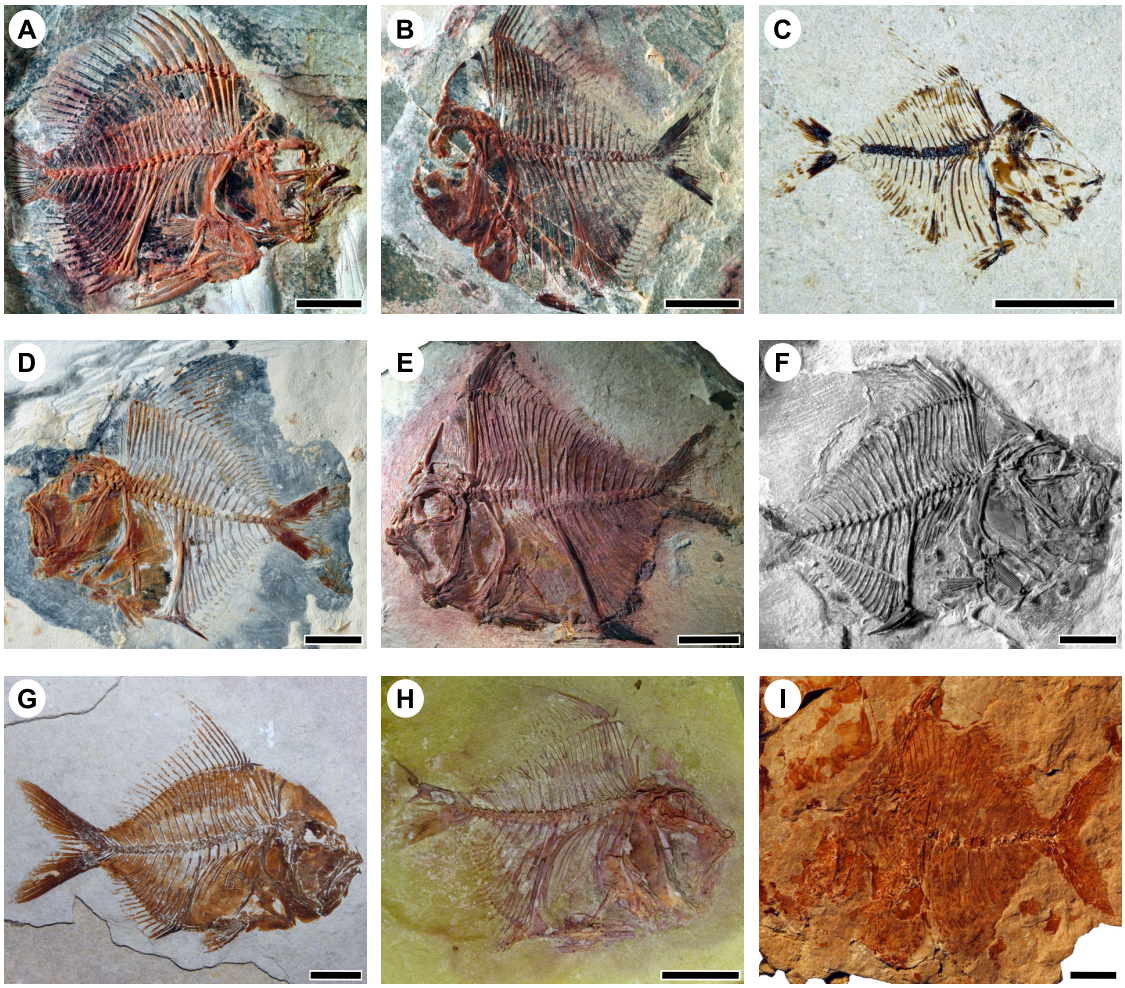

Figure 2.12: Other Cretaceous lampridomorphs. **A,** †*Pycnosteroides levispinosus*, MNHN. F. HDJ105 (photograph by C. Lemzaouda). **B,** †*Pharmacichthys numismalis*, holotype MNHN. F. HAK3 (photograph by C. Lemzaouda). **C,** †*Pharmacichthys venenifer*, NHMUK P. 62777 (photograph by D. J. Delbarre). **D,** †'*Aipichthys*' *minor*, MNHN. F. HAK94 (photograph by C. Lemzaouda). **E,** †'*Aipichthys*' *velifer*, MNHN. F. HAK57 (photograph by D. Davesne). **F,** †*Freigichthys elleipsis*, holotype FSL 573 015 (photograph by N. Podevigne, courtesy of O. Otero). **G,** †*Zoqueichthys carolinae*, holotype IHNFG-2224 (photograph by L. P. C. Machado, courtesy of J. Alvarado-Ortega). **H,** †*Aipichthyoides galeatus*, holotype EY 59a (photograph by Rivka Rabinovich). **I,** †*Aspesaipichthys cavaensis*, holotype MSNV Na 508 (photograph by M. Friedman). All scale bars represent 10 mm.

lampridomorphs (350 mm standard length), with a highly protusible premaxilla. Relatively large sizes and extreme jaw protrusion are two ecologically relevant features characteristic of crown lampridiforms. Our placement of †*Nardovelifer* on the lampridiform stem places the origin of these traits deeper within lampridomorph phylogeny than implied by previous interpretations of this genus as a crown lampridiform. The striking difference in habitus between early lampridomorphs on

one hand and †*Nardovelifer* plus crown lampridiforms on the other suggests that future fossil finds might play an important role in further clarifying the sequence of evolutionary changes leading to the unusual lampridiform bodyplan.

2.5.6 Implications for lampridomorph evolution

Cretaceous lampridomorphs are known from deposits that correspond to near-shore marine environments (Forey et al., 2003; Friedman et al., 2016). With the exception of †*Nardovelifer*, Cretaceous lampridomprphs are phenotypically similar to some extant near-shore bottom dwellers (e.g. Carangidae: *Alectis*, *Selene*; Patterson, 1964), which some have interpreted as convergence based on ecology (Rosenblatt and Bell, 1976). The phenotypic resemblance between †*Nardovelifer* and the deeply-bodied lampridomorphs implies that these taxa may have had a similar ecological role: slow and steady swimmers that are capable of burst-swimming to attain high speeds that can be used in prey capture (Rosenblatt and Johnson, 1976; Videler, 1993). Most extant lampridomorphs are found in the deep, pelagic ocean, although veliferids are found in near-shore environments (Olney, 2006; Nelson et al., 2016). As †*Nardovelifer* is found in coastal deposits, and it bears a strong resemblance to veliferids, it seems likely that †*Nardovelifer* would be more similar to veliferids than other deep-bodied lampridomorphs (Lampridae).

Despite most extant lampridiform clades being known from the fossil record (Bannikov, 1999; Carnevale, 2004; Bannikov, 2014a; Davesne, 2017), lampridomorphs are generally rare in the fossil record, as are extant lampridomorphs in modern oceans. Fossil lampridomorphs from the Cretaeceous appear to be more common than those from the Cenozoic. The pelagic lifestyle of non-veliferoid lampridiforms could explain the rarity of fossil representatives, as a change to a pelagic lifestyle in the deep sea would convey a lower preservation potential, whereas veliferids in marginal environments would have a higher preservation potential. However, as clades containing pelagic lampridiforms are known from the fossil record, the extreme morphologies that characterise these taxa – both very deep

bodied and elongated forms – may have evolved in near-shore environments, with the adoption of a pelagic lifestyle being secondary.

3

Anatomy of †*Aulolepis typus*, and the phylogenetic position of †Ctenothrissiformes and †Pattersonichthyiformes

Contents

3.1 Introduction 71
3.2 Materials and methods 74
3.3 Systematic palaeontology 84
3.4 Phylogenetic analyses 94
3.5 Hypothesis tests 99
3.6 Discussion 102

3.1 Introduction

Numbering over 18,500 living species, eurypterygian fishes represent a third of extant vertebrates. Eurypterygii unites three lineages: Aulopiformes, Myctophiformes and Acanthomorpha. Aulopiforms represent the sister group to a clade comprising acanthomorphs and myctophiforms: Ctenosquamata. Initial arguments for the monophyly of aulopiforms (Baldwin and Johnson, 1996; Sato and Nakabo, 2002; Davis, 2010), myctophiforms (Stiassny, 1996) and acanthomorphs (Stiassny, 1986;

Johnson and Patterson, 1993), as well as their mutual relationships (Rosen, 1973; Johnson, 1992), drew on morphological evidence, and have since been corroborated by molecular studies (e.g. Davis, 2010; Near et al., 2012; Betancur-R et al., 2013; Near et al., 2013; Chen et al., 2014).

Individually, these well-circumscribed extant eurypterygian lineages are represented by rich fossil records extending into the mid-Cretaceous. They are joined by two extinct eurypterygian groups of unclear phylogenetic placement: †Ctenothrissiformes and †Pattersonichthyiformes. Members of these nominal orders are small-bodied fishes (up to 20 cm in length), restricted to the early Late Cretaceous and best known from Cenomanian deposits in Lebanon (Hakel, Hadjoula) and the United Kingdom (English Chalk). Despite modest taxonomic diversity, relatively abundant fossil remains, and a long history of study, the monophyly of these groups, along with their relationships to one another and other eurypterygians, remains uncertain.

†Ctenothrissiformes contains three genera in two families: †Ctenothrissidae (†*Ctenothrissa* and †*Heterothrissa*) and †Aulolepidae (†*Aulolepis*). This represents a modification of earlier treatments that regarded both †*Ctenothrissa* and †*Aulolepis* as †ctenothrissids (Woodward, 1901), and was spurred by the revelation of conspicuous differences between these two genera by Patterson (1964). †*Heterothrissa* represents a later addition to the order (Gaudant, 1978c). Two other genera, †*Pateroperca* and †*Pattersonichthys*, were initially included in †Aulolepidae (Patterson, 1964; Goody, 1969) when they were described, but were later removed. Gaudant (1978b) considered †*Pateroperca* an *incertae sedis* ctenosquamate, and erected the order †Pattersonichthyiformes to accommodate †*Pattersonichthys* (Gaudant, 1976). Gaudant (1978c) later added two other species to †Pattersonichthyiformes: †*Phoenicolepis* and †*Humilichthys*.

A variety of hypotheses relating the taxa now recognized as †ctenothrissiforms and †pattersonichthyiforms to extant lineages have been proposed, spanning over a century of research. Early interpretations included an affinity to salmoniforms (Woodward, 1895) and clupeiforms (Woodward, 1899, 1900; Gregory, 1933; Berg,

1940; Bertin and Arambourg, 1958), primarily based on their primitive clupeoid-like jaws and primitive skull roof patterns with the parietals meeting at the midline, unseparated from one another by the supraocciptial. Still working in a pre-cladistic framework, Patterson (1964) suggested that †Ctenothrissiformes were similar to 'Myctophoidei' *sensu lato*, (including Myctophiformes of modern usage and Aulopiformes) as both possess a combination of primitive and advanced traits. However, Patterson (1964: pp. 245-246) did not believe that the †ctenothrissiforms and myctophoids were closely related, and hypothesised that the †ctenothrissiforms were ancestral to the acanthopterygians, branching off just before the percopsiforms. Greenwood et al. (1966) and Goody (1969) also supported a 'myctophiform' placement for these taxa. Rosen (1973) provided the first explicit cladistic argumentation bearing on †ctenothrissiforms, and regarded them as the sister lineage of acanthomorphs. He found nine characters commonly shared between acanthomorphs, myctophiforms and †ctenothrissiforms (Rosen, 1973: p. 463), although he hypothesised that the †ctenothrissiforms are the sister group to the acanthomorphs, primarily based on the moulded premaxillary articular and ascending processes (p. 468). Gaudant (1978c) proposed an affinity between †pattersonichthyiforms and myctophiforms, while later placing †Ctenothrissiformes as sister group to Acanthomopha + Myctophiformes + †Pattersonichthyiformes (Gayet, 1980c). Zehren (1979) studied †ctenothrissiforms, †pattersonichthyiforms and 'myctophoids' *sensu lato* in order to assess their relationships to acanthopterygians; he neglected to use the now commonplace taxonomic groupings, such as Acanthomorpha, that were introduced by Rosen (1973). Zehren concluded that all three groups have advanced traits and that they are more closely related to acanthopterygians than any other group, although it was not clear which were most closely related to Acanthopterygii. However, Zehren's 'myctophoids' were all aulopiforms or *incertae sedis* fossil taxa, with no myctophiforms included in the analysis.

In the more than three decades since the work of Zehren (1979) and Gayet (1980c), little has been added to our understanding of the anatomy of

†ctenothrissiforms and †pattersonichthyiforms, their relationships to one another, and their placements in eurypterygian phylogeny. With mature morphological (Johnson, 1992; Wiley and Johnson, 2010) and molecular (Near et al., 2012; Betancur-R et al., 2013; Near et al., 2013; Chen et al., 2014) datasets bearing on eurypterygian relationships now available, understanding of the relationships of these Cretaceous groups is principally limited by the lack of detailed anatomical data. In particular, key features relevant to ctenosquamate interrelationships pertain to the gill skeleton or details of the pelvic fin that are difficult to observe in crushed fossil material, and are not apparent from past descriptions of †pattersonichthyiforms and †ctenothrissiforms (e.g. Patterson, 1964; Goody, 1969; Gaudant, 1978c). Here I leverage advances in micro-computed tomography (µCT) to examine three-dimensionally preserved material of the 'primitive' †ctenothrissiform †*Aulolepis* from the Lower Chalk of the English Chalk Group of the UK, with two principal goals. First, I seek to evaluate key aspects of skeletal anatomy not apparent in older accounts of †*Aulolepis* specifically or †ctenothrissiforms generally. Second, I look to integrate these new observations with existing morphological and molecular data to critically evaluate the relationships of †ctenothrissiforms and †pattersonichthyiforms to one another and to other teleosts.

3.2 Materials and methods

3.2.1 Computed tomography scanning

The Metris X-Tek HMX ST 225 CT scanner at the Natural History Museum, London, UK was used for all µCT scans. Three specimens of †*Aulolepis typus* (two full body and one braincase) were initially scanned. However, only one of the scans (†*Aulolepis*: SMESC B. 9092) was of sufficient quality to permit extensive segmentation. µCT scans were segmented in Mimics (Materialise, 2015; version 15.01), with Blender (Blender Foundation, 2013; version 2.72b) used to produce the figure renders.

Table 3.1: Sources of morphological data used in the phylogenetic analysis. * indicates that CT scans of the specimen were studied. ** indicates that the specimen and CT scans of it were studied.

Taxa		Material consulted	
		Specimens studied	Literature
Lepisosteiformes	*Lepisosteus*	*L. osseus*: NHMUK 90.2.25.69 (3250) *L. platostomus*: NHMUK No reference (3250)	Jollie, 1984; Grande, 2010
Amiiformes	*Amia*	*A. calva*: NHMUK 12.4.6.87 (3180) *A. calva*: NHMUK No reference (3180)	Schultze and Arratia, 1989; Grande and Bemis, 1998; Springer and Johnson, 2004; Schultze and Arratia, 2013
†Leptolepiformes	†*Tharsis*	–	Nybelin, 1974; Patterson, 1975; Patterson and Rosen, 1977; Arratia, 1991
Elopiformes	*Elops*	*E. affinis*: NHMUK 1892.9.5.128 (3340) *E. saurus*: NHMUK 1888.11.6.57 (3340)	Ridewood, 1904; Forey, 1973; Rosen, 1973; Nybelin, 1979; Schultze and Arratia, 1989; Patterson and Johnson, 1995; Hilton, 2003; Springer and Johnson, 2004; Schultze and Arratia, 2013
Lepidogalaxiiformes	*Lepidogalaxias*	–	Rosen, 1974; Patterson and Johnson, 1995; Williams, 1997; Springer and Johnson, 2004; Mcdowall and Burridge, 2011
Salmoniformes	*Thymallus*	*T. brevirostris*: NHMUK 98.4.26.13 (4770) *T. vulgaris*: NHMUK 91.10.12.8 (4770)	Norden, 1961; Patterson and Johnson, 1995; Springer and Johnson, 2004
Stomiiformes	*Diplophos*	–	Fink and Weitzman, 1982; Fujita, 1990; Patterson and Johnson, 1995; Springer and Johnson, 2004
Osmeriformes	*Aplochiton*	*A. zebra*: NHMUK 1868.6.22.9 (5620)	Chapman, 1944; McDowall, 1969; Rosen, 1974; Williams, 1997; Mcdowall and Burridge, 2011
Ateleopodiformes	*Ateleopus*	–	Regan, 1911b; Rosen, 1973; Fujita, 1990; Olney et al., 1993; Springer and Johnson, 2004; Sasaki et al., 2006; Atsumi, 2016
Aulopiformes	*Synodus*	*S. lucioceps*: NHMUK 1890.11.15.288 (8090)	Rosen, 1973; Fujita, 1990; Stiassny and Moore, 1992; Patterson and Johnson, 1995; Baldwin and Johnson, 1996; Springer and Johnson, 2004
	Aulopus	*A. filamentosus*: NHMUK 62.6.14.3 (7980) *A. filamentosus*: NHMUK No reference (7980)	Goody, 1969; Rosen and Patterson, 1969; Rosen, 1973; Stiassny, 1986; Fujita, 1990; Patterson and Johnson, 1995; Baldwin and Johnson, 1996

Table 3.1: Species list continued

	Paraulopus	–	Sato and Nakabo, 2002
†Ctenothrissiformes	†*Aulolepis*	†*A. typus*: NHMUK 25908 †*A. typus*: NHMUK P.10458** †*A. typus*: SMESC B. 9092* †*A. typus*: SMESC B. 9093*	Woodward, 1900; Patterson, 1964, 1968; Rosen, 1973; Gaudant, 1978c
	†*Ctenothrissa*	†*C. microcephala*: NHMUK 47290 †*C. radians*: NHMUK PV. OR. 4029 †*C. radians*: NHMUK P. 5685 †*C. radians*: NHMUK P. 5699* †*C. radians*: NHMUK P. 11103 †*C. radians*: NHMUK P. 11233 †*C. radians*: NHMUK P. 44836a †*C. radians*: NHMUK P. 47912 †*C. vexillifer*: NHMUK P. 49493	Patterson, 1964, 1968; Rosen, 1973; Gaudant, 1978c
†Pattersonichthyiformes	†*Pattersonichthys*	†*P. delicatus*: NHMUK P. 9976	Goody, 1969; Gaudant, 1978c
Myctophiformes	*Neoscopelus*	*N. macrolepidotus*: NHMUK 1887.12.7:214 (8460)	Rosen and Patterson, 1969; Rosen, 1973; Stiassny, 1986; Fujita, 1990; Stiassny and Moore, 1992; Patterson and Johnson, 1995; Stiassny, 1996; Sato and Nakabo, 2002; Springer and Johnson, 2004
	Lampanyctus	*L. crocodilus*: NHMUK 1885.7.1.4 (8490)	Fujita, 1990; Stiassny and Moore, 1992; Stiassny, 1996; Springer and Johnson, 2004; Kobyliansky, 2016
Acanthomorpha	*Polymixia*	*P. japonica*: NHMUK 96.2.26.24 (26350) *P. nobilis*: NHMUK 95.5.28.1 (26350)	Rosen, 1973; Zehren, 1979; Stiassny, 1986; Fujita, 1990; Stiassny and Moore, 1992; Patterson and Johnson, 1995; Stiassny, 1996; Springer and Johnson, 2004
	†*Berycopsis*	†*B. elegans*: NHMUK P. 5696 †*B. elegans*: NHMUK P. 6465 †*B. elegans*: NHMUK P. 49053	Patterson, 1964
	Veliferidae	*Velifer hypselopterus*: NHMUK 49.10.9.16 (25890)	Rosen, 1973; Oelschläger, 1983; Fujita, 1990; Olney et al., 1993; Patterson and Johnson, 1995; Stiassny, 1996; Springer and Johnson, 2004
	Myripristis	*M. adusta*: NHMUK 58.4.21.239 (27170) *M. mudjan*: NHMUK 87.11.11.159 (27170)	Fujita, 1990

3.2.2 Phylogenetic analyses

3.2.2.1 Taxon sample

Two †ctenothrissiforms, †*Aulolepis* and †*Ctenothrissa*, and one †pattersonichthyiform, †*Pattersonichthys*, were included in the phylogenetic analyses. I included 18 additional neopterygian taxa (two fossil, 16 extant), including three aulopiforms (*Aulopus*, *Synodus* and *Paraulopus*), two myctophiforms (*Lampanyctus* and *Neoscopelus*) and four acanthomorphs (*Polymixia*, †*Berycopsis*, Veliferidae [*Metavelifer*/*Velifer*] and *Myripristis*). I also included a stem teleost (†*Tharsis*: Leptolepiformes) and a further six crown teleosts: *Elops* (Elopiformes), *Lepidogalaxias* (Lepidogalaxiiformes), *Thymallus* (Salmoniformes), *Aplochiton* (Osmeriformes) and *Ateleopus* (Ateleopodiformes). Finally, I included two holosteans: *Amia* (Amiiformes) and *Lepisosteus* (Lepisosteiformes).

3.2.2.2 Materials examined

Whenever possible, character data was collected directly, by studying osteological and fossil material (Table 3.1). The literature was consulted to aid with interpretation and to supplement the study of specimens (Table 3.1). In some cases it was not possible to directly study material, so all character data was sourced from the literature.

3.2.2.3 Morphological data

The character list (Table 3.2) contains 56 characters that define major neopterygian clades and the relationships between them. All characters had been described previously (see Table 3.2 for character sources), but they had not been used in this configuration before. The vast majority of characters were osteological in nature.

3.2.2.4 Molecular data

I assembled a molecular data set using five nuclear genes widely used in teleost phylogenetics: RAG1, ZIC1, PLAGL2, MYH6 and ENC1. Sequence data was downloaded from GenBank (Benson et al., 2005) (Table 3.3) using R (R Core

Table 3.2: List of morphological characters

Character number	Character description	References
1	Sagittal crest: **(0)** Absent or small; **(1)** Developed.	Stiassny, 1986; Olney et al., 1993
2	Spina occipitalis: **(0)** Absent; **(1)** Present.	Stiassny, 1986
3	Parietals: **(0)** Make contact for greater than half their length; **(1)** Separated by the supraoccipital along most of the length of the two bones.	Patterson, 1964; Zehren, 1979; Gayet, 1980c; Johnson and Patterson, 1996
4	Exoccipitals and basioccipital exposed posteriorly and joined in an inverted Y-shaped suture: **(0)** Absent; **(1)** Present.	Patterson, 1964; Rosen, 1973; Zehren, 1979; Johnson, 1992; Johnson and Patterson, 1996
5	Posttemporal fossa: **(0)** Roofed; **(1)** Unroofed.	Patterson, 1964; Rosen, 1973; Gayet, 1980b; Johnson and Patterson, 1996
6	Ridge or fossa on the neurocranium for articulation with the supratemporal: **(0)** Absent; **(1)** Present.	Patterson, 1964
7	Orbitosphenoid: **(0)** Present; **(1)** Absent.	Johnson and Patterson, 1996
8	Lateral ethmoid closely associated or fused to the vomer: **(0)** Absent; **(1)** Present.	Patterson, 1964; Stiassny, 1986
9	Articulation between the lateral ethmoid and lacrimal: **(0)** Absent; **(1)** Present.	Patterson, 1964; Zehren, 1979; Johnson and Patterson, 1996
10	Well-developed median dorsal keel on the mesethmoid: **(0)** Absent; **(1)** Present.	Regan, 1911b; Stiassny, 1986
11	Frontal branch of sensory canal running in a: **(0)** Closed tube; **(1)** Open groove.	Otero and Gayet, 1996
12	Autopalatine: **(0)** Ventral part expanded laterally; **(1)** No lateral expansion.	Sato and Nakabo, 2002
13	Oral margin of the jaw consists of: **(0)** The premaxilla and the maxilla; **(1)** The premaxilla and lacrimomaxillaries; **(2)** Just the premaxilla.	Patterson, 1964; Baldwin and Johnson, 1996; Johnson and Patterson, 1996; Grande, 2010
14	Form of premaxilla: **(0)** Attached to neurocranium; **(1)** Free from neurocranium.	Patterson, 1977; de Pinna, 1996
15	Ascending process of the premaxilla: **(0)** Absent; **(1)** Present.	Rosen, 1973; Zehren, 1979; Fink and Weitzman, 1982; Stiassny, 1986
16	Dentition on maxilla: **(0)** Present; **(1)** Absent.	Gayet, 1980c; Johnson and Patterson, 1996
17	Supraorbital bones: **(0)** Present; **(1)** Absent.	Patterson, 1964; Gaudant, 1978b; Zehren, 1979; Gayet, 1980c; Stiassny, 1986; Johnson and Patterson, 1996; Stiassny, 1996
18	Subocular shelf on infraorbitals: **(0)** Absent; **(1)** Present.	Rosen, 1973; Gayet, 1980c; Stiassny, 1996
19	Beryciform foramen on anterior ceratohyal: **(0)** Present; **(1)** Absent.	Patterson, 1964; McAllister, 1968; Rosen and Patterson, 1969; Johnson and Patterson, 1996
20	Number of branchiostegals articulating with posterior ceratohyal: **(0)** Three or more; **(1)** Two or less.	Patterson, 1964; McAllister, 1968; Zehren, 1979; Gayet, 1980c; Baldwin and Johnson, 1996; Johnson and Patterson, 1996; Stiassny, 1996
21	Posterior branchiostegal rays: **(0)** Most posterior one to three branchiostegals abruptly larger than anterior ones; **(1)** Similar size as anterior rays or get gradually larger posteriorly.	Fink and Weitzman, 1982

Table 3.2: continued

22	Uncinate process on second epibranchial: **(0)** Present, small; **(1)** Present, enlarged.; **(2)** Absent.	Rosen, 1973, 1974; Baldwin and Johnson, 1996; Johnson and Patterson, 1996
23	Toothplates fused to the third epibranchial: **(0)** Absent; **(1)** Single toothplate fused to EB3; **(2)** Lots of small toothplates associated with EB3.	Rosen, 1973; Johnson, 1992
24	Epibranchial 4 morphology: **(0)** Proximal end slender, without an uncinate process; **(1)** Proximal end expanded, without an uncinate process; **(2)** Proximal end slender with an uncinate process; **(3)** Proximal end expanded, with an uncinate process at the middle.	Sato and Nakabo, 2002
25	Fifth upper pharyngeal toothplate: **(0)** Absent; **(1)** Present.	Johnson, 1992; Stiassny, 1996
26	Large toothplate fused to proximal face of fourth ceratobranchial: **(0)** Toothplate absent or not fused to fourth ceratobranchial; **(1)** Present.	Stiassny, 1996
27	Number of vertebrae: **(0)** More than or equal to 60; **(1)** Greater than or equal to 40, less than 60; **(2)** Less than 40.	Zehren, 1979
28	First centrum has facets for articulation with exoccipital condyles: **(0)** Absent; **(1)** Present.	Rosen, 1985; Johnson, 1993
29	Parapophyses on the first centrum cone-like and meet in the middle: **(0)** Parapophyses absent or if present they are not cone-like and do not meet in the ventral midline; **(1)** Cone-like and meet in the ventral midline.	Stiassny, 1986, 1996
30	Accessory neural arch: **(0)** Absent; **(1)** Present.	Patterson and Johnson, 1995; Baldwin and Johnson, 1996; Johnson and Patterson, 1996; Stiassny, 1996
31	Neural arch on first vertebra: **(0)** Left and right elements separate; **(1)** Left and right elements fused together into a single unit.	Patterson, 1964; Stiassny, 1996
32	Fusion between anterior epineurals and neural arches: **(0)** Present; **(1)** Absent.	Patterson and Johnson, 1995; Johnson and Patterson, 1996; Stiassny, 1996
33	Epipleural series: **(0)** Absent; **(1)** Begin on V3 or further back; **(2)** Begin on V2 or V1.	Patterson and Johnson, 1995; Baldwin and Johnson, 1996; Johnson and Patterson, 1996
34	Origin of epipleurals: **(0)** All below the horizontal septum; **(1)** One or more displaced dorsally into horizontal septum.	Patterson and Johnson, 1995; Baldwin and Johnson, 1996
35	Number of supraneurals: **(0)** 15 or more; **(1)** Five to 14; **(2)** Four; **(3)** Three or less.	Gayet, 1980c; Patterson and Rosen, 1989; Johnson and Patterson, 1996
36	Form and development of supraneurals: **(0)** First supraneural similar in size/thickness to subsequent ones. No free neural spine between the first and subsequent supraneural; **(1)** First supraneural substantially larger/thicker than others, and separated from subsequent supraneural by one or more neural spines.	Johnson and Patterson, 1996
37	True fin spines on either/both the dorsal and anal fins: **(0)** Absent; **(1)** Present.	Patterson, 1964; Rosen, 1973; Johnson, 1993
38	Adipose fin: **(0)** Absent; **(1)** Present.	Patterson and Rosen, 1977; Gayet, 1980c; Johnson and Patterson, 1996
39	Caudal axis upturns: **(0)** Gradually from around PU5-3; **(1)** Sharply around PU1.	Patterson and Rosen, 1977; Schultze and Arratia, 2013
40	U1 and PU1: **(0)** Separate bones; **(1)** Fused together.	Zehren, 1979; Johnson and Patterson, 1996

Table 3.2: continued

41	Neural spine on preural centrum two: **(0)** Long, spine-like; **(1)** Short; **(2)** No neural spine.	Patterson, 1968; Rosen, 1973
42	Neural arch/spine on U1: **(0)** Present, and not greatly reduced; **(1)** Either greatly reduced (rudimentary) or absent.	Patterson and Rosen, 1977
43	Number of pairs of uroneurals: **(0)** None; **(1)** Three or more; **(2)** Two; **(3)** One.	Patterson and Rosen, 1977; Zehren, 1979; Johnson and Patterson, 1996
44	Number of hypurals: **(0)** Eight or more; **(1)** Seven or fewer.	Patterson, 1964; Patterson and Rosen, 1977; Zehren, 1979; Johnson and Patterson, 1996
45	Urodermal: **(0)** Present; **(1)** Absent.	Zehren, 1979; Johnson and Patterson, 1996
46	Dermal caudal scutes: **(0)** Present; **(1)** Absent.	Zehren, 1979; Gayet, 1980c; Johnson and Patterson, 1996
47	Position of the pectoral fins: **(0)** Low on the body (closer to the ventral midline); **(1)** High on the body (closer to the lateral midline).	Baldwin and Johnson, 1996
48	Mesocoracoid: **(0)** Present; **(1)** Absent.	Patterson, 1964; Zehren, 1979; Johnson and Patterson, 1996
49	Number of postcleithra: **(0)** One; **(1)** Three or more; **(2)** Two; **(3)** None.	Gottfried, 1989; Baldwin and Johnson, 1996; Johnson and Patterson, 1996; Stiassny, 1996
50	Position of pelvic fins: **(0)** Abdominal or Sub-abdominal; **(1)** Thoracic or Sub-thoracic; **(2)** Jugular.	Patterson, 1964; Zehren, 1979; Baldwin and Johnson, 1996
51	Association between the pelvic and pectoral girdle: **(0)** Pelvic and pectoral girdle do not make contact, and are not closely associated with one another; **(1)** Pelvic and pectoral girdles make contact, or are closely associated with one another.	Patterson, 1964
52	Form of medial processes of pelvic bones: **(0)** Medial processes absent or inconspicuous; **(1)** Medial processes elongated along the anterior posterior axis; **(2)** Medial processes extend medially as column-like processes.	Johnson, 1993; Baldwin and Johnson, 1996
53	Pelvic foramen: **(0)** No foramen in the pelvis bones; **(1)** A foramen present in the internal wing of the pelvic bone.	Regan, 1911b
54	Posterior processes of pelvis: **(0)** Small or absent; **(1)** elongated and widely separated.	Regan, 1911b
55	Fusion of ventral half of medial pelvic ray to medial pelvic radial: **(0)** Absent; **(1)** Present.	Gosline, 1961; Johnson, 1992
56	Number of pelvic fin rays: **(0)** Greater than or equal to 10; **(1)** 8-9; **(2)** 6-7; **(3)** 4 or less.	Patterson, 1964; Zehren, 1979

Team, 2016). The sequence data for each gene was opened in Jalview (Waterhouse et al., 2009; version 2.8.2) where it was aligned using ClustalW2 (Larkin et al., 2007). The alignment was then checked by hand and the ends of the sequences were trimmed. Fossil taxa were included within each alignment, but all data was coded as missing. The aligned sequences for the five genes were then combined

Table 3.3: GenBank accession numbers for the five genes used in the molecular dataset

Taxa		Genes				
		RAG1	ZIC1	PLAGL2	MYH6	ENC1
Lepisosteiformes	*Lepisosteus osseus*	AF137185	JN853449	EU002110	JN853376	JN853336
Amiiformes	*Amia calva*	AY430199	EF032909	EF033013	EF032922	EF032974
Elopiformes	*Elops saurus*	JN230876	EU001868	EU002097	EU001903	EU002014
Lepidogalaxiiformes	*Lepidogalaxias salamandroides*	JN232634	JX255596	JX255549	JX190440	–
Salmoniiformes	*Thymallus brevirostris*	JX190834	JX191292	JX190571	JX190444	–
Stomiiformes	*Diplophos taenia*	EU366724	EU366768	EU366676	FJ918866	EU366630
Osmeriformes	*Aplochiton zebra*	JN132661	JN132792	JN132591	JX190435	JN132482
Ateleopodiformes	*Ateleopus japonicus*	KC442191	JX191297	JX190575	JX190449	KF139370
Aulopiformes	*Synodus variegatus*	KF141375	EU366762	EU366673	KF140137	KF139375
	Aulopus filamentosus	EU366688	EU366733	EU366642	–	EU366593
	Paraulopus oblongus	EU366709	EU366752	EU366664	–	EU366615
Myctophiformes	*Neoscopelus microchir*	KC442197	JX191303	JX190581	JX190456	KF139376
	Lampanyctus macdonaldi	EU477497	KJ556246	–	KC827301	–
Polymixiiformes	*Polymixia lowei*	JN230906	JX189009	KF140820	KF140087	JX188837
Lampridiformes	*Metavelifer multiradiatus*	EF094949	EU366772	EU366679	–	EU366633
Beryciformes	*Myripristis violacea*	JX190861	JX191320	JX190597	EU001916	EU002026

with the morphological data and saved as a single NEXUS file.

3.2.2.5 Parsimony analyses

PAUP* (Swofford, 2003; version 4.0b10) was used to conduct all parsimony analyses (Appendix A). Both *Amia* and *Lepisosteus* were set as the outgroup in all analyses. For the morphology only dataset, the branch and bound algorithm was used. The heuristic search algorithm was used for the combined morphology and molecular dataset. All analyses using the heuristic search were run using 100 random addition sequence replicates. When more than one tree was retained a strict consensus tree was calculated. The consistency index, homoplasy index, retention index and the rescaled consistency index were also calculated using PAUP*. I calculated bootstrap (Bs) support values, using a bootstrap search that was run for 1000 replicates and used the heuristic search option. Bremer indexes (BI) were manually calculated in PAUP*. I initially conducted a heuristic search and generated a strict consensus tree to get the tree length. I then ran additional heuristic searches, increasing the tree length by one each time. After each additional heuristic search

a strict consensus tree was generated. This process was repeated, increasing the tree length each time, until all clades in the consensus tree had collapsed. Clades only present in the original heuristic tree were assigned a Bremer index of one. As the tree length was increased, the Bremer index value being tested was increased by the same value. Any clades still present in a consensus tree had a Bremer index of the value being tested, or greater.

3.2.2.6 Bayesian analyses

All Bayesian phylogenetic analyses were conducted in MrBayes (Huelsenbeck and Ronquist, 2001; version 3.2.6) (Appendix A). As only one taxon can be set as the outgroup, all taxa except the holosteans (*Amia* and *Lepisosteus*) were constrained to form a monophyletic group. Each of the five genes and the morphological dataset were treated as different partitions. Each gene was also split into three partitions, based on codon position.

For the morphological data (in both the morphology only and combined analyses), a single substitution rate (`nst = 1`) was used, with among-site rate distribution gamma distributed. A GTR model, where the rate of substitution was variable across sites, (`nst = 6`) was used with an invariable gamma distribution for the molecular partitions. The substitution rates of the GTR model, the character state frequencies, the gamma shape and the proportion of invariable sites were unlinked across partitions. The rates were also allowed to vary across partitions (`ratepr = variable`).

The morphology only and combined datasets were analysed using the Markov chain Monte Carlo (MCMC) algorithm. Two independent runs were performed for each analysis. Each run had three heated chains and one cold chain. The chain was sampled every 500 generations. The first 25% of each sample was discarded as burn-in. The morphology only and combined analyses were run for 1.5 and 6 million generations respectively. Both datasets were run until the standard deviation of split frequencies were ≤ 0.01, the potential scale reduction factor (PSRF) values were 1 ± 0.005 and minimum effective sample sizes (ESS)

Table 3.4: Criteria for interpreting Bayes factors (after Kass and Raftery, 1995)

$2 \log_e(\mathrm{BF})$	Interpretation
0 – 2	No/weak support
2 – 6	Positive support
6 – 10	Strong support
>10	Very strong support

were >200. The `sumt` command was used to generate a majority rule consensus tree with posterior probabilities (PP).

3.2.3 Hypothesis testing

Topological hypothesis tests were undertaken to evaluate support for several phylogenetic placements for key taxa. The choice of hypotheses to be tested was decided after the phylogenetic analyses had been completed. The stepping-stone algorithm (Xie et al., 2011), implemented in MrBayes, was used for all hypothesis tests. Each hypothesis was tested twice, once with each dataset. Each analysis was run for 50 steps, with a burn-in stage prior to commencing the first step. Each step contained 200,000 and 500,000 generations for the morphology only and the combined analyses respectively. The burn-in stage was equal to the length of one step. At the beginning of each step the first 25% of samples were also discarded as burn-in. All other parameters were set as described above for the MCMC analyses. The standard deviation of split frequencies was ≤ 0.03 for each step. For each hypothesis, the marginal log likelihoods were compared using Bayes factors (Kass and Raftery, 1995). Bayes factors were interpreted using the criteria set out by Kass and Raftery (1995) (Table 3.4), which are commonly used when undertaking phylogenetic hypothesis tests (e.g. Bergsten et al., 2013; Dembo et al., 2015). The Bayes factors were calculated by taking the difference between the marginal log likelihoods from the two hypotheses been compared, and then multiplying it by two.

3.3 Systematic palaeontology

3.3.1 †*Aulolepis typus*

Infraclass **Teleostei** Müller, 1846

Subcohort **Neoteleostei** Nelson, 1969

Infracohort **Eurypterygii** Rosen, 1973

Section **Ctenosquamata** Rosen, 1973

Order †**Ctenothrissiformes** Patterson, 1964

Family †**Aulolepidae** Patterson, 1964

Genus †***Aulolepis*** Agassiz, 1844

†***Aulolepis typus*** Agassiz, 1844

(Figs. 3.1, 3.2, 3.3, 3.4, 3.5, 3.6, 3.7)

1844 †*Aulolepis typus* Agassiz: 109, pl. lx a, figs 5 – 8.

1888 †*Aulolepis typus* Agassiz; Woodward: 324.

1895 †*Aulolepis typus* Agassiz; Woodward: 660 (in part), pl. XLIII, figs 4, 6.

1900 †*Aulolepis typus* Agassiz; Woodward: 324, pl. IX, fig. 2.

1901 †*Aulolepis typus* Agassiz; Woodward: 127.

1903 †*Aulolepis typus* Agassiz; Woodward: 85, pl. XIX, figs 3 – 4.

1964 †*Aulolepis typus* Agassiz; Patterson: 247, figs 14 – 22.

1968 †*Aulolepis typus* Agassiz; Patterson: 53, figs 2 – 3.

1973 †*Aulolepis typus* Agassiz; Rosen: 464, figs 81, 87.

Diagnosis. †Ctenothrissiform, and only species in the family †Aulolepidae, reaching approx 20 cm in length. Unlike other non-aulopiform eurypterygians, †*Aulolepis* possesses an elongated uncinate process of the second epibranchial. Differs from other ctenosquamates, in not having a subocular shelf on any of the infraorbitals. Similar to †*Pattersonichthys*, but different from other ctenosquamates, in having more than two branchiostegals (four) articulating with the posterior ceratohyal. Unlike †Ctenothrissidae, Myctophiformes and Acanthomorpha in having the parietals in contact for most of their length, and not separated by the supraoccipital. †*Aulolepis*

also differs from those taxa in not having a ridge or fossa for the supratemporal to articulate with the neurocranium. Alongside †Ctenothrissidae, differs from crown ctenosquamates with the two halves of the first neural arch not being fused to one another.

Material examined. SMESC B. 9092 (Fig. 3.1), a three-dimensionally preserved articulated specimen, containing the cranial region and most of the trunk. Much of the dorsal region of the trunk and the caudal fin are missing. The left side of the fossil has been extensively prepared.

Occurrence. Cenomanian English Chalk. SMESC B. 9092 is one of at least 13 known specimens from the English Chalk. SMESC B. 9092 is from the Lower Chalk of Southerham Lewes, UK (Woodward, 1900). †*Aulolepis* is also known from three other English Chalk localities: Burham, Dorking and Brighton. The Lower Chalk at Southerham is Cenomanian in age (Friedman et al., 2016). Woodward (1903) described the Burham and Dorking localities as of the zone of †*Holaster subglobosus*, which is also Cenomanian in age (Friedman et al., 2016). These localities correspond with the Zig Zag Chalk and West Melbury Formations of the Grey Chalk Subgroup (Hopson, 2005; Friedman et al., 2016).

Remarks. Diedrich (2012, 2014) also reports that †*Aulolepis typus* has been found in Upper Cenomanian deposits of Halle and Lengerich, Westphalia, Germany. However, available figures are insufficient to determine whether this attribution is correct.

3.3.1.1 Description

The description of †*Aulolepis* by Patterson (1964) is generally detailed, although the description of some important features, such as the branchial arches, is lacking. This description should be regarded as a supplement to Patterson's description that corrects errors and provides additional details. The following description is primarily based on µCT scans of SMESC B. 9092. There is a large accumulation

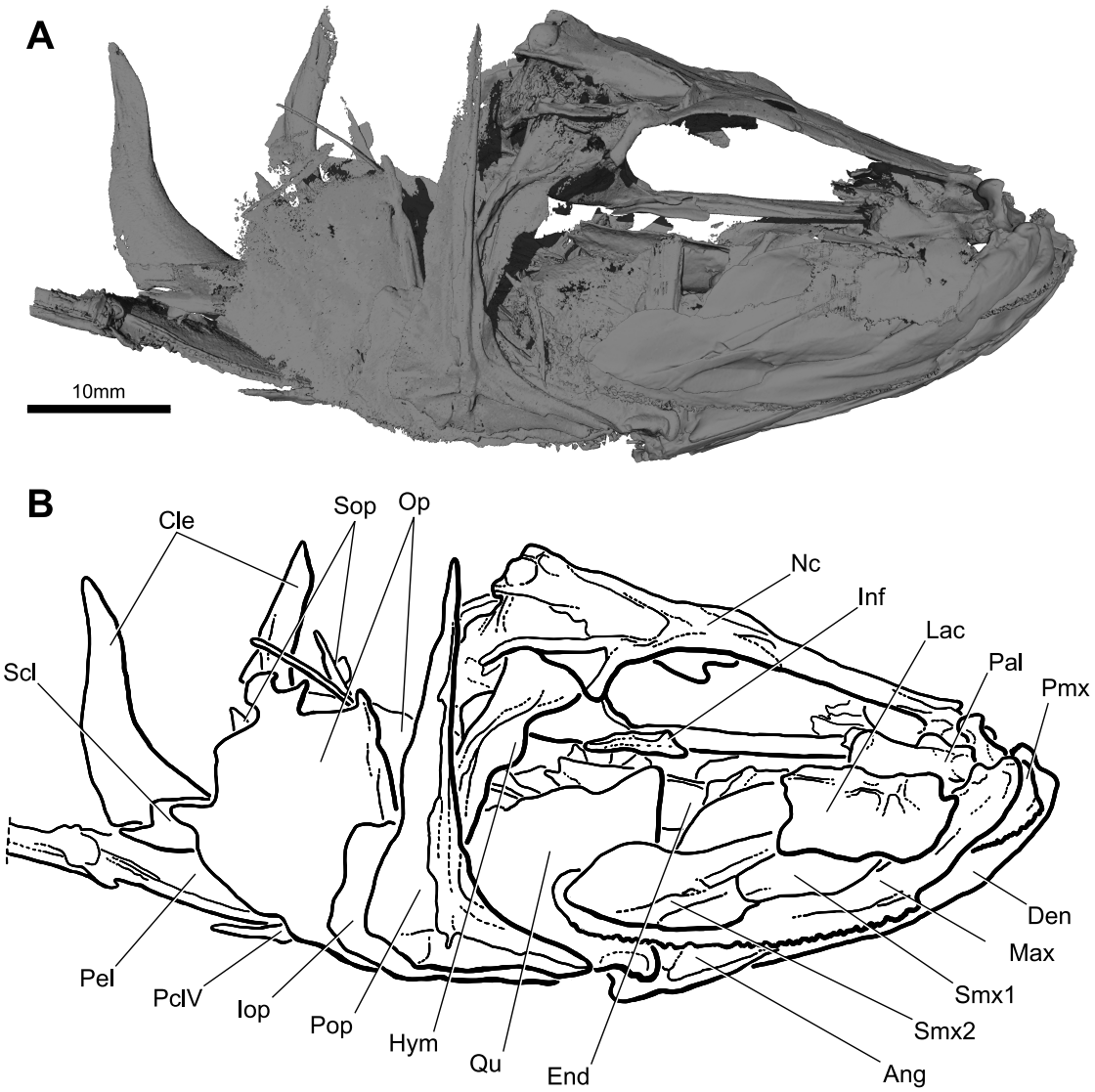

Figure 3.1: †*Aulolepis typus* SMESC B. 9092. Scale bar represents 10 mm. **A,** computed tomography scan in right lateral view. **B,** interpretative drawing.

of a dense material in this fossil that has destroyed some internal anatomy of the skull, particularly that of the left hand side of the specimen.

Infraorbital series. Four suborbital bones are visible, one of which is the lacrimal (Fig. 3.1). These bones are feeble and poorly ossified, so it is likely that more may have been present in life. There is no evidence of a subocular shelf on any of the suborbital bones. Patterson (1964) did not mention the presence of subocular shelves on the infraorbitals, so presumably he did not observe them either.

Patterson (1964: p. 250) refers to the antorbital as "an oval bone... [that]

articulates with the edge of the frontal and lateral ethmoid", and "ends in a thickened process which meets the lacrimal". In Patterson's figures of †*Aulolepis* (fig. 14), and †*Ctenothrissa* (figs. 2 – 3), the bone he refers to in text as the antorbital is labelled with the abbreviation "so". Patterson's justification for the bone being the antorbital was that in both †*Ctenothrissa* (p. 223) and †*Aulolepis* (p. 250) the infraorbital canal extended to this bone, and was homologous to the antorbital of primitive teleosts. Gaudant (1978c) re-examined Patterson's specimens and could not find a groove for the sensory canal. In her examination of two Lebanese species of †*Ctenothrissa*, Gaudant (1978c: figs. 1, 2; plate 2, fig. 2) observed and figured the true antorbital and refers to Patterson's 'antorbitals' as supraorbitals. Gaudant cited the similarity between the morphology of the supraorbital in *Elops* (Forey, 1973) and salmoniforms (Patterson, 1970), and Patterson's 'antorbital' as evidence that the bone is actually the supraorbital. There is also a strong resemblance, in terms of the size, shape and location of the bone, between Patterson's 'antorbital' and the supraorbital in stem teleosts (†*Tharsis*: Nybelin, 1974: fig. 23) and aulopiforms (*Aulopus*: Goody, 1969: fig. 88). Based on the above evidence, I am in agreement with Gaudant (1978c) that Patterson's original interpretation appears to be incorrect. To summarise, †*Aulolepis* does possess a supraorbital, but the nasals and true antorbitals, if they were present, are not known.

Hyoid arch. The description of the hyoid arch and branchiostegals presented by Patterson (1964) appears to be accurate. However, while Patterson (1964) figured the hyoid arch, he did not show the branchiostegals, either alone or in articulation with the hyoid arch. A figure of the branchiostegals in articulation with the hyoid arch is given in Figure 3.2 as a complement to Patterson's account. As described by Patterson, I also found that five and four of the branchiostegals articulated with anterior and posterior ceratohyals respectively.

Branchial arches. The branchial skeleton is relatively complete (Fig. 3.3). Bones preserved include two basibranchials, three hypobranchials, five ceratobranchials, four epibranchials and three pharyngobranchials.

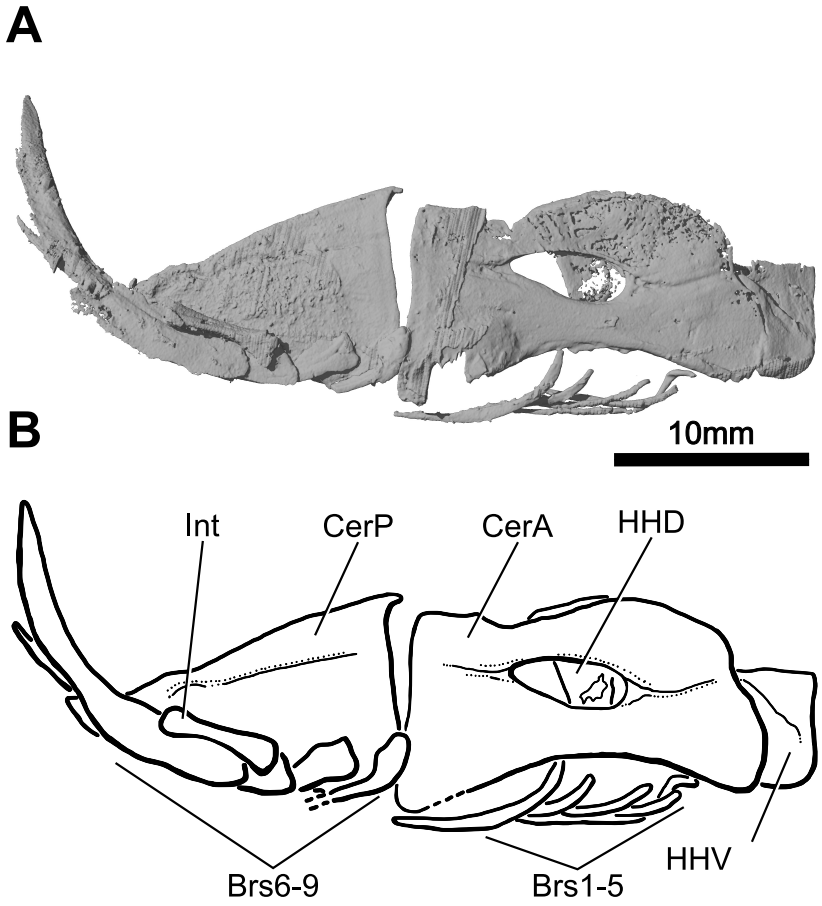

Figure 3.2: Hyoid arch of †*Aulolepis typus* SMESC B. 9092. Scale bar represents 10 mm. **A,** computed tomography scan in right lateral view. **B,** interpretative drawing.

The basihyal and basihyal toothplate are not preserved. The second and third basibranchials are preserved (Fig. 3.3). Basibranchials one and the typically cartilaginous basibranchial four are not preserved. The posterior of the large second basibranchial is not completely preserved. It has teeth on its dorsal surface. However these can only be seen towards the posterior of the bone and not along the full length as described by Patterson (1964). The third basibranchial appears to be slightly shorter than the second. It is broken and generally poorly preserved.

The three hypobranchials are preserved (Fig. 3.3). The first hypobranchial is a long, straight bone that articulates with the second basibranchial and the first ceratobranchial. There is a groove running along most of the length of the ventral surface of this bone. Only a small part of the second hypobranchial is preserved; most of it has been obscured by a dense mineral accumulation. Not

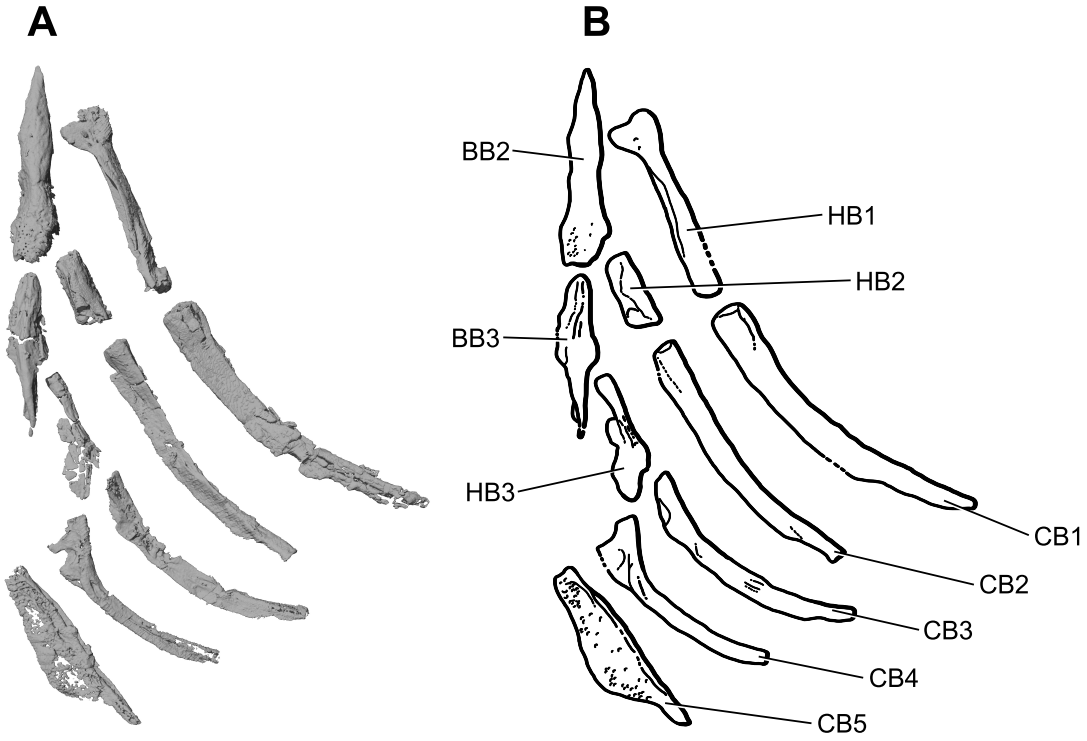

Figure 3.3: Ventral branchial skeleton of †*Aulolepis typus* SMESC B. 9092. The elements of the gill skeleton are disarticulated and have been rearranged here. Scale bar represents 5 mm. **A,** computed tomography scan in dorsal view. **B,** interpretative drawing.

much can be said of this bone except that it also bears a groove along its ventral surface. The third hypobranchial is much shorter than the first. It has a large posterior-lateral facet for articulation with the third ceratobranchial. The third hypobranchial tapers in towards the anterior apex where it presumably articulates with the third basibranchial.

There are five ceratobranchials (Fig. 3.3). The first ceratobranchial is the longest, with each subsequent ceratobranchial shorter than the former. Ceratobranchials one to four each have a large ventral groove running along the length of the bone. The anterior ends of the first three ceratobranchials articulate with the corresponding hypobranchials. The third and fourth ceratobranchials presumably articulated directly with a cartilaginous basibranchial four. The posterior ends of the first four ceratobranchials articulate with the corresponding epibranchials. There is a large toothplate on the dorsal surface of the fifth ceratobranchial. The toothplate extends posteromedially from the main body of the ceratobranchial and

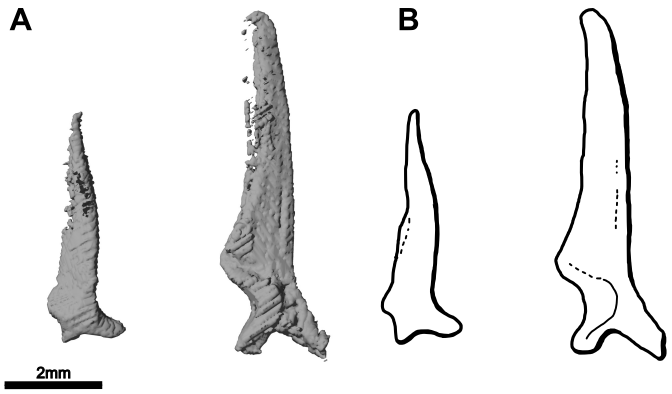

Figure 3.4: Gill rakers of †*Aulolepis typus* SMESC B. 9092. Scale bar represents 2 mm. **A,** computed tomography scan. **B,** interpretative drawing.

is covered with small denticles. This toothplate corresponds with the overlying upper pharyngeal toothplates.

The branchial skeleton bears well-developed gill rakers (Fig. 3.4). They are of varying size with the largest almost half the length of the first ceratobranchial. The gill rakers are blade-like in appearance, with a moulded base for articulation with the ceratobranchials. The gill rakers are not preserved in articulation with the ceratobranchials, so it is not possible to say how they were arranged in life.

Four epibranchials are preserved (Fig. 3.5). Each of the four epibranchials has a large groove running along the length of the bone. The posterior end of each epibranchial articulates with the posterior end of the corresponding ceratobranchial. The first epibranchial is the largest of the four. It articulates with the first pharyngobranchial dorsally. It has a moderately-sized uncinate process that articulated with the uncinate process of the second pharyngobranchial. The second epibranchial is an L-shaped bone, approximately two-thirds the length of the first epibranchial. The anterior end articulates with the second pharyngobranchial. There is a medially-directed elongated uncinate process that appears to have articulated directly with the third pharyngobranchial. The third epibranchial is slightly longer than the second, reaching three-quarters of the length of the first. The anterior end of this bone articulated with the posterior of the third pharyngobranchial and possibly the fourth pharyngobranchial as well. There is no evidence of an uncinate process or any dentition on this bone. The fourth epibranchial is much smaller than the

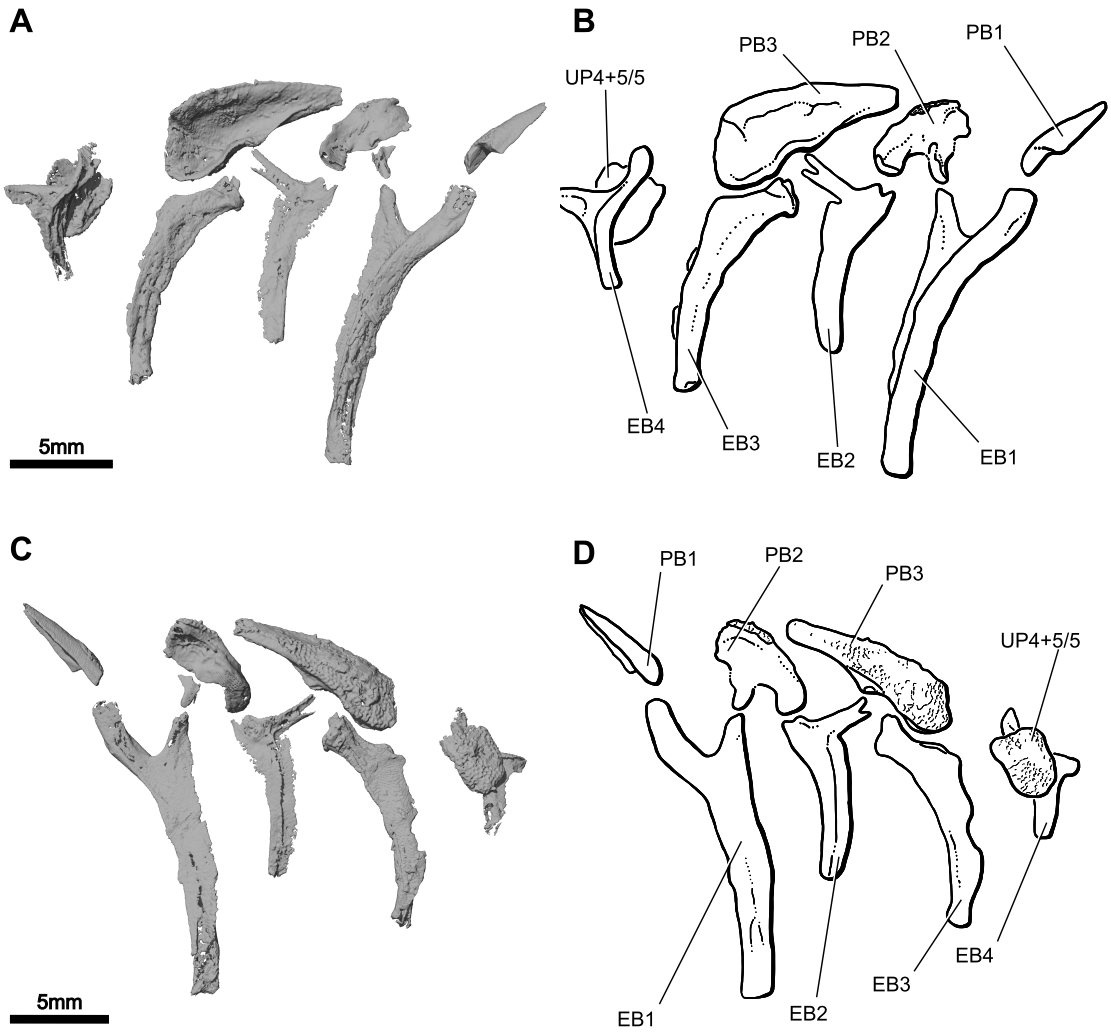

Figure 3.5: Dorsal branchial skeleton of †*Aulolepis typus* SMESC B. 9092. The elements of the gill skeleton are disarticulated and have been rearranged here. Scale bars represent 5 mm. **A,** computed tomography scan in dorsal view. **B,** interpretative drawing of A. **C,** computed tomography scan in ventral view. **D,** interpretative drawing of C.

others. It has a less well-defined groove, a slender posterior end and a small uncinate process. There is a toothplate on the dorsal surface of this bone. It appears to be either upper pharyngeal toothplate five or toothplate four fused to toothplate five. Its close association with epibranchial four suggests it is unlikely to be just upper pharyngeal toothplate four. This toothplate may be two individual toothplates (i.e. UP4 and UP5) fused together, although it is difficult to say with any certainty. Rosen (1973: fig. 81) figures two of the upper pharyngeal toothplates, one of which he labels as UP4. However, he does not figure the epibranchials, so it is not possible to say whether Rosen's UP4 is the same as the toothplate seen in this specimen.

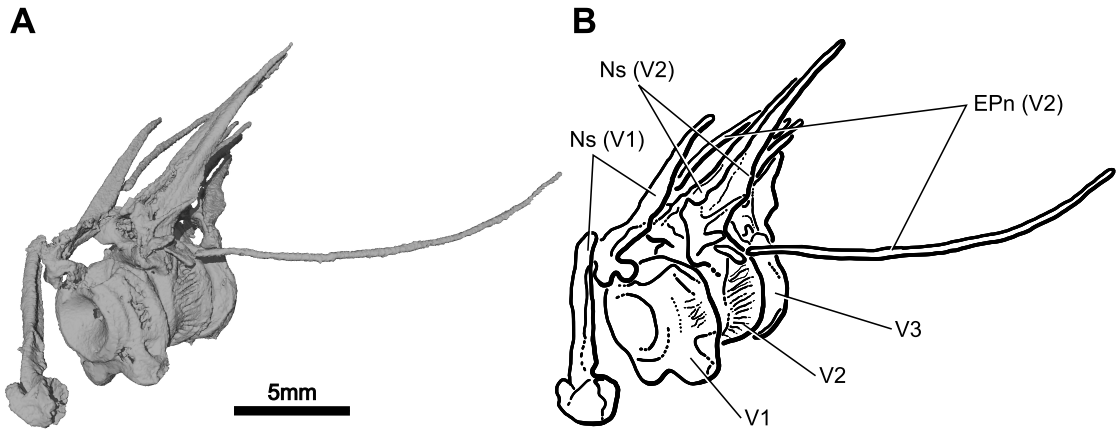

Figure 3.6: Anterior vertebrae of †*Aulolepis typus* SMESC B. 9092. Scale bar represents 5 mm. **A,** computed tomography scan in anterior-left lateral view. **B,** interpretative drawing.

Pharyngobranchials one to three are preserved (Fig. 3.5). Pharyngobranchial four is not preserved, although it is always cartilaginous (Nelson, 1969; Rosen, 1973). The unremarkable first pharyngobranchials are small and deeply concave on one side. These bones presumably articulated with the first epibranchial, although their life orientation is not clear. The posterior end of the second pharyngobranchial articulates with the second epibranchial. This bone has a small laterally directed uncinate process for articulation with the first epibranchial. The second upper pharyngeal toothplate is fused to the ventral surface of this bone. The third pharyngobranchial is a large bone with the third upper pharyngeal toothplate tightly fused to its ventral surface. The uncinate process of the second epibranchial articulated directly with the dorsal surface of the third pharyngobranchial.

Vertebral column. The vertebral column and its associated structures are highly disarticulated posteriorly. The two halves of the first neural arch are separate from one another and are not attached to the first vertebra. Only the first neural arch appears to be autogenous, unlike that of the specimen described by Patterson (1964: p. 260; NHM P. 10458), where the first few neural arches are described as autogenous. Patterson (1964: p. 260) indicates that the first two vertebrae bear intermuscular bones, but it is not clear from his description whether they bear both epineurals and epipleurals. In SMESC B. 9092, the only intermuscular

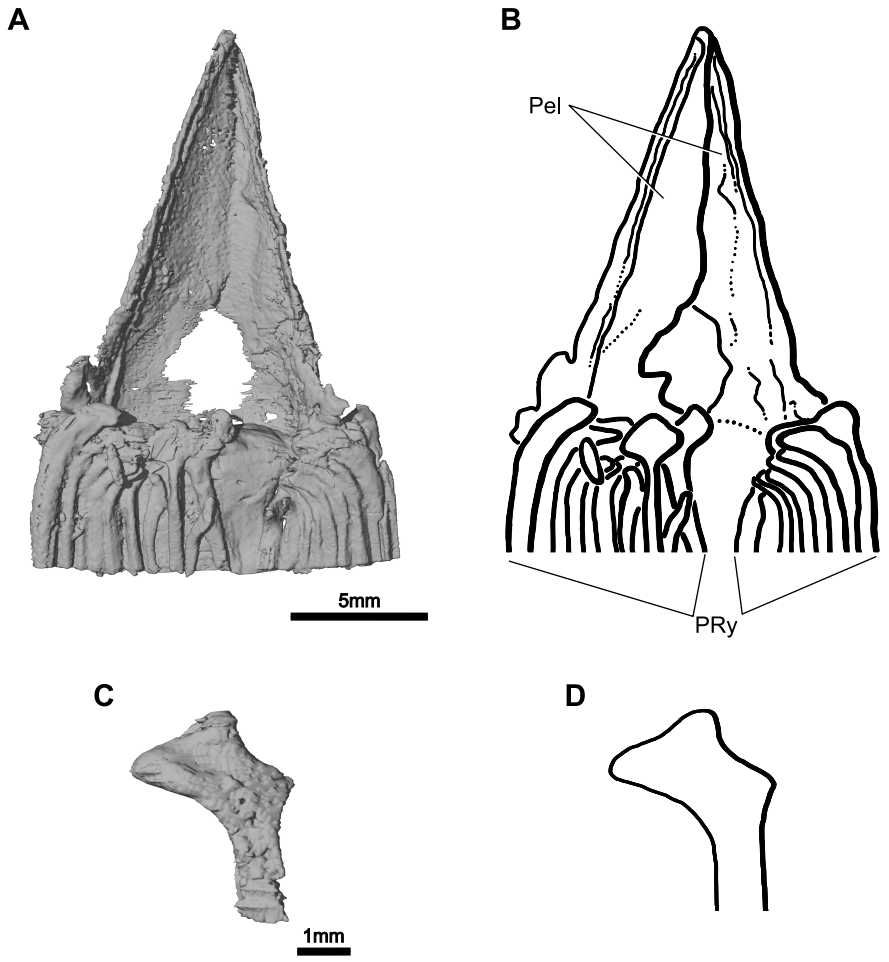

Figure 3.7: Pelvic girdle of †*Aulolepis typus* SMESC B. 9092. **A,** computed tomography scan of the pelvic girdle in ventral view. Scale bar represents 5 mm. **B,** interpretative drawing of A. **C,** computed tomography scan of the medial pelvic ray, fused to the medial pelvic radial. Scale bar represents 1 mm. **D,** interpretative drawing of C.

bones preserved in articulation are the epineurals of the second abdominal vertebra (Fig. 3.6). These epineurals articulate with — but are not fused to — the neural arch. It is not possible to say which neural arches the epipleurals articulated with, or where they originated (i.e. above or below the horizontal septum).

Pelvic girdle. Both pelvic bones and the pelvic rays are preserved (Fig. 3.7a – b). Patterson (1964: fig. 22, p. 261 – 262) figured and described the pelvic bones of †*Aulolepis*. However, he did not show the articulation between the pelvic bones, nor the fin rays, either alone or in articulation with the pelvic bones. Unfortunately, the posterior processes of the pelvic bones were not captured in the µCT scan, but these

Table 3.5: Morphological character matrix.

Taxa	Characters										
	1–5	6–10	11–15	16–20	21–25	26–30	31–35	36–40	41–45	46–50	51–55	56
Lepisosteus	0000-	00-0-	01100	?0010	0100?	00001	0-0-0	00000	00001	10000	00000	2
Amia	00000	00000	00000	01011	00010	00000	0-0-1	00000	00001	10000	00000	2
†*Tharsis*	000?0	?0000	0?01?	00000	00???	?1???	?????	?0?00	00100	0?0??	00000	0
Elops	00000	00000	00010	00010	02201	00001	00100	00010	10110	00010	01000	0
Lepidogalaxias	0001?	?1000	0?211	11-11	10010	01000	?-??0	10010	01311	10130	00000	3
Thymallus	0000?	01000	00010	00010	10011	0◇001	00101	10110	11111	10010	02000	0
Diplophos	00010	?1000	00010	00010	02121	?0001	00100	10011	11211	10010	01000	1
Aplochiton	00000	01010	0?21?	11011	12011	00001	000-0	10111	01211	1013	00000	2
Ateleopus	0011-	01000	??210	10011	12001	00100	010-3	10011	21011	11102	?0110	3
Synodus	00010	000?0	0121?	10010	11001	?◇001	0121?	10111	11211	11121	01111	1
Aulopus	00010	0◇000	01211	10010	11131	01001	01213	10111	1121◇	01111	01111	1
Paraulopus	00010	00000	?1211	10010	11131	0100◇	00103	10111	11210	11121	01011	1
Neoscopelus	00111	11011	00211	11111	?2120	12010	11102	10111	11210	11121	02001	1
Lampanyctus	00110	11011	00211	11111	12120	12010	1?10?	?0111	1121?	11121	02001	1
Polymixia	11111	10110	10211	11101	12120	02100	11103	01011	01211	11121	11001	2
†*Berycopsis*	11111	10110	1?211	11101	1????	?21?0	?????	01011	01211	111?1	1100?	2
Myripristis	11111	10110	10211	◇1111	12120	02100	1-203	01011	11211	11121	110?1	1
Veliferidae	10111	?0111	11211	11011	?2020	?2100	110-3	01011	11211	11101	11001	1
†*Aulolepis*	00011	00010	00011	00000	11021	02000	01???	?0011	1121?	01121	01001	1
†*Ctenothrissa*	00111	10010	00011	00101	1????	?20?0	0???3	00011	◇121◇	01121	1100?	1
†*Pattersonichthys*	000?0	?10?0	0?011	01100	1????	?2??0	????3	0?011	11210	01121	0100?	1

◇ Multiple states present (0 and 1)

are shown in Patterson's figure. No foramen can be seen in the pelvic bones. The ventral half of the medial pelvic ray is fused to the medial pelvic radial (Fig. 3.7c – d).

3.4 Phylogenetic analyses

3.4.1 Morphology only dataset

3.4.1.1 Parsimony

Analysis of the morphological data alone (Table 3.5), using parsimony, does not result in a fully resolved tree (Fig. 3.8). Acanthomorph and myctophiform monophyly are strongly supported (Bs $\geq$ 93; BI = 4). These clades are united as crown ctenosquamates with a moderate level of support (Bs = 66; BI = 2). †*Ctenothrissa* is recovered as the immediate sister taxon to crown ctenosquamates, although this

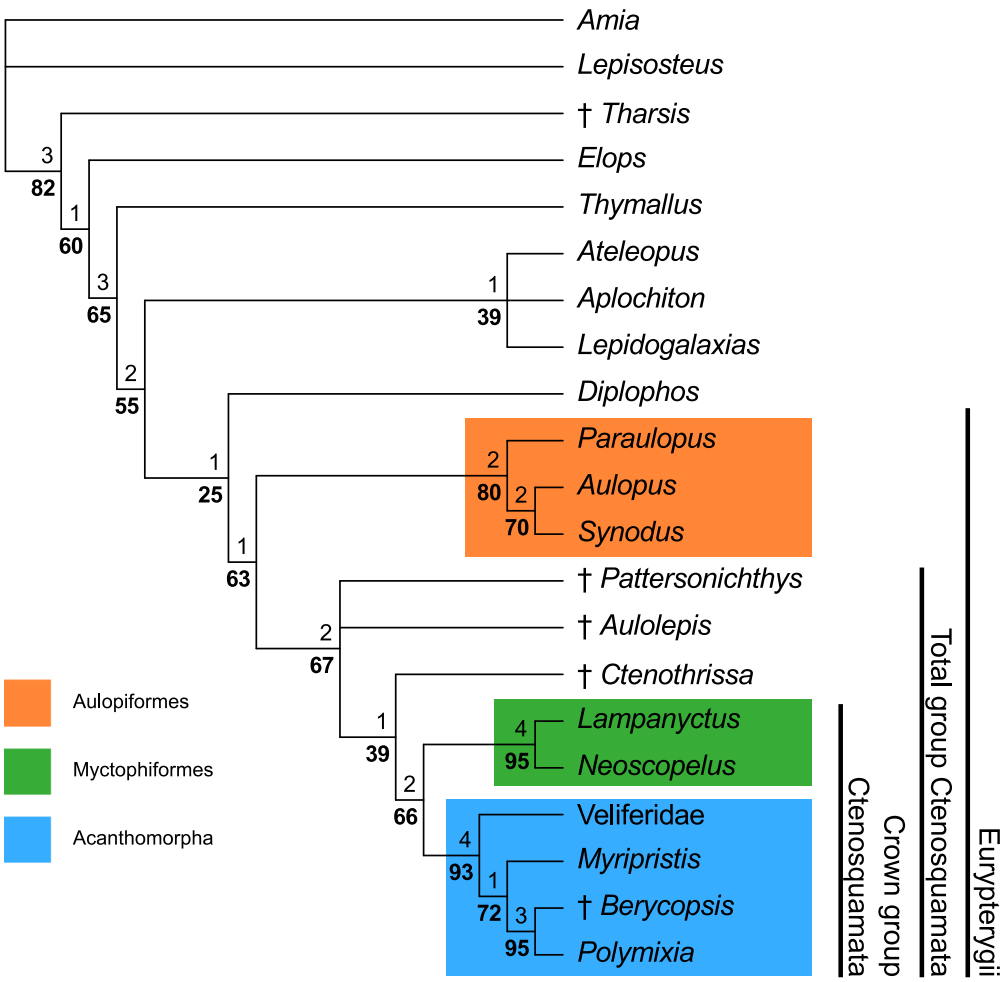

Figure 3.8: Strict consensus tree of four parsimonious trees using the morphology only dataset. Tree length = 154, consistency index = 0.48, homoplasy index = 0.52, retention index = 0.71, rescaled consistency index = 0.34. Numbers above branches are Bremer index support values, those below branches are Bootstrap support values.

placement is weakly supported (Bs = 39; BI = 1). †*Ctenothrissa* + crown-group Ctenosquamata, †*Aulolepis* and †*Pattersonichthys* are united in an unresolved polytomy, with moderate support (Bs = 67; BI = 2). Aulopiforms are recovered as monophyletic (Bs = 80; BI = 2) as is Eurypterygii (Bs = 63; BI = 1). The stomiiform *Diplophos* is recovered as the sister group to Eurypterygii. The atelopodiform *Ateleopus*, the galaxiid *Aplochiton* and the lepidogalaxiid *Lepidogalaxias* are placed in a polytomy that branches below the *Diplophos* + Eurypterygii clade. The salmoniform *Thymallus* is the sister taxon to all aforementioned taxa, and the most deeply branching euteleost.

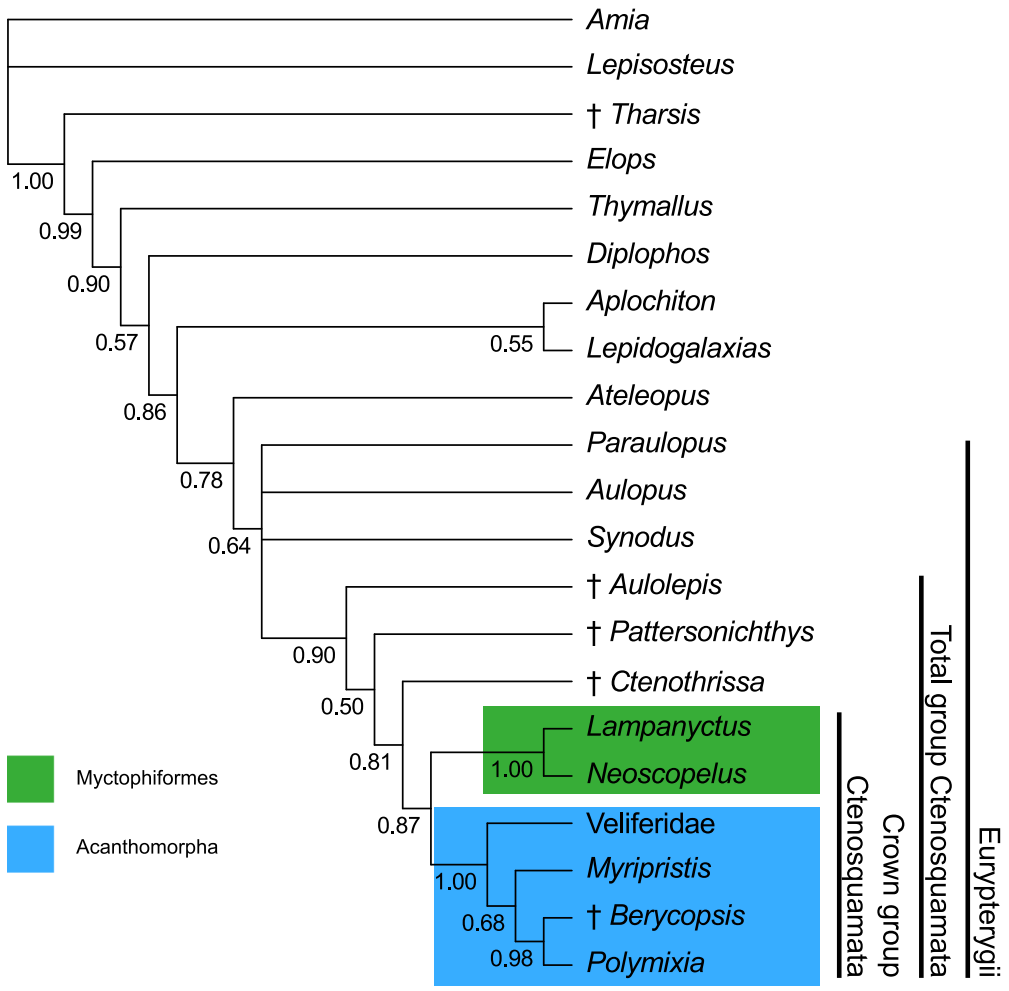

Figure 3.9: Majority rule consensus tree from the Bayesian morphology only dataset. Numbers below branches are posterior probabilities.

3.4.1.2 Bayesian

The Bayesian tree is more resolved than the parsimony tree (Fig. 3.9). Monophyletic Acanthomorpha and Myctophiformes are strongly supported (PP = 1.00), as is crown-group Ctenosquamata (PP = 0.87). Once again, †*Ctenothrissa* is recovered as the immediate sister taxon to the crown ctenosquamates; this placement is strongly supported (PP = 0.81). †*Pattersonichthys* is recovered as the sister taxon to †*Ctenothrissa* + crown ctenosquamates with weak support (PP = 0.50). †*Aulolepis* is recovered as the sister taxon to †*Pattersonichthys* + †*Ctenothrissa* + crown-group Ctenosquamata. Total-group Ctenosquamata, including †ctenothrissiforms and the †pattersonichthyiform, is strongly supported (PP = 0.90). Aulopiformes was not

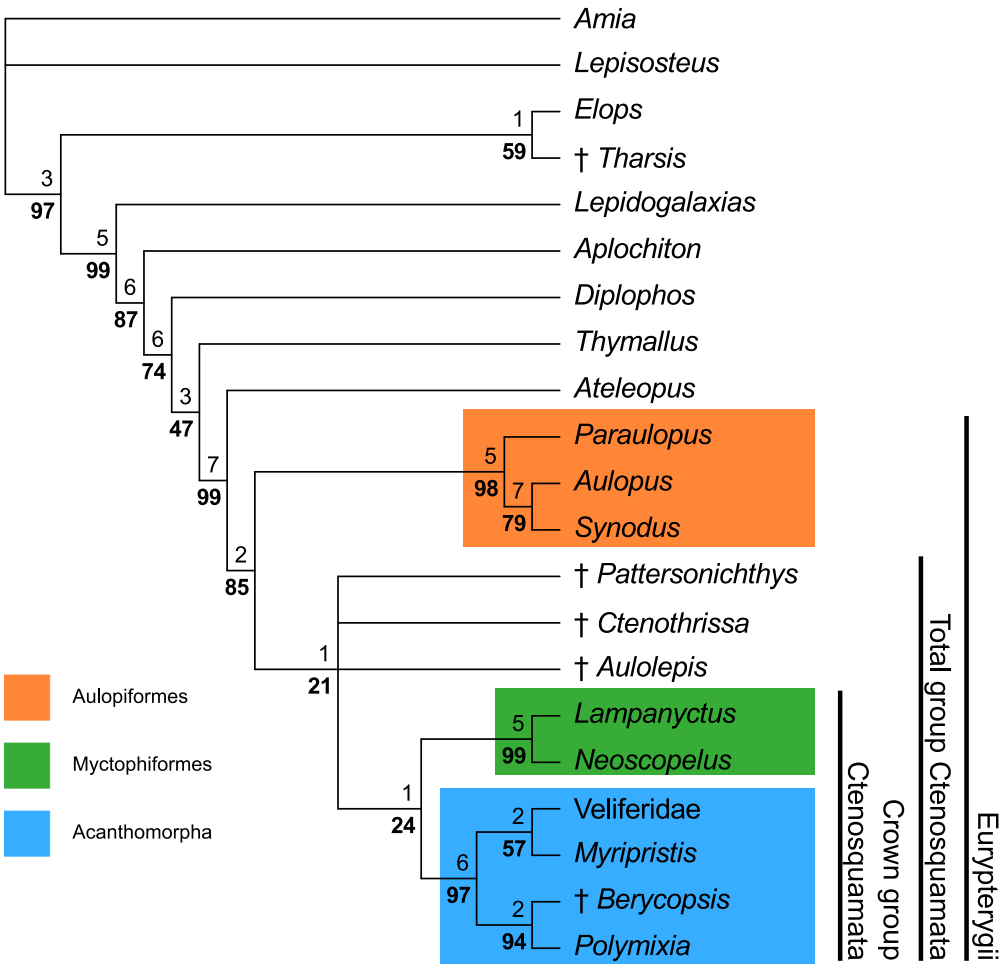

Figure 3.10: Strict consensus tree of five parsimonious trees using the combined dataset. Tree length = 6120, consistency index = 0.56, homoplasy index = 0.44, retention index = 0.38, rescaled consistency index = 0.21. Numbers above branches are Bremer index support values, those below branches are Bootstrap support values.

recovered as a monophyletic group in the 50% credibility tree (PP = 0.37). The aulopiform taxa are placed in a polytomy with a clade comprising all remaining eurypterygians. Eurypterygii as a whole is moderately supported (PP = 0.64). The ateleopodiform *Ateleopus* is recovered as the sister group of Eurypterygii (PP = 0.78). *Aplochiton* and *Lepidogalaxias* are united as a monophyletic group that is the sister group to Eurypterygii + *Ateleopus*. *Diplophos* is the sister group to all the above taxa. *Thymallus* is the sister taxon to all the other euteleosts.

3.4.2 Combined dataset

3.4.2.1 Parsimony

The combined dataset, analysed with parsimony, produced a tree that is fully resolved apart from at the level of the stem ctenosquamates (Fig. 3.10). Acanthomorph, myctophiform and aulopiform monophyly are strongly supported (Bs $\geq$ 97; BI $\geq$ 5). Crown-group Ctenosquamata is recovered in the consensus tree, although it is not strongly supported (Bs = 24; BI = 1). †*Aulolepis*, †*Ctenothrissa* and †*Pattersonichthys* are recovered as stem ctenosquamates, in a polytomy with crown-group Ctenosquamata; total-group Ctenosquamata is weakly supported (Bs = 21; BI = 1). Eurypterygii is recovered as a monophyletic group and it is strongly supported by the bootstrap analysis (Bs = 85), but weakly supported by the Bremer index (BI = 2). *Ateleopus* is recovered as the sister group to Eurypterygii (Bs = 99; BI = 7). All the other euteleosts are arranged as sister taxa to nested monophyletic groups, with *Thymallus* furthest from the root, followed by *Diplophos*, *Aplochtion* and *Lepidogalaxias*.

3.4.2.2 Bayesian

The Bayesian analysis using the combined data produced a similar tree to that of the parsimony analysis, although relationships between taxa are more resolved (Fig. 3.11). Acanthomorpha and Myctophiformes are recovered with very strong support (PP = 1.00). Crown-group Ctenosquamata is well supported (PP = 0.74), and total-group Ctenosquamata, including the †ctenothrissiform and †pattersonichthyiform taxa is reasonably well supported (PP = 0.60). Unlike the results of all the other analyses, the two †ctenothrissiforms and †pattersonichthyiform are united as a monophyletic group, with very strong posterior support (PP = 1.00). The three taxa are arranged in a polytomy but †*Aulolepis* and †*Pattersonichthys* united as sister taxa is the resolution with the highest posterior support (PP = 0.42). All other resolutions, including a monophyletic †Ctenothrissiformes, had lower posterior support (PP = 0.29). Aulopiformes and Eurypterygii are strongly supported (PP $\geq$ 0.94). *Ateleopus* is recovered as the sister group to Eurypterygii

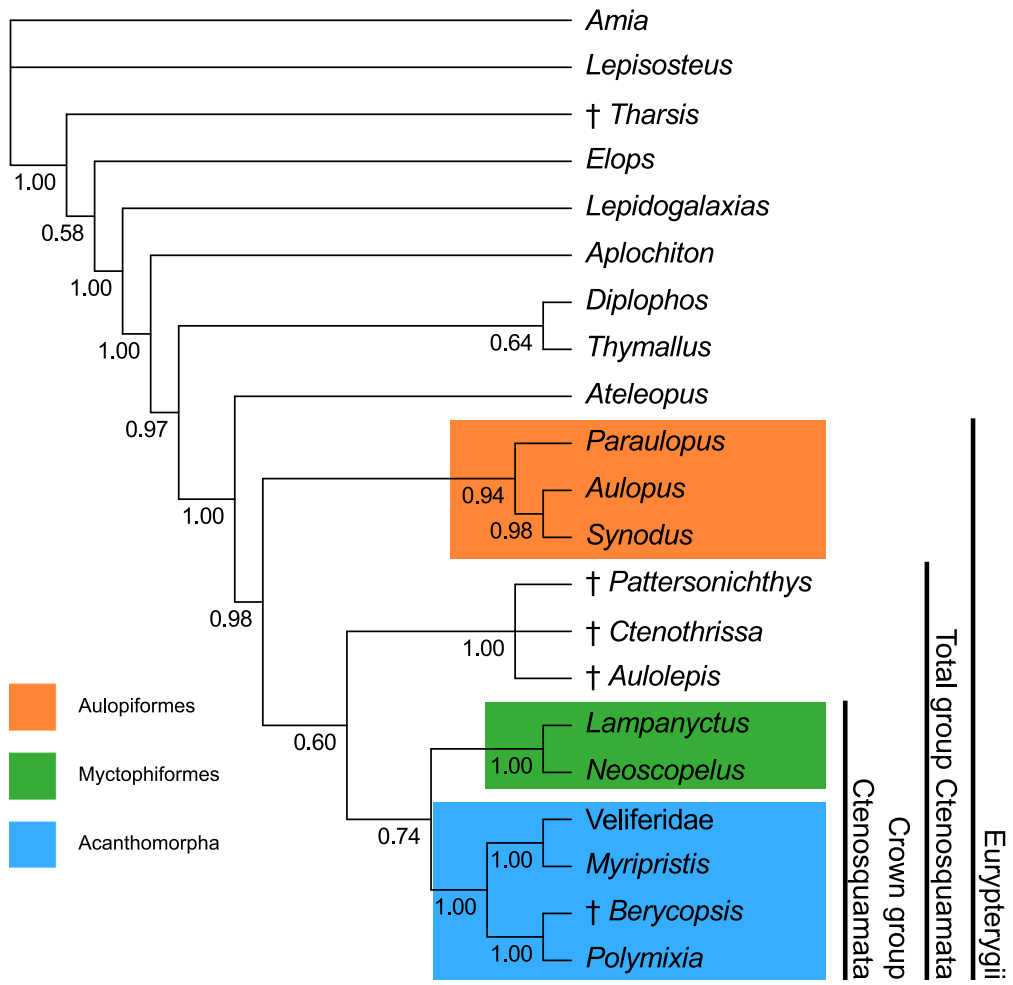

Figure 3.11: Majority rule consensus tree from the Bayesian combined dataset. Numbers below branches are posterior probabilities.

(PP = 1.00). *Diplophos* and *Thymallus* are united as a monophyletic group that is the sister group to Eurypterygii + *Ateleopus*. *Aplochiton* and *Lepidogalaxias* are arranged in the same manner as they are in the parsimony analysis.

3.5 Hypothesis tests

Following on from the results of the phylogenetic analyses, I decided to evaluate seven topological hypotheses (see Figs. 3.12, 3.13 for details of all hypotheses). Five of these hypotheses tested stem-group ctenosquamate placements for the †ctenothrissiform and †pattersonichthyiform taxa. Although none of the four phylogenetic analyses supported an aulopiform placement for these taxa, I decided to test two aulopiform

placements because of the presence of a key aulopiform synapomorphy in †*Aulolepis*: an elongated uncinate process on the second epibranchial (see Discussion).

3.5.1 Morphology only dataset

In the morphology dataset hypothesis tests, the best performing hypothesis was the same as the consensus tree obtained from the Bayesian morphology analysis (Fig. 3.12: H1). In this hypothesis, †*Ctenothrissa* is the sister taxon to crown-group Ctenosquamata, †*Pattersonichthys* is the sister taxon to †*Ctenothrissa* + crown group Ctenosquamata, and †*Aulolepis* is the sister taxon to †*Pattersonichthys* + †*Ctenothrissa* + crown-group Ctenosquamata. The next best hypothesis (H3) was similar to the preferred hypothesis (H1), with the exception of the location of †*Aulolepis* and †*Pattersonichthys*, whose placements were switched. These two hypotheses had similar marginal log likelihoods, and the low Bayes factor (BF = 0.84) indicates that there is no evidence to reject the alternative hypothesis. The third best hypothesis (H4) was the same as the preferred hypothesis, except that †*Aulolepis* and †*Pattersonichthys* were united as a monophyletic group. This hypothesis could not be completely rejected, but performed much worse than the preferred hypothesis (BF = 3.44). There was strong evidence to reject the four remaining hypotheses (BF $\geq$ 6.54), including the two hypotheses where aulopiform placements of the †ctenothrissiform and †pattersonichthyiform taxa were considered.

3.5.2 Combined dataset

As with the morphology only hypothesis tests, in the combined dataset tests the preferred hypothesis (Fig. 3.13: H2) was the same as the result of the corresponding phylogenetic analysis. In this hypothesis, †*Aulolepis*, †*Ctenothrissa* and †*Pattersonichthys* are united as a monophyletic group of stem ctenosquamates. In the next best-performing hypothesis (H7), the †ctenothrissiforms and †pattersonichthyiform are placed in an unresolved polytomy with the aulopiforms. This hypothesis had a small Bayes factor when compared to the best performing hypothesis (BF = 3.02) and could not be completely rejected. There was very strong

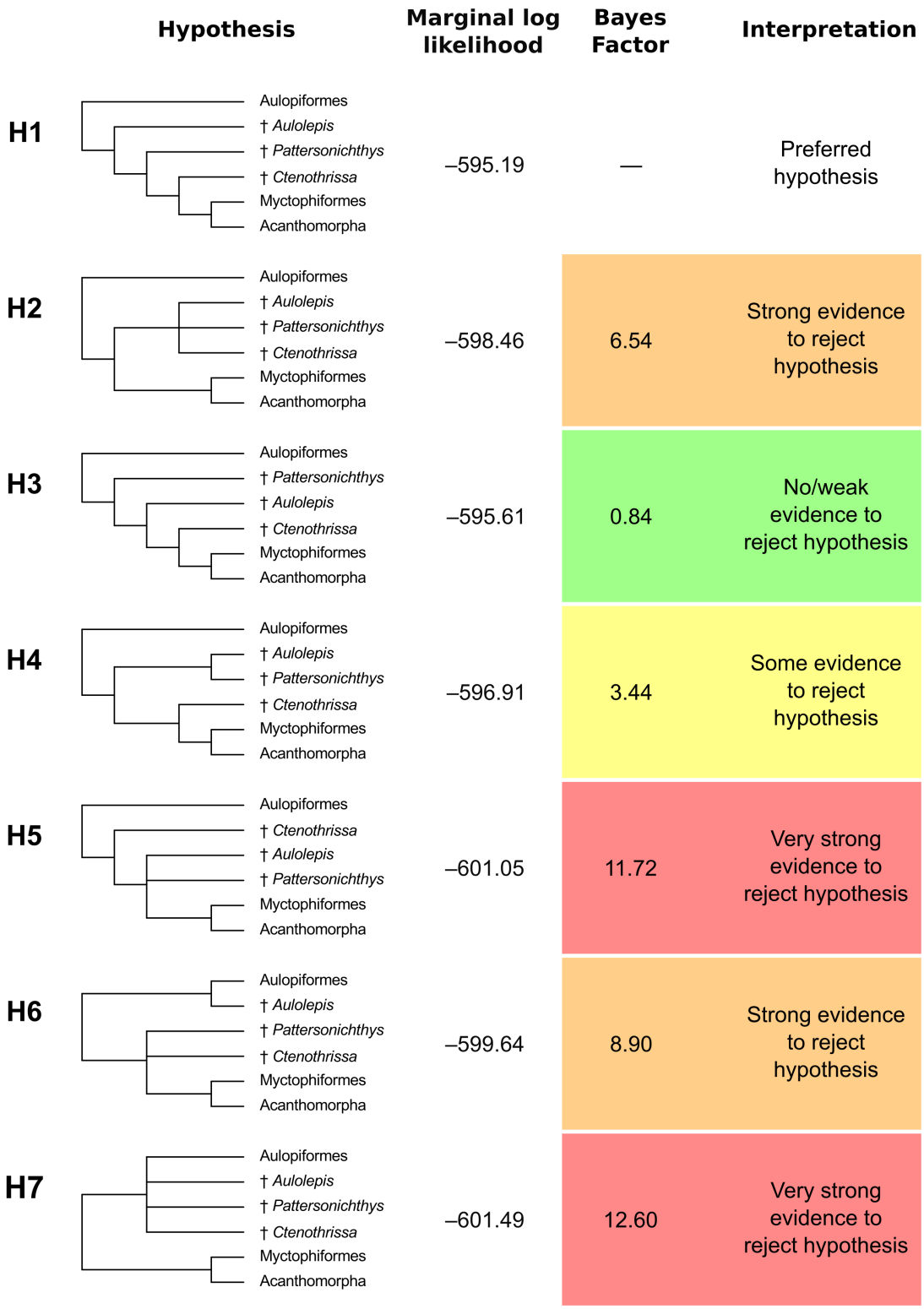

Figure 3.12: Phylogenetic hypothesis tests comparing marginal log likelihoods from Bayesian stepping-stone analyses using the morphology only dataset. The seven phylogenetic hypotheses are compared using Bayes factors, following the criteria established by Kass and Raftery (1995).

evidence to reject the five remaining hypotheses (BF $\geq$ 12.88). In all five of these hypotheses, the analysis was constrained in a way that prevented the †ctenothrissiform and †pattersonichthyiform taxa from forming a monophyletic group.

3.6 Discussion

3.6.1 Characters uniting Neoteleostei

Since Neoteleostei was established (Nelson, 1969), the lineages included within the subcohort have changed. Early interpretations only included Stomiiformes and Eurypterygii in Neoteleostei (Rosen, 1973; Johnson, 1992), before Olney et al. (1993) also placed Ateleopodiformes in the group. Subsequent molecular work has shown that the stomiiforms are not neoteleosts, but rather they are more closely related to osmeriiforms and retropinnids. However, these studies corroborate the placement of Ateleopodiformes as sister group to Eurypterygii (Near et al., 2012; Betancur-R et al., 2013; Near et al., 2013). Olney et al. (1993) justified the neoteleost placement of Ateleopodiformes using three characters: presence of a retractor dorsalis, a third internal levator inserting on UP5 and a tripartite occipital condyle. Here I am able to suggest two more characters that may support neoteleost monophyly (Ateleopodiformes + Eurypterygii). Two of these characters were identified by Regan (1911b) as evidence of affinity between *Ateleopus* and *Aulopus*, but which do not seem to have been discussed in subsequent studies. These two characters are: greatly elongated and widely separated posterior processes of the pelvic bones (character 54), and a pelvic foramen in each of the pelvic bones (character 53). Although these characters appear to unite Ateleopodiformes + Eurypterygii, they are only found in ateleopodiforms and deeply diverging aulopiforms. Therefore, these characters can be optimised in two different ways: as neoteleost synapomorphies, but lost in ctenosquamates and derived aulopiforms, or convergently evolved in ateleopodiforms and aulopiforms, but lost in derived aulopiforms.

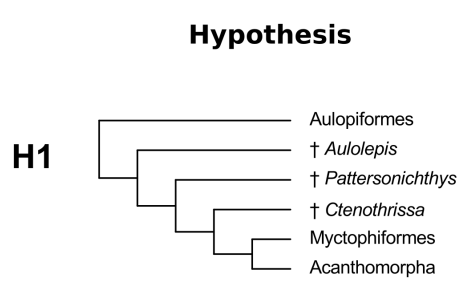

Hypothesis	Marginal log likelihood	Bayes Factor	Interpretation
H1	–30159.83	23.24	Very strong evidence to reject hypothesis
H2	–30148.21	—	Preferred hypothesis
H3	–30160.44	24.46	Very strong evidence to reject hypothesis
H4	–30154.65	12.88	Very strong evidence to reject hypothesis
H5	–30158.36	20.30	Very strong evidence to reject hypothesis
H6	–30156.73	17.04	Very strong evidence to reject hypothesis
H7	–30149.72	3.02	Some evidence to reject hypothesis

Figure 3.13: Phylogenetic hypothesis tests comparing marginal log likelihoods from Bayesian stepping-stone analyses using the combined dataset. The seven phylogenetic hypotheses are compared using Bayes factors, following the criteria established by Kass and Raftery (1995).

3.6.2 †Ctenothrissiformes and †Pattersonichthyiformes as eurypterygians

There are five eurypterygian synapomorphies, only two of which are applicable to fossil taxa: the ventral medial pelvic ray is fused to the medial half of the medial pelvic radial (Johnson, 1992; character 55) and a tooth plate fused to the third epibranchial (Johnson, 1992; character 23). The presence of these characters could not be confirmed in †*Ctenothrissa* or †*Pattersonichthys*. In †*Aulolepis*, the ventral medial pelvic ray is fused to the medial pelvic radial, but a tooth plate is not fused to the third epibranchial. However, third epibranchial toothplates are completely absent in some eurypterygians, including some deeply diverging aulopiform lineages (Johnson, 1992) and some percomorphs (Johnson, 1984, 1992). In all of my phylogenetic analyses, the †ctenothrissiform and †pattersonichthyiform taxa were recovered as crown-group eurypterygians (see below).

3.6.3 †Ctenothrissiformes and †Pattersonichthyiformes as stem aulopiforms

†*Aulolepis*, and other ctenothrissiforms, have not previously been attributed to Aulopiformes. †*Aulolepis* possesses one of the key aulopiform synapomorphies: an elongated uncinate process on the second epibranchial (character 22). The status of this character could not be confirmed in †*Ctenothrissa* and †*Pattersonichthys*. Of the seven synapomorphies and three possible synapomorphies of Aulopiformes (Wiley and Johnson, 2010), only three of these ten characters can be directly observed in fossils: an elongated uncinate process on the second epibranchial (character 22), epipleurals extending anteriorly to the second vertebra (character 33) and at least one epipleural displaced dorsally into the horizontal septum (character 34). The state of the two epipleural synapomorphies could not be confirmed in any of the †ctenothrissiform and †pattersonichthyiform taxa. However, there was character support for a ctenosquamate placement for these taxa (see below). One of the ten synapomorphies/possible synapomorphies of aulopiforms (Wiley and Johnson, 2010), the presence of a cartilaginous condyle on the third pharyngobranchial,

cannot be observed in fossils. However, the condyle typically allows for articulation between the second epibranchial and the third pharyngobranchial. With the loss of the condyle on the third pharyngobranchial, the elongated uncinate process of the second epibranchial articulates directly with the pharyngobranchial. Therefore, these characters are essentially duplicates of one another. Another one of the ten characters listed by Wiley and Johnson (2010) that cannot be observed in fossils, a cartilaginous join between the medial processes of the pelvic bones, is partially included here as a modified character (character 52), which captures the form of the medial processes. The five remaining synapomorphies/possible synapomorphies of Wiley and Johnson (2010) could not be observed in fossils, even partially: the presence of larval peritoneal pigment, absence of a gas bladder, a benthic habitus, the distinctive configuration of the retractor dorsalis and a simple sphincter of the oesophagus.

An aulopiform placement for the †ctenothrissiform and †pattersonichthyiform taxa was not supported by any of the four phylogenetic analyses, although, in the hypothesis test using the combined dataset, an aulopiform placement for these taxa could not be completely rejected. The presence of an elongated uncinate process of the second epibranchial may not be an aulopiform synapomorphy. Instead, it may be a eurypterygian synapomorphy that is lost in the crown, and potentially some of the stem (†Ctenothrissidae, †Pattersonichthyiformes), ctenosquamates. However, this optimisation is ambiguous, as there is the possibility that the character evolved convergently in Aulopiformes and †*Aulolepis*.

3.6.4 †Ctenothrissiformes and †Pattersonichthyiformes as stem ctenosquamates

A stem ctenosquamate placement for the †ctenothrissiform and †pattersonichthyiform taxa was supported by all four phylogenetic analyses and the two hypothesis tests. Although all of the analyses and hypothesis tests point towards a stem ctenosquamate placement for the †ctenothrissiforms and †pattersonichthyiforms, the relationships between these taxa are much less well-defined. The morphology only

Bayesian analysis and the morphology only hypothesis tests supported a placement of †*Ctenothrissa* as the sister taxon to the crown ctenosquamates, †*Pattersonichthys* as sister taxon to †*Ctenothrissa* + crown Ctenosquamata, and †*Aulolepis* as sister taxon to †*Pattersonichthys* + †*Ctenothrissa* + crown Ctenosquamata (H1). The morphology only parsimony analysis supported the placement of †*Ctenothrissa* as sister taxon to crown-group Ctenosquamata, but the relationships of †*Aulolepis* and †*Pattersonichthys* were not resolved. In the combined Bayesian analysis and combined hypothesis test, †*Aulolepis*, †*Pattersonichthys* and †*Ctenothrissa* were united as a monophyletic group (H2). In the morphology only parsimony analysis, †*Aulolepis*, †*Pattersonichthys* and †*Ctenothrissa* were recovered as stem ctenosquamates, although they were placed in a polytomy alongside the crown ctenosquamates.

Collectively, the results of the analyses suggest that hypotheses one and two are the most likely. Although the results of the analyses do not provide unanimous support for either hypothesis, studying character evolution based on the two topologies provides a useful means of assessing the anatomical support for each hypothesis. There are three characters that provide strong support for total-group Ctenosquamata (†Ctenothrissiformes, †Pattersonichthyiformes and crown-group Ctenosquamata) in both hypotheses. These are: articulation between the lateral ethmoids and the lacrimals (character 9), epibranchial four with an uncinate process and a slender posterior end (character 24; although the character state is unknown in †*Ctenothrissa* and †*Pattersonichthys*) and possessing less than 40 vertebrae (character 27).

There are five more characters supporting total group Ctenosquamata in hypothesis one. These are: an unroofed posttemporal fossa (character 5; state reversed in †*Pattersonichthys*), the oral margin of the jaw consisting of the premaxilla and the maxilla (character 13), dentition on the maxilla (character 16), a beryciform foramen on the anterior ceratohyal (character 19) and presence of dermal caudal scutes (character 46). All of these characters are optimised as reversals in crown group Ctenosquamata, although a beryciform foramen is present in polymixiiforms.

In hypothesis two, four of these characters (13, 16, 19, 46) are the only ones that support the monophyletic †ctenothrissiform-†pattersonichthyiform clade. However, these four characters are also found in stem teleosts (e.g. †*Tharsis*) and they are also present in a mosaic-like fashion in primitive teleosts (e.g. 3/4 present in *Elops*). Therefore, the condition found in †ctenothrissiforms and †pattersonichthyiforms is either convergent with primitive teleosts, or it has persisted up to the level of Eurypterygii.

There is some evidence that the characters supporting †ctenothrissiform + †pattersonichthyiform monophyly are in-fact primitive, and that they are common to the last common ancestor of eurypterygians and would have then been transformed convergently in individual eurypterygian lineages. There are three pieces of evidence that provide support for this view. First, for these primitive characters to have persisted up to the level of Eurypterygii, they would have had to have been lost multiple times as they are not seen in lineages branching closely to Eurypterygii. The fossil record of deeply diverging taxa from many teleost lineages is very poor, so our understanding of early character evolution in these groups is limited. This includes taxa branching close to Eurypterygii, such as ateleopodiforms, galaxiids and osmeriforms, whose extant representatives are highly derived and most likely do not represent the ancestral condition of their corresponding lineages. Second, if a broader perspective is taken, then developmental and ontological evidence supports the hypothesis that some of these characters have persisted up to the level of the euryptergians as they are present in their larvae. For example, Berry (1964: fig. 6) showed that in the larval form of an aulopiform (*Scopelosaurus*), two of the 'primitive' characters supporting †ctenothrissiform-†pattersonichthyiform monophyly in hypothesis two – the premaxilla and maxilla both forming the oral margin of the jaw, and a toothed maxilla – are present. Adult aulopiforms typically have a toothless maxilla that is excluded from the jaw, but during early development the maxilla is toothed and it is the primary bone of the upper jaw. As the larval form develops, its maxillary teeth are lost and the premaxilla develops posteriorly to exclude the maxilla from the jaw. Furthermore, †ctenothrissiforms are superficially

similar to some eurypterygian larvae. '*Macristium*', a poorly known larval/juvenile form with a toothed maxilla included in the oral margin of the jaw, was believed to be the larvae of an unknown living †ctenothrissiform (Marshall, 1961). This †ctenothrissiform affinity was primarily based on the upper jaw structure and arrangement of the fins. However, this form is now known to be a larval bathysaurid aulopiform (Rosen, 1971). Third, maxillary teeth are also found in some fossil and living eurypterygians. This includes a fossil aulopiform (†*Halec*), a fossil beryciform (†*Gnathoberyx*) and a living beryciform (*Myripristis*). Collectively, this evidence provides some support for the two jaw characters having been present in the last common ancestor of the eurypterygians. However, there are also some issues with this view. The persistence of these primitive characters is not the most parsimonious solution, as it requires a number of character losses in different teleost lineages. However, the likelihood of the four aforementioned characters appearing in unison both in primitive teleosts, and in the †ctenothrissiforms and †pattersonichthyiforms also seems unlikely.

If some or all of the four primitive characters mentioned above have persisted up to the level of the Eurypterygii, and they do not represent a reversal to the primitive condition, then the presence of these primitive characters cannot be used to define a monophyletic group. Rosen and Patterson (1969) echoed this view, stating that there are "no specialized features common to the three genera of ctenothrissoids" – with ctenothrissoids including †*Aulolepis*, †*Ctenothrissa* and †*Pateroperca*. For the †ctenothrissiform and †pattersonichthyiform taxa (amongst other eurypterygians) to possess the same array of characters as primitive teleosts it seems likely to be more than mere coincidence. In light of this, hypothesis two seems unlikely, as there is no real morphological support for the †ctenothrissiform-†pattersonichthyiform clade. Most of the early interpretations on †ctenothrissiform relationships indicated an affinity to the clupeiforms (Woodward, 1899, 1900; Gregory, 1933; Berg, 1940; Bertin and Arambourg, 1958), which also posses the four characters stated above. So instead of these characters uniting a clade, they

highlight the gaps in our understanding of character evolution spanning from the level of Clupeiformes up to Eurypterygii.

In contrast to hypothesis two, there is strong morphological support for the placement of the †ctenothrissiform and †pattersonichthyiform taxa in hypothesis one. Three characters support the †*Ctenothrissa* + crown-group Ctenosquamata clade: the complete, or almost complete, separation of the parietals (character 3), a reduction to two or fewer branchiostegals on the posterior ceratohyal (character 20) and close association/contact between the pelvic and pectoral girdles (character 51; reversed in Myctophiformes). The †*Pattersonichthys* + †*Ctenothrissa* + crown-group Ctenosquamata clade is supported by one character: a subocular shelf present on the infraorbitals (character 18). An additional character, a supratemporal fossa (character 5), will support one of these two clades, depending on the character state of †*Pattersonichthys*, which could not be determined.

3.6.5 †Ctenothrissiformes + †Pattersonichthyiformes monophyly

Based on the evidence presented above, hypothesis one seems to be the most likely topology depicting the relationships between the †ctenothrissiform and †pattersonichthyiform taxa. If this is the case, then †Ctenothrissiformes can no longer be considered to be a monophyletic group. Not only does †*Pattersonichthys* appear to be more closely related to †*Ctenothrissa*, than does †*Ctenothrissa* to †*Aulolepis*, but all three of these taxa appear to be from independent lineages. Therefore, the †ctenothrissiforms and †pattersonichthyiforms appear to represent a paraphyletic grade rather than true monophyletic groups.

Although only three of the six †ctenothrissiform and †pattersonichthyiform genera were included in the phylogenetic analyses, it is possible, using the descriptions and figures of Gaudant (1978c), to comment on the phylogenetic position of the remaining taxa. The other †ctenothrissiform genus, †*Heterothrissa*, seems to occupy a similar position to †*Ctenothrissa*, as it possess a subocular shelf, the skull proportions are similar and the parietals are separated for greater than

half their length. †*Heterothrissa* also has the same number of branchiostegals as †*Ctenothrissa*, although it is not possible to say how many articulated with the posterior ceratohyal. The other †pattersonichthyiform genera, †*Humilichthys* and †*Phoenicolepis*, display a similar array of characters as †*Pattersonichthys*: similar skull proportions, parietals in contact for most of their length, a subocular shelf present on the infraorbitals and three or more branchiostegals articulating with the posterior ceratohyal. Therefore, the six †ctenothrissiform-†pattersonichthyiform taxa appear to be divided into three groups: †Aulolepidae, †Pattersonichthyiformes and †Ctenothrissidae, with †Aulolepidae the most primitive and the †Ctenothrissidae closest to the ctenosquamate crown.

3.6.6 Refining the eurypterygian phylogeny

Although the relationships between the major extant eurypterygian lineages (Aulopiformes, Myctophiformes and Acanthomorpha) are well supported by morphological and molecular data, placing fossil taxa which fall outside of the crown groups of these lineages is somewhat problematic. In this study, I found strong support for a eurypterygian placement for the †ctenothrissiforms and †pattersonichthyiforms, although higher level placements were not as strongly supported. The primitive nature of the †ctenothrissiforms and †pattersonichthyiforms relative to the more derived condition found at the base of the three major eurypterygian clades leaves a 'morphological gap' that makes inference of phylogeny difficult. This 'morphological gap' could be bridged by studying other fossil taxa with uncertain eurypterygian affinities – such as †*Nematonotus* and †*Sardinoides*. Furthermore, the study of stem group fossil taxa which branch close to the crown of the major eurypterygian clades could help to improve our understanding of the characters found at the base of these groups. Collectively, the placement of these additional fossil taxa could help piece together the early evolutionary history of Eurypterygii and enable us to gain a deeper understanding of the origin of a third of extant vertebrates.

A deeper understanding of the internal anatomy of †*Aulolepis*, particularly of the gill skeleton, was crucial in helping to refine the placement of this taxon.

However, the lack of this data for †*Ctenothrissa* and †*Pattersonichthys* serves as a barrier to understanding their phylogenetic placement. For example, we do not know whether †*Ctenothrissa* and †*Pattersonichthys* possess an elongated uncinate process on the second epibranchial – an important character for resolving the phylogenetic placement of these fossils. If this data could be obtained, either from new specimens or from further CT scans of museum specimens, then this would significantly improve our ability to understand the phylogenetic placement of these taxa.

4

A phylogenetic framework for investigating the evolution of jaw protrusion in acanthomorphs: fossil data exposes a Late Cretaceous shift in evolutionary rates

Contents

4.1 Introduction 113
4.2 Materials and methods 117
4.3 Results 127
4.4 Discussion 140

4.1 Introduction

The evolution of upper jaw protrusion is a major evolutionary innovation in vertebrate feeding (Schaeffer and Rosen, 1961; Gosline, 1980; Holzman et al., 2008; Bellwood et al., 2015; Wainwright and Longo, 2017). Although jaw protrusion potentially has numerous functions (Motta, 1984), there are two principal ones. First, jaw protrusion enables fish to reduce the distance between their jaws and their

food, thus reducing the chance of their prey escaping (Alexander, 1967b; Lauder and Liem, 1981; Motta, 1984). Second, jaw protrusion can assist with suction feeding (Alexander, 1967b; Lauder, 1980; Motta, 1984), potentially increasing suction forces exerted on prey by up to 35% (Holzman et al., 2008). Upper jaw protrusion has evolved multiple times and it is present in both chondrichthyan and actinopterygian groups (Motta, 1984; Wilga et al., 2001; Westneat, 2004; Wainwright et al., 2015). While the function of jaw protrusion is similar in each of the different origins, independent lineages have different morphological adaptations to achieve protrusion. There are at least five independent actinopterygian origins of jaw protrusion (Westneat, 2004; Wainwright et al., 2015). Three of these origins occurred in groups represented by little extant diversity (<30 living species; Ascipenseriformes, a genus of characiforms [*Bivibranchia*] and a species of gonorynchiform [*Phractolaemus ansorgii*]), while the other two occurred in major radiations: the acanthomorphs (16,000 species) and the cypriniforms (3,000 species (Westneat, 2004; Wainwright et al., 2015). In cypriniforms the rotation of the kinethmoid, a bone unique to the group, causes the premaxilla to protrude anteriorly (Gidmark et al., 2012). While in acanthomorphs, depression of the lower jaw causes the maxilla to swing forward, with the head of the maxilla forcing the premaxilla to protrude (Alexander, 1967b; Motta, 1984).

The acanthomorphs, or spiny-finned teleosts, are one of the most successful vertebrate groups, containing one-third of all extant vertebrate species (Stiassny et al., 2004) and exhibiting huge morphological and ecological diversity (Friedman, 2010; Nelson et al., 2016; Wainwright and Longo, 2017). Classic studies anecdotally attribute the success of the acanthomorphs, and the percomorph sub-clade in particular, to the presence of protrusible jaws (Schaeffer and Rosen, 1961). Although they did not explicitly test this, Bellwood et al. (2015) hypothesised that the evolution of jaw protrusion alone was not necessarily associated with, or sufficient for, a rapid increase in diversification rates. The acanthomorph jaw protrusion mechanism most likely originated at the base of Acanthomorpha or a deeper branch (Westneat, 2004), possibly in the Cretaceous †ctenothrissiforms (Alexander, 1967b),

which were believed at the time to be close to ancestral acanthomorphs but are currently regarded as more remote relatives that branch from the ctenosquamate stem (see Chapter 3).

The ancestral protrusile premaxilla has been modified in many acanthomorph lineages, with up to 15 independent origins of significant jaw protrusion (Bellwood et al., 2015). Jaw protrusion has been extensively studied at the lower taxonomic levels, with particular emphasis on exceptional taxa such as the slingjaw wrasse *Epibulus insidiator* (e.g. Westneat and Wainwright, 1989; Westneat, 1991; Wainwright et al., 2004). However, it is possible to gain a broader understanding of patterns of evolution of jaw protrusion. In acanthomorphs, the length of the ascending process of the premaxilla has been shown to be an indicator of the extent that fish can protrude their jaws (Alexander, 1967b; Gosline, 1987; Hulsey et al., 2010; Bellwood et al., 2015). Using the length of the ascending process of the premaxilla has allowed for large-scale studies examining protrusion that sample broadly among both living and extinct taxa (e.g. Bellwood et al., 2015).

To date, jaw protrusion has not been studied using a large-scale, phylogenetic framework. Some studies have informally mapped the presence of protrusion, as a binary trait, onto phylogenies (e.g. Westneat, 2004; Wainwright et al., 2015), but this does not allow in-depth investigation of macroevolutionary trends. Jaw protrusion has a strong phylogenetic signal when it has been studied at a smaller scale (e.g. heroine cichlids: Hulsey et al., 2010). There are numerous tools available that allow for investigation of the evolution of traits, such as jaw protrusion, but these typically require a phylogenetic framework. These tools include comparative biological techniques, such as ancestral character reconstruction (Revell, 2012; Maddison and Maddison, 2016) and evolutionary rates analyses (Pagel et al., 2004; Eastman et al., 2011; Rabosky et al., 2014). Collectively, these methods allow for a multifaceted approach to investigating macroevolutionary trends and when used to study jaw protrusion, they have the potential to reveal the role that protrusion had in the evolution of the acanthomorphs.

In comparative studies, the inclusion of fossil taxa can provide temporal and historical data that studies limited to extant taxa lack. In particular, fossil data can aid inference of ancestral trait values and reveal otherwise hidden macroevolutionary trends (Finarelli and Flynn, 2006; Slater et al., 2012; Benson and Choiniere, 2013; Slater and Harmon, 2013; Betancur-R et al., 2015). Furthermore, fossil data can greatly improve our understanding of the evolution of jaw protrusion (Bellwood et al., 2015). The fossil record provides a unique insight into the evolution of acanthomorphs: Cretaceous deposits, such as the English Chalk (Woodward, 1902; Patterson, 1964) and those in Lebanon (e.g. Hakel and Hadjoula; Woodward, 1942; Gayet, 1980a), reveal primitive acanthomorphs from deeply diverging clades, while the Eocene Bolca locality famously yields early representatives from numerous extant percomorph lineages (Blot, 1969; Bannikov, 2014b). Generally, we have a good understanding of morphological characters underpinning monophyly of many individual acanthomorph lineages (Wiley and Johnson, 2010). However, prior to the onset of molecular phylogenetic methods it had been almost impossible to understand the relationships between many of these lineages – especially those within the percomorph "bush at the top" (Nelson, 1989), let alone understand how fossil taxa fit into a phylogenetic framework. The relationships between some extant and fossil acanthomorphs are well resolved; notable examples include lampridomorphs (Davesne et al., 2014; Chapter 2), tetraodontiforms (Santini and Tyler, 2004; Close et al., 2016) and zeiforms (Tyler and Santini, 2005; Davesne et al., 2017). Even for most fossil taxa whose phylogenetic positions are less well-defined, it is generally possible to propose well-supported identifications at the family level (Bannikov, 2014b).

In this study, I investigated the evolution of jaw protrusion in acanthomorphs using a phylogenetic framework that combines both fossil and extant taxa in order to pursue four lines of enquiry. First, I aimed to reconstruct patterns of jaw protrusion at the family level to see if the extent of protrusion present in individual lineages is characterised by broad clade-specific patterns. Second, I investigated whether evolutionary rates of change of protrusion were constant across

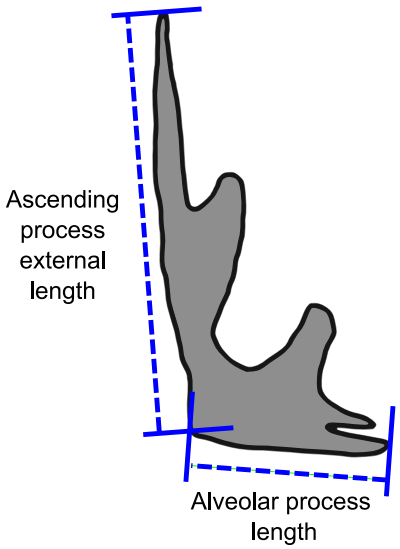

Figure 4.1: Measurements of the premaxilla that are used to calculate the jaw protrusion index (JPI).The JPI is calculated by dividing the external length of the ascending process by the length of the alveolar process.

acanthomorph lineages, or whether there were clades showing elevated or reduced rates of evolution in protrusion. Third, I investigated whether there are temporal trends in the evolution of protrusion that characterise the acanthomorph clade. Previous work has identified temporal trends in rates of lineage diversification (Near et al., 2013) and morphological disparity of overall body geometry (Friedman, 2010). I hoped to see how protrusion correlated with the results from these previous studies, and understand the role that the evolution of protrusion may have played in the Palaeogene radiation of the acanthomorphs. Fourth and finally, I wanted to establish the role that fossil data play in understanding the evolution of protrusion. In other taxonomic groups, the inclusion of fossil data has helped identify macroevolutionary trends that would have been otherwise hidden; I aimed to see if fossil data has a similar role in understanding the evolution of protrusion.

4.2 Materials and methods

4.2.1 Jaw protrusion index

The importance of the length of the ascending process of the premaxilla in the acanthomorph protrusion mechanism has been widely reported (e.g. Alexander,

1967b; Gosline, 1987; Westneat and Wainwright, 1989; Westneat, 1991; Hulsey et al., 2010; Bellwood et al., 2015; Wainwright et al., 2015). The extent that a fish can protrude its upper jaw is limited by the length of the ascending process, which acts as a guide for the premaxilla to protrude outwards (Hulsey et al., 2010). The correlation between the extent of protrusion and the length of the premaxillary ascending process has also been quantified in two previous studies (Hulsey et al., 2010; Bellwood et al., 2015). In order for the length of the ascending process to be compared across acanthomorphs, where the size of taxa can vary by several orders of magnitude, it must be standardised. Bellwood et al. (2015) used the length of the ascending process standardised by the standard length as a proxy for jaw protrusion. They selected this method after evaluating nine different metrics (Bellwood et al., 2015: table S1) to determine which was the most reliable at predicting protrusion in extant taxa. All of the linear measurements they considered were standardised using the standard length (anterior end of the snout to the posterior of the hypural plates of the caudal fin). When extrapolating beyond the original taxon sample of Bellwood et al. (2015), the use of the standard length as the standardisation method presents some problems. First, in taxa with elongated body forms (e.g. *Regalecus glesne*) the metric greatly underestimates protrusion. Second, fossil taxa with well-preserved premaxillae may be disarticulated or incompletely preserved, meaning that it is not possible to obtain standard length data.

To circumvent the issues with using the standard length to standardise the measurements, I used a novel metric, henceforth referred to as the jaw protrusion index (JPI), which can be applied to a wider range of taxa than the method of Bellwood et al. (2015). The extensive morphological diversity of the acanthomorphs presented some challenges in selecting alternatives to the standard length, as the dimensions of very few structures are well conserved across taxonomic groups. The role of the length of the alveolar process in protrusion has not been reported before. However, the premaxillae of acanthomorphs with high levels of protrusion typically share two characteristics: they have an elongated premaxillary ascending process relative to a short alveolar process. Taxa which cannot protrude their jaw at all

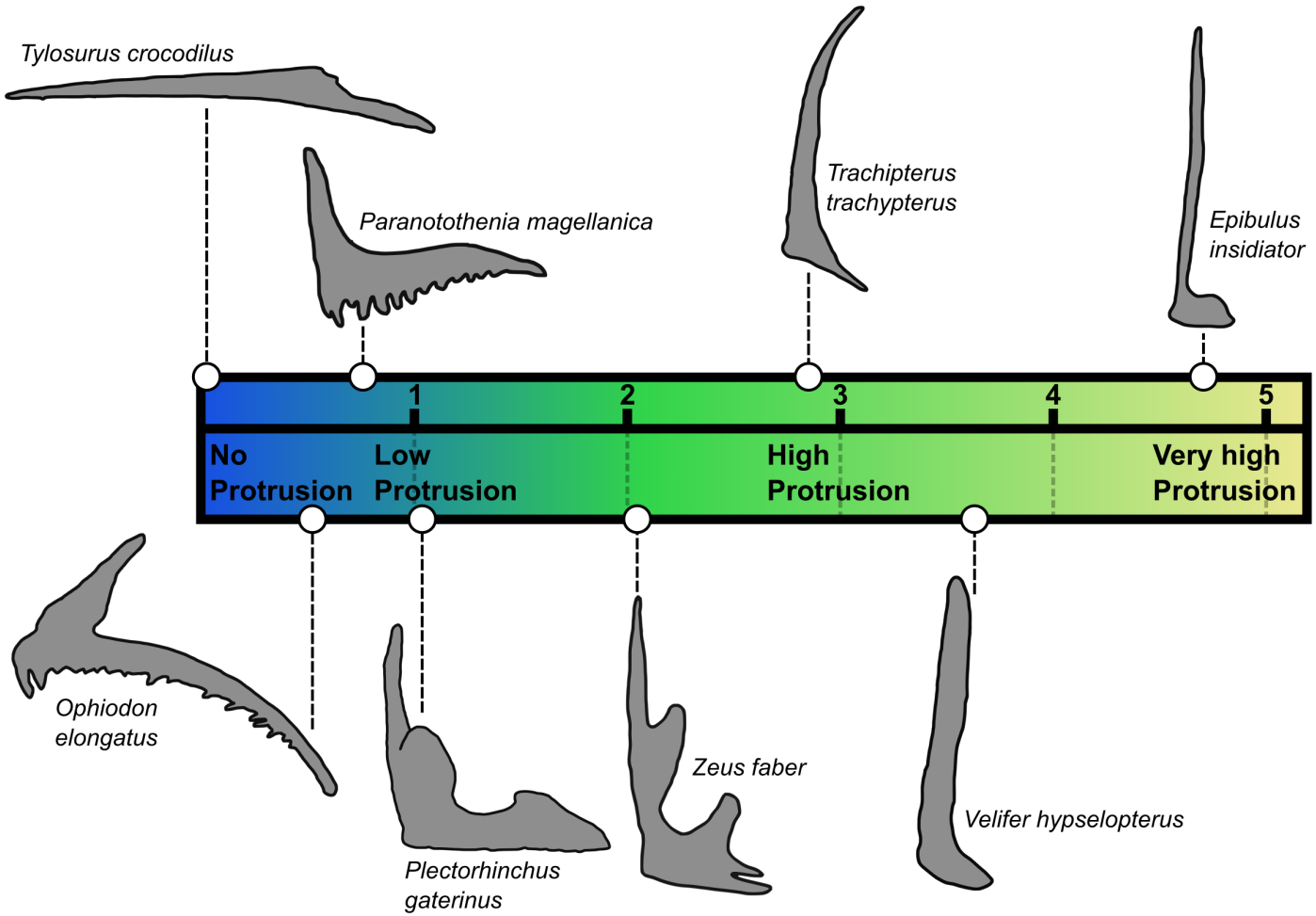

Figure 4.2: The jaw protrusion index (JPI) and premaxillary morphology. The JPIs are shown for the premaxillae of eight species of extant acanthomorphs with varying morphologies.

appear to have the opposite arrangement, with a small or non-existent ascending process relative to a long alveolar process. The JPI was calculated using the ratio between the length of the ascending process and the length of the alveolar process of the premaxilla (Fig. 4.1). The JPI is highest in taxa with a long premaxillary ascending process, and a short premaxillary alveolar process, and lowest in taxa with a short, or non-existent, ascending process and a long alveolar process (Fig. 4.2). All that is required to calculate the JPI is a complete premaxilla – and premaxillae can be obtained from taxa with vastly different body proportions. Transformations to the JPI were considered, but when the data was transformed it was not longer suitable for studying protrusion, as the premaxillae of some non-protruders have been modified to a much greater extent than the premaxillae of protruders. To give an example, the ratio between the longest and shortest of the two processes that are used to calculate the JPI for the most extreme protruder (*Epibulus insidiator*) and the most extreme non-protruder (*Xiphias galdius*) are 5:1 and 250:1 respectively – the ratio between the processes is 50 times greater in the extreme non-protruder. Because of this, when the JPI data is transformed, the signal for protrusion is lost and only extreme non-protrusion can be detected.

The JPI was evaluated by comparing the index to the protrusion data of Bellwood et al. (2015) and to the metric they used to estimate protrusion, the length of the premaxillary ascending process as a percentage of the standard length. When possible, the JPI and data of Bellwood et al. (2015) were compared using the same species, but if this was not possible then two species of the same genus were compared. When the JPI was compared to the protrusion data, which was standardised using the standard length, (Fig. 4.3A) there was a strong, positive correlation (Pearson's product-moment correlation: $r = 0.69$, $t = 3.56$, d.f. $= 14$, $p < 0.01$). However, as protrusion data was only available for extant taxa and there was limited crossover between the taxon samples, only 16 taxa could be compared. When the JPI was compared to the metric of Bellwood et al. (2015) (Fig. 4.3B) there was an even stronger, positive correlation between the two variables (Pearson's product-moment correlation: $r = 0.78$, $t = 8.02$, d.f. $= 42$, $p < 0.001$). In Figure 4.3B, most of the

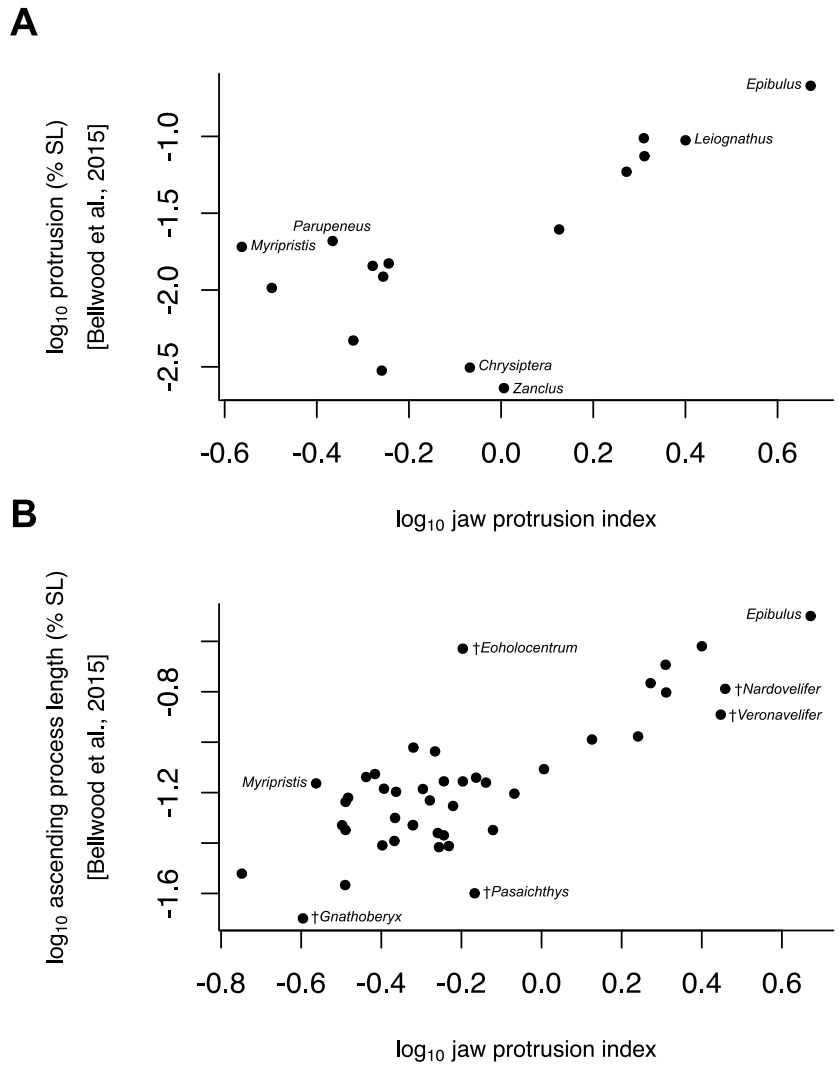

Figure 4.3: Correlation between the jaw protrusion index and data collected by Bellwood et al. (2015). All data was transformed to remove heteroscedasticity. Fossil taxa were removed from A as the extent of protrusion was estimated. **A,** Jaw protrusion index and the extent of protrusion, as a percentage of standard length. Pearson's product-moment correlation: r = 0.69, t = 3.56, d.f. = 14, $p < 0.01$. **B,** Jaw protrusion index and the premaxillary ascending process as a percentage of standard length. Pearson's product-moment correlation: r = 0.78, t = 8.02, d.f. = 42, $p < 0.001$.

outliers appear to be fossil taxa; this may reflect difficulty in obtaining accurate standard length measurements for fossil taxa. Bellwood et al. (2015: table S2) identified 15 lineages as having the potential for significant protrusion; all 15 lineages were represented in the taxon sample used in this work. Representatives from 12 of these lineages were found in the top 20% of JPIs, with nine in the top 10% of JPIs.

4.2.2 Data collection

4.2.2.1 Taxon sample

The premaxillae of 233 extant and 52 extinct fishes were measured. Of the extant taxa, all but ten were acanthomorphs. The ten non-acanthomorph taxa were selected as representatives from major euteleost clades. The 223 acanthomorphs were selected to provide a representative sample of the diversity present in the acanthomorphs. I aimed to select at least one representative from each acanthomorph family. Some families were not represented in the dataset because it was not possible to source material to obtain measurements. For large families, up to three taxa were included in the taxon sample. Taxonomic assignments were primarily sourced from *The Catalog of Fishes* (Eschmeyer et al., 2016).

Fossil taxa were only included in the analysis when they could be placed relative to living taxa. The fossil taxa were Cretaceous to Miocene in age, broken down as follows: Cretaceous (24 species), Paleocene (3 species), Eocene (24 species) and Miocene (1 species). Three of the fossil taxa were stem ctenosquamates, with the remaining taxa all from acanthomorph lineages. The majority of the fossil acanthomorphs were from non-percomorph lineages (33/49). Previous work has shown that in macroevolutionary analyses, constraint of deep nodes can improve trait inference (Finarelli and Flynn, 2006; Slater et al., 2012; Betancur-R et al., 2015). Therefore, the inclusion of deeply diverging fossil taxa (i.e. non-percomorphs) was prioritised.

The choice of representative taxa was primarily dependent on the availability of material for measuring. Although taxa with novel morphologies were included in the dataset, I endeavoured to ensure that the dataset was representative, and did not just contain taxa with the most extreme morphologies.

When discussing the taxonomy and phylogenetic placement of taxa, recognised clade names are used when applicable. A number of unnamed clades needed to be referred to in the text; when this was the case, these clades were denoted with letters (see Results for explanation of these clades).

4.2.2.2 Measurements

The majority of measurements were taken from photographs and radiographs of fossil and osteological specimens from museum collections (Appendix B). Additional images were sourced from the scientific literature. Because the approach to quantifying jaw protrusion rests on a simple ratio between the two processes of the premaxilla, images without scale bars could still be added to the dataset. Drawings were only used when they were judged to be accurate. All measurements were carried out in the image analysis software ImageJ (Schneider et al., 2012; version 1.50i).

4.2.3 Supertree construction

An informal supertree was constructed using the dated molecular phylogeny of Near et al. (2013) as a scaffold tree. Representatives from five additional families that were not present in the scaffold tree were inserted manually: two zeiform (Cyttidae and Oreosomatidae) and three lampridiform (Lophotidae, Radiicephalidae, Veliferidae) families. The phylogenetic placement of these taxa was based on the results of published phylogenetic analyses (Appendix B). Relationships between fossil taxa were fully reconstructed when phylogenetic hypotheses were available. When this was not possible, fossil taxa were placed in polytomies with extant taxa. A full breakdown of the source of phylogenetic placements for fossil taxa can also be found in Appendix B. The informal supertree was constructed using Mesquite (Maddison and Maddison, 2016; version 3.10) and the R (R Core Team, 2016) package ape (Paradis et al., 2004; version 4.0).

4.2.4 Supertree dating

The tree was dated in MrBayes (Huelsenbeck and Ronquist, 2001; version 3.2.6). A custom R script (Appendix C) was used to produce a NEXUS file containing constraints, calibrations and parameters. This script used the `createMrBayesConstraints` and `dateNodes` functions from the paleotree R package (Bapst, 2012; version 2.7). The relationships between all taxa in the tree were constrained as per the informal supertree. Node ages were calibrated for nodes that were present

in the scaffold tree; all other node ages were left uncalibrated. The nodes were calibrated as a uniform distribution using the 95% HPD values, from the Near et al. (2013) tree file, to set the upper and lower bounds. The tip ages were calibrated for all taxa: all extant taxa were given a fixed age of zero, whereas the ages of the fossil taxa were set using uniform distributions based on the beginning and end of the narrowest stratigraphic interval to which each taxon could be assigned to. Fossil taxa were not included in the tree when their age was not consistent with their placement in the supertree. The age of the root node was set using the `treeagepr` setting in MrBayes. The age was set as a uniform distribution of the 95% HPD values from the root node of the scaffold tree.

The analysis was run using the uniform clock setting with the `clockvarpr` set to an igr model. The sampling frequency was set to 1,000 generations. As I was dating a supertree, I ran the analysis with the `no data` setting active. The analysis was run for 20 million generations. The majority rule consensus tree that was generated by MrBayes was used for all further analyses.

4.2.5 Ancestral character reconstruction

The `contMap` function from the phytools R package (Revell, 2012; version 0.5–64) was used to map the JPI onto the time-calibrated supertree. The `contMap` function uses maximum likelihood to interpolate between the JPI values of the tips to estimate the node values. The JPI trait values were then mapped over the phylogeny using a colour scale. In order for the full range of protrusion abilities to be shown, the JPI data needed to be approximately normally distributed. As the raw data was positively skewed it was square-root-transformed before it was mapped onto the phylogeny. Finally, the phytools `fastAnc` function was used to compare node estimates from the datasets including and excluding fossil taxa. An R script (Appendix C) was used to identify nodes that were present in both datasets. The absolute differences between node estimates were then calculated. The relationship between the absolute differences of node estimates and node ages were analysed using linear regression.

4.2.5.1 Origins of high protrusion

The number of origins of high levels of jaw protrusion, and the timing of these origins, were assessed by studying the protrusion data mapped on to the supertree (see above). What quantifies as a high level of jaw protrusion is somewhat arbitrary. Therefore, I selected a cut-off JPI value by selecting the lowest JPIs from each of the 15 clades that were identified by Bellwood et al. (2015) as having high protrusion. I then averaged these JPI values (mean JPI = 1.53, rounded to 1.5), and used it as the cut-off value for classifying a JPI as representing a high level of protrusion.

4.2.6 Evolutionary rates analyses

I studied how the rates of evolutionary change in JPI varied across the supertree using the Bayesian reversible-jump Markov chain Monte Carlo method outlined in Eastman et al. (2011). I conducted two analyses: one using all the taxa in the supertree and the other with all the fossil taxa removed. Before running the analyses, all polytomies were resolved to zero length branches using the `multi2di` function in the ape R package. I performed the evolutionary rates analyses using the `rjmcmc.bm` algorithm of the R package geiger (Harmon et al., 2008; version 2.0.6), applying the relaxed-rates Brownian motion model that allows for multi-rate diffusion across the tree (Eastman et al., 2011). The proposal widths, which determine the way parameter space is explored, were estimated using the `calibrate.rjmcmc` function, although they were later refined after assessing the diagnostics of trial runs. The complete and extant only analyses were run with two chains for 10,000,000 generations. Each run was sampled every 1,000 generations and the first 25% of each run was discarded as burn-in. Diagnostics were performed in the R package coda (Plummer et al., 2006; version 0.19-1). Run parameters and convergence between runs were verified visually using autocorrelation and trace plots, and the effective sample size was >200 and the potential scale reduction factor was between 1 - 1.1 for each sampled parameter. The associated plot function was used to produce phylogenetic trees displaying the evolutionary rates data.

The rate of evolution is given in units of Brownian variance of the JPI per million years, which broadly corresponds to the rate in which the JPI is changing along a given branch. An increase or decrease in the evolutionary rate along a branch (relative to another branch) does not mean that the JPI is changing in the same direction as the change in rate – the JPI could be increasing or decreasing; when interpreting changes in evolutionary rate, the direction of change in a trait needs to be considered alongside the change in rate. With regards to the interpretation of evolutionary rate and the formation of macroevolutionary hypotheses, elevated rates correspond with change in the trait values occurring more quickly, relative to areas of the phylogeny where rates are lower. In this study, the JPI is designed to detect changes in the extent of protrusion, not gross premaxillary morphology. Therefore, the evolution of some traits, like long, sword-like jaws that are not protrusile, may correspond with low evolutionary rates if they occur in an area of the phylogeny where there are already low levels of protrusion, despite a considerable change in premaxillary morphology.

4.2.7 Tempo of jaw protrusion evolution

I studied the JPIs and age of taxa to see if there was any temporal pattern to the appearance of high protrusion morphologies. A robust regression method was used to see if there was any relationship between the JPI and the tip age of taxa. Robust regression uses an iteratively reweighted least squares method. Unlike ordinary least squared methods, robust regression can be used on data that is not normally distributed, where there are outliers, and when the variance changes with the independent variable. The analysis was carried out using the `rlm` function in the R package MASS (Venables and Ripley, 2002; version 7.3-45) and the regression was evaluated using `f.robftest`, a robust F-test function, in the R package sfsmisc (Maechler, 2016; version 1.1-0).

I wrote a custom function, `Evo.Rate.Time` (Appendix C), partially based on the concept of the `plotRateThroughTime` function that is implemented in the BAMMtools (Rabosky et al., 2014) R package. The `Evo.Rate.Time` function used

the posterior sample from the evolutionary rates analysis to investigate how rates of evolutionary change varied over time across the whole acanthomorph phylogeny, rather than on individual branches. These estimates were generated using a series of steps. The function calculated which branches of the supertree were present during a given time interval and then extracted the corresponding rates data for each branch from the posterior sample. The median, mean and 80% confidence intervals were then calculated across all branches present during a given time interval and plotted using LOESS smoothing. In this analysis, the temporal range of the phylogeny was divided into 500 intervals. The analysis was completed twice: once including all taxa and then with the fossil taxa excluded.

4.3 Results

4.3.1 Jaw protrusion index

The highest JPI I recorded (4.697) is in the labrid *Epibulus insidiator* and the lowest (0.004) in the swordfish *Xiphias galdius*. Most taxa have relatively low JPIs (Fig. 4.4): the average index is 0.74 and the median is 0.53. Only 66 of the 285 sampled taxa (23%) have an index of one or greater (i.e. the ascending process is at least the same length as the alveolar process).

4.3.2 Phylogenetic distribution of jaw protrusion

When the JPI is mapped onto the time-calibrated supertree (Fig. 4.5A), all non-acanthomorphs have very low JPIs (mean JPI = 0.25), with the exception of the ateleopodiform *Ateleopus* (JPI = 0.64). The mean JPI (0.77) is much higher in acanthomorphs. However, low levels of protrusion are typical in the most deeply-branching acanthomorph lineages. High levels of jaw protrusion are seen at the base of the zeiogadiform clade. All sampled zeiforms, *Stylephorus* and the most deeply diverging gadiform lineage (Macrouridae) exhibit high levels of protrusion (JPI $\geq$ 1.26). High protrusion appears to be primitive for gadiforms. The extent of protrusion is reduced in subsequent branching clades, with the youngest gadiform lineages – the gadids and lotids – having considerably lower JPI values (JPI $\leq$

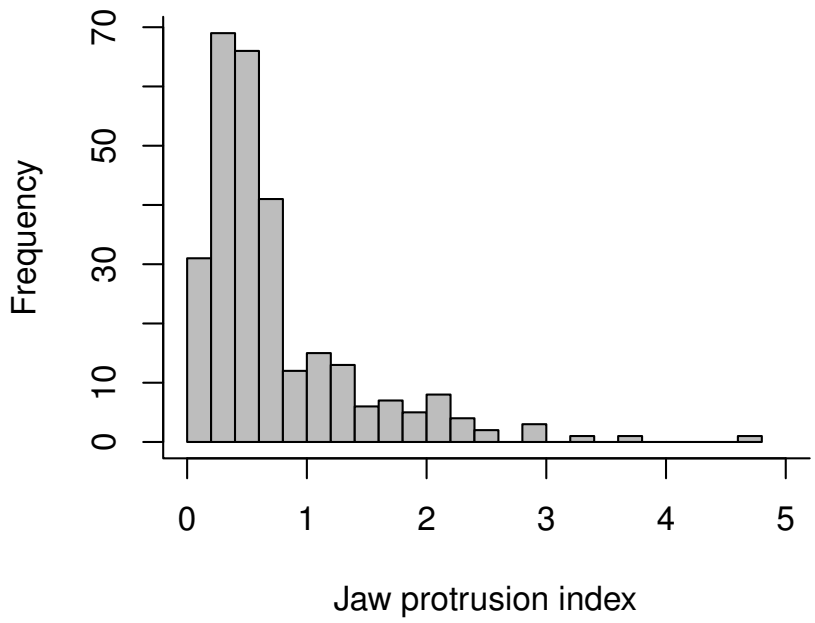

Figure 4.4: Histogram of the jaw protrusion indexes of all taxa included in taxon sample.

0.31) than all other zeiogadiform lineages. Primitive lampridomorphs have low to medium JPI values (0.32 – 0.73). However, in the clade containing †*Nardovelifer* and crown Lampridiformes, JPI values are consistently high (JPI $\geq$ 0.97; mean JPI = 2.22); this clade contains taxa with some of the highest values I recorded (e.g. *Velifer hypselopterus*: 3.62). The beryciform clade is characterised by relatively low JPI values (mean JPI = 0.44). The holocentrid *Sargocentron* is the only beryciform taxon to have a JPI greater than one (JPI = 1.04). The JPIs of all other sampled beryciforms are much lower ($\leq$ 0.69), with the rondeletiid *Rondeletia* having the lowest JPI (0.07).

In the percomorphs, the average JPI is slightly lower than in the acanthomorphs as a whole (mean JPI = 0.74). The earliest diverging percomorph lineages have low JPIs (percomorphs outside of Clade A: mean JPI = 0.41), with the exception of the Callionymidae + Dactylopteridae clade where JPI values are elevated (1.23 – 1.64). Within Clade A, an unnamed percomorph clade (see Fig. 4.5

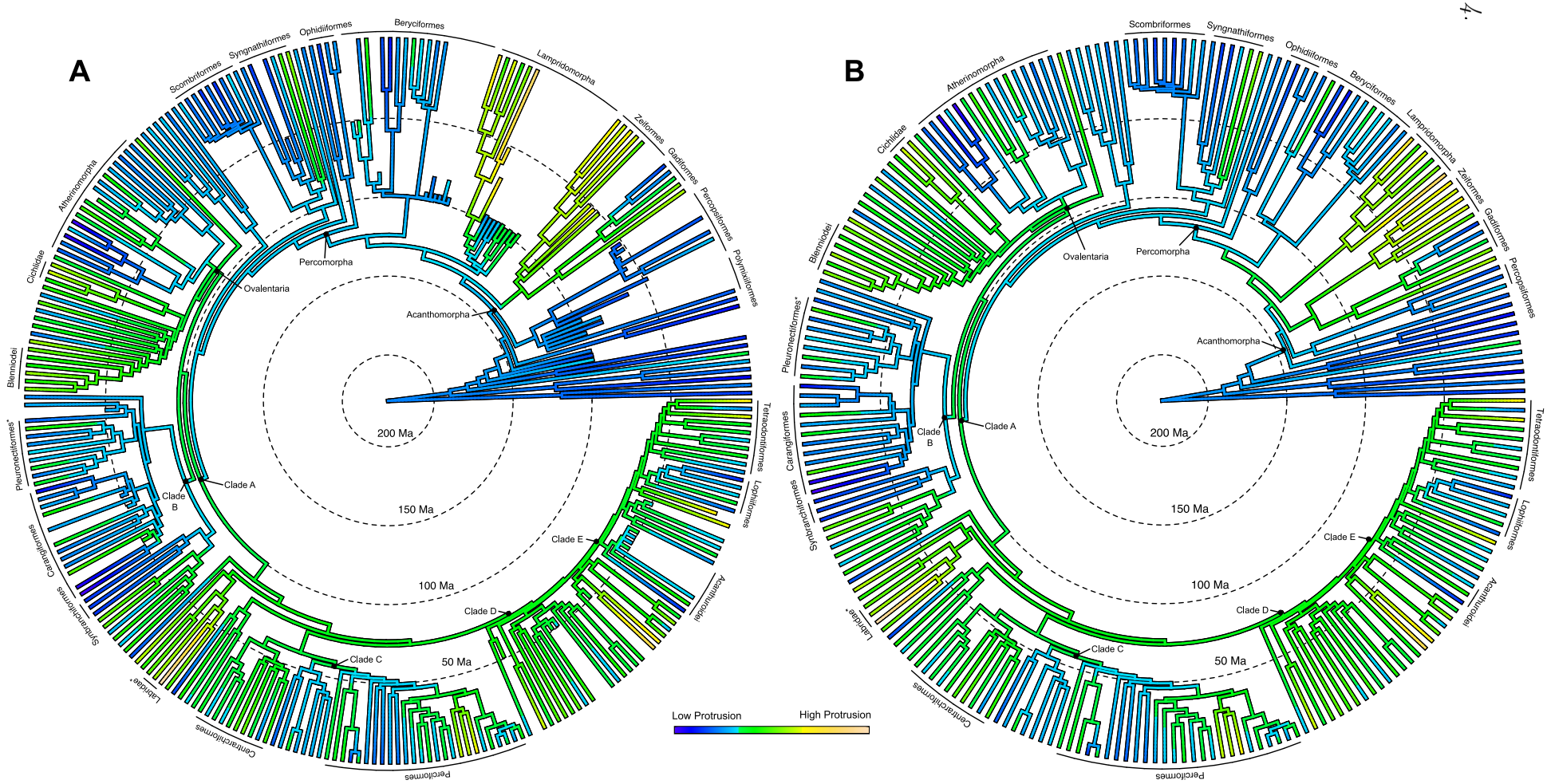

Figure 4.5: The phylogenetic distribution of jaw protrusion. Using maximum likelihood, the jaw protrusion index (JPI) is mapped onto a timescaled supertree of acanthomorphs and selected outgroups. **A,** extant and fossil taxa. **B,** extant taxa only.

for all clade definitions), there is much greater heterogeneity in JPI values, even among closely related lineages. In the labrids, a group which branches relatively deeply within clade A, I recorded the highest JPI value (*Epibulus insidiator*: 4.70). In the ovalentarians, JPI values are relatively high, especially in the cichlids (*Amphilophus citrinellus*: 2.04). However, a number of atherinomorph lineages have reverted to morphologies consistent with very low JPI values (Belonidae: JPI = 0.01, Zenarchopteridae: JPI = 0.02).

In Clades B and C there are a number of lineages that have reverted to morphologies represented by low JPI values while others have retained higher JPI values. In the carangiforms, three lineages have some of the lowest JPIs I recorded: Xiphiidae (JPI = 0.004), Istiophoridae (JPI = 0.02) and Echeneidae (JPI = 0.07). A clade of gasterosteiform perciforms (Aulorhynchidae + Gasterosteidae + Hypoptychidae) has particularly high JPI values, ranging from 1.94-2.28 – the highest of all perciform taxa.

With the exception of Lophiformes and Acanthuroidei, the JPIs of taxa in Clade D are generally high and more homogenous than those of taxa that diverge deeper within Clade A. Within Clade D there are a number of origins of high protrusion including the Leiognathidae + Chaetodontidae clade (JPI $\geq$ 2.52), Caproidae (JPI $\geq$ 2.19) and two tetraodontiform lineages: Triacanthidae (JPI = 2.47) and Triacanthodidae (JPI = 2.17).

When the JPI was mapped onto the phylogeny with the fossil taxa excluded (Fig. 4.5B), the overall pattern is near identical to that of the analysis including all taxa. However, the interpolated JPI node values vary between the two datasets. The estimated JPI root value is lower in the analysis including fossils (0.34) relative to the analysis excluding the fossil taxa (0.42). Of the nodes that are still present in the tree when the fossil taxa are removed, the absolute disparity between the JPI node estimates from the two datasets increases towards the root of the tree ($y = -6.1265 + 2.3686x$; Fig. 4.6). This relationship is highly significant (F-test: $R^2 = 0.39$; $F = 146$, d.f. $= 230$, $P < 0.001$).

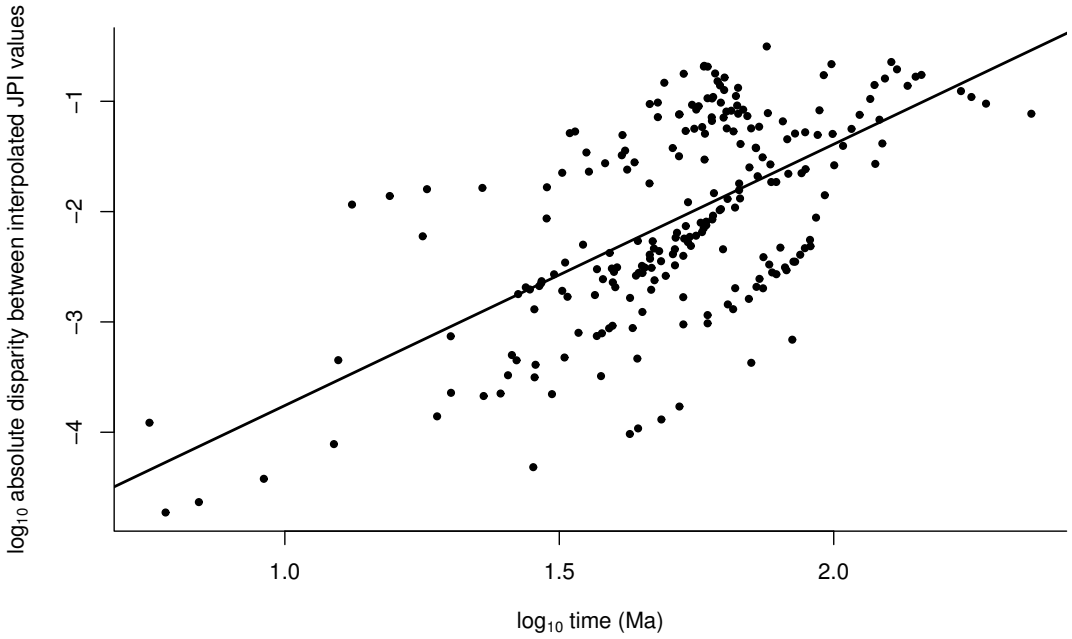

Figure 4.6: Relationship between age of nodes and the absolute disparity of estimated node values of the jaw protrusion index between the supertree including all taxa and the supertree where fossil data are removed. Only nodes that are found in both supertrees are included. Linear regression: y = -6.1265 + 2.3686x, F-test: $R^2 = 0.39$; F = 146, d.f. = 230, P <0.001.

4.3.3 Origins of significant jaw protrusion

When the JPI was mapped onto the supertree, 14 independent origins of high protrusion were identified (Table 4.1). The number of origins did not vary when fossil taxa were removed from the analysis, although the timing of two of the origins varied (reported below). Six of the origins are found in clades that originate during the Cretaceous period, the earliest of which is at the base of Zeiogadiformes (119 Ma). The next origin was in the lampridiforms. In the analysis including all taxa, protrusion originated in a clade with the stem lampridiform †*Nardovelifer* at its base (101 Ma), although in the analysis excluding fossil taxa, high protrusion originated in the crown lampridiforms, over 25 million years later (75 Ma). The four remaining Cretaceous origins were in the Callionymidae, Gerreidae, Gobiesocidae and Labridae. Four of the Cenozoic origins of high protrusion occur at the base of clades uniting extant percomorph groups: Triacanthodidae +

Table 4.1: Origins of high levels of jaw protrusion in acanthomorphs. Taxa with a JPI > 1.5 were judged to have high levels of protrusion. Ages of clades were extracted from the dated supertrees. Dates from the extant only tree are only specified when they differ from those of the tree containing both extant and fossil taxa.

Clade	Age of clade in supertree		Identified by Bellwood et al. (2015)
	All taxa	Extant only	as having high protrusion?
Zeiogadiformes	118.64	–	Zeiformes only
Lampridiformes	100.8	75.49	Yes
Callionymidae	82.28	–	Yes
Cichlidae	44.81	–	Yes
Gobiesocidae	70.04	–	No
Labrisomidae + Chaenopsidae + Dactyloscopidae	37.68	–	No
Gerreidae	78.57	–	Yes
Labridae	66.1	–	Yes
Hypoptychidae + Aulorhynchidae + Gasterosteidae	28.62	–	No
Drepaenidae	42.04	–	Yes
Chaetodontidae + Leiognathidae	46.21	–	Yes, separately
Datnoididae	15.53	–	No
Caproidae	58.58	64.05	Yes
Triacanthodidae + Molidae + Triacanthidae	51.35	–	No

Molidae + Triacanthidae (Tetraodontiformes), Chaetodontidae + Leiognathidae, Labrisomidae + Chaenopsidae + Dactyloscopidae (Blennioidei), and Hypoptychidae + Aulorhynchidae + Gasterosteidae (Gasterosteiformes). The four remaining Cenozoic origins occurred in isolated lineages: Caproidae, Cichlidae, Drepaenidae, and Datnoididae. The timing of the origin of high protrusion in the Caproidae varied between the analyses including (59 Ma) and excluding (64 Ma) fossil taxa.

4.3.4 Evolutionary rates analyses

4.3.4.1 Fossil and extant taxa

For the tree including fossil and modern taxa, I find low rates of change in JPI are typical from the base of the tree to the base of Clade A (Fig. 4.7). However, in this area of the phylogeny there are a number of rate shifts that are restricted to individual clades. The deepest rate shift is at the base of Zeiogadiformes and is well supported by the posterior (PP = 0.980; Table 4.2). In the zeiogadiforms, the elevated median evolutionary rate is consistent across the clade, except in the early

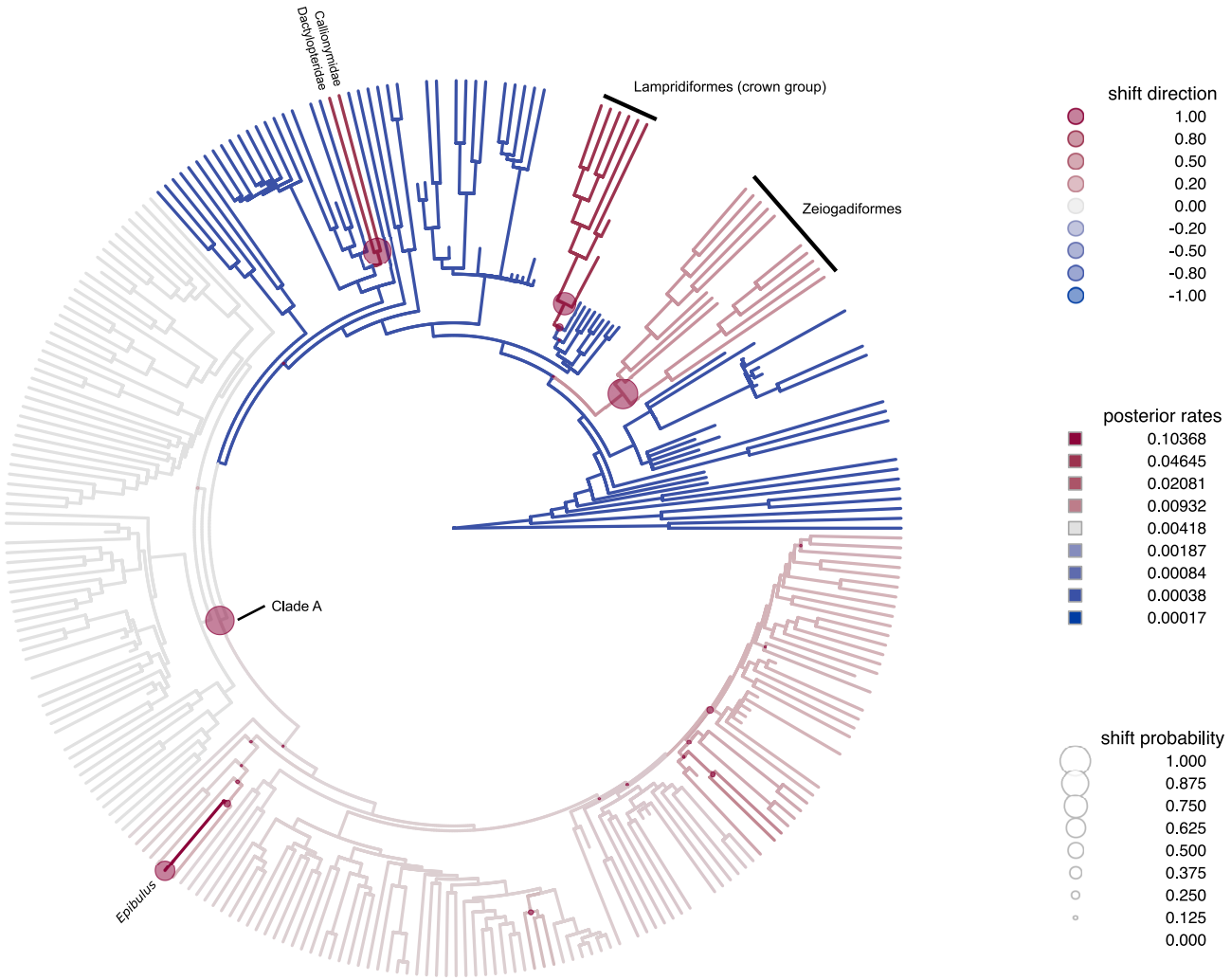

Figure 4.7: Rate of evolution of the jaw protrusion index using the supertree containing living and fossil taxa. Branch colours indicate the evolutionary rate of the corresponding branch. Coloured circles on nodes and branches indicate possible shifts in evolutionary rate. The colour of circles indicates the direction of the shift and the size of the circles indicates the posterior probability of the shift occurring.

Table 4.2: Posterior probabilities of shifts in evolutionary rate of the jaw protrusion index in the analyses including and excluding fossil taxa. Only shifts with a probability of ≥ 0.2 in at least one of the two rates analyses are included. Taxa denoted with an asterisk were not present in the extant only analysis.

Clade/Tip	All taxa	Fossils excluded
	Posterior Probability	Posterior Probability
Zeiogadiformes	0.98	0.004
Lampridiformes + †*Nardovelifer**	0.736	0.839
Lampridiformes + †*Nardovelifer* + †*Aipichthyoides*	0.221	–
Callionymidae + Dactylopteridae	0.906	0.001
Clade A	0.936	0.002
Epibulus + Scaridae	0.208	0.173
Epibulus	0.64	0.616
Gasterosteidae + Aulorhynchidae + Hypoptychidae	0.168	0.803
Clade E	0.198	0.392
Leiognathidae + Chaetodontidae	0.145	0.202
Triacanthodidae + Molidae + Triacanthidae	0.028	0.236

zeiforms †*Archaeozeus* and †*Bajaichthys*, where there is a further slight increase. In the zeiogadiforms, the median evolutionary rate is 19 times greater than that of the preceding node (0.0070 versus 0.0004). In the lampridomorphs there is a rate shift in the Lampridiformes + †*Nardovelifer* clade (PP = 0.736) and two weakly supported shifts in the preceding two clades, reflecting some uncertainty as to where the shift occurred. In deeply diverging lampridomorphs, the evolutionary rate is the same as that of the backbone of the phylogeny (0.0004). In Lampridiformes + †*Nardovelifer* the evolutionary rate increases by two orders of magnitude relative to the preceding lampridomorph node (0.0447 versus 0.0004).

There is one rate shift in the deeply diverging percomorphs: there is a strongly supported shift in rate at the base of the Callionymidae + Dactylopteridae clade (PP = 0.906), where there is an increase in rate by two orders of magnitude. At the base of Clade A there is a rate shift, corresponding with an increase of one order of magnitude in median evolutionary rate (0.00419 versus 0.00038), with strong posterior support (PP = 0.936). Up until the level of Clade D, the evolutionary rate is fairly consistent, although there are a number of isolated changes in evolutionary rate. There is a shift with moderate support in the branch leading to the labrid

Epibulus (PP = 0.640). There are four additional rate shifts in each of the four nodes branching below *Epibulus*; collectively, these nodes lead to labrids, scarids, odacids and gerreids. However, all four shifts have low posterior support (PP $\leq$ 0.207) and reflect uncertainty as to where (and if) the shift occurred. In the four nodes with low posterior support for a shift in rate, the median evolutionary rate increases gradually from the deepest node: 0.00427 up to 0.00493. In the branch leading to *Epibulus*, the rate is considerably higher (0.13636) – the highest rate estimate in the analysis. Another shift in rate was detected in the Gasterosteidae + Aulorhynchidae + Hypotychidae clade, although this is also weakly supported by the posterior sample (PP = 0.168) and there is only a twofold increase in median evolutionary rate relative to the preceding node.

In Clade D, eight shifts in evolutionary rate were detected. However, all eight have low posterior support (PP $\leq$ 0.198). The eight shifts are dispersed across Clade D, with three of them occurring along the backbone of the phylogeny, three at nodes branching below the leiognathid + chaetodontid clade, one at the base of Caproidae, and one at the base of the Triacanthodidae + Molidae + Triacanthidae clade. In clade D, there is a small and gradual increase in evolutionary rate along the backbone of the phylogeny, with the deepest node having the lowest value (0.00431); the highest rate is in the Leiognathidae + Chaetodontidae clade (0.00804).

4.3.4.2 Extant taxa only

When the fossil taxa are excluded from the analysis (Fig. 4.8), the general evolutionary rate across the tree is higher, and more homogenous, than in the analysis including fossils. On the deepest branches, in the analysis excluding fossils, the median evolutionary rate (0.00192) is over five times higher than that in the analysis including them (0.00036). In the analysis with no fossil taxa, there is no shift in evolutionary rate at the base of the zeiogadiform clade, although there is very weak support (PP = 0.035) for a shift in the preceding node. As in the analysis containing all taxa, there is strong support for an increase in evolutionary rate in Lampridiformes (PP = 0.839). At the base of the lampridiform clade, the

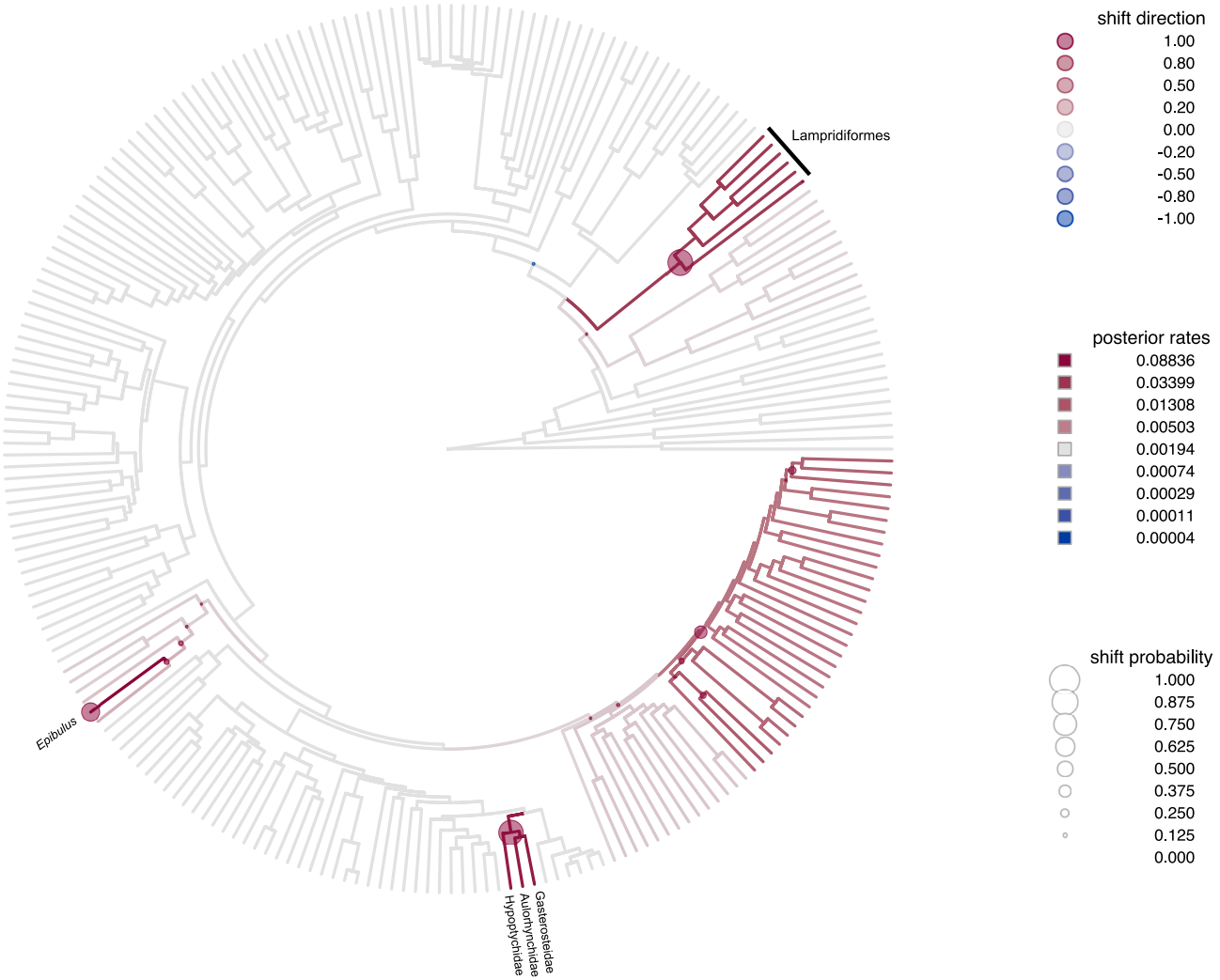

Figure 4.8: Rate of evolution of the jaw protrusion index using the supertree only containing living taxa. Branch colours indicate the evolutionary rate of the corresponding branch. Coloured circles on nodes and branches indicate possible shifts in evolutionary rate. The colour of circles indicates the direction of the shift and the size of the circles indicates the posterior probability of the shift occurring.

median evolutionary rate is nearly 14 times higher than that of the preceding node (0.02730 versus 0.00196).

There is no support for a shift in evolutionary rate in the Callionymidae + Dactyopteridae clade or at the base of Clade A; in these two clades the evolutionary rate is nearly identical to that of the preceding nodes. As with the analysis including all taxa, there is moderate support for a rate shift in the branch leading to *Epibulus* (PP = 0.616) and weak support for shifts in the preceding four clades (PP $\leq$ 0.207). The shift in the Gasterosteidae + Aulorhynchidae +Hypoptychidae clade, that is weakly supported in the analysis containing all taxa, is strongly supported in this analysis (PP = 0.803); the median evolutionary rate is over 30 times greater than the value of the preceding node (0.06008 versus 0.00194).

Clade D is the area of the tree that most closely resembles the tree from the analysis including fossil taxa. Eight rate shifts are detected, none of which have a posterior probability >0.392; five have posterior probabilities <0.2. Three of these shifts occur along the backbone of the phylogeny, three occur on nodes leading to the leiognathids and chaetodontids, and two lead to tetraodontiform lineages with high protrusion.

4.3.5 Tempo of jaw protrusion evolution

In the acanthomorphs, there is a slight increase in JPI values towards the present. Using robust regression, I identified a slight negative linear relationship between the JPIs and ages of tips (y = -0.0018x + 0.6613; Fig. 4.9), although this was not significant (Robust F-test: F = 3.22, d.f. = 272, P = 0.074). The highest JPIs (JPI >3) are found in modern taxa, although some high values (JPI >2) are also found in Eocene and Cretaceous taxa. The lowest protrusion values (JPI <0.01) are only found in modern taxa, although some Eocene taxa have JPIs that are consistent with limited protrusile abilities (JPI <0.2).

When the relative evolutionary rates were averaged across the acanthomorph tree, the global pattern varied greatly between the datasets including and excluding fossils (Fig. 4.10). In both of these analyses, the mean evolutionary rate is strongly

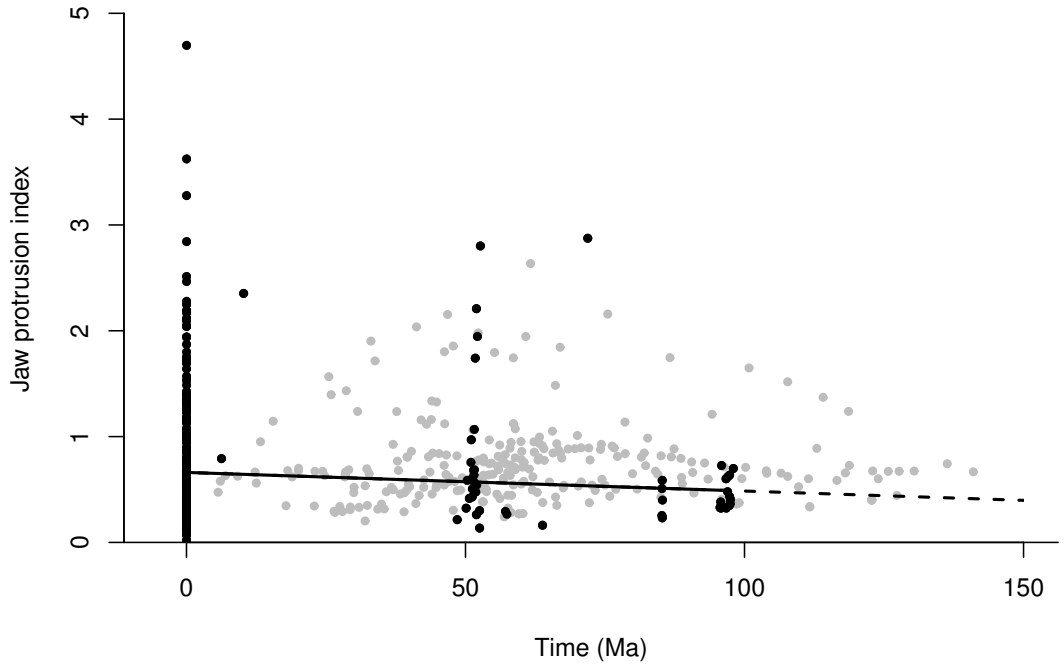

Figure 4.9: Relationship between the jaw protrusion index (JPI) and age of the tips (black data points). Grey data points show the estimates of the JPI node values and the node ages. The grey points are included for illustrative reasons and are not used in the regression analysis. Robust linear regression: y = -0.0018x + 0.6613, Robust F-test: F = 3.22, d.f. = 272, P = 0.074.

influenced by substantial rate increases in isolated lineages – particularly at the base of the tree where there are few branches. The median evolutionary rate provides a more reliable metric for estimating the average rate across the tree as it is less strongly influenced by outliers. In the analysis including fossil taxa (Fig. 4.10A), the global median evolutionary rate at the base of the acanthomorph tree is low (0.0004) and relatively constant, with a small peak in rate (0.00047) at 135 – 130 Ma. Between 100 – 88 Ma there is a steady increase in global median rate. At 88 Ma, the global median evolutionary rate sharply increases from 0.0009 to 0.0031 – a threefold increase. The global evolutionary rate is relatively constant up to 70 Ma where there is another slight increase in rate, before stabilising, and remaining relatively constant. In the analysis excluding fossils (Fig. 4.10B), the global median evolutionary rate is near-constant ($\sim$ 0.002) from the base of the acanthomorph tree up until the present day. The only feature that stands out is a slight increase

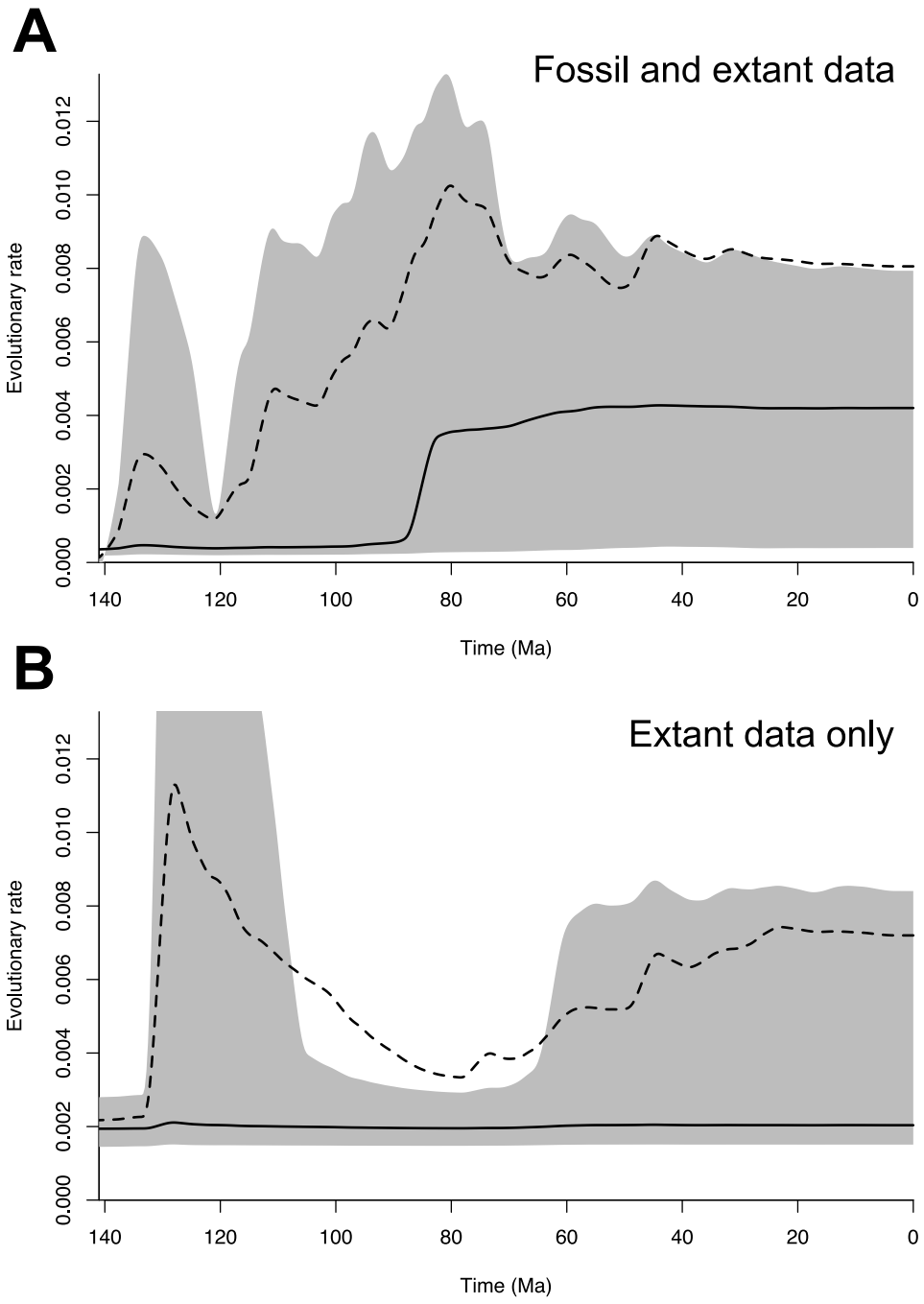

Figure 4.10: The evolutionary rate of the jaw protrusion index averaged across the acanthomorph supertree. **A,** The analysis of the supertree containing both living and fossil taxa. **B,** The analysis of the supertree that only contains extant taxa. The solid black line indicates the median evolutionary rate, while the dashed black line shows the mean evolutionary rate. Only the 80% confidence interval is shown (grey area) to improve visibility of the trend lines. Both panels are shown using the same axis scales for ease of comparison.

in rate (0.00018) at 130 Ma, after which the median global rate stabilises.

4.4 Discussion

4.4.1 Jaw protrusion and morphology

The high correlation between the JPI and the method used by Bellwood et al. (2015) indicates that the JPI is a good stand-in for the more complex approach applied by Bellwood et al. (2015). The JPI has the additional advantage of being able predict protrusion in taxa with vastly different body proportions and in incompletely preserved fossils. A long premaxillary ascending process has been shown to give an indication of the extent of jaw protrusion (Alexander, 1967b; Gosline, 1987; Hulsey et al., 2010; Bellwood et al., 2015). However, the size of the alveolar process relative to the size of the ascending process had not been investigated previously. Taxa reported as having high protrusion in previous studies (e.g. Bellwood et al., 2015: table s2) have long ascending processes and they, typically, have short alveolar processes. When a fish protrudes its upper jaw the minimum gape size is dependent on the length of the alveolar process (e.g. Hulsey et al., 2010: fig. 1), thus possessing long ascending and alveolar processes are not congruent, as a long alveolar process would make protrusion impossible, or at least considerably restrict its use. At the other end of the scale, taxa with long swordfish-like jaws, have no need for an ascending process, as the premaxillae are fused to the skull and cannot be protruded.

Dentition is greatly reduced or lost in taxa with considerable protrusion, whereas taxa with moderate or low levels of protrusion retain much of their dentition. This suggests that taxa with moderate levels of protrusion are optimised for a mixed feeding strategy where the benefits of protrusion are balanced with the need to use the oral jaws for prey retention or reduction. Pharyngeal jaws are found in a number of percomorph lineages, including those, such as labrids (Liem and Sanderson, 1986) and cichlids (Liem, 1973), which have high JPI values. Liem (1973) hypothesised that the evolution of pharyngeal jaws decoupled food capture and processing, allowing the oral and pharyngeal jaws to evolve independently. More recent work supports Liem's hypothesis, showing that in heroine cichlids the oral jaw evolves

independently to the pharyngeal jaw (Hulsey et al., 2006). If this is the case, then the evolution of pharyngognathy could explain the evolution of high protrusion morphologies in taxa, such as labrids and cichlids, which possess pharyngeal jaws. However, it is worth noting that pharyngeal jaws are also found in lineages with low protrusion (e.g. the atherinomorph families Hemiramphidae and Exocoetidae). Pharyngognathy has evolved at least six times in percomorphs (Wainwright et al., 2012) and does not always correlate with high protrusion morphologies.

The origin of the acanthomorph jaw protrusion mechanism has been considered by a number of authors (Alexander, 1967b; Gosline, 1980, 1981; Motta, 1984; Gosline, 1987; Westneat, 2004). Alexander (1967b) proposed that the †ctenothrissiform upper jaw has all the necessary fundamentals for the acanthopterygian jaw protrusion mechanism. The †ctenothrissiform premaxilla has both ascending and articular processes, although the ascending process is short. While these taxa may have had limited protrusile abilities, the advanced state of the premaxillary processes would have allowed the premaxilla to rock back and forth on the base of the neurocranium (Gosline, 1987). However, a similar premaxilla is also found in more deeply diverging teleosts, such as the clupeiforms (Alexander, 1967b; Gosline, 1981), implying that the acanthopterygian jaw could have had a much deeper origin than at the level of the †ctenothrissiforms (see Chapter 3 for a discussion on the presence of primitive characters in †Ctenothrissiformes). Initial modifications to the general teleost jaw may not have initially correlated with high jaw protrusion, and thus would not have been picked up by the JPI (e.g. the rocking mechanism found in †ctenothrissiforms). In order to gain a deeper understanding of the origin of the acanthomorph protrusion mechanism, in-depth functional and anatomical investigation is necessary in taxa in which initial modifications may have occurred. Focus would need to be directed towards non-acanthomorph taxa to identify stepwise changes in osteological and soft-tissue morphology leading up to the level of the acanthomorphs. Part of the challenge in undertaking this task will be understanding the optimization of morphological change across teleost phylogeny.

4.4.2 Jaw protrusion and macroevolution

Jaw protrusion was nearly completely absent in the non-acanthomorph euteleosts that I sampled. In line with previous work (Bellwood et al., 2015), I find that significant protrusion is not phylogenetically restricted: taxa with high JPI values were dispersed across the supertree. In the acanthomorphs, considerable jaw protrusion appears to have originated 14 times. Bellwood et al. (2015) identified 15 lineages with the potential for significant protrusion, 10 of which are identified here, at least in part, as possessing highly protrusile jaws. The two deepest origins, in terms of both time and phylogenetic position, of acanthomorph jaw protrusion occur in the lampridomorphs and at the base of Zeiogadiformes. The area of the phylogeny where these clades originate is characterised by low JPI values and rates of evolutionary change in the JPI. Higher up in the tree a percomorph subclade (Clade A), is characterised by high rates of evolution and contains taxa with a range of JPI values. The taxa within Clade A are morphologically diverse and exhibit morphologies consistent with both high and low protrusion. Taxa exhibiting low and high protrusion are well dispersed across the tree with, seemingly, multiple origins of both of these extreme states. There also appeared to be greater heterogeneity in jaw morphologies (i.e. high vs. low protrusion) in the percomorphs. Schaeffer and Rosen (1961) hypothesised that the general condition of the acanthomorph premaxilla could predispose it to modification. The range of JPI values, representing high levels of diversity in acanthomorph, particularly percomorph, premaxillae indicate that the premaxilla has undergone significant modification from its ancestral condition.

The weak relationship between acanthomorph JPI values and time before present gives a different result to previous work, which found that average protrusion had increased between the Eocene and the present (Bellwood et al., 2015: fig. 4). The heterogeneity between the results presented here and those of Bellwood et al. (2015) can possibly be explained by methodological differences. Bellwood et al. (2015) used discrete time bins that were compared with a PERMANOVA analysis. Here, robust regression was used to see if there was any relationship between the JPI and tip ages of taxa in the sample. The robust regression method that was used here

down-weighs the influence of outliers. Therefore, it is able to better track general acanthomorph trends, while reducing the influence of extreme values in isolated lineages that do not reflect global patterns of protrusion. Following the extinction of non-acanthomorph predatory fish (i.e. those with low protrusion) at the end of the Cretaceous (Cavin, 2002; Friedman, 2009), acanthomorphs filled the vacant morphospace these taxa vacated (Friedman, 2010). The weak slope of the regression between the JPI and time indicates that in acanthomorphs, the ratio between the adoption of low and high protrusion morphologies is relatively constant through time – and highlights the group's success in monopolising a wide range of ecological niches. As the most extreme JPI values, both low and high, are only found in modern taxa, there may be a tendency for acanthomorphs to continue exploring morphospace and new ecological niches. However, there is the possibility that fossil taxa with extreme JPI values are simply not known due to the incompleteness of the fossil record.

Many of the major acanthomorph lineages diverged prior to the end-Cretaceous extinction event (Near et al., 2013), suggesting that in at least some of these lineages the premaxillae had already been modified to both high and low protrusion morphologies. Most of the shifts in jaw protrusion evolutionary rate, with reasonably strong support, predated the Palaeogene. The substantial increase in the median evolutionary rate in the middle Late Cretaceous was followed by a period of gradual rate increase in the late Late Cretaceous before stabilising in the Paleocene. My results suggest that a considerable increase in evolutionary rate of change in protrusion occurred 22 million years before the start of the Paleocene, although there was a very slight increase in rate following the end-Cretaceous extinction event. The timing of this Late Cretaceous shift in rate is consistent with the cranial disparity estimates of Sallan and Friedman (2012), who found that there was a significant increase in acanthomorph cranial disparity between the early and late Late Cretaceous. My results also support the hypothesis put forward by Bellwood et al. (2015) that the adoption of high protrusion morphologies may have laid the foundations for the acanthomorph radiation, rather than directly responded to it. However, the link between the diversification of acanthomorph

lineages and the evolution of protrusion is less clear. In Clade A, the shift in evolutionary rate follows an increase in diversification rate that occurred 7.5 million years earlier (Near et al., 2013). This implies that as new lineages of acanthomorphs evolved they started to explore morphospace and develop modifications to the premaxilla. Conversely, other percomorph innovations, such as the evolution of pharyngeal jaws, did not result in an increase in diversification rate (Alfaro et al., 2009). Developmental plasticity, which can facilitate adaptation, morphological novelty and the exploration of morphospace (West-Eberhard, 2005; Moczek et al., 2011; Susoy et al., 2015), could explain a link between an increase in protrusion and diversification rates. Some acanthomorphs reportedly have ecophenotypic premaxillae, where different ecological conditions, such as the type of available prey, can lead to phenotypic differences, including variation in the length of ascending processes (Witte, 1984; Wintzer and Motta, 2005; Crichigno et al., 2014). This plasticity could lead to increased speciation, where different phenotypes of the same species diverge, which provides a link between increases in diversification rates and increases in the evolutionary rate of change in protrusion.

Acanthomorph lineage diversification rates did not respond to the end-Cretaceous extinction event, although there was a steep decline in diversification rate during the Eocene ($\sim$ 50 Ma; Near et al., 2013). There was no post-Cretaceous decline in the evolutionary rate of change in the JPI. For the evolutionary rate of jaw protrusion to remain high in acanthomorphs, but lineage diversification rates to decline, it suggests that, in this instance, these two variables are not directly linked. There are a few possible explanations for this trend. First, instead of the high evolutionary rate of premaxillary change allowing acanthomorphs to diversify and occupy vacant niches, the elevated evolutionary rate could be sustained by an evolutionary arms race between acanthomorphs and their prey (Bellwood et al., 2015). If the ecological niches that were left vacant at the end of the Cretaceous period were rapidly filled by early Palaeogene acanthomorphs, then a high evolutionary rate of change in the JPI could be sustained by continued adaptation to prey defences. Second, high protrusion may not correlate with

high species richness. Bellwood et al. (2015) suggested that some lineages with independently evolved origins of protrusion are species poor. The results of this study support this view. Across all sampled taxa the JPI data was highly positively skewed, indicating that very few taxa have very high levels of protrusion. Some of these taxa are from groups with few species and occupy specialised ecological niches (e.g. Lampridiformes). The lack of diversity among some extreme protruders implies that extreme protrusion may be a specialist feeding strategy. Therefore, elevated rates of evolutionary change in the JPI would not necessarily correlate with an increase in diversification rate.

While elevated rates of morphological evolution can correlate with high rates of speciaition (e.g. Ricklefs, 2004; Rabosky et al., 2013), morphological evolution can be decoupled from speciation events (e.g. Adams et al., 2009; Venditti et al., 2011; Bapst, 2012). In the context of studying jaw protrusion, using the JPI, an increase in evolutionary rate does not necessarily correspond with higher levels of protrusion, as a reduction in protrusion would also be associated with an increase in evolutionary rate. Therefore, in clades which are phenotypically versatile, elevated rates of protrusion could be sustained. There are a number of acanthomorph clades, such as blennies, cichlids, labrids and tetraodontiforms, that are characterised by highly versatile jaw morphology and high rates of evolution of the JPI. However, these clades are also highly speciose ($>$ 350 species), so a link between elevated rates of diversification and morphological evolution cannot be discredited. There are less speciose clades with very high rates of evolution of protrusion: the zeiforms and lampridiforms. The premaxillae in these taxa appear to be conservative, as they all tend to use protrusion and suction feeding as a primary feeding mechanism. However, the extent of protrusion does vary in some of these taxa. For example, in the lampridform *Regalecus* its JPI is considerably lower than in all other lineages of crown lampridiforms. It is also worth noting that the general morphology of the lampridiforms is highly variable between lineages. Therefore, the lampridiforms could be regarded as being morphologically highly versatile. Both the lampridiforms and zeiforms are specialised deep-sea forms, so in

these groups, elevated rates of evolution could correlate with specialisation, rather than speciation. A caveat with this study is that the JPI can only detect changes in protrusile ability, and not gross changes in premaxillary morphology (i.e. the adoption of morphologies consistent with other feeding methods). Therefore, if a lineage that belongs to a clade that is already characterised by low levels of protrusion, evolved an extreme structure, such as a sword-like jaw, then the rate of evolutionary change in the JPI would be low. For a more in-depth investigation into the link between phenotypic versatility of the feeding morphology and the rate of morphological evolution, a different index to the JPI will be required.

4.4.3 Inclusion of fossil data in macroevolution analyses

The inclusion of fossil data has been shown to help aid the detection of macroevolutionary trends that otherwise could not have been apparent from studying extant taxa in isolation (Finarelli and Flynn, 2006; Slater et al., 2012; Benson and Choiniere, 2013; Slater and Harmon, 2013; Betancur-R et al., 2015). In this study, the disparity between JPI node estimates from the datasets including and excluding fossil taxa increased with time before present. This increase in disparity is likely due to the lack of constraint for deep nodes in the analysis excluding fossils (Finarelli and Flynn, 2006; Slater et al., 2012; Betancur-R et al., 2015). Fossil taxa – particularly those that branch deeply, in areas of the tree with long branches – act as calibration points that aid inference of JPI values at deep nodes.

There was a stark contrast between the results of the evolutionary rates analyses that included and excluded fossil taxa. In both analyses, the evolutionary rate estimates were similar in the parts of the tree furthest from the root (e.g. Clade D). However, in the extant only analysis, at the base of the tree, where there are long branches, the rate of evolution was elevated relative to the analysis where fossil taxa were included. Furthermore, when the large-scale trends that characterise the acanthomorph clade were studied, there were substantial differences between the two datasets. In the analysis including fossils, the rate of evolutionary change in the JPI was low in early acanthomorphs, before sharply increasing in the

Late Cretaceous and stabilising in the Palaeogene. However, when fossil taxa were excluded, the evolutionary rate was near-constant over the entire 140 million years of acanthomorph evolutionary history. In this instance, the inclusion of fossil data exposes heterogeneity in evolutionary rate that would otherwise not be apparent.

The inclusion of fossil data does not always result in different estimates of ancestral trait values or evolutionary rates compared to analyses only containing extant taxa, although the confidence of estimates may be increased (Puttick and Thomas, 2015).Here, the inclusion of fossil data did not change the inferred number of origins of high levels of protrusion. Nearly all of the fossil taxa that were included within this study belong to extant families. However, most of the fossil acanthomorphs that could not be included in this study due to a lack of phylogenetic hypotheses defining their relationships, are still closely related to, and morphologically similar to extant taxa (Patterson, 1993; Bannikov, 2014b). Therefore, the inclusion of these taxa is unlikely to help identify further origins of protrusion, although the location and timing of origins could be refined, as they were for the lampridiforms and caproids in this study. The effect that the inclusion of fossil data has on an analysis is not something that can be determined *a priori*. Therefore, macroevolutionary analyses that neglect to include fossil data are likely missing valuable information that will either improve confidence in estimates obtained from studying extant taxa in isolation, or, as is the case in this study, reveal otherwise hidden macroevolutionary trends.

5 Conclusion

Contents

5.1 The rise of the acanthomorphs: a few secrets revealed 149
5.2 The evolution of primitive acanthomorph groups . . . 150
5.3 The origins of the acanthomorphs 151
5.4 Acanthomorph macroevolution 152
5.5 The importance of revisiting 'old' fossils 153
5.6 Reconstructing relationships between living and fossil taxa 155
5.7 Summary 156

5.1 The rise of the acanthomorphs: a few secrets revealed

With over 18,500 living species and hundreds of known fossil taxa, unravelling all the secrets behind the success of the acanthomorphs will be a long, laborious, and most likely, impossible task. In the past, there has been a tendency to view palaeontological and neontological datasets as separate entities, instead of combining them to gain a more complete picture of acanthomorph evolution. The overarching goal of this thesis was to understand the effect that combining palaeontological and neontological data has on interpreting the evolutionary history of one of the most successful extant groups of vertebrates, the acanthomorph fishes. I aimed to achieve

this by undertaking three projects, with each one focusing on a different aspect of acanthomorph evolution, which collectively would have the potential to enhance our understanding of their origins, innovations and evolutionary history.

5.2 The evolution of primitive acanthomorph groups

In Chapter 2, I aimed to augment our understanding of the relationships of a primitive acanthomorph group, the lampridomorphs. The chapter began with detailed anatomical descriptions of two Late Cretaceous lampridomorphs, †*Aipichthys pretiosus* and †'*Aipichthys*' *nuchalis*, which was followed by a phylogenetic analysis, where they were placed relative to 10 extant and 15 extinct taxa. Prior to this work, †*A. pretiosus*, †'*A.*' *nuchalis*, and three other extinct species were regarded as being part of the same genus; the results of the anatomical investigation and phylogenetic analysis do not support this view. Instead, †*A. pretiosus* is shown to be distinct from all other species that were previously included in †*Aipichthys*. The inclusion of †*Nardovelifer altipinnis* and †*Gigapteryx tethyestris* in the phylogenetic analysis also yielded some important results. †*Nardovelifer* was previously viewed as a crown lampridiform (Veliferidae); this view now appears to be incorrect, and †*Nardovelifer* is placed as a stem-lampridiform. †*Gigapteryx* appears to be one of the most deeply-diverging lampridomorphs, and not an acanthopterygian as it was originally assigned. Collectively, these findings help to reveal the origins of the extant lampridiform bodyplan, and show how character evolution may have occurred up to the level of the crown-group.

Fossil taxa that are now assigned to Lampridomorpha have been included in a number of phylogenetic analyses (e.g. Otero and Gayet, 1996; Alvarado-Ortega and Than-Marchese, 2012; Davesne et al., 2014; Chapter 2). As a result of this, the relationships of the lampridomorphs are now some of the most well-known of all acanthomorph groups with fossil representatives. Other groups of acanthomorphs now need to be subjected to similar in-depth phylogenetic analyses. The availability of a phylogeny that unites the extinct and extant members of a group of living and fossil acanthomorphs unleashes the potential of those fossil taxa as a data

source to evolutionary biologists, as they can then be included in further analyses with much more ease (e.g. phylogenetic comparative methods). Extant taxa from the most deeply-diverging acanthomorph lineages are connected by long branches. Understanding how fossil taxa are related to these extant taxa has the potential to break up these long branches and provide insight into the evolution of these groups. Deeply diverging acanthomorph lineages in which the relationships to fossil relatives are poorly known should initially be targeted, as there is the most to gain from studying these groups. Lineages that meet this criteria include Polymixiiformes and Beryciformes, whose relationships are currently poorly defined. Although the phylogenetic relationships of fossil percomorphs are some of the most poorly known, when most of these lineages first appear in the fossil record in the Eocene they are already anatomically modern (Greenwood et al., 1966; Patterson, 1993; Maisey, 1996). Therefore, targeting primitive acanthomorphs is likely to provide greater insight into acanthomorph evolution at this stage.

5.3 The origins of the acanthomorphs

In Chapter 3, the origin of the acanthomorph clade was investigated by studying two lineages of extinct fishes with uncertain affinities: the †ctenothrissiforms and †pattersonichthyiforms. First, the anatomy of †*Aulolepis typus* (†Ctenothrissiformes) was reappraised in light of new insights from computed tomography (CT) scanning. †*Aulolepis*, †*Ctenothrissa* (†Ctenothrissiformes), †*Pattersonichthys* (†Pattersonichthyiformes) and 18 additional taxa (living and fossil) were included in morphology only and combined morphology and molecular datasets, which were analysed using parsimony and Bayesian methods, before being subjected to Bayesian topological hypothesis tests. Although a stem acanthomorph position has been previously considered for the †ctenothrissiforms, I find that the †ctenothrissiforms and †pattersonichthyiforms are stem ctenosquamates. The placement of these taxa as stem ctenosquamates provides insight into the primitive condition that was present at the base of Acanthomorpha. However, the results of the analyses support two alternative topologies. Analysis of the characters supporting the two

topologies seems to suggest that one of the hypotheses, where the three taxa of interest represent a grade of stem ctenosquamates, is more likely.

While broad eurypterygian relationships are strongly supported by numerous morphological (Rosen, 1973; Lauder and Liem, 1983; Stiassny, 1986; Johnson, 1992; Stiassny and Moore, 1992; Johnson and Patterson, 1993; Grande et al., 2013) and molecular (Chen et al., 2003; Dettai and Lecointre, 2005; Broughton, 2010; Near et al., 2012; Betancur-R et al., 2013; Grande et al., 2013; Near et al., 2013; Chen et al., 2014) analyses, the placements of fossil taxa that branch outside of the crown-groups of the major lineages (Aulopiformes, Myctophiformes and Acanthomorpha) are less than certain. Although I found strong support for a stem ctenosquamate placement for the †ctenothrissiforms and †pattersonichthyiform, character evolution among fossil taxa in this area of the tree is complicated. The polarity of primitive teleost characters found in fossil taxa at the level of Eurypterygii is hard to discern and needs further investigation. Areas of focus could include the placement of eurypterygians with uncertain affinity (e.g. †*Nematonotus*, †*Sardinoides*) and developing our knowledge of the early evolution of teleost lineages that branch prior to Eurypterygii. This two-pronged approach could enhance our understanding of character evolution up to the level of the eurypterygians, revealing the primitive acanthomorph condition.

5.4 Acanthomorph macroevolution

The aim of Chapter 4 was to investigate the evolution of jaw protrusion in the acanthomorphs. Using a timescaled informal supertree of 275 acanthomorphs (223 extant, 49 extinct) and a novel metric that acts as a proxy for protrusion, I produced the first large-scale phylogenetic study of the evolution of jaw protrusion. Ancestral character reconstruction was used to map the evolution of protrusion across the supertree, revealing broad patterns of protrusion in the acanthomorphs. The rate of evolution of jaw protrusion was studied using a Bayesian methodology, where there were strongly supported increases in evolutionary rate in two primitive acanthomorph lineages (Zeiogadiformes, Lampridomorpha) and three percomorphs

clades (Callionymidae + Dactylopteridae, a large unnamed percomorph clade [Clade A], and the branch leading to *Epibulus*). When averaged across the acanthomorph tree, there is a strong increase in median evolutionary around 88 Ma, after which it remains high. These findings provide insight into the role that protrusion may have played in the acanthomorph's rise to dominance in the Recent. However, the inclusion of fossil data played an important role in the detection of these macroevolutionary patterns. When fossil taxa were excluded from the ancestral character reconstruction there were incongruities in estimated node values, which were elevated towards the root of the tree. The exclusion of fossil taxa from the evolutionary rates analyses led to a higher, but more homogenous rate of evolution across the tree. When this data is averaged across the tree there is no global increase in evolutionary rate – it is near constant throughout the entire evolutionary history of the acanthomorphs.

My work on jaw protrusion was the first instance of a large-scale macroevolutionary analysis of the acanthomorphs that used an underlying phylogenetic framework of living and fossil taxa. Because of the lack of phylogenetic hypotheses for many fossil acanthomorphs, a full resolved acanthomorph tree of life does not exist and is unlikely to exist for some time. Supertrees can be used as a proxy for the tree of life and can provide researchers with a framework for asking macroevolutionary questions that are pertinent to understanding their evolution. The supertree method that I used here to create the first acanthomorph supertree, has the potential to unveil many more insights into acanthomorph evolution: it could be used to investigate the evolution of other functional traits (e.g. fin spines, pharyngeal jaws), clade-specific patterns of gross body morphology (e.g. body size and shape), and morphological disparity between clades, to give a few examples.

5.5 The importance of revisiting 'old' fossils

Most extinct vertebrates, including acanthomorphs, are primarily known from their fossilised skeletal remains. Consequently, if we wish to understand how these extinct taxa evolved, then studying their skeletal remains is the only way of doing so. When

viewed through a modern lens, early anatomical descriptions (i.e. 19th – early 20th century) of fossil fish are insufficient. Early anatomical descriptions of fossils were usually based on the anatomical characters that were considered important at the time for classifying the fossil taxon being studied. As the methods for reconstructing phylogenetic relationships matured and our knowledge of synapomorphies that define those relationships has developed, our knowledge of anatomy has become much deeper. As a consequence, early anatomical descriptions lack much of the character data that is considered important to a modern systematist. In this thesis, the re-descriptions of †*A. pretiosus*, †'*A.*' *nuchalis* and †*Aulolepis*, all of which were first described in the mid-1800s and most recently described in the 1960s, revealed numerous anatomical details which had not been previously known – some of which had significant phylogenetic implications. However, the significance of these anatomical details could not have been known to the palaeontologists of the past. As a result of this, previously described taxa need to be reappraised, and if necessary re-described, in light of developments to our knowledge of characters that have phylogenetic significance. Even though the description of †*Aulolepis* that is presented by Patterson (1964) is highly detailed, spans 15 pages and contains eight figures, there were still details lacking that are now considered phylogenetically important. Therefore, even if an anatomical description appears detailed and complete, there will always be scope to update it in light of new developments. Finally, the now widespread use of CT scanning technology in palaeontology also has the potential to reveal new anatomical details that were hidden from researchers of the past. This includes phylogenetically important structures like the gill skeleton, which was described for †*Aulolepis* in this thesis. Hopefully the re-descriptions included in this thesis illustrate the potential that revisiting previously described taxa has on developing our understanding of the evolution of the acanthomorphs, and other taxonomic groups. While fieldwork may be the primary source of new data for palaeontologists, revisiting the millions of specimens that are already held in museum collections can provide new and insightful discoveries.

5.6 Reconstructing relationships between living and fossil taxa

If as biologists we want to reconstruct a complete tree of life, then we must understand how fossil taxa are related to living taxa. There are three types of dataset that an evolutionary biologist can choose to use when undertaking a phylogenetic analysis: morphology, molecular, and combined morphology and molecular datasets. Of course, a molecular dataset is not directly useful for understanding the relationships between fossil and living taxa (but see below). Therefore, to place extinct taxa amongst extant taxa, either a morphology or combined dataset must be used. In Chapter 3, I compared the results of a morphology only and a combined dataset, both of which were evaluated using parsimony and Bayesian methodologies. Although the broad tree structure was similar, and the †ctenothrissiform and †pattersonichthyiform taxa were all placed as stem ctenosquamates, there was some heterogeneity in results of all four of these analyses. The inconsistencies between these results highlight the importance of dataset and model selection when undertaking phylogenetic analyses. The lack of congruence between analyses can be used to highlight areas of uncertainty in the topology. Conversely, there are some analyses where the addition of molecular data is unlikely to improve inference. In the phylogenetic analysis of the lampridomorphs in Chapter 2, 15 fossil taxa were arranged as a grade of stem lampridomorphs with six branching events leading up to the crown-group. The addition of molecular data is unlikely to refine the relationships of the fossil taxa that are found in this area of the tree, although it may have further resolved other areas of the topology. In Chapter 4, I built a supertree to investigate how jaw protrusion evolved in the acanthomorphs. Although fossil taxa cannot be included in a molecular dataset, the resulting phylogenies from these analyses can be used to understand the relationships of fossil taxa. The availability of a well-resolved molecular phylogeny spanning the whole of Acanthomorpha was essential to be able to reconstruct this supertree. For many of the fossil taxa in the tree their family level assignment was the most detailed information documenting their relationships to living taxa. In

this case, familial assignments were sufficient to place them on the supertree. More finely detailed hypotheses of relationships would be necessary for supertrees where sub-family level relationships are required; currently, the acanthomorphs would not be a suitable taxonomic group for use in this scenario.

5.7 Summary

In the three research-based chapters that form the core part of this thesis, the juxtaposition of palaeontological and neontological data has provided new insights into the evolution of the acanthomorphs, and the dawn of the "Second Age of Fishes" (Near et al., 2012). Unlike some other well-studied taxonomic groups, such as the dinosaurs, our understanding of the evolution of the acanthomorphs is at a much more primitive state. For those researchers interested in understanding the evolution of life and the origins of modern biodiversity, the acanthomorphs are an untapped well. We are only just beginning to solve the puzzle that is the Palaeogene acanthomorph radiation, and there are many secrets left to reveal.

References

Abel, R. L., Laurini, C. R., and Richter, M. (2012). A palaeobiologist's guide to 'virtual' micro-CT preparation. *Palaeontologia Electronica* 15.2, pp. 1–16.

Adams, D. C., Berns, C. M., Kozak, K. H., and Wiens, J. J. (2009). Are rates of species diversification correlated with rates of morphological evolution? *Proceedings of the Royal Society B: Biological Sciences* 276.1668, pp. 2729–2738.

Agassiz, L. (1844). Recherches sur les poissons fossiles. Book V. Neuchatel: Imprimerie de Petitpierre, p. 160.

Alexander, R. (1967a). Functional Design in Fishes. London: Hutchinson & Co, p. 160.

— (1967b). The functions and mechanisms of the protrusible upper jaws of some acanthopterygian fish. *Journal of Zoology* 151.1, pp. 43–64.

Alfaro, M. E., Brock, C. D., Banbury, B. L., and Wainwright, P. C. (2009). Does evolutionary innovation in pharyngeal jaws lead to rapid lineage diversification in labrid fishes? *BMC Evolutionary Biology* 9.1, p. 255.

Alvarado-Ortega, J. and Than-Marchese, B. A. (2012). A Cenomanian aipichthyoid fish (Teleostei, Acanthomorpha) from America, *Zoqueichthys carolinae* gen. and sp. nov. from El Chango Quarry (Cintalapa member, Sierra Madre Formation), Chiapas, Mexico. *Revista Mexicana de Ciencias Geologicas* 29.3, pp. 735–748.

Anderson, J. S. (2001). The phylogenetic trunk: maximal inclusion of taxa with missing data in an analysis of the Lepospondyli (Vertebrata, Tetrapoda). *Systematic Biology* 50.2, pp. 170–193.

Arcila, D., Alexander Pyron, R., Tyler, J. C., Ortí, G., and Betancur-R., R. (2015). An evaluation of fossil tip-dating versus node-age calibrations in tetraodontiform fishes (Teleostei: Percomorphaceae). *Molecular Phylogenetics and Evolution* 82.PA, pp. 131–145.

Arratia, G. (1991). "The caudal skeleton of Jurassic teleosts: a phylogenetic analysis". In: *Early Vertebrates and Related Problems in Evolutionary Biology*. Ed. by G. R. Zhang, M.-M. Chang, and Y. H. Liu. Beijing: Science Press, pp. 249–430.

Atsumi, K. (2016). Anatomical features of the pelvic girdle in the family Ateleopodidae (Pisces: Ateleopodiformes). *Bulletin of Fisheries Sciences, Hokkaido University* 66.2, pp. 59–61.

Baciu, D.-S., Bannikov, A. F., and Tyler, J. C. (2005). Revision of the fossil fishes of the family Caproidae (Acanthomorpha). *Bollettino del Museo Civico di Storia Naturale di Verona* 11, pp. 7–74.

Baldwin, C. C. and Johnson, G. D. (1996). "Interrelationships of Aulopiformes". In: *Interrelationships of fishes*. Ed. by M. L. J. Stiassny, L. R. Parenti, and G. D. Johnson. San Diego, pp. 355–404.

Bannikov, A. F. (1990). An Eocene veliferoid (Teleostei, Lampridiformes) from Bolca. *Studi e Ricerche sui Giacimenti Terziari di Bolca* 6, pp. 161–174.

— (1999). A review of fossil Lampridiformes (Teleostei) finds with a description of a new Lophotidae genus and species from the Oligocene of the Northern Caucasus. *Paleontological Journal* 33.1, pp. 68–76.

— (2014a). A new genus of the family Palaeocentrotidae (Teleostei, Lampridiformes) from the Oligocene of the northern Caucasus and comments on other fossil Veliferoidei. *Paleontological Journal* 48.6, pp. 624–632.

— (2014b). The systematic composition of the Eocene actinopterygian fish fauna from Monte Bolca, northern Italy, as known to date. *Miscellanea paleontologica* 12, pp. 22–34.

Bannikov, A. F. and Tyler, J. C. (1995). Phylogenetic revision of the fish families Luvaridae and Kushlukiidae (Acanthuroidei), with a new genus and two new species of Eocene luvarids. *Smithsonian Contributions to Paleobiology* 81, pp. 1–45.

Bapst, D. W. (2012). paleotree : an R package for paleontological and phylogenetic analyses of evolution. *Methods in Ecology and Evolution* 3.5, pp. 803–807.

— (2013). A stochastic rate-calibrated method for time-scaling phylogenies of fossil taxa. *Methods in Ecology and Evolution* 4.8. Ed. by G. Slater, pp. 724–733.

— (2014). Assessing the effect of time-scaling methods on phylogeny-based analyses in the fossil record. *Paleobiology* 40.03, pp. 331–351.

Bassani, F. (1882). Descrizione dei pesci fossili di Lesina, accompagnata da appunti su alcune alter ittiofaune Cretace. *Denkschriften Akademie der Wissenschaften in Wien* 45, pp. 195–288.

Baum, B. R. (1992). Combining trees as a way of combining data sets for phylogenetic inference, and the desirability of combining gene trees. *Taxon* 41.1, p. 3.

Bellwood, D. R., Goatley, C. H., Bellwood, O., Delbarre, D. J., and Friedman, M. (2015). The rise of jaw protrusion in spiny-rayed fishes closes the gap on elusive prey. *Current Biology* 25.20, pp. 2696–2700.

Benson, D. A., Karsch-Mizrachi, I., Lipman, D. J., Ostell, J., and Wheeler, D. L. (2005). GenBank. *Nucleic Acids Research* 33.Database issue, pp. D34–D38.

Benson, R. B. J. and Choiniere, J. N. (2013). Rates of dinosaur limb evolution provide evidence for exceptional radiation in Mesozoic birds. *Proceedings of the Royal Society B: Biological Sciences* 280.1768, p. 20131780.

Benton, M. J. and Ayala, F. (2003). Dating the tree of life. *Science* 300.5626, pp. 1698–1700.

Berg, L. S. (1940). A classification of fishes, both recent and fossil. *Akademiia nauk SSSR. Zoologicheskiĭ institut* 5, pp. 87–517.

Bergsten, J., Nilsson, A. N., and Ronquist, F. (2013). Bayesian tests of topology hypotheses with an example from diving beetles. *Systematic Biology* 62.5, pp. 660–673.

Berry, F. H. (1964). Aspects of the development of the upper jaw bones in teleosts. *Copeia* 1964.2, pp. 375–384.

Bertin, L. and Arambourg, C. (1958). "Super-ordre des Téléostéens". In: *Traité de Zoologie: Anatomie, Systématique, Biologie, Tome 13: Agnathes et Poissons, Fascicule 3*. Ed. by P.-P. Grassé. Paris: Masson et Cie, pp. 2204–2500.

Betancur-R, R., Broughton, R. E., Wiley, E. O., Carpenter, K., Lopez, J. A., Li, C., Holcroft, N. I., Arcila, D., Sanciangco, M., Cureton, J. C., Zhang, F., Buser, T., Campbell, M. A., Ballesteros, J. A., Roa-Varón, A., Willis, S., Borden, W. C., Rowley, T., Reneau, P. C., Hough, D. J., Lu, G., Grande, T., Arratia, G., and Ortí, G. (2013). The Tree of Life and a New Classification of Bony Fishes. *Tree of Life*, pp. 1–54.

Betancur-R, R., Ortí, G., and Pyron, R. A. (2015). Fossil-based comparative analyses reveal ancient marine ancestry erased by extinction in ray-finned fishes. *Ecology Letters* 18.5, pp. 441–450.

Bininda-Emonds, O. R. P., Gittleman, J. L., and Steel, M. A. (2002). The (super)tree of life: procedures, problems, and prospects. *Annual Review of Ecology and Systematics* 33.1, pp. 265–289.

Bininda-Emonds, O. R. P. and Sanderson, M. J. (2001). Assessment of the accuracy of matrix representation with parsimony analysis supertree construction. *Systematic Biology* 50.4, pp. 565–579.

Bininda-Emonds, O. R. (2004). The evolution of supertrees. *Trends in Ecology & Evolution* 19.6, pp. 315–322.

Blender Foundation (2013). *Blender*. Amsterdam.

Block, B., Booth, D., and Carey, F. (1992). Direct measurement of swimming speeds and depth of blue marlin. *Journal of Experimental Biology* 166, pp. 267–284.

Blot, J. (1969). Les poissons fossiles du Monte Bolca classes jusqu'ici dans les familles des Carangidae, Menidae, Ephip- pidae, Scatophagidae. *Studi e Ricerche sui Giacimenti Terziari di Bolca* 1, pp. 1–526.

Bonde, N. (1987). Moler its origin and its fossils, especially fishes. Nykøbing Mors: Morsø Bogtrykkeri, p. 47.

Boulenger, G. A. (1904). "Fishes (systematic account of Teleostei)". In: *Cambridge Natural History, Volume 7*. Ed. by S. F. Harmer and A. E. Shipley. London: Macmillian and Co., pp. 541–727.

Broughton, R. E. (2010). "Phylogeny of teleosts based on mitochondrial genome sequences". In: *Origin and Phylogenetic Interrelationships of Teleosts*. Ed. by

J. S. Nelson, H.-P. Schultze, and M. V. H. Wilson. Munich: Verlag Dr. Friedrich Pfeil, pp. 61–76.

Caldwell, M. W. and Cooper, J. A. (1999). Redescription, palaeobiogeography and palaeoecology of *Coniasaurus crassidens* Owen, 1850 (Squamata) from the Lower Chalk (Cretaceous; Cenomanian) of SE England. *Zoological Journal of the Linnean Society* 127, pp. 523–452.

Carnevale, G. (2004). The first fossil ribbonfish (Teleostei, Lampridiformes, Trachipteridae). *Geological Magazine* 141.5, pp. 573–582.

Carnevale, G. and Pietsch, T. W. (2010). Eocene handfishes from Monte Bolca, with description of a new genus and species, and a phylogeny of the family Brachionichthyidae (Teleostei: Lophiiformes). *Zoological Journal of the Linnean Society* 160.4, pp. 621–647.

— (2012). †*Caruso*, a new genus of anglerfishes from the Eocene of Monte Bolca, Italy, with a comparative osteology and phylogeny of the teleost family Lophiidae. *Journal of Systematic Palaeontology* 10.1, pp. 47–72.

Casier, E. (1966). Faune Ichthyologique du London Clay. London: Trustees of the British Museum (Natural History), p. 496.

Cavin, L. (2002). "Effects of the Cretaceous-Tertiary boundary event on bony fishes". In: *Geological and biological effects of impact events*. Ed. by E. Buffetaut and C. Koeberl. Berlin, Heidelberg: Springer, pp. 141–158.

Cavin, L., Jurkovšek, B., and Kolar-Jurkovšek, T. (2000). Stratigraphic succession of the Upper Cretaceous fish assemblages of Kras (Slovenia). *Geologija* 43.2, pp. 165–195.

Chapman, W. M. (1944). On the osteology and relationships of the South American fish, *Aplochiton zebra* Jenyns. *Journal of Morphology* 75.1, pp. 149–165.

Chen, W.-J., Bonillo, C., and Lecointre, G. (2003). Repeatability of clades as a criterion of reliability: a case study for molecular phylogeny of Acanthomorpha (Teleostei) with larger number of taxa. *Molecular phylogenetics and evolution* 26.2, pp. 262–88.

Chen, W.-J., Santini, F., Carnevale, G., Chen, J.-N., Liu, S.-H., Lavoué, S., and Mayden, R. L. (2014). New insights on early evolution of spiny-rayed fishes (Teleostei: Acanthomorpha). *Frontiers in Marine Science* 1.53.

Clarke, J. T., Lloyd, G. T., and Friedman, M. (2016). Little evidence for enhanced phenotypic evolution in early teleosts relative to their living fossil sister group. *Proceedings of the National Academy of Sciences* 113.41, pp. 11531–11536.

Close, R. A., Johanson, Z., Tyler, J. C., Harrington, R. C., and Friedman, M. (2016). Mosaicism in a new Eocene pufferfish highlights rapid morphological innovation near the origin of crown tetraodontiforms. *Palaeontology* 59.4. Ed. by J. Sigwart, pp. 499–514.

Collar, D. C., O'Meara, B. C., Wainwright, P. C., and Near, T. J. (2009). Piscivory limits diversification of feeding morphology in centrarchid fishes. *Evolution* 63.6, pp. 1557–1573.

Cope, E. D. (1871). Observations on the Systematic Relations of the Fishes. *The American Naturalist* 5.8/9, pp. 579–593.

Cornwell, W. and Nakagawa, S. (2017). Phylogenetic comparative methods. *Current Biology* 27.9, R333–R336.

Cracraft, J. (2002). The seven great questions of systematic biology: an essential foundation for conservation and the sustainable use of biodiversity. *Annals of the Missouri Botanical Garden* 89.2, p. 127.

Cracraft, J. and Donoghue, P. C. J. (2004). Assembling the Tree of Life. Oxford: Oxford University Press, p. 592.

Crichigno, S. A., Battini, M. Á., and Cussac, V. E. (2014). Diet induces phenotypic plasticity of *Percichthys trucha* (Valenciennes, 1833) (Perciformes, Percichthyidae) in Patagonia. *Zoologischer Anzeiger* 253.3, pp. 192–202.

Darwin, C. (1859). On the Origin of Species by Means of Natural Selection, or the Preservation of Favoured Races in the Struggle for Life. London: John Murray, p. 502.

Davenport, J. (1994). How and why do flying fish fly? *Reviews in Fish Biology and Fisheries* 4.2, pp. 184–214.

Davesne, D. (2017). A fossil unicorn crestfish (Teleostei, Lampridiformes, Lophotidae) from the Eocene of Iran. *PeerJ* 5, e3381.

Davesne, D., Carnevale, G., and Friedman, M. (2017). *Bajaichthys elegans* from the Eocene of Bolca (Italy) and the overlooked morphological diversity of Zeiformes (Teleostei, Acanthomorpha). *Palaeontology* 60.2. Ed. by Z. Johanson, pp. 255–268.

Davesne, D., Friedman, M., Barriel, V., Lecointre, G., Janvier, P., Gallut, C., and Otero, O. (2014). Early fossils illuminate character evolution and interrelationships of Lampridiformes (Teleostei, Acanthomorpha). *Zoological Journal of the Linnean Society* 172.2, pp. 475–498.

Davesne, D., Gallut, C., Barriel, V., Janvier, P., Lecointre, G., and Otero, O. (2016). The phylogenetic intrarelationships of spiny-rayed fishes (Acanthomorpha, Teleostei, Actinopterygii): fossil taxa increase the congruence of morphology with molecular data. *Frontiers in Ecology and Evolution* 4, pp. 1–20.

Davis, M. P. (2010). "Evolutionary relationships of the Aulopiformes (Euteleostei: Cyclosquamata): a molecular and total evidence approach". In: *Origin and Phylogenetic Interrelationships of Teleosts*. Ed. by J. S. Nelson, H.-p. Schultze, and M. V. H. Wilson. Munich: Verlag Dr. Friedrich Pfeil, pp. 545–567.

De Pinna, M. C. C. (1996). "Teleostean monophyly". In: *Interrelationships of Fishes*. Ed. by M. L. J. Stiassny, L. R. Parenti, and G. D. Johnson. San Diego: Academic Press, pp. 147–162.

Delbarre, D. J., Davesne, D., and Friedman, M. (2016). Anatomy and relationships of †*Aipichthys pretiosus* and †'*Aipichthys*' *nuchalis* (Acanthomorpha: Lampridomorpha), with a review of Late Cretaceous relatives of oarfishes and their allies. *Journal of Systematic Palaeontology* 14.7, pp. 545–567.

Dembo, M., Matzke, N. J., Mooers, A. Ø., and Collard, M. (2015). Bayesian analysis of a morphological supermatrix sheds light on controversial fossil hominin relationships. *Proceedings of the Royal Society B: Biological Sciences* 282.1812, p. 20150943.

d'Erasmo, G. (1946). L'ittiofauna cretacea di Comeno nel Carso triestino. *Atti della Accademis Science Fische, Mathematiche, Napoli (3a)* 2, pp. 1–136.

Dettai, A. and Lecointre, G. (2005). Further support for the clades obtained by multiple molecular phylogenies in the acanthomorph bush. *Comptes Rendus - Biologies* 328.7, pp. 674–689.

Diedrich, C. G. (2012). Stomach and gastrointestinal tract contents in Late Cenomanian (Upper Cretaceous) teleosts from Black Shales of Germany and analysis of fish mortality and food chains in the upwelling-influenced pre-North Sea basin of Europe. *New Mexico Museum of Natural History and Science Bulletin* 57, pp. 241–254.

— (2014). Skeleton of the fossil shark *Isurus denticulatus* from the Turonian (Late Cretaceous) of Germany — ecological coevolution with prey of mackerel sharks. *Paleontology Journal* 2014, p. 934235.

Dixon, F. (1850). The Geology and Fossils of the Tertiary and Cretaceous formation of Sussex. London: Longman, Brown, Green and Longmans, p. 573.

Dodd, M. S., Papineau, D., Grenne, T., Slack, J. F., Rittner, M., Pirajno, F., O'Neil, J., and Little, C. T. S. (2017). Evidence for early life in Earth's oldest hydrothermal vent precipitates. *Nature* 543.7643, pp. 60–64.

Domenici, P., Wilson, A. D. M., Kurvers, R. H. J. M., Marras, S., Herbert-Read, J. E., Steffensen, J. F., Krause, S., Viblanc, P. E., Couillaud, P., and Krause, J. (2014). How sailfish use their bills to capture schooling prey. *Proceedings of the Royal Society B: Biological Sciences* 281.1784, pp. 20140444–20140444.

Donoghue, M. J., Doyle, J. a., Gauthier, J., Kluge, a. G., and Rowe, T. (1989). The Importance of fossils in phylogeny reconstruction. *Annual Review of Ecology and Systematics* 20.1, pp. 431–460.

Donoghue, P. C. and Benton, M. J. (2007). Rocks and clocks: calibrating the tree of life using fossils and molecules. *Trends in Ecology & Evolution* 22.8, pp. 424–431.

Dornburg, A., Townsend, J. P., Friedman, M., and Near, T. J. (2014). Phylogenetic informativeness reconciles ray-finned fish molecular divergence times. *BMC Evolutionary Biology* 14.1, p. 169.

Eastman, J. M., Alfaro, M. E., Joyce, P., Hipp, A. L., and Harmon, L. J. (2011). A novel comparative method for identifying shifts in the rate of character evolution on trees. *Evolution* 65.12, pp. 3578–3589.

Endo, H. (2002). Phylogeny of the order Gadiformes (Teleostei, Paracanthopterygii). *Memoirs of the Graduate School of Fisheries Sciences, Hokkaido University* 49.2, pp. 75–149.

Eschmeyer, W. N., Fricke, R., and van der Laan, R. (2016). Catalog of Fishes: Genera, Species, References.

Ezard, T. H. G., Thomas, G. H., and Purvis, A. (2013). Inclusion of a near-complete fossil record reveals speciation-related molecular evolution. *Methods in Ecology and Evolution* 4.8, pp. 745–753.

Fastovsky, D. E. and Weishampel, D. B. (2016). Dinosaurs: A Concise Natural History. Cambridge: Cambridge University Press, p. 432.

Fedotov, V. F. and Bannikov, A. F. (1989). "On the phylogenetic relationships of fossil Gadidae". In: *Papers on the Systematics of Gadiform Fishes*. Ed. by D. M. Cohen. Los Angeles: Natural History Museum of Los Angeles County, pp. 187–196.

Fierstine, H. L., Bannikov, A. F., and Monsch, K. A. (2008). A new species of the extinct billfish genus *Palaeorhynchus* (Perciformes, Xiphioidei, Palaeorhynchidae) from the late Early Eocene of Bolca in northern Italy. *Miscellanea Paleontologica, Studi e Ricerche sui Giacimenti Terziari di Bolca, Museo Civico di Storia Naturale di Verona* 12.1996, pp. 7–27.

Fierstine, H. L. and Monsch, K. A. (2002). Redescription and phylogenetic relationships of the family Blochiidae (Perciformes: Scombroidei), Middle Eocene, Monte Bolca, Italy. *Studi e Ricerche sui Giacimenti Terziari di Bolca* 9, pp. 121–163.

Finarelli, J. A. and Flynn, J. J. (2006). Ancestral state reconstruction of body size in the Caniformia (Carnivora, Mammalia): the effects of incorporating data from the fossil record. *Systematic Biology* 55.2, pp. 301–313.

Fink, W. L. and Weitzman, S. H. (1982). Relationships of the stomiiform fishes (Teleostei), with a description of *Diplophos*. *Bulletin of the Museum of Comparative Zoology* 150.2, pp. 31–93.

Forey, P. L. (1973). A revision of the elopiform fishes, fossil and recent. *Bulletin of The British Museum (Natural history) Geology* Supplement, pp. 1–222.

Forey, P. L., Yi, L., Patterson, C., and Davies, C. E. (2003). Fossil fishes from the Cenomanian (Upper Cretaceous) of Namoura, Lebanon. *Journal of Systematic Palaeontology* 1.4, pp. 227–330.

Friedman, M. (2008). The evolutionary origin of flatfish asymmetry. *Nature* 454.7201, pp. 209–212.

— (2009). Ecomorphological selectivity among marine teleost fishes during the end-Cretaceous extinction. *Proceedings of the National Academy of Sciences* 106.13, pp. 5218–5223.

— (2010). Explosive morphological diversification of spiny-finned teleost fishes in the aftermath of the end-Cretaceous extinction. *Proceedings of the Royal Society B: Biological Sciences* 277.1688, pp. 1675–1683.

Friedman, M., Beckett, H. T., Close, R. A., and Johanson, Z. (2016). The English Chalk and London Clay: two remarkable British bony fish Lagerstätten. *Geological Society, London, Special Publications* 430.1, pp. 165–200.

Friedman, M. and Sallan, L. C. (2012). Five hundred million years of extinction and recovery: a phanerozoic survey of large-scale diversity patterns in fishes. *Palaeontology* 55.4, pp. 707–742.

Fujita, K. (1990). The Caudal Skeleton of Teleostean Fishes. Tokyo: Tokai University Press, p. 897.

Gaudant, J. (1979). *Pachylebias crassicaudus* (Agassiz) (Poisson Téléostéen, Cyprinodontiforme), un constituant majeur de l'ichthyofaune du Messinien continental du bassin Méditerranéen. *Geobios* 12.1, pp. 47–73.

Gaudant, M. (1976). Sur la création d'un ordre nouveau de poissons téléostéens, les Pattersonichthyiformes, et sur ses relations phylogénétiques. *Comptes rendus de l'Académie des sciences, Paris, Série D* 283, pp. 1629–1631.

— (1978a). Contribution a l' etude anatomique et systematique de l'ichthyofaune Cenomanienne du Portugal. *Comunicacòes dos Servic os Geológicos du Portugal* 63, pp. 105–149.

— (1978b). Nouvelles observations sur l'anatomie et sur la position systématique d'un poisson téléostéen du Cénomanien du Liban: *Pateroperca* woodward. *Géobios* 11.2, pp. 189–211.

— (1978c). Recherches sur l'anatomie et la systématique des Cténothrissiformes et des Pattersonichthyiformes (poissons téléostéens) du Cénomanien du Liban. *Memoires du Museum National D'Histoire Naturelle, Paris, Série C, Science de la Terre* 41, pp. 1–124.

Gayet, M. (1980a). Contribution a l'etude anatomique et systematique des poissons Cenomamiens du Liban, anciennement places dans les Acanthopterygiens. *Memoires du Museum National D'Histoire Naturelle, Paris, Série C, Science de la Terre,* 44, pp. 1–149.

— (1980b). Recherches sur l'ichthyofaunce Cenomanienne des Monts de Judee: Les Acanthopterygiens. *Annales de Paleontologie (Vertebres)* 66.2, pp. 75–128.

— (1980c). Relations phylogénétiques des poissons Eurypterygii non Acanthomorpha. *Bulletin du Muséum national d'Histoire naturelle, Paris, Série C* 2, pp. 321–337.

Gidmark, N. J., Staab, K. L., Brainerd, E. L., and Hernandez, L. P. (2012). Flexibility in starting posture drives flexibility in kinematic behavior of the kinethmoid-mediated premaxillary protrusion mechanism in a cyprinid fish, *Cyprinus carpio*. *Journal of Experimental Biology* 215.13, pp. 2262–2272.

Gill, T. (1872). Arrangement of the families of fishes. *Smithsonian Miscellaneous Collections* 11, pp. 1–49.

Goody, P. C. (1969). The relationships of certain upper Cretaceous teleosts with special reference to the myctophids. *Bulletin of the British Museum (Natural History)* Supplement, pp. 1–255.

Gorjanovic-Kramberger, C. (1892). *Aigialosaurus*: ein neue eidechse aus den kreideschiefern der insel Lesina mit Rücksicht auf die bereits beschriebenen Lacertiden von Comen und Lesina. *Glasnika Hrvatskoga Naravoslovogna Druztva* 7, pp. 74–106.

— (1895). De piscibus fossilibus Comeni, Mrzleci, Lesinae et M. Libanonis. *Djela Jugoslavenske Akademije* 16, pp. 1–67.

Gosline, W. A. (1961). Some osteological features of modern lower teleostean fishes. *Smithsonian Miscellaneous Collections* 142.3, pp. 1–42.

— (1980). The evolution of some structural systems with reference to the interrelationships of modern lower teleostean fish groups. *Japanese Journal of Ichthyology* 27.1, pp. 1–28.

— (1981). The evolution of the premaxillary protrusion system in some teleostean fish groups. *Journal of Zoology* 193.1, pp. 11–23.

— (1987). Jaw structures and movements in higher teleostean fishes. *Japanese Journal of Ichthyology* 34.1, pp. 21–32.

Gottfried, M. D. (1989). Homology and terminology of higher teleost postcleithral elements. *Transactions of the San Diego Society of Natural History* 21.18, pp. 283–290.

Grande, L. (2010). An empirical synthetic pattern study of gars (Lepisosteiformes) and closely related species, based mostly on skeletal anatomy. The resurrection of Holostei. *Copeia* 2A, supplement, pp. 1–871.

Grande, L. and Bemis, W. E. (1998). A comprehensive phylogenetic study of amiid fishes (Amiidae) based on comparative skeletal anatomy. An empirical search for interconnected patterns of natural history. *Journal of Vertebrate Paleontology* 18.sup001, pp. 1–696.

Grande, T., Borden, W. C., and Smith, W. L. (2013). "Limits and relationships of Paracanthopterygii: a molecular framework for evaluating past morphological hypotheses". In: *Mesozoic Fishes 5 - Global Diversity and Evolution*. Ed. by G. Arratia, H.-P. Schultze, and M. V. H. Wilson. Munich: Verlag Dr. Friedrich Pfeil, pp. 385–418.

Greenwood, P. H., Rosen, D. E., Weitzman, S. H., and Myers, G. S. (1966). Phyletic studies of teleostean fishes, with a provisional classification of living forms. *Bulletin of the American Museum of Natural History* 131.4, pp. 339–456.

Gregory, W. K. (1933). Fish skulls: a study of the evolution of natural mechanisms. *Transactions of the American Philosophical Society* 23.2, pp. 75–481.

Habegger, M. L., Dean, M. N., Dunlop, J. W. C., Mullins, G., Stokes, M., Huber, D. R., Winters, D., and Motta, P. J. (2015). Feeding in billfishes: inferring the role of

the rostrum from a biomechanical standpoint. *Journal of Experimental Biology* 218.6, pp. 824–836.

Haeckel, E. H. P. A. (1866). Generelle Morphologie der Organismen. Berlin: Georg Reimer.

— (1889). Natürliche Schöpfungsgeschichte-Geschichte (Vertebrata). 8th ed. Berlin: Georg Reimer.

— (1895). Systematische Phylogenie der Wirbelthiere. Berlin: Georg Reimer.

Hardenbol, J., Thierry, J., Farley, M. B., Jacquin, T., de Graciansky, P.-C., and Vail, P. R. (1998). Mesozoic and Cenozoic sequence chronostratigraphic framework of European basins. *Mesozoic and Cenozoic Sequence Stratigraphy of European Basins, SEPM Special Publication* 60, pp. 763–786.

Harmon, L. J., Weir, J. T., Brock, C. D., Glor, R. E., and Challenger, W. (2008). GEIGER: investigating evolutionary radiations. *Bioinformatics* 24.1, pp. 129–131.

Harris, V. A. (1960). On the locomotion of the mudskipper *Periophthalmus koelreuteri* (Pallas): (Gobiidae). *Journal of Zoology* 134.1, pp. 107–135.

Hay, O. P. (1903). Some remarks on the fossil fishes of Mount Lebanon, Syria. *American Naturalist* 37.442, pp. 685–695.

Hedman, M. M. (2010). Constraints on clade ages from fossil outgroups. *Paleobiology* 36.01, pp. 16–31.

Hennig, W. (1950). Grundzüge einer Theorie der phylogenetischen Systematik. *Deutscher Zentralverlag*, p. 370.

Hennig, W. (1965). Phylogenetic Systematics. *Annual Review of Entomology* 10, pp. 97–116.

Hilton, E. J. (2003). Hilton, 2003, Comparative osteology and phylogenetic systematics of fossil and living bony-tongue fishes (Actinopterygii, Teleostei, Osteoglossomorpha), pp. 1–100.

Holzman, R. A., Day, S. W., Mehta, R. S., and Wainwright, P. C. (2008). Jaw protrusion enhances forces exerted on prey by suction feeding fishes. *Journal of The Royal Society Interface* 5.29, pp. 1445–1457.

Hoogland, R., Morris, D., and Tinbergen, N. (1956). The spines of sticklebacks (*Gasterosteus* and *Pygosteus*) as means of defence against predators (*Perca* and *Esox*). *Behaviour* 10.3/4, pp. 205–236.

Hopson, P. M. (2005). A stratigraphical framework for the Upper Cretaceous Chalk of England and Scotland with statements on the Chalk of Northern Ireland and the UK Offshore Sector. *British Geological Survey Research Reports* RR/05/01, pp. 1–102.

Huelsenbeck, J. P. and Ronquist, F. (2001). MRBAYES: Bayesian inference of phylogenetic trees. *Bioinformatics* 17.8, pp. 754–755.

Huelsenbeck, J. P. (1991). When are fossils better than extant taxa in phylogenetic analysis? *Systematic Biology* 40.4, pp. 458–469.

Hulsey, C. D., Hollingsworth, P. R., and Holzman, R. A. (2010). Co-evolution of the premaxilla and jaw protrusion in cichlid fishes (Heroine: Cichlidae). *Biological Journal of the Linnean Society* 100.3, pp. 619–629.

Hulsey, C. (2006). Function of a key morphological innovation: fusion of the cichlid pharyngeal jaw. *Proceedings of the Royal Society B: Biological Sciences* 273.1587, pp. 669–675.

Hulsey, C., García de León, F. J., and Rodiles-Hernández, R. (2006). Micro- and macroevolutionary decoupling of cichlid jaws: a test of Liem's key innovation hypothesis. *Evolution* 60.10, pp. 2096–2109.

Hunt, G. and Slater, G. (2016). Integrating paleontological and phylogenetic approaches to macroevolution. *Annual Review of Ecology, Evolution, and Systematics* 47.1, pp. 189–213.

International Commission on Zoological Nomenclature (2000). International Code of Zoological Nomenclature. Fourth edition. London: International Trust for Zoological Nomenclature, p. 306.

Jetz, W., Thomas, G. H., Joy, J. B., Hartmann, K., and Mooers, A. O. (2012). The global diversity of birds in space and time. *Nature* 491.7424, pp. 444–448.

Johnson, G. D. (1984). "Percoidei: development and relationships". In: *Ontogeny and Systematics of Fishes*. Ed. by H. G. Moser, W. J. Richards, D. M. Cohen, M. P. Fahay, A. W. Kendall, and S. L. Richardson. Lawrence, Kansas: American Society of Icthyologists and Herpetologists, pp. 464–498.

— (1992). Monophyly of the Euteleostean Clades: Neoteleostei, Eurypterygii, and Ctenosquamata. *Copeia* 1992.1, pp. 8–25.

— (1993). Percomorph phylogeny: progress and problems. *Bulletin of Marine Science* 52.1, pp. 3–28.

Johnson, G. D. and Patterson, C. (1993). Percomorph phylogeny: a survey of acanthomorphs and a new proposal. *Bulletin of Marine Science* 52.1, pp. 554–626.

— (1996). Relationships of lower euteleostean fishes. *Interrelationships of fishes* 1981, pp. 251–332.

Jollie, M. (1984). Development of cranial and pectoral girdle bones of *Lepisosteus* with a note on scales. *Copeia* 1984.2, pp. 476–502.

Kass, R. E. and Raftery, A. E. (1995). Bayes Factors. *Journal of the American Statistical Association* 90.430, pp. 773–795.

Kobyliansky, S. G. (2016). Anatomy of fishes of genus *Lampanyctus* (*sensu lato*), its taxonomic structure, and status in the Lampanyctini (Myctophidae) tribe system. *Journal of Ichthyology* 56.2, pp. 181–199.

Larkin, M., Blackshields, G., Brown, N., Chenna, R., McGettigan, P., McWilliam, H., Valentin, F., Wallace, I., Wilm, A., Lopez, R., Thompson, J., Gibson, T., and Higgins, D. (2007). Clustal W and Clustal X version 2.0. *Bioinformatics* 23.21, pp. 2947–2948.

Lauder, G. V. (1980). The suction feeding mechanism in sunfishes (*Lepomis*): an experimental analysis. *Journal of Experimental Biology* 88, pp. 49–72.

Lauder, G. V. and Drucker, E. G. (2004). Morphology and experimental hydrodynamics of piscine control surfaces. *IEEE Journal of Oceanic Engineering* 29.3, pp. 556–571.

Lauder, G. V. and Liem, K. F. (1981). Prey capture by *Luciocephalus pulcher*: implications for models of jaw protrusion in teleost fishes. *Environmental Biology of Fishes* 6.3/4, pp. 257–268.

— (1983). The evolution and interrelationships of the actinopterygian fishes. *Bulletin of the Museum of Comparitive Zoology at Harvard College* 150.3, pp. 95–197.

Liem, K. F. (1973). Evolutionary strategies and morphological innovations: cichlid pharyngeal jaws. *Systematic Zoology* 22.4, pp. 425–441.

Liem, K. F. and Sanderson, S. L. (1986). The pharyngeal jaw apparatus of labrid fishes: a functional morphological perspective. *Journal of Morphology* 187.2, pp. 143–158.

Linnaeus, C. (1735). Systema Naturae. Leiden: Theodor Haak.

Lloyd, G. T., Wang, S. C., and Brusatte, S. L. (2012). Identifying heterogeneity in rates of morphological evolution: discrete character change in the evolution of lungfish (Sarcopterygii; Dipnoi). *Evolution* 66.2, pp. 330–348.

Maddison, W. P. and Maddison, D. R. (2016). *Mesquite: a modular system for evolutionary analysis*.

Maechler, M. (2016). *sfsmisc: utilities from "Seminar fuer Statistik" ETH Zurich*.

Maisey, J. G. (1996). Discovering Fossil Fishes. New York: Henry Holt and Company, p. 218.

Marshall, N. B. (1961). A young *Macristium* and the ctenothrissid fishes. *Bulletin of the British Museum (Natural History) Zoology* 7.8, pp. 353–370.

May, R. M. (2010). Tropical arthropod species, more or less? *Science* 329.5987, pp. 41–42.

McAllister, D. E. (1968). The evolution of branchiostegals and associated opercular, gular, and hyoid bones and the classification of teleostome fishes, living and fossil. *Bulletin of the National Museum of Canada* 221, pp. 1–239.

McDowall, R. M. (1969). Relationships of Galaxioid fishes with a further discussion of Salmoniform classification. *Copeia* 1969.4, pp. 796–824.

Mcdowall, R. M. and Burridge, C. P. (2011). Osteology and relationships of the southern freshwater lower euteleostean fishes. *Zoosystematics and Evolution* 87.1, pp. 7–185.

Moczek, A. P., Sultan, S., Foster, S., Ledon-Rettig, C., Dworkin, I., Nijhout, H. F., Abouheif, E., and Pfennig, D. W. (2011). The role of developmental plasticity in evolutionary innovation. *Proceedings of the Royal Society B: Biological Sciences* 278.1719, pp. 2705–2713.

Monsch, K. A. (2000). "The phylogeny of the scombroid fishes". PhD thesis. University of Bristol, p. 273.

Moore, J. A. (1993). "The phylogeny and evolution of the Trachichthyiformes (Teleostei: Percomorpha), with comments on the intrarelationships of the Acanthomorpha". PhD thesis. Yale University, p. 271.

Mora, C., Tittensor, D. P., Adl, S., Simpson, A. G. B., and Worm, B. (2011). How many species are there on Earth and in the ocean? *PLoS Biology* 9.8. Ed. by G. M. Mace, e1001127.

Motta, P. J. (1984). Mechanics and functions of jaw protrusion in teleost fishes: a review. *Copeia* 1, pp. 1–18.

Müller, J. (1846). Über den bau und die grenzen der ganoiden und über das natürliche system der fische. *Abhandlungen der Königlichen Akademie der Wissenschaften zu Berlin* 1846.117-216.

Murray, A. M. and Wilson, M. V. H. (1999). "Contributions of fossils to the phylogenetic relationships of the percopsiform fishes (Teleosteii: Paracanthopterygii): order restored". In: *Mesozoic Fishes 2: Systematics and Fossil Record*. Ed. by G. Arratia and H.-p. Schultze. Munich: Verlag Dr. Friedrich Pfeil, pp. 397–411.

— (2014). Four new basal acanthomorph fishes from the Late Cretaceous of Morocco. *Journal of Vertebrate Paleontology* 34.1, pp. 34–48.

Near, T. J., Dornburg, A., Eytan, R. I., Keck, B. P., Smith, W. L., Kuhn, K. L., Moore, J. A., Price, S. A., Burbrink, F. T., Friedman, M., and Wainwright, P. C. (2013). Phylogeny and tempo of diversification in the superradiation of spiny-rayed fishes. *Proceedings of the National Academy of Sciences* 110.31, pp. 12738–12743.

Near, T. J., Eytan, R. I., Dornburg, A., Kuhn, K. L., Moore, J. A., Davis, M. P., Wainwright, P. C., Friedman, M., and Smith, W. L. (2012). Resolution of ray-finned fish phylogeny and timing of diversification. *Proceedings of the National Academy of Sciences of the United States of America* 109.34, pp. 13698–13703.

Near, T. J. and Sanderson, M. J. (2004). Assessing the quality of molecular divergence time estimates by fossil calibrations and fossil-based model selection. *Philosophical Transactions of the Royal Society B: Biological Sciences* 359.1450, pp. 1477–1483.

Nelson, G. J. (1969). Gill arches and the phylogeny of fishes, with notes on the classification of vertebrates. *Bulletin of the American Museum of Natural History* 141.4, pp. 475–552.

— (1989). "Phylogeny of major fish groups". In: *Hierarchy of Life: Molecules and Morphology in Phylogenetic Analysis*. Ed. by B. Fernholm, K. Bremer, and H. Jörnvall. Amsterdam: Excerpta Medica, pp. 325–336.

Nelson, J. S., Grande, T., and Wilson, M. V. H. (2016). Fishes of the World. New Jersey: John Wiley & Sons, p. 752.

Norden, C. R. (1961). Comparative Osteology of Representative Salmonid Fishes, with Particular Reference to the Grayling (*Thymallus arcticus*) and its Phylogeny. *Journal of the Fisheries Research Board of Canada* 18.5, pp. 679–791.

Nybelin, O. (1974). A revision of leptolepid fishes. *Acta Regiae Societatis Scientiarum et Litterarum Gothoburgensis, Zoologica* 9, pp. 1–202.

— (1979). Contributions to taxonomy and morphology of the genus *Elops* (Pisces, Teleostei). *Acta Regiae Societatis Scientiarum et Litterarum Gothoburgensis, Zoologica* 12, pp. 1–37.

Oelschläger, H. A. (1983). Vergleichende und funktionelle Anatomie der Allotriognathi (= Lampridiformes), ein Beitrag zur Evolutionsmorphologie der Knochenfische. *Abhandlungen der Senckenbergischen Naturforschenden Gesellschaft* 541, pp. 1–127.

Olney, J. E. (2006). "Order Lampridiformes". In: *Early Atlantic Fishes: An Idenfitication Guide for the North Atlantic*. Boca Raton, Florida: CRC Press, pp. 991–993.

Olney, J. E., Johnson, G. D., and Baldwin, C. C. (1993). Phylogeny of lampridiform fishes. *Bulletin of Marine Science* 52.1, pp. 137–169.

O'Reilly, J. E., dos Reis, M., and Donoghue, P. C. (2015). Dating tips for divergence-time estimation. *Trends in Genetics* 31.11, pp. 637–650.

Orr, J. W. (1995). "Phylogenetic relationships of gasterosteiform fishes (Teleostei: Acanthomorpha)". PhD thesis. University of Washington, p. 813.

Otero, O. (1997). A new genus of Aipichthyoidea (Teleostei, Acanthomorpha) from the Lower Cenomanian of Hgula (Lebanon): description and phylogenetic relationships. *Comptes Rendus de l'Academie des Science: Series IIA: Earth and Planetary Science* 325.6, pp. 453–458.

— (2004). Anatomy, systematics and phylogeny of both Recent and fossil latid fishes (Teleostei, Perciformes, Latidae). *Zoological Journal of the Linnean Society* 141.1, pp. 81–133.

Otero, O., Dutour, Y., and Gayet, M. (1995). Hgulichthys, nouveau genre de Lissoberycinae (Trachichthyiformes, Trachichthyoidea) du Cénomanien inférieur marin de Hgula (Liban). Implications phylogénétiques. *Geobios* 28.6, pp. 711–717.

Otero, O. and Gayet, M. (1995). Étude phylogénétique des Aipichthyides, poissons téléostéens de la Tethys Cenomanienne. *Geobios* 28.S2, pp. 221–224.

— (1996). Anatomy and phylogeny of the Aipichthyoidea nov. of the Cenomanian Tethys and their place in the Acanthomorpha (Teleostei). *Neues Jahrbuch fur Geologie und Palaontologie Abhandlungen* 202.3, pp. 313–344.

Page, R. D. M. (2001). *Nexus Data Editor*.

Pagel, M., Meade, A., Barker, D., and Thorne, J. (2004). Bayesian estimation of ancestral character states on Phylogenies. *Systematic Biology* 53.5, pp. 673–684.

Paradis, E., Claude, J., and Strimmer, K. (2004). APE: analyses of phylogenetics and evolution in R language. *Bioinformatics* 20.2, pp. 289–290.

Patterson, C. (1964). A review of Mesozoic acanthopterygian fishes, with special reference to those of the English Chalk. *Philosophical Transactions of the Royal Society B: Biological Sciences* 247.739, pp. 213–482.

— (1968). The caudal skeleton in Mesozoic acanthopterygian fishes. *Bulletin of the British Museum (Natural History) Geology* 17.2, pp. 47–102.

— (1970). Two Upper Cretaceous salmoniform fishes from the Lebanon. *Bulletin of the British Museum (Natural History) Geology* 19.5, pp. 205–296.

— (1975). The braincase of pholidophorid and leptolepid fishes, with a review of the actinopterygian braincase. *Philosophical Transactions of the Royal Society B: Biological Sciences* 269.899, pp. 275–579.

— (1977). "The contribution of palaeontology to teleostean phylogeny". In: *Major patterns in vertebrate evolution*, pp. 579–643.

— (1993). An overview of the early fossil record of acanthomorphs. *Bulletin of Marine Science* 52.1, pp. 29–59.

Patterson, C. and Johnson, G. D. (1995). The intermuscular bones and ligaments of teleostean fishes. *Smithsonian Contributions to Zoology* 559, pp. 1–83.

Patterson, C. and Rosen, D. E. (1977). Review of ichthyodectiform and other Mesozoic teleost fishes and the theory and practice of classifying fossils. *Systematic Zoology* 26.3, p. 358.

— (1989). "The Paracanthopterygii revisited: order and disorder". In: *Papers of the Systematics of Gadiform Fishes*. Ed. by D. M. Cohen. Los Angeles: Natural History Museum of Los Angeles County, pp. 5–36.

Pictet, F. J. (1850). Déscription de quelques poissons fossiles du Mont Liban. Geneva: Imprimerie de Jules-Guillaume Fick, p. 59.

Pietsch, T. W. and Grobecker, D. B. (1987). Frogfishes of the World. Systematics, Zoogeography, and Behavioral Ecology. Stanford: Stanford University Press, p. 420.

Plummer, M., Best, N., Cowles, K., and Vines, K. (2006). CODA: convergence diagnosis and output analysis for MCMC. *R News* 6.1, pp. 7–11.

Price, S. A., Schmitz, L., Oufiero, C. E., Eytan, R. I., Dornburg, A., leo Smith, W., Friedman, M., Near, T. J., and Wainwright, P. C. (2014). Two waves of colonization straddling the K?Pg boundary formed the modern reef fish fauna. *Proceedings of the Royal Society Biological Sciences* 281.1783, p. 20140321.

Puttick, M. N. and Thomas, G. H. (2015). Fossils and living taxa agree on patterns of body mass evolution: a case study with Afrotheria. *Proceedings of the Royal Society B: Biological Sciences* 282.1821, p. 20152023.

Pyron, R. A. and Burbrink, F. T. (2012). Trait-dependent diversification and the impact of palaeontological data on evolutionary hypothesis testing in New World ratsnakes (tribe Lampropeltini). *Journal of Evolutionary Biology* 25.3, pp. 497–508.

Pyron, R. A. (2011). Divergence time estimation using fossils as terminal taxa and the origins of Lissamphibia. *Systematic Biology* 60.4, pp. 466–481.

R Core Team (2016). *R: A Language and Environment for Statistical Computing*. Vienna.

Rabosky, D. L., Grundler, M., Anderson, C., Title, P., Shi, J. J., Brown, J. W., Huang, H., and Larson, J. G. (2014). BAMMtools: An R package for the analysis of evolutionary dynamics on phylogenetic trees. *Methods in Ecology and Evolution* 5.7, pp. 701–707.

Rabosky, D. L., Santini, F., Eastman, J., Smith, S. A., Sidlauskas, B., Chang, J., and Alfaro, M. E. (2013). Rates of speciation and morphological evolution are correlated across the largest vertebrate radiation. *Nature Communications* 4, p. 1958.

Ragan, M. A. (1992). Phylogenetic inference based on matrix representation of trees. *Molecular Phylogenetics and Evolution* 1.1, pp. 53–58.

Raup, D. M. (1991). Extinction: Bad Genes or Bad Luck? New York: Norton, p. 210.

Regan, C. (1911a). The anatomy and classification of the teleostean fishes of the orders Berycomorphi and Xenoberyces. *Annals and Magazine of Natural History* 7, pp. 1–9.

— (1911b). The osteology and classification of the teleostean fishes of the order Iniomi. *Annals and Magazine of Natural history* 7.8, pp. 120–133.

Revell, L. J. (2012). phytools: An R package for phylogenetic comparative biology (and other things). *Methods in Ecology and Evolution* 3.2, pp. 217–223.

Ricklefs, R. E. (2004). Cladogenesis and morphological diversification in passerine birds. *Nature* 430.6997, pp. 338–341.

Ridewood, W. G. (1904). On the cranial osteology of the fishes of the families Elopidae and Albulidae, with remarks on the morphology of the skull in the lower teleostean fishes generally. *Proceedings of the Zoological Society of London* 74, pp. 35–81.

Ronquist, F., Klopfstein, S., Vilhelmsen, L., Schulmeister, S., Murray, D. L., and Rasnitsyn, A. P. (2012). A total-evidence approach to dating with fossils, applied to the earlyr radiation of the Hymenoptera. *Systematic Biology* 61.6, pp. 973–999.

Rosen, D. E. (1971). The Macristiidae, a ctenothrissiform family based on juvenile and larval scopelomorph fishes. *American Museum Novitates* 2542, pp. 1–22.

— (1973). "Interrelationships of higher euteleostean fishes". In: *Interrelationships of Fishes*. Ed. by P. Greenwood, R. S. Miles, and C. Patterson. London: Linnean Society, pp. 397–513.

— (1974). Phylogeny and zoogeography of salmoniform fishes and relationships of *Lepidogalaxias salamandroides*. *Bulletin of the American Natural History* 153.2, pp. 265–326.

— (1985). An essay on euteleostean classification. *American Museum Novitates* 2827, pp. 1–57.

Rosen, D. E. and Patterson, C. (1969). The structure and relationships of the paracanthopterygian fishes. *Bulletin of the American Museum of Natural History* 141.3, pp. 357–474.

Rosenblatt, R. H. and Bell, M. A. (1976). Osteology and relationships of the roosterfish *Nematistius pectoralis* Gill. *Contributions in Science* 279, pp. 1–23.

Rosenblatt, R. H. and Johnson, G. D. (1976). Anatomical considerations of pectoral swimming in the opah, *Lampris guttatus*. *Copeia* 1976.2, pp. 367–370.

Ruta, M., Wagner, P. J., and Coates, M. I. (2006). Evolutionary patterns in early tetrapods. I. Rapid initial diversification followed by decrease in rates of character change. *Proceedings of the Royal Society B: Biological Sciences* 273.1598, pp. 2107–2111.

Sallan, L. C. and Friedman, M. (2012). Heads or tails: staged diversification in vertebrate evolutionary radiations. *Proceedings of the Royal Society B: Biological Sciences* 279.1735, pp. 2025–2032.

Sanderson, M. J., Purvis, A., and Henze, C. (1998). Phylogenetic supertrees: assembling the trees of life. *Trends in Ecology & Evolution* 13.3, pp. 105–109.

Santini, F. and Tyler, J. C. (2003). A phylogeny of the families of fossil and extant tetraodontiform fishes (Acanthomorpha, Tetraodontiformes), Upper Cretaceous to Recent. *Zoological Journal of the Linnean Society* 139.4, pp. 565–617.

— (2004). The importance of even highly incomplete fossil taxa in reconstructing the phylogenetic relationships of the Tetraodontiformes (Acanthomorpha: Pisces). *Integrative and comparative biology* 44.5, pp. 349–357.

Santini, F., Tyler, J. C., Bannikov, A. F., and Baciu, D.-S. (2006). A phylogeny of extant and fossil buckler dory fishes, family Zeidae (Zeiformes, Acanthomorpha). *Cybium* 30.2, pp. 99–107.

Sasaki, K., Tanaka, Y., and Takata, Y. (2006). Cranial morphology of *Ateleopus japonicus* (Ateleopodidae: Ateleopodiformes), with a discussion on metamorphic mouth migration and lampridiform affinities. *Ichthyological Research* 53.3, pp. 254–263.

Sato, T. and Nakabo, T. (2002). Paraulopidae and *Paraulopus*, a new family and genus of aulopiform fishes with revised relationships within the order. *Ichthyological Research* 49.1973, pp. 25–46.

Schaeffer, B. and Rosen, D. E. (1961). Major adaptive levels in the evolution of the actinopterygian feeding mechanism. *American Zoologist* 1.2, pp. 187–204.

Schneider, C. A., Rasband, W. S., and Eliceiri, K. W. (2012). NIH Image to ImageJ: 25 years of image analysis. *Nature Methods* 9.7, pp. 671–675.

Schultze, H.-P. and Arratia, G. (1989). The composition of the caudal skeleton of teleosts (Actinopterygil: Osteichthyes). *Zoological Journal of the Linnean Society* 97.3, pp. 189–231.

— (2013). The caudal skeleton of basal teleosts, its conventions, and some of its major evolutionary novelties in a temporal dimension. *Mesozoic Fishes 5 - Global Diversity and Evolution*, pp. 187–246.

Sereno, P. C. (1999). The evolution of dinosaurs. *Science* 284.5423, pp. 2137–2147.

Sibert, E. C. and Norris, R. D. (2015). New age of fishes initiated by the Cretaceous-Paleogene mass extinction. *Proceedings of the National Academy of Sciences* 112.28, pp. 8537–8542.

Slater, G. J. and Harmon, L. J. (2013). Unifying fossils and phylogenies for comparative analyses of diversification and trait evolution. *Methods in Ecology and Evolution* 4.8. Ed. by R. Freckleton, pp. 699–702.

Slater, G. J., Harmon, L. J., and Alfaro, M. E. (2012). Integrating fossils with molecular phylogenies improves inferences of trait evolution. *Evolution* 66, pp. 3931–3944.

Smith, a. B. (1998). What does palaeontology contribute to systematics in a molecular world? *Molecular Phylogenetics and Evolution* 9.3, pp. 437–447.

Smith, A. B. and Peterson, K. J. (2002). Dating the time of origin of major clades: molecular clocks and the fossil record. *Annual Review of Earth and Planetary Sciences* 30.1, pp. 65–88.

Smith, C. L. and Bailey, R. M. (1962). The subocular shelf of fishes. *Journal of Morphology* 110.1, pp. 1–17.

Smith, N. D. (2012). Body mass and foraging ecology predict evolutionary patterns of skeletal pneumaticity in the diverse "waterbird" clade. *Evolution* 66.4, pp. 1059–1078.

Smith, W. L. and Wheeler, W. C. (2006). Venom evolution widespread in fishes: a phylogenetic road map for the bioprospecting of piscine venoms. *Journal of Heredity* 97.3, pp. 206–217.

Sorbini, C. and Sorbini, L. (1999). The Cretaceous fishes of Nardó. 10º. *Nardovelifer altipinnis*, gen. et sp. nov. (Teleostei, Lampridiformes, Veliferidae). *Studi e Ricerche sui Giacimenti Terziari di Bolca, Museo Civico di Storia Naturale* 8, pp. 11–27.

Sorenson, M. D. (1999). *TreeRot*. Boston.

Springer, V. G. and Johnson, G. D. (2004). Study of the dorsal gill-arch musculature of teleostome fishes, with special reference to the Actinopterygii. *Bulletin of the Biological Society of Washington* 11, p. 260.

Steindachner, F. (1860). Beiträge zur Kenntnis der fossilen fische Österreichs. II Folge. I Ueber einen neuen Vomer-ahnlichen fische von Comen an Karst. *Sitzungsberichte der Akademie der Wissenschaften, Wien* 38, pp. 763–777.

Stewart, J. D. (1984). "Taxonomy, paleoecology, and stratigraphy of the halecostome-inoceramid associations of the North American Upper Cretaceous epicontinental seaways". PhD thesis. University of Kansas, p. 201.

Stiassny, M. L. J. (1986). The limits and relationships of the acanthomorph teleosts. *Journal of Zoology* 1.2, pp. 411–460.

— (1996). "Basal ctenosquamate relationships and the interrelationships of the Myctophiform (Scopelomorph) fishes". In: *Interrelationships of fishes*, pp. 405–426.

Stiassny, M. L. J. and Moore, J. A. (1992). A review of the pelvic girdle of acanthomorph fishes, with comments on hypotheses of acanthomorph intrarelationships. *Zoological Journal of the Linnean Society* 104.3, pp. 209–242.

Stiassny, M. L. J., Wiley, E. O., Johnson, G. D., and de Carvalho, M. R. (2004). "Gnathostome fishes". In: *Assembling the Tree of Life*. Ed. by J. Cracraft and M. J. Donoghue. New York: Oxford University Press USA, pp. 410–429.

Susoy, V., Ragsdale, E. J., Kanzaki, N., and Sommer, R. J. (2015). Rapid diversification associated with a macroevolutionary pulse of developmental plasticity. *eLife* 4, e05463.

Swofford, D. L. (2003). *PAUP*, Phylogenetic Analysis Using Parsimony *and other methods*.

Taverne, L. (2004). Les poissons crétacés de Nardò. 17°. *Aspesaipichthys cavaensis* gen. et sp. nov. (Teleostei, Acanthomorpha, Aipichthyoidea). *Bollettino del Museo Civico di Storia Naturale di Verona, Geologia, Paleontologia, Preistoria* 28, pp. 3–15.

Tyler, J. C. and Santini, F. (2005). A phylogeny of the fossil and extant zeiform-like fishes, Upper Cretaceous to Recent, with comments on the putative zeomorph clade (Acanthomorpha). *Zoologica Scripta* 34.2, pp. 157–175.

Tyler, J. C. and Sorbini, L. (1996). New superfamily and three new families of tetraodontiform fishes from the Upper Cretaceous : the earliest and most morphologically primitive plectognaths. *Smithson. Contr. Paleobiol.* 82, pp. 1–68.

Venables, W. N. and Ripley, B. D. (2002). Modern Applied Statistics with S. Fourth Edition. New York: Springer, p. 495.

Venditti, C., Meade, A., and Pagel, M. (2011). Multiple routes to mammalian diversity. *Nature* 479.7373, pp. 393–396.

Videler, J. J. (1993). Fish Swimming. London: Chapman & Hall, p. 260.

Wainwright, P. C. (1988). Morphology and ecology: functional basis of feeding constraints in Caribbean labrid fishes. *Ecology* 69.3, pp. 635–645.

Wainwright, P. C. (2005). "Functional morphology of the pharyngeal jaw apparatus". In: *Fish Physiology*. San Diego: Academic Press, pp. 77–101.

Wainwright, P. C., Bellwood, D. R., Westneat, M. W., Grubich, J. R., and Hoey, A. S. (2004). A functional morphospace for the skull of labrid fishes: patterns of diversity in a complex biomechanical system. *Biological Journal of the Linnean Society* 82.1, pp. 1–25.

Wainwright, P. C. and Longo, S. J. (2017). Functional innovations and the conquest of the oceans by acanthomorph fishes. *Current Biology* 27.11, R550–R557.

Wainwright, P. C., McGee, M. D., Longo, S. J., and Hernandez, L. P. (2015). Origins, innovations, and diversification of suction feeding in vertebrates. *Integrative and Comparative Biology* 55.1, pp. 134–145.

Wainwright, P. C., Smith, W. L., Price, S. A., Tang, K. L., Sparks, J. S., Ferry, L. A., Kuhn, K. L., Eytan, R. I., and Near, T. J. (2012). The evolution of pharyngognathy: a phylogenetic and functional appraisal of the pharyngeal jaw key innovation in labroid fishes and beyond. *Systematic Biology* 61.6, pp. 1001–1027.

Waterhouse, A. M., Procter, J. B., Martin, D. M. A., Clamp, M., and Barton, G. J. (2009). Jalview Version 2–a multiple sequence alignment editor and analysis workbench. *Bioinformatics* 25.9, pp. 1189–1191.

Webb, P. W. (1984). Form and function in fish swimming. *Scientific American* 251.1, pp. 72–82.

West-Eberhard, M. J. (2005). Developmental plasticity and the origin of species differences. *Proceedings of the National Academy of Sciences* 102.Supplement 1, pp. 6543–6549.

Westneat, M. W. (1991). Linkage Biomechanics and evolution of the unique feeding mechanism of *Epibulus Insidiator* (Labridae: Teleostei). *Journal of Experimental Biology* 159, pp. 165–184.

— (2004). Evolution of levers and linkages in the feeding mechanisms of fishes. *Integrative and Comparative Biology* 44.5, pp. 378–389.

Westneat, M. W. and Wainwright, P. C. (1989). Feeding mechanism of *Epibulus insidiator* (Labridae; Teleostei): evolution of a novel functional system. *Journal of Morphology* 202.2, pp. 129–150.

Whitlock, J. A. (2010). Phylogenetic relationships of the Eocene percomorph fishes †*Priscacara* and †*Mioplosus*. *Journal of Vertebrate Paleontology* 30.4, pp. 1037–1048.

Wiley, E. O. and Johnson, G. D. (2010). "A teleost classification based on monophyletic groups". In: *Origin and Phylogenetic Interrelationships of Teleosts*. Munich: Verlag Dr. Friedrich Pfeil, pp. 123–182.

Wiley, E. O., Johnson, G. D., and Dimmick, W. W. (1998). The phylogenetic relationships of lampridiform fishes (Teleostei: Acanthomorpha), based on a total-evidence analysis of morphological and molecular data. *Molecular Phylogenetics and Evolution* 10.3, pp. 417–425.

Wilga, C. D., Hueter, R. E., Wainwright, P. C., and Motta, P. J. (2001). Evolution of upper jaw protrusion mechanisms in elasmobranchs. *American Zoologist* 41, pp. 1248–1257.

Williams, R. R. G. (1997). Bones and muscles of the suspensorium in the galaxioids and *Lepidogalaxias salamandroides* (Teleostei: Osmeriformes) and their phylogenetic significance. *Records of the Australian Museum* 49.2, pp. 139–166.

Wintzer, A. P. and Motta, P. J. (2005). Diet-induced phenotypic plasticity in the skull morphology of hatchery-reared Florida largemouth bass, *Micropterus salmoides floridanus*. *Ecology of Freshwater Fish* 14.4, pp. 311–318.

Witte, F. (1984). Consistency and functional significance of morphological differences between wild-caught and domestic *Haplochromis squamipinnis* (Pisces, Cichlidae). *Netherlands journal of zoology* 34.4, pp. 596–612.

Woodward, A. S. (1887). XLV.—On the so-called *Microdon nuchalis*, Dixon, from the chalk of Sussex, a new species of *Platax*. *Journal of Natural History* 20.119, pp. 342–344.

— (1888). A synopsis of the vertebrate fossils of the English Chalk. *Proceedings of the Geologists' Association* 10, pp. 273–338.

— (1895). A description of the so-called salmonoid fishes of the English Chalk. *Proceedings of the Zoological Society of London* 1894, pp. 655–664.

— (1899). Note on some Cretaceous clupeoid fishes with pectinated scales (*Ctenothrissa* and *Pseudoberyx*). *Annals and Magazine of Natural History: Series 7* 3, pp. 489–492.

— (1900). On a new specimen of Clupeoid fish *Aulolepis typus* from the English Chalk. *Annals and Magazine of Natural History: Series 7* 5, pp. 324–326.

— (1901). Catalogue of Fossil Fishes in the British Museum (Natural History), Part IV. London: Trustees of the British Museum (Natural History), p. 636.

— (1902). The Fossil Fishes of the English Chalk. Part I. London: The Palaeontographical Society, p. 56.

— (1903). The Fossil Fishes of the English Chalk. Part II. London: The Palaeontographical Society, p. 39.

— (1942). XLV.— Some new and little-known Upper Cretaceous fishes from Mount Lebanon. *Annals and Magazine of Natural history: Series 11* 9.56, pp. 537–568.

Xie, W., Lewis, P. O., Fan, Y., Kuo, L., and Chen, M.-H. (2011). Improving marginal likelihood estimation for Bayesian phylogenetic model selection. *Systematic Biology* 60.2, pp. 150–160.

Zehren, S. J. (1979). The Comparitive Osteology and Phylogeny of the Beryciformes (Pisces: Teleostei). Chicago: University of Chicago, p. 389.

Zuckerkandl, E. and Pauling, L. (1962). "Molecular disease, evolution and genetic heterogeneity". In: *Horizons in Biochemistry*. Ed. by M. Kasha and B. Pullman. New York: Academic Press, pp. 189–225.

Appendices

A

Scripts for phylogenetic analyses from Chapter 3

A.1 Parsimony analyses

All parsimony analyses were performed in PAUP*.

Morphology-only

```
#NEXUS

BEGIN TAXA;
       DIMENSIONS NTAX = 21;
       TAXLABELS
              LEPISOSTEUS AMIA THARSIS ELOPS LEPIDOGALAXIAS THYMALLUS
                  DIPLOPHOS APLOCHITON ATELEOPUS SYNODUS AULOPUS
                  PARAULOPUS NEOSCOPELUS LAMPANYCTUS POLYMIXIA BERYCOPSIS
                   MYRIPRISTIS VELIFERIDAE AULOLEPIS CTENOTHRISSA
                  PATTERSONICHTHYS
       ;
END;

BEGIN CHARACTERS;
       DIMENSIONS NCHAR=56;
       FORMAT DATATYPE = STANDARD GAP = - MISSING = ? SYMBOLS = " 0 1 2 3
           4 5 6";

MATRIX
[morphological character matrix inserted here]
       ;
```

```
END;

BEGIN PAUP;
OUTGROUP LEPISOSTEUS AMIA;
BANDB;
LOG FILE = Aulolepis_Morph_log.log;
CONTREE ALL / TREEFILE = Aulolepis_morph_contree_paup.tre;
DESCRIBETREES;

[bootstrap analysis]
BOOTSTRAP NREPS = 1000 SEARCH = HEURISTIC / ADDSEQ = RANDOM NREPS = 100;
SAVETREES FROM = 1 TO = 1 SAVEBOOTP = NODELABELS FILE =
   Aulolepis_morph_bootstrap.tre;

[Bremer index]
HSEARCH ADDSEQ = RANDOM NREPS=100; [Base tree for the bremer indexes.
   Indexes need to be computed manually]
CONTREE ALL; [To get tree length X]
HSEARCH KEEP = [X+Y] ADDSEQ=RANDOM NREPS = 100; [Y = X+1 is for Bremer
   index of 2; Y = X+2 would be for an index of 3]
CONTREE ALL; [Clades still present in this tree have a Bremer index of at
    least the value used above]
LOG STOP;

END;
```

Combined

```
#NEXUS

BEGIN TAXA;
       DIMENSIONS NTAX = 21;
       TAXLABELS
              LEPISOSTEUS AMIA THARSIS ELOPS LEPIDOGALAXIAS THYMALLUS
                  DIPLOPHOS APLOCHITON ATELEOPUS SYNODUS AULOPUS
                  PARAULOPUS NEOSCOPELUS LAMPANYCTUS POLYMIXIA BERYCOPSIS
                   MYRIPRISTIS VELIFERIDAE AULOLEPIS CTENOTHRISSA
                  PATTERSONICHTHYS
       ;
END;

BEGIN CHARACTERS;
       DIMENSIONS NCHAR = 4561;
       FORMAT DATATYPE = STANDARD MISSING = ? GAP = - SYMBOLS = "0123
           ACGTKYMRSWN" INTERLEAVE;
MATRIX
[molecular and morphology character matrix inserted here]
[RAG1 1436bp 1 to 1436]
[ZIC1 870 bp 1437 to 2306]
```

```
[PLAGL2 660bp 2307 to 2966]
[ENC1 810bp 3696 to 4505]
[morphology 56 char 4506 to 4561]
       ;
END;

BEGIN PAUP;
OUTGROUP LEPISOSTEUS AMIA;
HSEARCH ADDSEQ = RANDOM NREPS = 100;
LOG FILE = Aulolepis_combined_log.log;
CONTREE ALL/TREEFILE = Aulolepis_combined_contree_paup.tre;
DESCRIBETREES;

[bootstrap analysis]
BOOTSTRAP NREPS = 1000 SEARCH = HEURISTIC /ADDSEQ=RANDOM NREPS = 100;
SAVETREES FROM = 1 TO = 1 SAVEBOOTP = NODELABELS FILE =
   Aulolepis_combined_bootstrap.tre;

[Bremer index]
[See morphology only analysis for instructions]
HSEARCH ADDSEQ = RANDOM NREPS = 100;
CONTREE;
HSEARCH KEEP = [X+Y] ADDSEQ = RANDOM NREPS = 100;
CONTREE ALL;
LOG STOP;

END;
```

A.2 Bayesian analyses

All Bayesian analyses were performed in MrBayes.

Morphology-only

```
#NEXUS

BEGIN MRBAYES;
       EXECUTE AULOLEPIS_NEW_MORPH_BAYES_V1.NEX; [morphology character
          matrix]
       LSET RATES = GAMMA;
       LSET NST = 1;
       CONSTRAINT OUTGROUP = 3-21; [*hypothesis tests same until this
          point]
       PRSET TOPOLOGYPR = CONSTRAINTS(OUTGROUP);
       MCMC NGEN = 1500000 APPEND = NO;
       SUMP;
       SUMT;
END;
```

Combined

```
#NEXUS

BEGIN MRBAYES;
        EXECUTE AULOLEPIS_NEW_COMBINED_BAYES_V1.NEX; [morphology and
            molecular character matrix]
        CHARSET RAG1_1 = 1-1436\3;
        CHARSET RAG1_2 = 2-1436\3;
        CHARSET RAG1_3 = 3-1436\3;
        CHARSET ZIC1_1 = 1437-2306\3;
        CHARSET ZIC1_2 = 1438-2306\3;
        CHARSET ZIC1_3 = 1439-2306\3;
        CHARSET PLAGL2_1 = 2307-2966\3;
        CHARSET PLAGL2_2 = 2308-2966\3;
        CHARSET PLAGL2_3 = 2309-2966\3;
        CHARSET MYH6_1 = 2967-3695\3;
        CHARSET MYH6_2 = 2968-3695\3;
        CHARSET MYH6_3 = 2969-3695\3;
        CHARSET ENC1_1 = 3696-4505\3;
        CHARSET ENC1_2 = 3697-4505\3;
        CHARSET ENC1_3 = 3698-4505\3;
        CHARSET MORPHOLOGY = 4506-4561;
        PARTITION PARTY = 16: RAG1_1, RAG1_2, RAG1_3, ZIC1_1, ZIC1_2,
            ZIC1_3, PLAGL2_1, PLAGL2_2, PLAGL2_3, MYH6_1, MYH6_2, MYH6_3,
            ENC1_1, ENC1_2, ENC1_3, MORPHOLOGY;
        SET PARTITION = PARTY;
        LSET APPLYTO = (1,2,3,4,5,6,7,8,9,10,11,12,13,14,15) NST = 6 RATES
             = INVGAMMA;
        UNLINK REVMAT = (ALL) STATEFREQ = (ALL) SHAPE = (ALL) PINVAR = (
            ALL);
        LSET APPLYTO = (16) RATES = GAMMA;
        PRSET APPLYTO=(ALL) RATEPR = VARIABLE;
        CONSTRAINT OUTGROUP = 3-21; [*hypothesis tests same until this
            point]
        PRSET TOPOLOGYPR = CONSTRAINTS(OUTGROUP);
        MCMC NGEN = 6000000 APPEND = NO;
        SUMP;
        SUMT;
END;
```

A.3 Hypothesis tests

All hypothesis tests were performed in MrBayes. Scripts below are for running single analyses, which test one hypothesis. The analyses need to be repeated (with the constraints amended) for each additional hypothesis that needs to be tested.

Details of the hypotheses are not shown below, but are detailed in Chapter 3.

Morphology-only

```
[*resume from marked point in Bayesian analyses]

CONSTRAINT [name constraint here] = [numbers of taxa in constraint];
[add additional constraints here; repeat above line]
PRSET TOPOLOGY PR = CONSTRAINTS(OUTGROUP [list all other constraints here
    , separated by commas]);
MCMCP FILENAME = [insert file name here, different for each hypothesis]
SS NGEN = 10200000;
END;
```

Combined

```
[*resume from marked point in Bayesian analyses]

CONSTRAINT [name constraint here] = [numbers of taxa in constraint];
[add additional constraints here; repeat above line]
PRSET TOPOLOGY PR = CONSTRAINTS(OUTGROUP [list all other constraints here
    , separated by commas]);
MCMCP FILENAME = [insert file name here, different for each hypothesis]
SS NGEN = 25500000;
END;
```

B

Supplementary tables for Chapter 4

Table B.1: Taxa included in the jaw protrusion analyses. Taxa that are included in the supertree, the source of their phylogenetic placement and their jaw protrusion index (JPI) are shown. The JPIs are rounded to four decimal places.

Tip label	Taxon (if different from label)	Source of phylogenetic placement	JPI
†'*Aipichthys*' *minor*	–	Chapter 2	0.4333
†'*Aipichthys*' *velifer*	–	Chapter 2	0.4786
†*Acrogaster daviesii*	–	Friedman, 2009	0.5866
†*Aipichthyoides galeatus*	–	Chapter 2	0.3242
†*Amphiplaga brachyptera*	–	Murray and Wilson, 1999	0.1356
†*Apricenaichthys italicus*	–	Friedman, 2009	0.4004
†*Archaeozeus skamolensis*	–	Tyler and Santini, 2005	1.7412
†*Aulolepis typus*	–	Chapter 3	0.5307
†*Bajaichthys elegans*	–	Davesne et al., 2017	2.2087
†*Berybolcensis leptacanthus*	–	Friedman, 2009	0.5422
†*Berycopsis elegans*	–	Friedman, 2009	0.3649
†*Ctenocephalichthys longispinus*	–	Friedman, 2009	0.5088
†*Ctenothrissa microcephala*	–	Chapter 3	0.2805
†*Ellaserrata monksi*	–	Bannikov, 2014b	0.6865
†*Eoaulostomus bolcense*	–	Bannikov, 2014b	0.2621
†*Eoholocentrum macrocephalum*	–	Friedman, 2009	0.6360
†*Eolates gracilis*	–	Otero, 2004	0.4162
†*Eorandallius rectifrons*	–	Bannikov, 2014b	0.5057
†*Eoscatophagus frontalis*	–	Bannikov, 2014b	0.5869
†*Erismatopterus levatus*	–	Murray and Wilson, 1999	0.2998
†*Gigapteryx tethyestris*	–	Chapter 2	0.7265
†*Gnathoberyx stigmosus*	–	Friedman, 2009	0.2538
†*Homonotichthys dorsalis*	–	Friedman, 2009	0.3487
†*Hoplopteryx lewesiensis*	–	Friedman, 2009	0.3838
†*Lateopisculus turrisfumosus*	–	Murray and Wilson, 1999	0.2660
†*Libanoberyx spinulosus*	–	Friedman, 2009	0.3434
†*Libotonius blakeburnensis*	–	Murray and Wilson, 1999	0.2151
†*Lichia veronensis*	–	Bannikov, 2014b	0.3234
†*Lissoberyx dayi*	–	Friedman, 2009	0.3240
†*Massamorichthys wilsoni*	–	Murray and Wilson, 1999	0.2931
†*McConichthys longispinnis*	–	Murray and Wilson, 1999	0.1623
†*Mene rhombeus*	–	Bannikov, 2014b	0.9702
†*Nardovelifer altipinnis*	–	Chapter 2	2.8743
†*Pachylebias crassicaudas*	–	Gaudant, 1979	0.7914
†*Padovathurus gaudryi*	–	Bannikov, 2014b	0.7564
†*Pasaichthys pleuronectiformis*	–	Blot, 1969	0.6808
†*Pattersonichthys delicatus*	–	Chapter 3	0.1786
†*Pharmacichthys judensis*	–	Chapter 2	0.6983
†*Pharmacichthys numismalis*	–	Chapter 2	0.6013
†*Pharmacichthys venenifer*	–	Chapter 2	0.6203
†*Priscacara clivosa*	–	Whitlock, 2010	1.0674
†*Proacanthurus tenuis*	–	Bannikov, 2014b	0.4292
†*Proantigonia radobojana*	–	Baciu et al., 2005	2.3528
†*Protozeus kuehnei*	–	Tyler and Santini, 2005	1.9469
†*Pseudosparnodus microstomus*	–	Bannikov, 2014b	0.5704
†*Pycnosterinx russeggeri*	–	Friedman, 2009	0.2322
†*Pycnosteroides levispinosus*	–	Chapter 2	0.6361
†*Seriola prisca*	–	Bannikov, 2014b	0.4771
†*Stichopteryx lewisi*	–	Friedman, 2009	0.3289
†*Tylerichthys nuchalis*	–	Bannikov, 2014b	0.5957
†*Veronavelifer sorbinii*	–	Bannikov, 1990	2.8016
†*Zoqueichthys carolinae*	–	Chapter 2	0.4043
Acanthurus xanthopterus	–	Near et al., 2013	0.5508
Achiridae	*Catathyridium jenynsii*	Near et al., 2013	0.5733
Acropomatidae	*Acropoma japonicum*	Near et al., 2013	0.5263
Adrianichthyidae	*Oryzias latipes*	Near et al., 2013	0.6430
Agonidae	*Podothecus accipenserinus*	Near et al., 2013	0.5641
Ambassidae	*Ambassis buruensis*	Near et al., 2013	0.4071
Amblyopsidae	*Amblyopsis spelaea*	Near et al., 2013	0.4854
Ammodytidae	*Ammodytes* sp.	Near et al., 2013	0.1636
Amphilophus citrinellus	–	Near et al., 2013	2.0426
Anabantidae	*Sandelia capensis*	Near et al., 2013	1.0808

Table B.1: continued

Anarhichadidae	*Anarhichas lupus*	Near et al., 2013	0.4583
Anomalopidae	*Photoblepharon palpebratum*	Near et al., 2013	0.5828
Anoplogastridae	*Anoplogaster cornuta*	Near et al., 2013	0.3411
Anoplopomatidae	*Anoplopoma fimbria*	Near et al., 2013	0.3949
Antennariidae	*Fowlerichthys avalonis*	Near et al., 2013	0.5602
Aphredoderidae	*Aphredoderus sayanus*	Near et al., 2013	0.2393
Aphyonidae	*Barathronus multidens*	Near et al., 2013	0.3541
Apogonidae	*Apogonichthyoides taeniatus*	Near et al., 2013	0.3941
Aracanidae	*Kentrocapros aculeatus*	Near et al., 2013	0.5892
Argyrosomus regius	–	Near et al., 2013	0.4777
Ateleopodidae	*Ateleopus japonicus*	Near et al., 2013	0.6389
Atherina breviceps	–	Near et al., 2013	0.3698
Atherinopsidae	*Chirostoma lucius*	Near et al., 2013	0.3251
Aulorhynchidae	*Aulorhynchus flavidus*	Near et al., 2013	1.9398
Aulostomus maculatus	–	Near et al., 2013	0.1594
Badidae	*Badis kyar*	Near et al., 2013	1.3918
Balistidae	*Balistes capriscus*	Near et al., 2013	0.6627
Bathymasteridae	*Bathymaster signatus*	Near et al., 2013	0.5224
Batrachoididae	*Batrachoides pacifici*	Near et al., 2013	0.2981
Bedotiidae	*Rheocles vatosoa*	Near et al., 2013	0.2479
Belonidae	*Tylosurus crocodilus*	Near et al., 2013	0.0077
Bembridae	*Brachybembras aschemeieri*	Near et al., 2013	0.2085
Berycidae	*Centroberyx affinis*	Near et al., 2013	0.4706
Blenniidae	*Hypsoblennius brevipinnis*	Near et al., 2013	0.9459
Bodianus diplotaenia	–	Near et al., 2013	1.3363
Bothidae	*Arnoglossus thori*	Near et al., 2013	0.6947
Bovichtidae	*Bovichtus chilensis*	Near et al., 2013	0.7738
Bramidae	*Brama brama*	Near et al., 2013	0.2720
Bythitidae	*Pseudonus squamiceps*	Near et al., 2013	0.3192
Caesionidae	*Caesio* sp.	Near et al., 2013	0.6551
Calamus brachysomus	–	Near et al., 2013	1.1413
Callanthiidae	*Callanthias ruber*	Near et al., 2013	1.2445
Callionymidae	*Callionymus lyra*	Near et al., 2013	1.6398
Capros aper	–	Near et al., 2013	2.1856
Caranx caninus	–	Near et al., 2013	0.3929
Carapidae	*Carapus bermudensis*	Near et al., 2013	0.1538
Caristiidae	*Platyberyx andriashevi*	Near et al., 2013	0.2950
Centrarchidae	*Archoplites interruptus*	Near et al., 2013	0.3391
Centriscidae	*Aeoliscus strigatus*	Near et al., 2013	0.5000
Centrolophidae	*Hyperoglyphe antarctica*	Near et al., 2013	0.2292
Centropomidae	*Centropomus unionensis*	Near et al., 2013	0.2781
Cepolidae	*Cepola macrophthalma*	Near et al., 2013	0.3502
Chaenopsidae	*Emblemaria hypacanthus*	Near et al., 2013	0.9490
Chaetodontidae	*Heniochus acuminatus*	Near et al., 2013	3.2776
Champsodontidae	*Champsodon nudivittis*	Near et al., 2013	0.1848
Channichthyidae	*Chaenocephalus aceratus*	Near et al., 2013	0.1150
Channidae	*Parachanna obscura*	Near et al., 2013	0.4544
Chaunacidae	*Chaunax* sp.	Near et al., 2013	0.4542
Cheilodactylidae	*Cheilodactylus variegatus*	Near et al., 2013	1.4206
Cheimarrichthyidae	*Cheimarrichthys fosteri*	Near et al., 2013	0.5833
Chiasmodontidae	*Dysalotus oligoscolus*	Near et al., 2013	0.1211
Cirrhitidae	*Cirrhitus rivulatus*	Near et al., 2013	0.5931
Clinidae	*Heteroclinus perspicillatus*	Near et al., 2013	0.8726
Coris julis	–	Near et al., 2013	1.7298
Coryphaenidae	*Coryphaena hippurus*	Near et al., 2013	0.3017
Cottidae	*Myoxocephalus scorpius*	Near et al., 2013	0.8065
Creediidae	*Limnichthys nitidus*	Near et al., 2013	0.2121
Cryptacanthodidae	*Cryptacanthodes maculatus*	Near et al., 2013	0.3798
Cyclopteridae	*Cyclopsis tentacularis*	Near et al., 2013	0.6402
Cynoglossidae	*Cynoglossus senegalensis*	Near et al., 2013	0.2625
Cyprinodon latifasciatus	–	Near et al., 2013	0.4323
Cyttidae	*Cyttus australis*	Tyler and Santini, 2005	2.0937
Dactylopteridae	*Dactyloptena orientalis*	Near et al., 2013	1.2294
Dactyloscopidae	*Dactyloscopus tridigitatus*	Near et al., 2013	1.5315
Datnioididae	*Datnioides polota*	Near et al., 2013	1.7037
Dicentrarchus labrax	–	Near et al., 2013	0.5303

Table B.1: continued

Diodontidae	*Diodon hystrix*	Near et al., 2013	0.3827
Diretmidae	*Diretmus argenteus*	Near et al., 2013	0.2741
Drepaneidae	*Drepane punctuata*	Near et al., 2013	2.0468
Echeneidae	*Remora remora*	Near et al., 2013	0.0688
Elassomatidae	*Elassoma zonatum*	Near et al., 2013	1.1511
Eleginopsidae	*Eleginops maclovinus*	Near et al., 2013	0.9735
Eleotridae	*Gobiomorus dormitor*	Near et al., 2013	0.4089
Embiotocidae	*Rhacochilus toxotes*	Near et al., 2013	1.3307
Emmelichthyidae	*Emmelichthys ruber*	Near et al., 2013	1.3638
Enoplosidae	*Enoplosus armatus*	Near et al., 2013	1.2429
Ephippidae	*Chaetodipterus zonatus*	Near et al., 2013	0.6546
Epibulus insidiator	–	Near et al., 2013	4.6968
Esociformes	*Esox lucius*	Near et al., 2013	0.1430
Exocoetidae	*Cheilopogon arcticeps*	Near et al., 2013	0.2871
Fistulariidae	*Fistularia tabacaria*	Near et al., 2013	0.1380
Fundulidae	*Fundulus rubrifrons*	Near et al., 2013	0.7321
Gadidae	*Gadus morhua*	Near et al., 2013	0.3083
Gasterosteidae	*Spinachia spinachia*	Near et al., 2013	2.2783
Gempylidae	*Ruvettus pretiosus*	Near et al., 2013	0.2653
Gerreidae	*Gerres cinereus*	Near et al., 2013	1.8714
Gigantactinidae	*Gigantactis* sp.	Near et al., 2013	0.1112
Gobiesocidae	*Acyrtus rubiginosus*	Near et al., 2013	1.7301
Gobiidae	*Mauligobius nigri*	Near et al., 2013	0.5225
Haemulidae	*Plectorhinchus gaterinus*	Near et al., 2013	1.0236
Helostomatidae	*Helostoma temminkii*	Near et al., 2013	0.5376
Hemiramphidae	*Hyporhamphus* sp.	Near et al., 2013	0.2204
Hexagrammidae	*Ophiodon elongatus*	Near et al., 2013	0.5170
Howellidae	*Howella sherborni*	Near et al., 2013	0.4325
Hypoptychidae	*Aulichthys japonicus*	Near et al., 2013	1.9416
Indostomidae	*Indostomus paradoxus*	Near et al., 2013	0.1471
Ipnopidae	*Bathypterois pectinatus*	Near et al., 2013	0.1232
Isonidae	*Iso nesiotes*	Near et al., 2013	0.4524
Istiophoridae	*Makaira nigricans*	Near et al., 2013	0.0173
Kuhliidae	*Kuhlia malo*	Near et al., 2013	0.6424
Kurtidae	*Kurtus indicus*	Near et al., 2013	0.2762
Kyphosidae	*Graus nigra*	Near et al., 2013	0.7389
Labrisomidae	*Labrisomus philippii*	Near et al., 2013	1.6926
Lampridae	*Lampris guttatus*	Near et al., 2013	1.4879
Lates niloticus	–	Near et al., 2013	0.4046
Leiognathidae	*Leiognathus equulus*	Near et al., 2013	2.5130
Lethrinidae	*Lethrinus lentjan*	Near et al., 2013	1.3113
Liparidae	*Liparis* sp.	Near et al., 2013	0.5524
Lobotidae	*Lobotes pacificus*	Near et al., 2013	0.6513
Lophiidae	*Lophius budegassa*	Near et al., 2013	0.2323
Lophotidae	*Lophotus lacepede*	Olney et al., 1993	0.9739
Lotidae	*Lota lota*	Near et al., 2013	0.1571
Lutjanidae	*Lutjanus argentiventris*	Near et al., 2013	0.6476
Luvaridae	*Luvarus imperialis*	Near et al., 2013	0.1245
Macrouridae	*Coelorinchus caelorhincus*	Near et al., 2013	1.5700
Malacanthidae	*Caulolatilus affinis*	Near et al., 2013	0.5941
Mastacembelidae	*Mastacembelus congicus*	Near et al., 2013	0.1335
Melamphaidae	*Poromitra capito*	Near et al., 2013	0.3703
Melanotaeniidae	*Pelangia mbutaensis*	Near et al., 2013	0.3566
Mene maculata	–	Near et al., 2013	1.2941
Microdesmidae	*Gunnellichthys irideus*	Near et al., 2013	0.3868
Molidae	*Ranzania makua*	Near et al., 2013	0.3002
Monacanthidae	*Monacanthus chinensis*	Near et al., 2013	0.7491
Monocentridae	*Monocentris japonica*	Near et al., 2013	0.6806
Monodactylus sebae	–	Near et al., 2013	0.7824
Mugilidae	*Mugil curema*	Near et al., 2013	0.4046
Mullidae	*Parupeneus macronemus*	Near et al., 2013	0.4308
Muraenolepididae	*Muraenolepis* sp.	Near et al., 2013	0.6248
Myctophidae	*Lampanyctus crocodilus*	Near et al., 2013	0.0677
Myripristis murdjan	–	Near et al., 2013	0.2737
Nandidae	*Nandus nandus*	Near et al., 2013	1.3365
Nematistiidae	*Nematistius pectoralis*	Near et al., 2013	0.7991

Table B.1: continued

Nemipteridae	*Parascolopsis inermis*	Near et al., 2013	0.5317
Neoscopelidae	*Neoscopelus macrolepidotus*	Near et al., 2013	0.1649
Nototheniidae	*Paranotothenia magellanica*	Near et al., 2013	0.7530
Odacidae	*Odax pullus*	Near et al., 2013	1.0446
Odontobutidae	*Odontobutis obscura*	Near et al., 2013	0.4881
Ogcocephalidae	*Ogcocephalus vespertilio*	Near et al., 2013	0.6814
Ophidiidae	*Brotula clarkae*	Near et al., 2013	0.3128
Opistognathidae	*Opistognathus whitehursti*	Near et al., 2013	0.2817
Oplegnathidae	*Oplegnathus insignis*	Near et al., 2013	0.5391
Oreochromis niloticus	–	Near et al., 2013	0.8449
Oreosomatidae	*Neocyttus rhomboidalis*	Tyler and Santini, 2005	1.2625
Osmeridae	*Osmerus eperlanus*	Near et al., 2013	0.0590
Osphronemidae	*Osphronemus goramy*	Near et al., 2013	1.0472
Ostraciidae	*Lactophrys trigonus*	Near et al., 2013	0.5299
Ostracoberycidae	*Ostracoberyx dorygenys*	Near et al., 2013	0.4346
Paralichthyidae	*Cyclopsetta querna*	Near et al., 2013	0.2715
Paralonchurus peruanus	–	Near et al., 2013	1.4249
Parazenidae	*Stethopristes eos*	Near et al., 2013	2.2468
Paretroplus polyactis	–	Near et al., 2013	1.7549
Pempheridae	*Pempheris poeyi*	Near et al., 2013	0.4201
Pentacerotidae	*Pentaceropsis recurvirostris*	Near et al., 2013	0.7557
Percichthys melanops	–	Near et al., 2013	0.7413
Percidae	*Perca fluviatilis*	Near et al., 2013	0.3669
Percopsis omiscomaycus	–	Near et al., 2013	0.1918
Phallostethidae	*Phallostethus dunckeri*	Near et al., 2013	1.0317
Pholidae	*Apodichthys flavidus*	Near et al., 2013	0.9018
Pholidichthyidae	*Pholidichthys leucotaenia*	Near et al., 2013	0.6243
Pinguipedidae	*Pinguipes chilensis*	Near et al., 2013	0.6813
Platycephalidae	*Platycephalus indicus*	Near et al., 2013	0.2457
Plesiopidae	*Paraplesiops meleagris*	Near et al., 2013	0.6767
Pleuronectidae	*Pleuronectes platessa*	Near et al., 2013	0.7313
Poeciliidae	*Priapichthys annectens*	Near et al., 2013	1.1864
Polycentridae	*Monocirrhus polyacanthus*	Near et al., 2013	1.3212
Polymixia nobilis	–	Near et al., 2013	0.2126
Polynemidae	*Polydactylus plebeius*	Near et al., 2013	0.3179
Polyprionidae	*Polyprion oxygeneios*	Near et al., 2013	0.3706
Pomacanthidae	*Pomacanthus paru*	Near et al., 2013	0.4890
Pomacentridae	*Chrysiptera bleekeri*	Near et al., 2013	0.8553
Pomatomidae	*Pomatomus saltatrix*	Near et al., 2013	0.5270
Priacanthidae	*Heteropriacanthus cruentatus*	Near et al., 2013	0.6679
Psettodidae	*Psettodes erumei*	Near et al., 2013	0.2092
Pseudochromidae	*Congrogadus subducens*	Near et al., 2013	1.0591
Pseudomugilidae	*Kiunga ballochi*	Near et al., 2013	0.4022
Rachycentridae	*Rachycentron canadum*	Near et al., 2013	0.4368
Radiicephalidae	*Radiicephalus elongatus*	Olney et al., 1993	2.1173
Regalecidae	*Regalecus glesne*	Near et al., 2013	1.0663
Rondeletiidae	–	Near et al., 2013	0.0732
Salmoniformes	*Salmo salar*	Near et al., 2013	0.2917
Samaridae	*Samariscus corallinus*	Near et al., 2013	1.1795
Sargocentron rubrum	–	Near et al., 2013	1.0368
Scaridae	*Scarus ghobban*	Near et al., 2013	1.2369
Scatophagus argus	–	Near et al., 2013	0.5684
Scomberesocidae	*Cololabis saira*	Near et al., 2013	0.5921
Scombridae	*Thunnus albacares*	Near et al., 2013	0.3880
Scophthalmidae	*Scophthalmus maximus*	Near et al., 2013	0.4677
Sebastidae	*Sebastolobus alascanus*	Near et al., 2013	0.3834
Serranidae	*Epinephelus analogus*	Near et al., 2013	0.6398
Siganidae	*Siganus javus*	Near et al., 2013	0.5546
Sillaginidae	*Sillago maculata*	Near et al., 2013	1.1285
Soleidae	*Phyllichthys sclerolepis*	Near et al., 2013	0.3410
Sphyraenidae	*Sphyraena idiastes*	Near et al., 2013	0.2915
Stephanoberycidae	*Stephanoberyx monae*	Near et al., 2013	0.1803
Sternoptychidae	*Argyropelecus aculeatus*	Near et al., 2013	0.4446
Stichaeidae	*Xiphister atropurpureus*	Near et al., 2013	0.7641
Stomiidae	*Echiostoma* sp.	Near et al., 2013	0.2099
Stromateidae	*Peprilus paru*	Near et al., 2013	0.5972

Table B.1: continued

Stylephoridae	*Stylephorus chordatus*	Near et al., 2013	1.8002
Synbranchidae	*Ophisternon bengalense*	Near et al., 2013	0.1246
Syngnathidae	*Syngnathus* sp.	Near et al., 2013	0.3058
Synodontidae	*Synodus scituliceps*	Near et al., 2013	0.1139
Terapontidae	*Terapon jarbua*	Near et al., 2013	0.5702
Tetraodontidae	*Sphoeroides annulatus*	Near et al., 2013	0.5488
Toxotidae	*Toxotes chatareus*	Near et al., 2013	0.3151
Trachichthyidae	*Hoplostethus mediterraneus*	Near et al., 2013	0.5226
Trachinotus blochii	–	Near et al., 2013	0.9898
Trachipteridae	*Trachipterus trachypterus*	Near et al., 2013	2.8429
Triacanthidae	*Triacanthus biaculeatus*	Near et al., 2013	2.4652
Triacanthodidae	*Paratriacanthodes retrospinis*	Near et al., 2013	2.1679
Trichiuridae	*Aphanopus carbo*	Near et al., 2013	0.1263
Trichodontidae	*Trichodon trichodon*	Near et al., 2013	0.4710
Triglidae	*Prionotus ruscarius*	Near et al., 2013	0.2475
Triodontidae	*Triodon macropterus*	Near et al., 2013	0.7761
Tripterygiidae	*Enneapterygius signicauda*	Near et al., 2013	1.4156
Uranoscopidae	*Kathetostoma laeve*	Near et al., 2013	0.9864
Velifer hypselopterus	–	Olney et al., 1993	3.6240
Xiphiidae	*Xiphias gladius*	Near et al., 2013	0.0040
Zanclidae	*Zanclus cornutus*	Near et al., 2013	1.0141
Zeidae	*Zeus faber*	Near et al., 2013	2.0400
Zenarchopteridae	*Dermogenys pusilla*	Near et al., 2013	0.0169
Zenionidae	*Zenion* sp.	Near et al., 2013	2.1905
Zoarcidae	*Lycodes frigidus*	Near et al., 2013	0.6041

Table B.2: Stratigraphic ages of extinct taxa that were used to date the supertree.

Taxon	End of interval	Start of interval
†*Acrogaster daviesii*	Santonian	Santonian
†*Aipichthyoides galeatus*	Cenomanian	Cenomanian
†'*Aipichthys*' *minor*	Cenomanian	Cenomanian
†'*Aipichthys*' *velifer*	Cenomanian	Cenomanian
†*Amphiplaga brachyptera*	Ypresian	Ypresian
†*Apricenaichthys italicus*	Santonian	Santonian
†*Archaeozeus skamolensis*	Ypresian	Ypresian
†*Aulolepis typus*	Cenomanian	Cenomanian
†*Bajaichthys elegans*	Ypresian	Ypresian
†*Berybolcensis leptacanthus*	Ypresian	Ypresian
†*Berycopsis elegans*	Cenomanian	Cenomanian
†*Ctenocephalichthys longispinus*	Santonian	Santonian
†*Ctenothrissa microcephala*	Cenomanian	Cenomanian
†*Ellaserrata monksi*	Ypresian	Ypresian
†*Eoaulostomus bolcense*	Ypresian	Ypresian
†*Eoholocentrum macrocephalum*	Ypresian	Ypresian
†*Eolates gracilis*	Ypresian	Ypresian
†*Eorandallius rectifrons*	Ypresian	Ypresian
†*Eoscatophagus frontalis*	Ypresian	Ypresian
†*Erismatopterus levatus*	Ypresian	Ypresian
†*Gigapteryx tethyestris*	Mid Cenomanian	Mid Cenomanian
†*Gnathoberyx stigmosus*	Santonian	Santonian
†*Homonotichthys dorsalis*	Cenomanian	Cenomanian
†*Hoplopteryx lewesiensis*	Cenomanian	Cenomanian
†*Lateopisculus turrisfumosus*	Thanetian	Selandian
†*Libanoberyx spinulosus*	Cenomanian	Cenomanian
†*Libotonius blakeburnensis*	Lutetian	Ypresian
†*Lichia veronensis*	Ypresian	Ypresian
†*Lissoberyx dayi*	Cenomanian	Cenomanian
†*Massamorichthys wilsoni*	Thanetian	Selandian
†*McConichthys longispinnis*	Danian	Danian
†*Mene rhombeus*	Ypresian	Ypresian
†*Nardovelifer altipinnis*	Early Maastrichtian	Late Campanian
†*Pachylebias crassicaudas*	Messinian	Messinian

Table B.2: continued

†*Padovathurus gaudryi*	Ypresian	Ypresian
†*Pasaichthys pleuronectiformis*	Ypresian	Ypresian
†*Pattersonichthys delicatus*	Cenomanian	Cenomanian
†*Pharmacichthys judensis*	Cenomanian	Cenomanian
†*Pharmacichthys numismalis*	Cenomanian	Cenomanian
†*Pharmacichthys venenifer*	Cenomanian	Cenomanian
†*Priscacara clivosa*	Ypresian	Ypresian
†*Proacanthurus tenuis*	Ypresian	Ypresian
†*Proantigonia radobojana*	Tortonian	Serravallian
†*Protozeus kuehnei*	Ypresian	Ypresian
†*Pseudosparnodus microstomus*	Ypresian	Ypresian
†*Pycnosterinx russeggeri*	Santonian	Santonian
†*Pycnosteroides levispinosus*	Cenomanian	Cenomanian
†*Seriola prisca*	Ypresian	Ypresian
†*Stichopteryx lewisi*	Cenomanian	Cenomanian
†*Tylerichthys nuchalis*	Ypresian	Ypresian
†*Veronavelifer sorbinii*	Ypresian	Ypresian
†*Zoqueichthys carolinae*	Cenomanian	Cenomanian

C
R scripts from Chapter 4

C.1 Supertree constraints and calibrations

```
library(ape)
library(paleotree)
library(phytools)

JPtree <- read.tree("JP_export_tree.tre")

##########

#Create a list of taxa for the character matrix. One character added as
   MrBayes won't accept the file without it.
Taxalist <- paste0("#NEXUS

    begin data;
    dimensions ntax=", Ntip(JPtree), " nchar=1;
    format datatype=standard interleave=no missing=?;
    matrix

                  ")
Taxalist2 <- paste0(JPtree$tip.label, " 0")
Taxalist2.2 <- gsub("\\+", "", Taxalist2)
Taxalist2.3 <- gsub("\\?", "", Taxalist2.2)
Taxalist3 <- paste0("
                   ;

      end;

  begin mrbayes;")
write(Taxalist, file = "JP_Bayes_Constraints_Calibrations.nex")
```

```
write(Taxalist2.3, file = "JP_Bayes_Constraints_Calibrations.nex", append
    = T)
write(Taxalist3, file = "JP_Bayes_Constraints_Calibrations.nex", append =
    T)

##########

#NODECONSTRAINTS. Constraints for topology shape. All taxa
#Create the the constraint for the root (not created automatically)
JPNodeConstraint <- paste0("constraint noderoot = 1-. ;")
write(JPNodeConstraint, file = "JP_Bayes_Constraints_Calibrations.nex",
   append = T)

#Create list of constraints for use in Mr Bayes
JPNodeConstraints2 <- createMrBayesConstraints(JPtree, partial = FALSE)

##########

#NODE AGES. Near et al. taxa only. Taxa without node dates given zero
   length branches in phylo.
#Get calibration dates for nodes. Tip dates will be included.
JP.NA <- dateNodes(JPtree)
JP.NA <- round(JP.NA, digits = 5)

#Remove the tip dates, so left with dates of nodes only
JP.NA2 <- JP.NA[(Ntip(JPtree)+1):(Nnode(JPtree)+Ntip(JPtree))]

#Remove the nodes not found in Near et al.
JPtreeNO <- read.tree("JP_export_Near_Only.tre")

#Get Node dates for NearOnly tree and filter out tips as above
JPNO.NA <- dateNodes(JPtreeNO)
JPNO.NA <- round(JPNO.NA, digits = 5)
JPNO.NA2 <- JPNO.NA[(Ntip(JPtreeNO)+1):(Nnode(JPtreeNO)+Ntip(JPtreeNO))]

#Remove the unique nodes - those not found in Near et al.
JP.NA3 <- JP.NA2[JP.NA2 %in% JPNO.NA2]

#Renumber the nodes to correspond with the Bayes calibrations
NR <- Ntip(JPtree)
NR2 <- as.numeric(names(JP.NA3))
NR3 <- NR2[]-NR-1
NR4 <- as.character(NR3)
NR4[1] <- "root"
names(JP.NA3) <- NR4

#Need to get the Min and Max 95%HPD values for each node.
#First read the table containing the 95% values and the node ages found
```

```
    in the tree
#Then match the node ages to those associated with the 95% values
#Good idea to visually check JP.NA.MM2 to make sure nodes arent being
    removed because of problems with rounding etc.
JP.NA.MM <- read.csv(file = "JP_Min_Max_ages2.csv")
JP.NA.MM$Node_height <- (trunc(JP.NA.MM$Node_height*10^3)/10^3)
JP.NA.MM2 <- data.frame(Node_name = names(JP.NA3), Node_age = (trunc(JP.
    NA3*10^3)/10^3), Node_Min = 0, Node_Max = 0)
JP.NA.MM2$Node_Min <- JP.NA.MM$Min_height_95[match(JP.NA.MM2$Node_age, JP
    .NA.MM$Node_height)]
JP.NA.MM2$Node_Max <- JP.NA.MM$Max_height_95[match(JP.NA.MM2$Node_age, JP
    .NA.MM$Node_height)]
JP.NA.MM3 <- na.omit(JP.NA.MM2)

#Format the calibrations
JPNodeCalibrations <- paste0("CALIBRATE node", JP.NA.MM3$Node_name, " =
    uniform (", JP.NA.MM3$Node_Min, ", ", JP.NA.MM3$Node_Max, ");")

##########

#TIP AGES.All extant fixed to 0. Fossils given age ranges.

#Read the csv files for the tip ages. Separate files for extant and
    extinct taxa.
JPTip.Live <- read.csv("JP_Tip_dates_extant.csv")
JPTip.Dead <- as.matrix(read.csv("JP_Tip_dates_extinct.csv"))

#Read the table for converting stages to dates
JPFossilAges <- read.csv("JP_fossil_ages.csv")

#Convert the fossil stages to dates
JPTip.Dead2 <- matrix(nrow=length(JPTip.Dead[,1]), ncol= 3)
JPTip.Dead2[,1] <- JPTip.Dead[,1]
JPTip.Dead2[,2] <- JPFossilAges$Min[match(JPTip.Dead[,2], JPFossilAges
    [,1])]
JPTip.Dead2[,3] <- JPFossilAges$Max[match(JPTip.Dead[,3], JPFossilAges
    [,1])]

#Format the tip ages for the extant taxa.
JPTip.Live2 <- paste0("CALIBRATE ", JPTip.Live[,1], " = fixed (", JPTip.
    Live[,2], ");")

#Format the tip ages for the extinct taxa.
JPTip.Dead3 <- paste0("CALIBRATE ", JPTip.Dead2[,1], " = uniform (",
    JPTip.Dead2[,2], ", ", JPTip.Dead2[,3], ");")

#########
```

```
#Combine all of the constraints and calibrations into one file
JPCombined <- c(JPNodeConstraints2, JPNodeCalibrations, JPTip.Live2,
    JPTip.Dead3)
JPCombined.2 <- gsub("\\+", "", JPCombined)
JPCombined.3 <- gsub("\\?", "", JPCombined.2)
JPCombined.4 <- gsub("\xa3", "", JPCombined.3)
JPCombined2 <- paste0("
prset brlenspr = clock:uniform;
prset nodeagepr = calibrated;
prset clockvarpr = igr;
prset treeagepr = uniform (", JP.NA.MM3[1,3], ", ", JP.NA.MM3[1,4], ");",
     "

end;
                     ")
write(JPCombined.4, file = "JP_Bayes_Constraints_Calibrations.nex",
    append = T)
write(JPCombined2, file = "JP_Bayes_Constraints_Calibrations.nex", append
     = T)
```

C.2 Disparity between node estimates

```
#COMPARE THE INTERPOLATED CONTMAP VALUES FOR TREES CONTAINING ALL TAXA
    AND FOSSILS ONLY

JP.contree.NP <- multi2di(JP.contree)
JP.contree.NP.NF <- drop.extinct(JP.contree.NP, tol = 0.001)
Nodes.trees <- list()
Nodes.trees[[1]] <- JP.contree.NP
Nodes.trees[[2]] <- JP.contree.NP.NF

JP.protrusion.index.cont <- JP.protrusion.data$No_transform
names(JP.protrusion.index.cont) <- rownames(JP.protrusion.data)

JP.protrusion.index.cont_NF <- JP.protrusion.index.cont[names(JP.
    protrusion.index.cont) %in% JP.contree.NP.NF$tip.label]

Nodes <- list()
Nodes[[1]] <- fastAnc(Nodes.trees[[1]], JP.protrusion.index.cont)
Nodes[[2]] <- fastAnc(Nodes.trees[[2]], JP.protrusion.index.cont_NF)

Descend_nodes <- list()

for (i in 1:2) {
  a = list()
  for (j in (Ntip(Nodes.trees[[i]])+1):(Ntip(Nodes.trees[[i]])+Nnode(
      Nodes.trees[[i]]))) {
    b = getDescendants(Nodes.trees[[i]], j)
```

```
    a[[j]] = b[b %in% 1:Ntip(Nodes.trees[[i]])]
  }
  Descend_nodes[[i]] <- a
}

a = which(Nodes.trees[[1]]$tip.label %in% Nodes.trees[[2]]$tip.label)
for (i in 1:length(Descend_nodes[[1]])) {
  if (is.null(Descend_nodes[[1]][[i]]) == FALSE) {
    b = Descend_nodes[[1]][[i]][which(Descend_nodes[[1]][[i]] %in% a)]
    Descend_nodes[[1]][[i]] <- b
  }
}

Nodes.same <- data.frame(All = integer(0), Extant_only = integer(0))
for (i in 1:length(Descend_nodes[[1]])) {
  if (is.null(Descend_nodes[[1]][[i]]) == FALSE & length(Descend_nodes
      [[1]][[i]]) != 0) {
    for (j in 1:length(Descend_nodes[[2]])) {
      if (is.null(Descend_nodes[[2]][[j]]) == FALSE & length(
          Descend_nodes[[2]][[j]]) != 0) {
        x = Nodes.trees[[1]]$tip.label [Descend_nodes[[1]][[i]]] %in%
          Nodes.trees[[2]]$tip.label [Descend_nodes[[2]][[j]]]
        y = Nodes.trees[[2]]$tip.label [Descend_nodes[[2]][[j]]] %in%
          Nodes.trees[[1]]$tip.label [Descend_nodes[[1]][[i]]]
        if (all(x == TRUE) & all(y == TRUE)) {
          z = nrow(Nodes.same)+1
          Nodes.same[z,1] <- i
          Nodes.same[z,2] <- j
        }
      }
    }
  }
}

#Remove the duplicate extant only tree clades
#Keep the most recent of the clades
a = NULL
for (i in min(Nodes.same[,2]):max(Nodes.same[,2])) {
  b = which(Nodes.same[,2] == i)
  if (length(b) >1) {
    b = b[-(which(b == max(b)))]
    a = c(a, b)
  }
}
Nodes.same <- Nodes.same[-a,]

#Get the ages of the branches
Ages <- list()
```

```
Ages[[1]] <- dateNodes(Nodes.trees[[1]])
Ages[[2]] <- dateNodes(Nodes.trees[[2]])

#For checking that the ages match from the two trees
A <- data.frame(Age1 = integer(0), Age2 = integer(0))
for (i in 1:2) {
  for (j in 1:nrow(Nodes.same)) {
    A[j,i] <- round(Ages[[i]][names(Ages[[i]]) %in% Nodes.same[j,i]],3)
  }
}

Nodes_traits <- matrix(ncol = 4, nrow = nrow(Nodes.same))
colnames(Nodes_traits) <- c("Age", "All", "Extant_only", "Difference")
Nodes_traits[,1] <- (Ages[[1]][names(Ages[[1]]) %in% Nodes.same[,1]])
for (i in 1:2) {
  for (j in 1:nrow(Nodes_traits)) {
    Nodes_traits[j,(i+1)] <- Nodes[[i]][names(Nodes[[i]]) %in% Nodes.same
        [j,i]]
  }
}
Nodes_traits[,4] <- Nodes_traits[,2] - Nodes_traits[,3]
Nodes_traits[,4] <- abs(Nodes_traits[,4])
```

C.3 Evo.Rate.Time

```
library(phangorn)

#Function to plot the evo rates through time using Geiger data
#Assumes the base tree is the same as that which the rates data was
    derived from

Evo.Rate.Time <- function(phy, Rates.data, Burnin = 0.25, Min = 0, Max,
    Slices, Keep, quantiles = 0.90,
                        quantilesmoothing = 0.05, linesmoothing = 0.05,
                           ylimit) {
  #Calculate the age and length of each branch in the phylogeny
  l <- Nnode(phy) + Ntip(phy)
  ERT.data <- matrix(ncol = 5, nrow = l)
  colnames(ERT.data) <- c("Branch", "Min", "Max", "Length", "Weights")
  nd <- dateNodes(phy)
  for (i in c(1:Ntip(phy), (Ntip(phy)+2):(Ntip(phy)+Nnode(phy)))) {
    ERT.data[i,1] <- i
    ERT.data[i,2] <- nd[i]
    x <- Ancestors(phy, i, type = "parent")
    ERT.data[i,3] <- nd[x]
    ERT.data[i,4] <- ERT.data[i,3] - ERT.data[i,2]
  }
  #Remove the root row
```

```
ERT.data <- ERT.data[! is.na(ERT.data[,2]),]
rownames(ERT.data) <- 1:nrow(ERT.data)
}

#Extract and format the rates data. Remove burnin too
ERT.rates <- as.matrix(Rates.data)
cn <- c(1:length(JP.evo.rj$phy$hash))
cn <- cn[-(Ntip(JP.evo.rj$phy)+1)]
colnames(ERT.rates) <- cn
b <- round(Burnin * nrow(ERT.rates))
ERT.rates <- ERT.rates[-c(1:b),]

#Remove any unwated taxa from the ERT.data matrix
if (!missing(Keep)) {
  X = getDescendants(phy, Keep)
  Y = which(ERT.data[,1] %in% X)
  ERT.data <- ERT.data[Y,]
  }

#Round the dates as the ages for extant taxa do not =0 exactly
ERT.data[,2:3] <- round(ERT.data[,2:3], 3)

#Calculate the age of each slice
#Then extract the rates data for each slice and calculate mean, median
    and quantiles
ERT.slices <- matrix(ncol = 5, nrow = Slices)
colnames(ERT.slices) <- c("Slice", "Mean", "Median", "Q1", "Q2")
if (Max > max(ERT.data[,3])) {
  Max = max(ERT.data[,3])
}

TL <- list()

ERT.slices[,1] <- seq(from = Min, to = Max, length.out = Slices)
for (i in 1:nrow(ERT.slices)) {
  A = NULL
  for (j in 1:nrow(ERT.data)) {
    X = ERT.data[j,1]
    if(ERT.data[j,2] <= ERT.slices[i,1] & ERT.data[j,3] >= ERT.slices[i
        ,1]) {
      A <- c(A, X)
    }
  }
  TL [[i]] <- A
  B <- which(colnames(ERT.rates) %in% A)
  C <- ERT.rates[,B]
  ERT.slices[i,2] <- mean(C)
  ERT.slices[i,3] <- median(C)
```

```
    D = 0+(1 - quantiles)/2
    D[2] = 1-(1 - quantiles)/2
    Q <- quantile(C, c(D[1], D[2]))
    ERT.slices[i,4] <- Q[1]
    ERT.slices[i,5] <- Q[2]
  }

  p1 <- loess(ERT.slices[,4] ~ ERT.slices[,1], span = quantilesmoothing,
      surface = "direct", degree = 1)
  p2 <- loess(ERT.slices[,5] ~ ERT.slices[,1], span = quantilesmoothing,
      surface = "direct", degree = 1)
  p3 <- matrix(ncol = 2, nrow = length(p1$fitted)*2)
  p3[,1] <- c(rev(p2$x[,1]), p1$x[,1])
  p3[,2] <- c(rev(p2$fitted), p1$fitted)
  p3[which(p3[,2] < 0),2] <- 0

  # #Plot the rate through time data
  #Customisble y axis limits should be set as ylimit = c(i,j)
  if (missing(ylimit) == TRUE) {
    ylimit = 0
    ylimit[2] = max(p3[,2])
  }
  Max2 = p3[4,1]
  plot(ERT.slices[,1], ERT.slices[,2],
       type = "l",
       xlim = c(Max, Min),
       ylim = c(ylimit[1], ylimit[2]),
       xlab = "Time (Ma)",
       ylab = "Evolutionary rate",
       bty = "l",
       col = "white",
       xaxs = "i",
       yaxs = "i")

  #Add the polygon
  #clip(x1 = Min, x2 = Max2, y1 = 0, y2 = yl)
  polygon(p3, col = "grey", border = NA)
  l1 <- loess(ERT.slices[,2] ~ ERT.slices[,1], span =linesmoothing,
      surface = "direct", degree = 1)
  l2 <- loess(ERT.slices[,3] ~ ERT.slices[,1], span = linesmoothing,
      surface = "direct", degree = 1)
  lines(l1$x, l1$fitted, lwd = 2, lty = 2)
  lines(l2$x, l2$fitted, lwd = 2, lty = 1)

  return(list(ERT.data, ERT.slices, ylimit))
}
```

Below are the settings that were used for the two analyses in Chapter 4.

```
Slices_all <- Evo.Rate.Time(phy = JP.evo.rj$phy, Rates.data = JP.evo.
    rj$rates, Max = 205, Slices = 500, Keep = 299, quantiles = 0.8,
    linesmoothing = 0.05)

Slices_nofossil <- Evo.Rate.Time(phy = JP.evo.rj$phy, Rates.data = JP.evo
    .rj$rates, Max = 205, Slices = 500, Keep = 244, quantiles = 0.8,
    linesmoothing = 0.05, ylimit = Slices_all[[3]])
```

D

The rise of jaw protrusion in spiny-rayed fishes closes the gap on elusive prey

Here I include a publication I co-authored while completing my DPhil. This work, published in *Current Biology*, is the first study to investigate protrusion in both extant and fossil taxa – and acts as a precursor to my own work on the evolution of jaw protrusion in acanthomorphs (Chapter 4). This work is not intended to form part of the main body of the thesis and is included to illustrate other relevant work that I have been involved in during my time at Oxford.

CellPress

Current Biology
Report

The Rise of Jaw Protrusion in Spiny-Rayed Fishes Closes the Gap on Elusive Prey

David R. Bellwood,[1,2,*] Christopher H.R. Goatley,[1,2] Orpha Bellwood,[1] Daniel J. Delbarre,[3] and Matt Friedman[3]
[1]College of Marine and Environmental Science, James Cook University, Townsville, QLD 4811, Australia
[2]Australian Research Council Centre of Excellence for Coral Reef Studies, James Cook University, Townsville, QLD 4811, Australia
[3]Department of Earth Sciences, University of Oxford, South Parks Road, Oxford OX1 3AN, UK
*Correspondence: david.bellwood@jcu.edu.au
http://dx.doi.org/10.1016/j.cub.2015.08.058

SUMMARY

Jaw protrusion is one of the most important innovations in vertebrate feeding over the last 400 million years [1, 2]. Protrusion enables a fish to rapidly decrease the distance between itself and its prey [2, 3]. We assessed the evolution and functional implications of jaw protrusion in teleost fish assemblages from shallow coastal seas since the Cretaceous. By examining extant teleost fishes, we identified a robust morphological predictor of jaw protrusion that enabled us to predict the extent of jaw protrusion in fossil fishes. Our analyses revealed increases in both average and maximum jaw protrusion over the last 100 million years, with a progressive increase in the potential impact of fish predation on elusive prey. Over this period, the increase in jaw protrusion was initially driven by a taxonomic restructuring of fish assemblages, with an increase in the proportion of spiny-rayed fishes (Acanthomorpha), followed by an increase in the extent of protrusion within this clade. By increasing the ability of fishes to catch elusive prey [2, 4], jaw protrusion is likely to have fundamentally changed the nature of predator-prey interactions and may have contributed to the success of the spiny-rayed fishes, the dominant fish clade in modern oceans [5].

RESULTS AND DISCUSSION

Predicting Jaw Protrusion in Fishes

Fishes have been important predators in aquatic systems for more than 400 million years. Throughout this time, they have been faced with a key problem: how to catch elusive prey. Today, many fishes use jaw protrusion to reduce predator-prey distances. Although jaw protrusion has arisen independently in multiple lineages, including elasmobranchs and several groups of actinopterygian fishes [2, 3, 6], premaxillary protrusion is the most common mode of jaw protrusion in modern fishes [2] (Figure 1). The evolution of jaw protrusion in teleosts—the most abundant and diverse fish group—is a textbook staple, but it remains unclear how this significant innovation has changed in magnitude or frequency over time. Equally uncertain are the implications of such changes for aquatic ecosystems.

The first goal of the present study, therefore, was to find a simple morphological indicator of premaxillary protrusion in fishes. We examined protrusion in 60 species from 37 families of extant coastal marine fishes. Regression tree and ordination analyses of nine morphological features potentially associated with jaw protrusion both identified the external length of the ascending process of the premaxilla as the best predictor of the extent of observed jaw protrusion in extant fishes (Table S1; Figure S1). Ascending process length and observed jaw protrusion exhibited a strong linear relationship ($y = [0.478x] - 0.014$; $r^2 = 0.74$; Figure 1C).

The Rise of Protrusion in Marine Teleost Fishes

We found a marked change in potential protrusion in fish assemblages over time. We document changes in both the frequency and extent of jaw protrusion in fishes using three "snapshots" from similar marine environments, from the first fossil evidence of teleost protrusion at the beginning of the Late Cretaceous to the modern day. Fishes from the Late Cretaceous were estimated to have a mean protrusion of only 0.68% ± 0.14% of the body length (standard length; mean ± SE), compared to 2.03% ± 0.25% in the Eocene and 3.16% ± 0.42% in Recent fishes (Figure 2). These values reflect a significant difference in protrusion among intervals (permutational ANOVA [PERMANOVA]: pseudo-$F_{2,283} = 32.82$, p[perm] = 0.001), with pairwise tests revealing significant differences among all intervals (K/Eo: t = 5.70, p[perm] = 0.001; K/R: t = 7.65, p[perm] = 0.001; Eo/R: t = 2.44, p[perm] = 0.01).

The trend seen in mean protrusion across the three intervals was mirrored in maximum protrusion values, with a maximum of 8.16% of body length in †*Cretazeus rinaldii* (Zeiformes) in the Late Cretaceous, 13.31% in †*Zorzinichthys annae* (†Zorzinichthyidae) in the Eocene, and 21.36% in the Recent *Epibulus insidiator* (Labridae) (Figure 3). The initial driver of changing protrusion abilities was an increase in the proportion of spiny-rayed (acanthomorph) fishes (from 38% in the Late Cretaceous sample to 98% in the Eocene). This change was subsequently boosted by a greater degree of protrusion among Recent acanthomorph taxa (Figure 4). Non-acanthomorph teleosts were consistently unable to protrude, reflecting the abilities of all teleost fishes prior to the Early Cretaceous (Figures 3 and 4).

From the first definitive evidence of teleost protrusion in the Late Cretaceous (~100 million years ago) to modern marine ecosystems, there has been a distinct increase in the frequency of this feeding strategy. This increase reflects the ascendance of

 ©2015 Elsevier Ltd All rights reserved

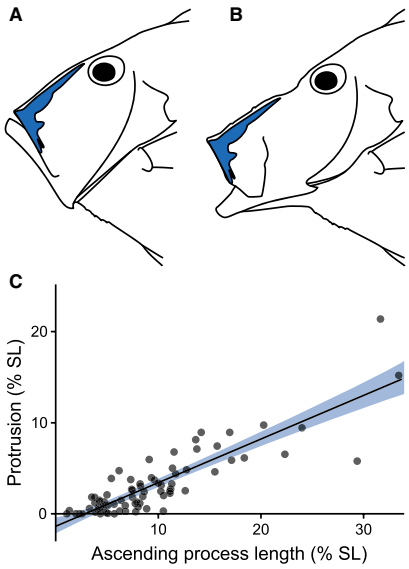

Figure 1. The Position of the Premaxilla and the Relationship with Jaw Protrusion in Recent Fishes

(A and B) The position of the premaxilla in the jaws of *Zeus faber* with the jaws closed (A) and jaws protruded (B). The premaxilla is the main tooth-bearing bone in the upper jaw. The ascending process extends from the top of the jaws toward the eye.

(C) The relationship between ascending process length and protrusion in extant fishes (±95% confidence interval; each dot represents the mean value of one species [n = 76] from 40 families).

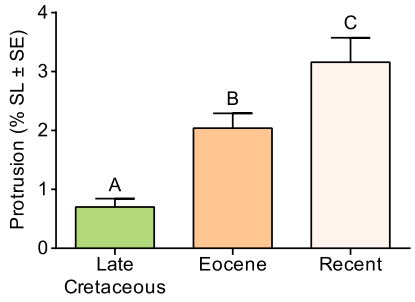

Figure 2. Estimated Jaw Protrusion Abilities of Fishes over the Last 100 Million Years

Data are presented as average percent of standard length (mean ± SE). Letters above bars indicate significant subgroups determined using a pairwise PERMANOVA of predicted protrusion and ascending process length. See also Figure S2.

spiny-rayed (acanthomorph) fishes to their modern position of prominence [5]. Today, the vast majority of modern fishes with protrusible jaws are acanthomorphs.

This increase in protrusion represents a potential shift in predator-prey dynamics that encompassed, but did not appear to respond to, the Cretaceous-Paleogene (K/Pg) mass extinction event. This lack of a response contrasts markedly with previous studies that have emphasized the extent of changes at, or shortly after, the K/Pg boundary. These changes include the loss of once-dominant Mesozoic fish clades [7, 8], the appearance of numerous new family-level lineages [5, 9], increasing disparity [10], and the rise of new functional traits [11–14]. Our findings point to a much earlier expansion in the functional abilities of teleost fishes. Indeed, the Paleogene radiation of acanthomorphs includes the first appearance of new lineages with reduced or no capacity for jaw protrusion, like scombrids and billfishes, which replaced extinct groups also characterized by limited protrusion [7].

Jaw protrusion appears to represent a general acanthomorph feature and thus may be traced to the Early Cretaceous (~140 million years ago) origin of the clade implied by molecular analyses [5]. Unlike previous marine studies that have largely focused on coral reef [11, 12, 15, 16] or pelagic fishes [7, 10], a functional rearrangement arising from increasing protrusion in teleosts probably applied to a wide range of marine habitats. Today, fishes with protruding jaws are found in all shallow benthic marine habitats. There also appears to have been a similar expansion in protrusion in freshwater systems, including an independent origin in the non-acanthomorph cyprinids [1, 3, 17]. The increased protrusion reported herein, therefore, appears to represent part of a global functional rearrangement that has operated over the past 100 million years.

The marked increase in the number of clades with protrusion (Figure 4) is strongly supported by existing molecular phylogenetic evidence. When mapped on a recent phylogeny of fishes [5], our observations suggest that there have been at least 8 and possibly 15 independent origins of significant protrusion (i.e., >5% of body length; Table S2). These observations are all in agreement with our fossil evidence: in the marine settings examined, protrusion is restricted entirely to the spiny-rayed fishes, with the vast majority being in widely separated lineages that first appear in the fossil record after the K/Pg boundary. The initial (Cretaceous to Eocene) increase in protrusion seen in Figure 2 therefore may be a result of repeated evolution, convergence, and replacement rather than expansion of protrusion within a restricted number of lineages.

The Ecological Implications of Protrusion

The ability to rapidly protrude the jaws, by up to 20% of the length of the body, has transformed the ability of fishes to feed on elusive prey [2–4, 18] and is likely to have fundamentally changed the nature of predator-prey interactions in marine ecosystems. Once protrusion arose, especially in fishes with well-developed visual abilities, elusive prey would be far more vulnerable to fish predation [2]. This is likely to have significantly enhanced predation-avoidance mechanisms. Logically, one would predict that prey would (1) increase infaunalization (to hide within the substratum), (2) increase armor (to resist dislodgement or capture), (3) develop faster escape mechanisms (to avoid capture if detected), and/or (4) reduce visual detection (by decreasing size or increasing nocturnality to

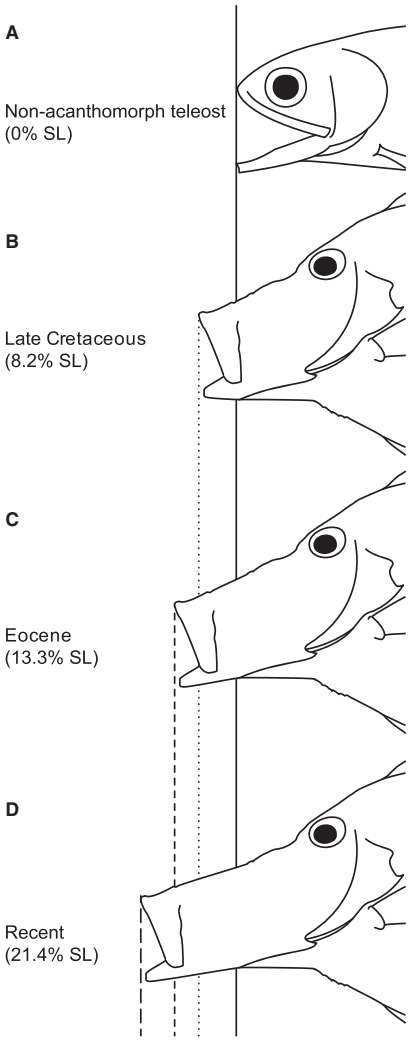

Figure 3. Differences in Estimated Maximum Jaw Protrusion over Time

Data are presented as percent of standard length (SL) between non-acanthomorph teleost fishes (A) (represented by †*Ctenodentelops striatus*) and acanthomorph fishes from Late Cretaceous (B), Eocene (C), and Recent species (D) (acanthomorph reconstructions based on the extant zeiform *Zeus faber*).

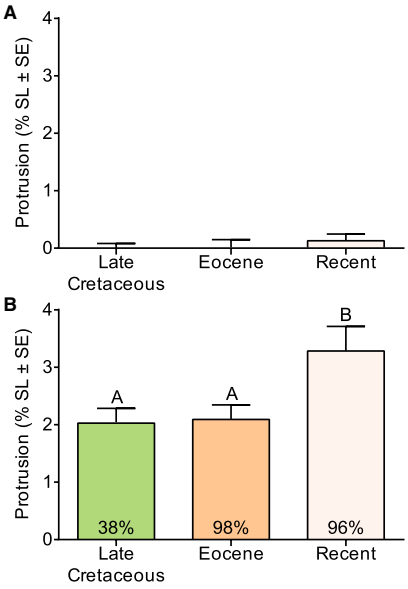

Figure 4. Estimated Protrusion Abilities of Non-acanthomorph and Acanthomorph Teleost Fishes over the Last 100 Million Years

Data (mean ± SE) are separated into non-acanthomorph (A) and acanthomorph (B) fishes. Letters above bars indicate significant subgroups determined using a pairwise PERMANOVA of predicted protrusion and ascending process length. Percentages within bars represent the proportion of sampled species in the assemblages assigned to the Acanthomorpha.

emerge under the cover of darkness). Evidence of infaunalization and increased armor have been suggested previously as responses to changes in the abilities of fish and invertebrate predators in the Paleozoic [19] and early Mesozoic [20]. However, infaunalization and/or increased armor reduce mobility and thus render prey less elusive. Faster escape mechanisms have not been documented, to our knowledge, but the evolution of structures associated with predation avoidance [15] and the diversification of coral-associated prey taxa [9] in the Neogene may reflect increasing predation pressure.

The most effective response to increasing protrusion in predators is likely to be for prey to reduce the chances of visual detection. Size reduction has been previously suggested as a predation-avoidance mechanism in copepods [21], and there is evidence that reef-associated crabs decreased in size in the Cretaceous [22]. Indeed, on modern coral reefs, the mean size of crustaceans is only 0.8 mm [23]. Interestingly, there have been significant evolutionary changes in fish feeding ecology that may reflect the impact of increasing protrusion. In the Eocene, there was an increase in high-precision diurnal feeding characterized by fishes with small mouths and large eyes [16], suggesting that fishes were indeed feeding on progressively smaller prey. Likewise, an increase in the proportion of potentially nocturnal fishes on coral reefs [16] may reflect a move to exploit the larger nektonic crustaceans, which emerge at night [24], presumably to avoid visual detection. As with size reduction in diurnal crustaceans, increased protrusion may have pushed larger elusive crustaceans to develop nocturnal habits.

These changes in diurnal precision and nocturnality suggest that there may have been a progressive escalation in

predation pressure: a trophic evolutionary arms race. In this respect it is noteworthy that the appearance of jaw protrusion is not associated with any rapid increase in diversification [5]. Indeed, some lineages of ray-finned fishes that have independently evolved jaw protrusion are both species poor and morphologically conservative (e.g., Acipenseriformes, Ateleopodiformes), indicating that protrusion in isolation is not a sufficient ingredient for diversification [2, 5]. However, a burst of new lineages may not be the only means by which innovations can underpin subsequent evolutionary radiation. Protrusion may be an example of a key innovation that, rather than producing an explosive radiation, laid the foundations for a more sustained influence marked by a prolonged and sequential expansion.

Overall, we observed an increase in jaw protrusion in fishes from the Late Cretaceous to the present. A concomitant increase in the ability of fishes to capture elusive prey is likely to have markedly changed marine predator-prey dynamics. This change may have led to a decrease in prey size and an increase in nocturnal and high-precision diurnal feeding, and may have underpinned the success of acanthomorph fishes. Today, these spiny-rayed fishes represent about a third of all extant fish biodiversity [5]. Furthermore, one of their key characteristics, jaw protrusion, represents one of the most important innovations in fish feeding in the past 400 million years. Protrusion has steadily increased to such an extent that it is a familiar characteristic of Recent marine fishes, one that we almost take for granted. Nevertheless, this characteristic has profoundly changed the abilities of fish to capture elusive prey.

EXPERIMENTAL PROCEDURES

To assess the best morphological predictors of protrusion, we conducted an initial morphological analysis on 73 freshly thawed specimens from 60 species in 37 families of extant marine fishes from coastal habitats (predominantly from the Indo-Pacific; collections followed James Cook University ethics approval A2181). In addition to measuring protrusion, we collected one angle and nine distance measurements from each specimen (see Table S1). We selected measurements that were likely to be functionally associated with premaxillary protrusion (cf. [18, 25]). To standardize data, we converted length measurements to percent of standard length and the angle measurement to the percent of a circle (360°). To evaluate allometric relationships, we plotted standardized data against standard length and, where regressions were significant, calculated residuals [15]. To allow data transformations, we removed negative values from the data by adding a constant (+0.1).

To identify potential morphological predictors of protrusion, we conducted a principal coordinates analysis (PCoA) of square-root-transformed data (morphologies and protrusion) using a Gower's dissimilarity matrix (PERMANOVA+ for PRIMER [26]). The Gower's matrix and PCoA were selected as they are more robust than PCA to the different forms of data in the analysis. The results were compared to those from a boosted regression tree. Both analyses revealed that the best predictor of protrusion was the external length of the ascending process of the premaxilla (hereafter "ascending process length"; Table S1; Figure S1). This trait measurement was then plotted against protrusion (as a percent of standard length) incorporating a further 16 species, from which it was not possible to collect the complete morphological dataset. The relationship between protrusion and ascending process length was then calculated for the full 76 species from 40 families.

To estimate the potential protrusion in fossil fishes, we measured the standard length and ascending process length from photographs, published images, or scaled reconstructions of teleosts from two periods: the Cretaceous (120 species), and Eocene (89 species). Cretaceous fossils were predominantly from the Cenomanian deposits of Lebanon (Namoura, Hakel, Hajoula, and Sahel Alma [27]), supplemented with specimens from six other localities (all from the Late Cretaceous; Table S3). Eocene fossils were from the Ypresian deposits of the Pesciara and Monte Postale localities of Bolca, Italy [28]. All selected localities had diverse fish assemblages and were most likely to span a broad range of tropical/subtropical coastal marine deposits, comparable to the sources of the extant species used in this study.

We standardized the ascending process length of fossil fishes against standard length, as per the extant fishes. The equation from the plot of ascending process length versus protrusion in Recent fishes was used to predict the potential protrusion of the fossil fishes (Table S4). Changes in the extent of protrusion between the periods were then assessed using a one-way permutational ANOVA (PERMANOVA [26]). This was conducted using relative values of predicted protrusion and ascending process length as variables and was based on a Euclidean distance resemblance matrix of square-root-transformed data. This analysis was selected because it accounts for the difference in sample sizes among periods and the distance-based nature of the data.

SUPPLEMENTAL INFORMATION

Supplemental Information includes two figures, four tables, and Supplemental Experimental Procedures, and can be found with this article online at http://dx.doi.org/10.1016/j.cub.2015.08.058.

ACKNOWLEDGMENTS

We wish to thank A. Aspes, A.F. Bannikov, G. Carnevale, P.L. Forey, U. Göhlich, J. Kriwet, J.G. Maisey, C. Patterson, O. Rauhut, M. Richter, O. Schultz, W. Simpson, L. Sorbini, J.C. Tyler, A. Vaccari, M. Véran, R. Wood, R. Zorzin, and two anonymous reviewers for their helpful comments and/or access to specimens under their care. Financial support was provided by the Australian Research Council (D.R.B.), the Natural Environment Research Council (NE/I005536/1 to M.F.), and the Leverhulme Trust (RPG 2012-658 and PLP 2012-130 to M.F.).

Received: August 12, 2015
Revised: August 24, 2015
Accepted: August 25, 2015
Published: October 8, 2015

REFERENCES

1. Staab, K.L., Holzman, R., Hernandez, L.P., and Wainwright, P.C. (2012). Independently evolved upper jaw protrusion mechanisms show convergent hydrodynamic function in teleost fishes. J. Exp. Biol. *215*, 1456–1463.
2. Wainwright, P.C., McGee, M.D., Longo, S.J., and Hernandez, L.P. (2015). Origins, innovations, and diversification of suction feeding in vertebrates. Integr. Comp. Biol. *55*, 134–145.
3. Ferry-Graham, L.A., Gibb, A.C., and Hernandez, L.P. (2008). Premaxillary movements in cyprinodontiform fishes: an unusual protrusion mechanism facilitates "picking" prey capture. Zoology (Jena) *111*, 455–466.
4. Waltzek, T.B., and Wainwright, P.C. (2003). Functional morphology of extreme jaw protrusion in Neotropical cichlids. J. Morphol. *257*, 96–106.
5. Near, T.J., Dornburg, A., Eytan, R.I., Keck, B.P., Smith, W.L., Kuhn, K.L., Moore, J.A., Price, S.A., Burbrink, F.T., Friedman, M., and Wainwright, P.C. (2013). Phylogeny and tempo of diversification in the superradiation of spiny-rayed fishes. Proc. Natl. Acad. Sci. USA *110*, 12738–12743.
6. Wilga, C.D., Hueter, R.E., Wainwright, P.C., and Motta, P.J. (2001). Evolution of upper jaw protrusion mechanisms in elasmobranchs. Am. Zool. *41*, 1248–1257.
7. Friedman, M. (2009). Ecomorphological selectivity among marine teleost fishes during the end-Cretaceous extinction. Proc. Natl. Acad. Sci. USA *106*, 5218–5223.

8. Cavin, L. (2002). Effects of the Cretaceous-Tertiary boundary event on bony fishes. In Geological and Biological Effects of Impact Events, E. Buffetaut, and C. Koeberl, eds. (Springer), pp. 141–158.
9. Cowman, P.F., and Bellwood, D.R. (2011). Coral reefs as drivers of cladogenesis: expanding coral reefs, cryptic extinction events, and the development of biodiversity hotspots. J. Evol. Biol. *24*, 2543–2562.
10. Friedman, M. (2010). Explosive morphological diversification of spiny-finned teleost fishes in the aftermath of the end-Cretaceous extinction. Proc. Biol. Sci. *277*, 1675–1683.
11. Bellwood, D.R., Hoey, A.S., Bellwood, O., and Goatley, C.H.R. (2014). Evolution of long-toothed fishes and the changing nature of fish-benthos interactions on coral reefs. Nat. Commun. *5*, 3144.
12. Bellwood, D.R. (2003). Origins and escalation of herbivory in fishes: a functional perspective. Paleobiology *29*, 71–83.
13. Wainwright, P.C., Smith, W.L., Price, S.A., Tang, K.L., Sparks, J.S., Ferry, L.A., Kuhn, K.L., Eytan, R.I., and Near, T.J. (2012). The evolution of pharyngognathy: a phylogenetic and functional appraisal of the pharyngeal jaw key innovation in labroid fishes and beyond. Syst. Biol. *61*, 1001–1027.
14. Bellwood, D.R., Goatley, C.H.R., Cowman, P.F., and Bellwood, O. (2015). The evolution of fishes on coral reefs: fossils, phylogenies, and functions. In Ecology of Fishes on Coral Reefs, C. Mora, ed. (Cambridge University Press), pp. 55–63.
15. Bellwood, D.R., Goatley, C.H.R., Brandl, S.J., and Bellwood, O. (2014). Fifty million years of herbivory on coral reefs: fossils, fish and functional innovations. Proc. Biol. Sci. *281*, 20133046.
16. Goatley, C.H.R., Bellwood, D.R., and Bellwood, O. (2010). Fishes on coral reefs: changing roles over the past 240 million years. Paleobiology *36*, 415–427.
17. Staab, K.L., Ferry, L.A., and Hernandez, L.P. (2012). Comparative kinematics of cypriniform premaxillary protrusion. Zoology (Jena) *115*, 65–77.
18. Wainwright, P.C., Ferry-Graham, L.A., Waltzek, T.B., Carroll, A.M., Hulsey, C.D., and Grubich, J.R. (2001). Evaluating the use of ram and suction during prey capture by cichlid fishes. J. Exp. Biol. *204*, 3039–3051.
19. Signor, P.W., and Brett, C.E. (1984). The Mid-Paleozoic precursor to the Mesozoic Marine Revolution. Paleobiology *10*, 229–245.
20. Vermeij, G. (1977). The Mesozoic Marine Revolution: evidence from snails, predators and grazers. Paleobiology *3*, 245–258.
21. Boxshall, G.A. (1981). Community structure and resource partitioning – the plankton. In The Evolving Biosphere, P.L. Forey, ed. (Cambridge University Press), pp. 143–156.
22. Klompmaker, A.A., Schweitzer, C.E., Feldmann, R.M., and Kowalewski, M. (2015). Environmental and scale-dependent evolutionary trends in the body size of crustaceans. Proc. Biol. Sci. *282*, 20150440.
23. Kramer, M.J., Bellwood, D.R., and Bellwood, O. (2014). Benthic Crustacea on coral reefs: a quantitative survey. Mar. Ecol. Prog. Ser. *511*, 105–116.
24. Marnane, M.J., and Bellwood, D.R. (2002). Diet and nocturnal foraging in cardinalfishes (Apogonidae) at One Tree Reef, Great Barrier Reef, Australia. Mar. Ecol. Prog. Ser. *231*, 261–268.
25. Wainwright, P.C., Bellwood, D.R., Westneat, M.W., Grubich, J.R., and Hoey, A.S. (2004). A functional morphospace for the skull of labrid fishes: patterns of diversity in a complex biomechanical system. Biol. J. Linn. Soc. Lond. *82*, 1–25.
26. Anderson, M.J., Gorley, R.N., and Clarke, K.R. (2008). PERMANOVA+ for PRIMER: Guide to Software and Statistical Methods (PRIMER-E Ltd.).
27. Forey, P.L., Yi, L., Patterson, C., and Davies, C.E. (2003). Fossil fishes from the Cenomanian (Upper Cretaceous) of Namoura, Lebanon. J. Syst. Palaeontol. *1*, 227–330.
28. Bannikov, A.F. (2014). The systematic composition of the Eocene actinopterygian fish fauna from Monte Bolca, northern Italy, as known to date. Studi e Ricerche sui Giacimenti Terziari di Bolca *15*, 23–34.

 ©2015 Elsevier Ltd All rights reserved